Year : 2021

Mixing of Rhône River water in Lake Geneva (Léman):Implications on the biogeochemistry of the lake

Cotte Gabriel

Cotte Gabriel, 2021, Mixing of Rhône River water in Lake Geneva (Léman):Implications on the biogeochemistry of the lake

Originally published at : Thesis, University of Lausanne

Posted at the University of Lausanne Open Archive http://serval.unil.ch
Document URN : urn:nbn:ch:serval-BIB_A16B0E629D4F0

UNIL | Université de Lausanne
Faculté des géosciences
et de l'environnement

Mixing of Rhône River water in Lake Geneva (Léman): Implications on the biogeochemistry of the lake

Thèse de doctorat

Présentée à la
Faculté des géosciences et de l'environnement de l'Université de Lausanne,
Institut des Dynamiques de la Surface Terrestre, par

Gabriel Cotte
Master en sciences de l'environnement
Université des Sciences de Montpellier

Jury :

Directeur de thèse : M. le Professeur Torsten Vennemann
Experte interne : Mme la Professeure Marie-Elodie Perga
Expert externe : M. le Docteur Jean-Luc Loizeau
Expert externe : M. le Professeur Mathew Wells
Sous la présidence de M. le Professeur Christian Kull

Lausanne, 2021

UNIL | Université de Lausanne
Faculté des géosciences et de l'environnement
bâtiment Géopolis bureau 4631

IMPRIMATUR

Vu le rapport présenté par le jury d'examen, composé de

Président de la séance publique :	M. le Professeur Christian Kull
Président du colloque :	M. le Professeur Christian Kull
Directeur de thèse :	M. le Professeur Torsten Vennemann
Experte interne :	Mme la Professeure Marie-Elodie Perga
Expert externe :	M. le Professeur Mathew Wells
Expert externe :	M. le Docteur Jean-Luc Loizeau

Le Doyen de la Faculté des géosciences et de l'environnement autorise l'impression de la thèse de

Monsieur Gabriel COTTE

Titulaire d'un Master en sciences de l'environnement
de l'Université des Sciences et Techniques du Languedoc/Montpellier 2

intitulée

Mixing of Rhône River water in Lake Geneva (Léman): Implications on the biogeochemistry of the lake

Lausanne, le 26 mars 2021

Pour le Doyen de la Faculté des géosciences et de l'environnement

Professeur Christian Kull

La Vierge des glaces

(Conte d'Hans Christian Andersen - 1861)

Au sommet des montagnes suisses, au creux des grands glaciers, vit la Vierge des glaces, redoutable reine des neiges éternelles.

Sa plus grande passion est d'écraser quiconque s'aventure dans son royaume.

Un jour, une mère décida de traverser ces hautes montagnes avec son bébé afin de passer du canton du Valais à l'Oberland bernois.

Avant d'atteindre Grindelwald, ils durent traverser un dernier glacier. Malheureusement, ils tombèrent dans une crevasse et la mère y perdit la vie.

Peu de temps après, une équipe de secours arriva et sauva le jeune Rudy d'une mort certaine.

Adulte, le jeune Rudy devint le meilleur chasseur de chamois du Valais.

La Vierge des glaces ayant juré de retrouver cet enfant qu'on lui avait volé jadis tenta par maints sortilèges de remettre la main sur Rudy.

Rien n'y fît, Rudy était trop intrépide…

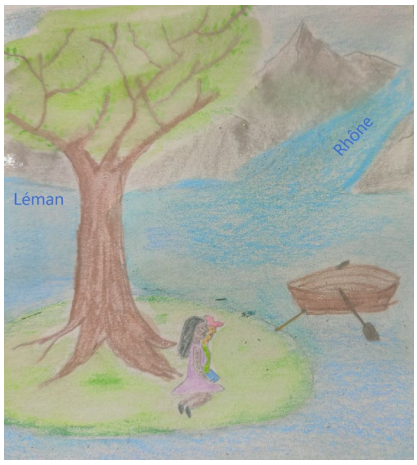

Un jour, Rudy et sa jeune femme, la fille du riche meunier de Bex, partirent au bord du Léman.

Ils décidèrent un soir de se rendre sur une île toute proche de l'embouchure du Rhône pour y admirer le coucher du soleil.

Soudain, la corde qui retenait leur barque se rompît.

Rudy plongea à l'eau pour récupérer leur seul moyen de rejoindre le littoral. C'est à ce moment-là que la Vierge des glaces emprunta l'intrusion du Rhône, se saisit de Rudy et l'entraina dans les abysses du Léman…

Cartographie du Royaume de la Vierge des glaces

(Sentinel-2A data courtesy of ESA)

Thèse de doctorat

Merci à Elfie S. pour les dessins et à Gilles A. pour la découverte.

Table of contents

Chapter I

Rhône River dispersion in Lake Geneva during the thermal stratification period

Chapter II

Mixing of the Rhône River intrusion into Lake Geneva at different thermal conditions

Chapter III

Processes driving nutrient dispersion in Lake Geneva during the stratification period

(study using the LéXPLORE platform)

Chapter IV

Hydrodynamic, physico-chemical, and biological aspects of the transition zone between the Rhône River and Lake Geneva

Conclusion

List of figures

Introduction

Chapter I

Chapter II

Chapter III

Chapter IV

Conclusion

List of Tables

Introduction

Chapter I

Chapter II

Chapter III

Conclusion

Remerciements

Je voudrais tout d'abord remercier le professeur Torsten Vennemann pour m'avoir donné l'opportunité de faire cette thèse. Je voudrais ensuite remercier tou.te.s mes collègues de l'IDYST pour le cadre agréable et stimulant de travail à l'Université de Lausanne, pour les moments incroyables passés lors des sorties d'institut et pour les souvenirs des conférences EGU à Vienne. Je voudrais aussi remercier Sabrina Damiani et Carole Schröcker pour leur sympathie et leur aide concernant les tâches administratives, mais aussi Laetitia Monbaron, Micaela Faria et Jorge Spangenberg pour leur présence et leur coup de main aux laboratoires. Je remercie également chaleureusement Aurélien Ballu pour son aide précieuse dans mes deux derniers projets de thèse riches en terrain et en galères techniques. Un remerciement amical est adressé à Philippe Arpagaus, capitaine du navire scientifique la Licorne, pour ces mémorables journées sur le lac et le partage de son amour pour le beau Léman. Je remercie également mes compagnons de départ qui, en partageant leur passion pour les sciences de l'eau, m'ont inspiré et beaucoup aidé dans mes premiers projets : Christophe Borel, Gelare Moradi et Romain Cardot. Je voudrais également remercier les membres de la team LAKE arrivés plus tard qui ont nourri mes connaissances sur ce grand lac : Nicolas Escoffier, Thibault Lambert et Pascal Perolo. Je remercie aussi les membres du projet « River-Lake Transition » avec qui nous avons monté cette belle collaboration : Frédéric Soulignac, Fabio dos Santos Correia et Matthieu Fallet et par la même occasion tous les moussaillons qui ont aidé lors des différentes campagnes de prélèvement (voir remerciements des chapitres).

Enfin, je voudrais remercier l'immense équipe de donkeys pour leur amitié, leur amour et ces moments inoubliables ! Merci c't'équipe !

Morges, novembre 2020 Dr Gab

Abstract

Determining the path of river intrusions into lakes is essential, both for a better understanding of the lake circulation as well as the nutrient transport and the distribution of pollutants introduced by the rivers. Lake Geneva has been on the way of re-oligotrophication since measures have been implemented to control the cultural eutrophication experienced during the second half of the 20th century. Despite a successful control of the nutrient fluxes with time, phosphorus becoming the limiting factor controlling primary production, the phytoplankton biomass increased in the lake. Today, with the additional effect of climate change, the euphotic zone becomes depleted in nutrients earlier during the year. The Rhône River, as the main tributary of Lake Geneva, has also been identified as the major source of nutrients, including phosphate, to the lake. The objective of this thesis is to determine the Rhône River water dispersion and its impact on the nutrient dynamics and primary production of the lake. Given the previous success of the unique stable isotope composition of the Rhône River as a conservative tracer of the influx of its waters, these measurements have been used to assess the dispersion of the Rhône River water and hence, comparing such measurements with the nutrient dispersion dynamics, relate this to the general biogeochemistry of the lake.

Several sampling campaigns, covering different seasons and focussing on different regions of the lake, have been organised in order to examine the varied patterns of dispersion for the Rhône River water. In spring, the Rhône River starts to intrude in the metalimnion at the onset of the stratification of the lake. As the Rhône River mouth is located in the eastern part of the lake, the Rhône interflow is first detected in this part called the Haut-Lac. Approximately after several weeks of well-established stratification, the interflow can reach the central lake. Over the summer, with the exception of flood events, the metalimnion layer is continuously fed by the interflow, reaching on average a proportion of around 10 % of Rhône water. The stronger the thermal stratification is, the more concentrated and vertically constrained will also be the Rhône interflow. Moreover, during the summer the Rhône interflow is dispersed throughout the whole basin by the general circulation within the lake, controlled by different gyres established under different meteorological conditions. The interflow can reach the Petit-Lac in less than four months. During autumn, lower ambient air temperatures and generally stronger

winds cool the surface waters, allowing to mix the epilimnion waters down to deeper levels. The progressive erosion of the stratification and the related plunge of the thermocline induce a deeper interflow of the Rhône River waters. As a consequence, the metalimnion enriched in Rhône River water is progressively mixed with waters from the epilimnion. In winter, the lake temperature profile is quasi-homogeneous and the Rhône River discharge is low. Deep Rhône River interflows can, however, be detected in the Haut-Lac following a progressive mixing with the ambient lake water during an underflow stage. Hence, important spatial heterogeneities of the dispersion of the Rhône River have been measured depending on the season.

Water of the metalimnion has been continuously sampled at the LéXPLORE platform from mid-September to the end of October 2019, in order to improve our understanding of possible short term changes in the nutrient dynamics during the stratification period of the lake. The vertical advection of nutrient-enriched waters from the deeper metalimnion has been identified as a major control of these dynamics during agitated periods. Indeed, the direction of circulation imposed on the surface water by the gyral motions and the direct wind forcing induce rapid changes in the thermocline depths. As the core zone of the Rhône interflow is located below the thermocline, these vertical motions provoke also oscillations of the Rhône interflow water. Hence, a coupled rise of silica-enriched water from 30 meters depth and from the Rhône River water at the thermocline has been noted during an upwelling event. In contrast, there was no notable increase in the orthophosphate concentrations as the phosphorus depletion extends down to 50 meters at this period. Meanwhile, the release or consumption of oxygen by metabolic processes is difficult to detect during agitated periods as the oxygen saturation is influenced by the vertical motions. However, biologically induced remineralization and recycling of the nutrients has been observed during periods with lesser wind agitation. Thereby, a higher resolution of the nutrient dynamics coupled to the actual monitoring of the water quality of the lake would be relevant to distinguish the processes driving the nutrient dispersion, including the influence that may be brought about by the Rhône River interflow.

An additional, multidisciplinary study examined the transition zone between the Rhône River and Lake Geneva in a number of short-range transects. The aim was to improve the understanding of the complexities and controls of phytoplankton growth in this specific river mouth area. Nutrient gradients of orthophosphate and silica related to the Rhône River intrusion have been measured in April and September 2019. In spring, an earlier onset of the stratification in the Haut-Lac due to the sheltering effect of the

surrounding mountains with the direct input of Rhône River induced nutrients makes this part of the lake particularly favourable for the vernal algal bloom. At the end of summer, the deep river intrusion, out of the turbid and turbulent near field of the river mouth, offers an equilibrium between the nutrients transported by the interflow and the other limiting factors within the lake, such as sunlight, low flow speed and temperature. In summary, the results of this part of the study identified the Rhône River mouth as a dynamic zone that punctually present optimal conditions for phytoplankton growth.

In conclusion, this thesis underlines the importance of the river-lake transition zone on the primary production of the lake and the importance of the interflow to the trophic evolution in this part of the lake. Thus, the Rhône River dispersion into the lake has to be taken into account in the lake ecosystem survey. Finally, studies of the nutrient dynamics such as initiated at the LéXPLORE platform, coupled with the historical monitoring by CIPEL, together with 3D modelling of lake circulation patterns, would allow to better assess the different biogeochemical processes within the lake.

Résumé

Etudier le parcours des intrusions de rivière dans les lacs est primordial pour comprendre leur circulation ainsi que le transport des nutriments et la distribution des polluants amenés par les rivières. Le Lac Léman est sur la voie de la re-oligotrophisation depuis que des mesures ont été prises pour contrôler l'eutrophisation qui impacta le lac pendant la deuxième moitié du XX^{ème} siècle. Malgré un contrôle efficace des apports en nutriments au lac, avec le phosphore étant devenu élément limitant de la production primaire, cette-dernière augmenta dans le lac. Actuellement, avec l'effet supplémentaire du changement climatique, les couches supérieures du lac sont appauvries en nutriments plus tôt dans l'année. Le Rhône, principal affluent du Léman, a été identifié comme source majeure de phosphore dans le lac. L'objectif de cette thèse est donc de déterminer la dispersion des eaux du Rhône et leurs impacts sur la biogéochimie du lac et, particulièrement, sur la dynamique des nutriments et la production primaire. La composition en isotopes stables de l'eau a été utilisée comme traceur conservatif des eaux du Rhône dans le lac.

Plusieurs campagnes de prélèvement ont été organisées à diverses conditions thermiques afin d'évaluer les différentes manières dont les eaux du Rhône se dispersent dans le Léman. Au printemps, le Rhône s'introduit dans le métalimnion et forme un écoulement intermédiaire à mesure que la stratification thermique se met en place. Comme l'embouchure du Rhône se situe dans la partie orientale du lac, cet écoulement intermédiaire est d'abord détecté dans cette zone appelée le Haut-Lac. Il lui faut ensuite plusieurs semaines de forte stratification pour atteindre le centre du lac. Au cours de l'été, excepté lors des crues, le métalimnion est continuellement alimenté par cet écoulement, atteignant en moyenne 10 % d'eau du Rhône. Plus la stratification est marquée, plus les eaux du Rhône seront concentrées et verticalement contraintes. De plus, à cette saison, les eaux du Rhône sont dispersées dans tout le bassin par les courants du lac et recirculent au gré du sens de rotation des gyres. Elles peuvent ainsi atteindre le Petit-Lac en moins de quatre mois. En automne, les températures de l'air plus basses et les vents plus forts refroidissent et mélange peu à peu les couches de surface. L'érosion de la stratification, et l'approfondissement de la thermocline qui s'en suit, provoque une intrusion du Rhône plus profonde. En parallèle, le métalimnion enrichi en eaux du Rhône est progressivement mélangé à l'épilimnion. En hiver, le profil thermique du lac est quasiment homogène et

le débit du Rhône est faible. Cependant, des intrusions profondes peuvent être détectées dans le Haut-Lac après qu'un mélange progressif du courant de gravité du Rhône et des eaux du lac ait eu lieu. Ces résultats montrent ainsi d'importantes hétérogénéités spatiales de dispersion des eaux du Rhône selon la saison.

Des échantillons d'eau du métalimnion ont été régulièrement collectés à la plateforme LéXPLORE de mi-Septembre à fin Octobre 2019 dans le but d'étudier la dynamique des nutriments en période de stratification. L'advection verticale d'eau profonde enrichie en nutriments a été identifiée comme principal vecteur de nutriments pendant les périodes de colonne d'eau agitée. En effet, la rotation des gyres et l'action directe du vent provoquent des oscillations de la thermocline. Le centre de l'écoulement des eaux du Rhône étant situé en-dessous de la thermocline, ces mouvements verticaux génèrent des déplacements ascendant et descendant de la couche d'eau du Rhône. Ainsi, une remontée d'eau enrichie en silice, provenant à la fois des couches plus profondes de la colonne d'eau et des eaux du Rhône, a pu être constatée lors d'un upwelling. Cependant, aucune augmentation de la concentration en orthophosphate n'a été détectée car la couche appauvrie en phosphore s'étends jusqu'à 50 mètres de profondeur à cette période. De plus, la production et consommation d'oxygène par les processus métaboliques sont difficilement mesurables pendant ces périodes agitées du fait que le taux de saturation en oxygène est corrélé à ces mouvements verticaux. Le recyclage des nutriments par la production primaire a tout de même été observé lors de périodes plus calmes. Ainsi, une meilleure résolution de la dynamique des nutriments couplée à l'actuel monitoring de la qualité du lac permettrait de distinguer les processus en jeu dont la contribution du Rhône.

Enfin, une étude multidisciplinaire s'est portée sur la zone de transition entre le Rhône et le Léman avec comme objectif de comprendre les conditions de croissance du phytoplancton dans cette zone d'estuaire. Des gradients de phosphore et de silice liés à l'intrusion des eaux du Rhône ont été constatés en Avril et Septembre 2019. Au printemps, une stratification thermique précoce se mets en place dans le Haut-Lac dû à l'effet de protection des montagnes avoisinantes. Ajoutant à cela l'apport direct en nutriment du Rhône, le Haut-lac apparait alors comme une zone privilégiée pour la croissance algale printanière. A la fin de l'été, l'intrusion profonde du Rhône, en dehors de la zone turbide et turbulente proche de l'embouchure, apporte un équilibre entre les nutriments transportés par la rivière et les autres facteurs limitant du lac comme la lumière, les faibles courants et la température. Ainsi, l'embouchure du Rhône dans le

Léman apparait comme une zone dynamique présentant ponctuellement des conditions favorables à la croissance du phytoplancton.

Les résultats de cette thèse ont pu mettre en évidence l'importance de la zone de transition entre le Rhône et le Léman pour la production primaire du lac. Son suivi devrait donc être étudié afin de comprendre l'évolution trophique du lac. De plus, la dispersion des eaux du Rhône dans le lac devrait être prise en compte dans le suivi de cet écosystème lacustre. Enfin, l'étude de la dynamique des nutriments initiée à LéXPLORE associée au monitoring existant de la CIPEL, ensemble intégrés par la modélisation hydrodynamique 3D, permettront de mieux comprendre les différents processus biogéochimiques du lac.

Résumé grand public

Le Léman, situé à la frontière entre la Suisse et la France, est le plus grand lac d'Europe occidentale. Il alimente en eau potable environ 900 000 habitants vivant le long de ses côtes. En plus de soutenir l'activité de quelques 140 pêcheurs professionnels, le lac accueille une large diversité de plantes et d'animaux.

Pendant la deuxième moitié du 20ème siècle, le Léman a souffert d'eutrophisation. Ce phénomène de croissance algale accrue fut provoquée par l'augmentation des apports en nutriments dans ces eaux, due à l'intensification des activités humaines. Entre autres, le phytoplancton, ces algues se développant dans la zone pélagique du lac, c'est-à-dire dans sa colonne d'eau, ont considérablement proliféré suite à l'augmentation des concentrations en phosphore. Ces plantes utilisent la lumière du soleil et les nutriments dissous dans l'eau pour effectuer la photosynthèse et ainsi croître. Un fois mortes, elles sont décomposées par les bactéries du lac. Ce processus consomme de l'oxygène présent sous forme dissoute dans l'eau. La prolifération des algues a donc entraîné une forte diminution de la teneur en oxygène dans l'eau. Ce phénomène, appelé hypoxie, peut provoquer d'intenses bouleversements dans les écosystèmes aquatiques. Par exemple, l'hypoxie des couches profondes du Léman a provoqué une forte diminution de la population de corégone, ce poisson ne pouvant survivre en dessous d'une certaine concentration en oxygène. Par ailleurs, l'eutrophisation des plans d'eau peut déclencher l'apparition d'espèces toxiques d'algues telles que les cyanobactéries.

Afin de lutter contre ce phénomène répertorié dans de nombreux lacs autour du monde, la CIPEL (Commission Internationale pour la Protection du Léman) a mis en place des mesures de réduction d'apport en phosphore au lac à partir des années 70. De nouvelles stations d'épuration ont été construites et des systèmes de déphosphatation des eaux usées ont été installés. De plus, les détergents à base de phosphate ont progressivement été interdits. Ces mesures ont permis une diminution de la concentration en phosphore dans le lac et une amélioration de qualité de l'eau. Cependant, la quantité d'algue mesurée chaque année n'a pas diminué. Ce paradoxe amène à la question suivante : pourquoi le phytoplancton croit-il toujours autant avec moins de nutriments ? Actuellement, l'effet supplémentaire du changement climatique perturbe l'écosystème lémanique et empêche un retour aux conditions d'avant 1950. En effet, le réchauffement climatique provoque une augmentation de la température de l'eau et une extension de la

saison de croissance des algues. Dans ce contexte, il est primordial de bien comprendre la dynamique des nutriments à travers le lac pour comprendre et prévoir l'évolution de cet écosystème.

Le fleuve Rhône, qui prend sa source dans le canton du Valais à 160 km en amont du Léman, est le principal affluent du lac. Le glacier du Rhône qui recouvrait l'emplacement du Léman lors du dernier maximum glaciaire, il y a environ 20 000 ans, se trouve maintenant au fond de sa vallée à 2341 m. En plus d'être le principal apport en eau et en sédiment, le Rhône apporte au lac la majorité du phosphore indispensable à la croissance des algues. Pour son développement, le phytoplancton a besoin d'un équilibre entre plusieurs paramètres : la lumière, la température et la concentration en nutriments. Au cours du printemps, la couche de surface qui reçoit les rayons du soleil, appelée zone euphotique, est progressivement appauvrie en nutriments par la photosynthèse. L'apport en nouveaux nutriments ne s'effectue donc que par le recyclage des algues mortes ou par les rivières. Selon le mélange des eaux de la rivière avec les eaux du lac qui les reçoit, différents effets de fertilisation peuvent être observés. Si la rivière, moins dense que les eaux du lac, flotte sur ce dernier, les nutriments qu'elle transporte seront alors directement (bio)disponibles pour le phytoplancton. En revanche, si la rivière plus dense, plonge au fond du lac, ses nutriments n'atteindront pas la zone euphotique et ne produiront pas d'effet de fertilisation. Et donc, qu'en est-il du rôle du Rhône dans la fertilisation du Léman ? Cette thèse s'est ainsi portée sur la dispersion des eaux du Rhône et de ses nutriments dans le Léman et à leur effet de fertilisation engendré dans le lac.

La première question posée a été celle de la dispersion du Rhône : où retrouve-t-on ses eaux dans le Léman selon la saison ? Il a été observé du printemps à l'automne un scénario intermédiaire aux deux présentés ci-dessus. Le Rhône, entre 8 et 12°C à cette période de l'année, va tout d'abord plonger dans les couches de surface plus chaudes du Léman avant de s'introduire dans la colonne d'eau à la profondeur où sa densité équivaut celle du lac. Cet écoulement, mesuré entre 10 et 20 m en été, est ensuite dirigé par les courants du Léman. Ces courants prennent la forme de tourbillons, comme dans les océans, appelés gyres. Ceux-ci sont provoqués par la force du vent et de la rotation de la Terre, dite de Coriolis. Il a ainsi pu être constaté que cet écoulement d'eau du Rhône était dispersé à l'échelle de tout le lac par ces gyres et qu'il pouvait atteindre le Petit-Lac en seulement trois mois.

Par la suite, la question de l'impact de ce transport des eaux du Rhône dans la dynamique des nutriments du Léman s'est posée. Pour y répondre, une étude a été menée

à la nouvelle plateforme scientifique LéXPLORE, ancrée à 500 m du port de Pully, à l'Est de Lausanne. Il en est ressorti qu'un apport important en nitrates et en silice des eaux plus profondes pouvait avoir lieu lorsque le lac était agité par de forts vents. De plus, l'apport en silice du Rhône, via l'écoulement intermédiaire décrit plus haut, a pu être mis en évidence au niveau de cette station située au milieu du Grand-Lac.

Enfin, dans le but de déterminer le rôle de fertilisation du Rhône dans sa zone d'embouchure, une étude multidisciplinaire menée par des équipes de recherche de l'UNIL, l'UNIGE et l'EPFL s'est portée sur la zone du Haut-Lac. Les résultats ont montré que cette partie orientale du lac pouvait être une zone privilégiée pour la croissance du phytoplancton du fait de la fertilisation directe des eaux du Léman par les nutriments du Rhône.

Les conclusions de cette thèse permettent de mieux comprendre la relation entre le Léman et son tributaire principal, le Rhône, et son rôle dans la fertilisation de cet écosystème lacustre.

Introduction

1. Motivations

1.1. Large lake services

Lakes and other lentic systems contain more than 90 % of the liquid surface freshwater of our planet (ILEC and UNEP, 2016). Hence, they represent an important reservoir of the Earth's global water cycle. They provide ecosystem services for the human population and contain a large diversity of organisms (Table 0-1). Worldwide, a large range in size and morphology of lakes exists, from small ponds to the deepest lake Baïkal with its maximum depth of 1741 m and its volume of 23 000 km^3. Indeed, most lakes are small and shallow and only 1719 lakes on the planet have a surface area greater than 100 km^2 (Jenny et al., 2020). However, these large lakes account for almost 90 % of the total surface and volume of the world's lakes. A list of the main services that lakes provide for natural systems is described below.

Table 0-1: List of services provided by lakes. From Jenny et al. (2020).

Ecosystem services	Examples
Provisioning services	Food, drinking water, industrial water and hydroelectricity, water for navigation, genetic resources, medicinal resources
Regulating services	Water flow regulation, local climate regulation, water quality regulation, regulation of natural risks, transfers or sequestration of elements . . .
Supporting services	Habitats for nursery and reproduction (plant and animal), maintenance of aquatic fauna and flora from micro-organisms to macro-organisms, support of migratory species and wildlife, hot spots of biodiversity
Cultural services	Aesthetics, recreation, inspiration for culture and art, spiritual experience, cognitive and scientific development

1.2. Large lake pressures

A recent paper, co-written by researchers from more than 30 different institutes, addressed a second warning to humanity concerning the rapid degradation of the world's large lakes (Jenny et al., 2020). They claimed that these ecosystems are particularly sensitive to anthropogenic and climate stressors. Indeed, their larger characteristics compared to others waterbodies (larger water volume, watershed, water inflows, greater depth, shoreline length and wind influence) have a direct and indirect influence on the exposure of stressors, the intensity of the impacts, the effectiveness of environmental management actions and the duration of recovery. About 131 million people are currently

living in their littoral zones. In the context of the Anthropocene, with a growing population and an intensification of human activities, large lakes are exposed to a wide variety of stressors. These stressors cause disturbance in the structure or the function of their ecosystems, leading to a deterioration of their services (Figure 0-1). Among the major disturbances, we can cite cultural eutrophication, triggered by an increase of nutrient loading as a result of human activities (Richardson and Jørgensen, 2013) and climate change (IPCC, 2018) that modifies the thermal structure of lakes and so their mixing regimes (Woolway and Merchant, 2019). Shoreline modification induces also pressures on coastal ecosystems with inputs of nutrients and pollutants and physical alterations that threaten the habitat's diversity (Schmieder, 2004; Vadeboncoeur et al., 2011).

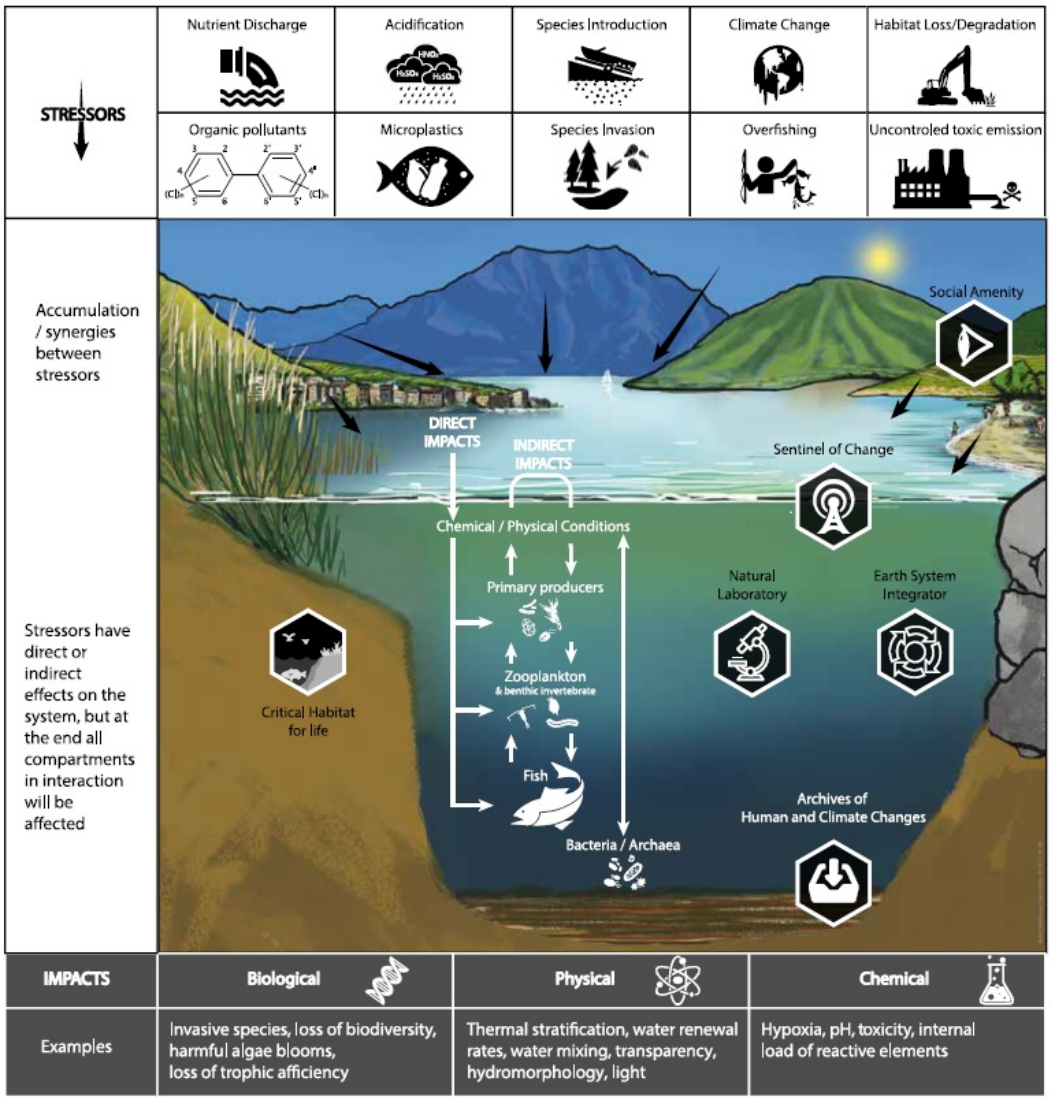

Figure 0-1: Overview of most known stressors, and of their impacts on lakes. White arrows highlight direct or indirect impacts. From Jenny et al. (2020).

1.3. Eutrophication as worldwide issue

The global spread of hypoxia in freshwater ecosystems has been identified as a worldwide problem (Jenny et al., 2016). The increased tendency of oxygen depletion of deep lake waters observed during the last century is related to the combined effect of cultural eutrophication and climate change. An intensification of human activities and nutrients released in aquatic ecosystems, especially after the 1950's, triggered an increase in primary production. The large amount of biomass induced an important consumption of dissolved oxygen and lead to a switch of trophic state in many lakes around the world (see below 2.1.).

The Alps are considered as the "water tower" of Europe. Two of the largest European rivers start to flow in the Swiss Alps (the Rhône and the Rhine). This global trend of cultural eutrophication was also measured in Swiss lakes (Figure 0-2) resulting in a degradation of the water quality and important changes in the ecosystem biota.

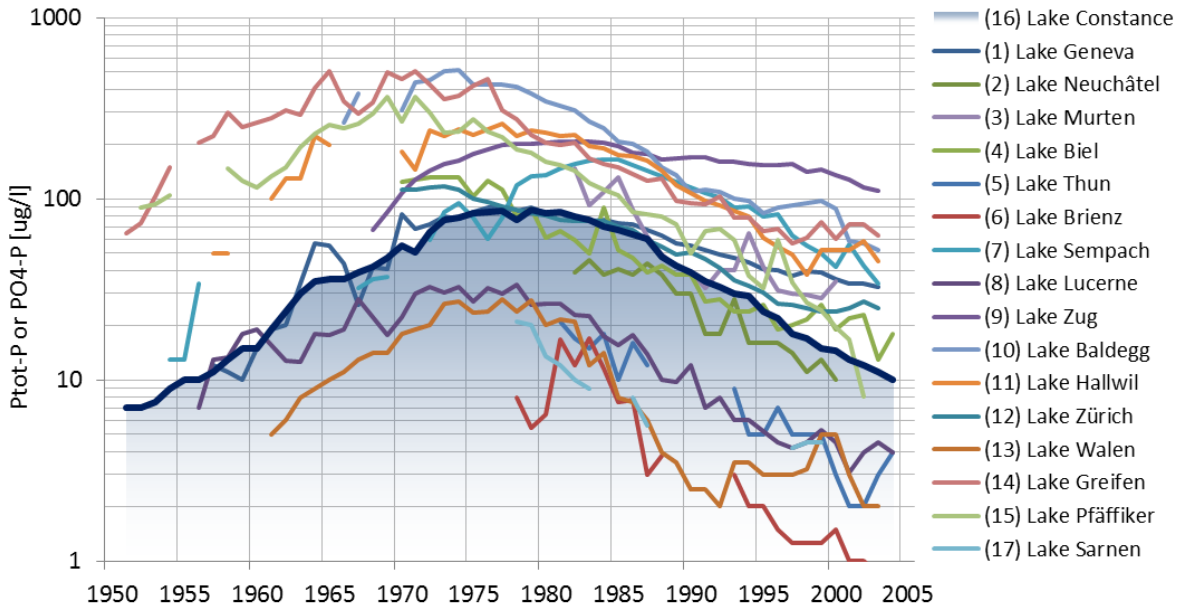

Figure 0-2: Change in phosphorus concentration through time in 17 Swiss lakes. From Vonlanthen et al. (2012).

1.4. Lake Geneva context

Lake Geneva, the largest fresh water reservoir of Western Europe, is located at the border between France and Switzerland. More than a million of people are living in its watershed (CIPEL, 2020). The lake is a major source of drinking water for almost

900’000 inhabitants via 10 pumping stations. It is hosting a wide diversity of plants and animals and it is sustaining the activity of about 140 professional fishermen in both countries. It is also important for the tourism and recreation sectors.

Lake Geneva has suffered from eutrophication since the 1950’s and has experienced a regime shift with consequential modifications of its ecological processes (Rimet et al., 2020). Using paleoecological data, Bruel et al. (2021) showed that this recent shift in the trophic state of the lake made it more vulnerable to climate change. Moreover, Lake Geneva is suffering from an intense artificialization of its shoreline and from the appearance of emergent pollutants, such as micropollutants (Chevre, 2018) and new invasive species (e.g., the quagga mussel). As remind by the second warning of lake researchers (Jenny et al., 2020), the combined effect of stressors generates a complex response of the lake and poses challenges to the lake management.

The present study focuses on the dispersion of the lake’s main tributary, the Rhône River, in the *Lac Léman* basin and the impact on the biogeochemistry of the lake in the context of its re-oligotrophication.

2. State of the art

2.1. Lakes along the aquatic continuum

Lakes as receptors and bioreactors

The hydrographic networks consist of an alternation of lotic and lentic systems. On this aquatic continuum, lakes are the receptors of the water, the sediment, the nutrients and other compounds from the watershed. They are also considered, since the 1990's, as reactors because they receive and transform particulate and dissolved materials from the catchment. As such, the influence of the watershed via the river input depends on the retention time within the lake basin. In other words, the most important is the water residence time, the most efficient will be the nutrient transformation within the lake (Engel et al., 2018 ; Figure 0-3). It will also vary according to the riverine pathway. These transformations occur via different biogeochemical reactions (Tranvik et al., 2009):

The photosynthesis processed by autotrophic species transforms the dissolved inorganic nutrients (C, N, P) into organic compounds using energy from light following the equation:

$$6\ CO_2 + 12\ H_2O + \text{Light/Energy} \rightarrow C_6H_{12}O_6 + 6\ O_2 + 6\ H_2O$$

The amount of photosynthate produced by photosynthesis corresponds to the primary production (PP). These photosynthates can be transferred into higher trophic levels via consumption.

The organic matter produced within the lake (autochthone) or imported from the watershed (allochthone) can be re-mineralized by different processes. The reverse reaction of photosynthesis, the respiration, is processed by autotrophic and heterotrophic organisms to obtain their vital energy. It consumes oxygen and releases dissolved inorganic nutrients. In lakes, one of the main organic matter degradation pathways is processed by bacteria as part of the microbial loop.

Residual organic and inorganic material can then be sedimented and hence be exported to the bottom of the lake. Sediments can process nutrients (e.g., remineralization of organic matter), trap material (e.g. particulate P) but can also release nutrients back to the water column (remobilization).

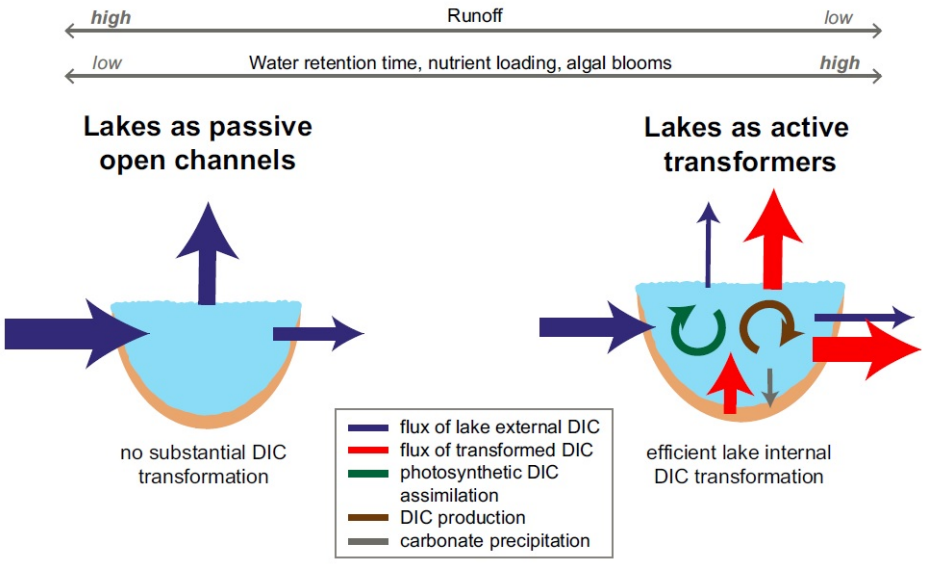

Figure 0-3: Conceptual figure showing two ends of a continuum of lake functions in the cycling of dissolved inorganic carbon (DIC). From Engel et al. (2018).

Each lake has its own way to transform terrestrial material depending on the multiple drivers that characterise it: climate, lake morphology, hydrology, ecological status, vegetation, soil types, land cover, geology, inputs, etc. Finally, lakes can act as source or sink for the nutrients, depending on the balance between hydrology and biology (e.g. P assimilation by bacteria = sink, versus P mobilization from the sediments = source).

Eutrophication

The term eutrophication corresponds to an enrichment of inorganic nutrients (mainly forms of N and P) and organic matters of a particular water body. Lakes naturally tend to accumulate organic matter and detrital material at their bottom, increasing the sediment thickness and thus decreasing the height of the water column with time. This process greatly varies in time across lakes as it depends on the bioproductivity of the lake, the supply of organic matter and other nutrients from the watershed and efficiency of remineralization both within the water column and the sediment (Björk, 2010). Thus, according to the phosphorus concentration, the concentration of chlorophyll *a* (Chl *a*) or the production rate of organic matter, different trophic levels of lakes can be defined (Table 0-2). With time, the filling up of lakes may thus transform them into wetlands, and eventually also be overgrown by emergent vegetation. However, if we refer to an eutrophication process inducing disequilibrium in the organic matter fluxes compare to the exportation capacity of the lake, the term dystrophization is more appropriate.

Likewise, Nixon (1995) proposed that eutrophication alludes to an increase in the production rate of organic carbon in aquatic ecosystem. Since the 1950's, with increasing human activities, we assist of an acceleration of these processes worldwide via the excessive use of fertilizers and phosphate-based detergents (i.e. cultural eutrophication; Smith, 1998).

Table 0-2: Characteristic features in lakes of different trophic levels. From Vollenweider and Kerekes (OECD, 1980)

Trophic level	Total P ($mg.m^{-3}$)	Chl a ($mg.m^{-3}$)	Annual production ($gC\ m^{-2}\ y^{-1}$)
Ultra-oligotrophic	<3	<0.1	<12.5
Oligotrophic	3-10	<1	12.5-38
Mesotrophic	5-40	<10	38-140
Eutrophic	20-400	<100	140-640
Hypertrophic	>100	<1000	>640

Primary producers are the first to be affected by eutrophication. Indeed, through higher nutrient supply, phytoplankton, but also floating and submerged macrophytes, proliferate and decrease water transparency. This organic matter ultimately sinks and is re-mineralized in the microbial loop, causing an increase of bacterial oxygen consumption and sedimentation rates. As a result, depending on the intensity of eutrophication and the intrinsic characteristics of each lake, hypoxia can occur and drastically change the lake's biogeochemical cycles (Jenny et al., 2016). Moreover, eutrophication can provoke harmful algal blooms with the development of potentially toxic cyanobacteria (Paerl et al., 2011).

Re-oligotrophication

Since the 1970's, the scientific community and a wide range of national and international management programs put efforts into the restoration of lakes (Jenny et al., 2020). Investigations were carried out to address the limiting nutrient responsible of the algal growth. Schindler (1974, 1977) identified phosphorus and demonstrated the importance of controlling its concentration to reduce unwanted seasonal algal blooms. Consequently, measures of reduction of phosphorus inputs to lakes were widely applied (Sas, 1990).

However, several lakes did not follow the phytoplankton reduction pattern expected and have known a persistence of hypolimnetic hypoxia (Jenny et al., 2016). Some of them even showed an increase in both PP and Chl *a* concentrations (Jeppesen et al., 2005). If we refer to Table 0-2, it has been shown that the classification of the trophic level of a lake based on the chemical definition does not necessarily coincide with the biological classification. Some studies attributed these non-return to original biological conditions to the storage of nutrients in the lake (Schindler, 2012) or in their watershed (Withers et al., 2014), or also to the impact of climate change that improve the eutrophication effects (Finger et al., 2013; Jenny et al., 2014). Indeed, the climate warming increases the water temperature and extends the growing season with a longer stratification period (Anneville et al., 2013). Other studies evaluate the capacity of the phytoplankton to adapt to long-term environmental changes. Moisset (2017) referred to a shift in the phytoplankton community from species characteristic of eutrophic waters towards those characteristic of meso-oligotrophic waters in Lake Geneva. Anneville et al. (2018) also suggested that phytoplankton communities adapted by changing their seasonal dynamics of species assemblages. Furthermore, Finger et al. (2013) argued that a reduction of phytoplankton abundance in lakes increases the euphotic depth and leads to an increase of the productive water volume, counter balancing the effect of oligotrophication, as illustrated in Fig. 0-4 for Lake Lucerne.

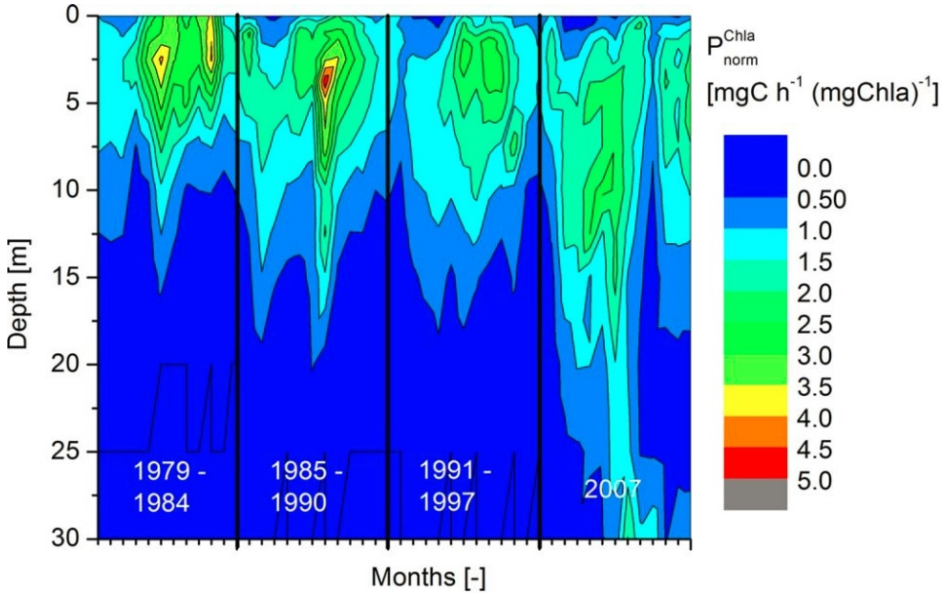

Figure 0-4: Mean monthly specific C assimilation rates per unit chlorophyll a, normalized to the reference water temperature and averaged for specific periods. From Finger et al. (2013).

Moreover, Wentzky et al. (2018) defined mechanisms, like mixotrophy, able to prevent a decrease in phytoplankton biomass after phosphorus reductions in a German drinking water reservoir. With this capacity to adapt the nutrient sources, they showed the considerable plasticity of phytoplankton abundance at a given nutrient content. Finally, Müller et al. (2019) proved, by showing an increase of the C:P ratio of the settled material, that phytoplankton community is able to maintain maximum biomass production by counteracting the decreasing P supply by a more efficient P utilization.

2.2. Mixing and transport in lakes

Thermal stratification

Aquatic physics of inland waters is primordial to understand aquatic ecosystem functioning. Knowledge about transport and mixing in lakes is a requirement in order to understand how and where chemical and biological processes can develop. Many lakes show vertical stratification of their water masses, at least for some extended time periods. Density differences in water bodies facilitate the compartmentation in layers of different chemical characteristics with many consequences for the biology (Boehrer and Schultze, 2008). The density of natural waters depends on temperature, pressure, dissolved substances and suspended sediment concentration (SSC). Usually, the main source of heat comes from the atmosphere and the solar radiation. As a result, thermal stratification of warm monomictic lakes takes place during the warm season and water column homogenisation can occur during the cold season. Overturns and deep mixing events are important for the renewal of deep waters and their oxygenation (e.g., Bouffard and Wüest, 2018). During the stratification period, the top-most layer exposed at the surface to the atmosphere is called the epilimnion. Below is the metalimnion, the layer with a large temperature gradient. In this layer, the plane where the temperature gradient is the highest is called the thermocline. Below the metalimnion is the so-called hypolimnion, the coldest layer that shows very little temperature change with depth (Figure 0-5). The thermal and chemical exchange between the epilimnion and the hypolimnion is hindered as the degree of stratification and so the stability of the water column increases throughout the warm season. During fall, the temperature of the epilimnion water decreases as the air temperature gets cooler and the solar radiation decreases. Hence, a progressive erosion of the metalimnion occurs until a possible homogenization of the lake by wind mixing and

water cooling leads to a complete overturn in winter or early spring (Wetzel and Likens, 1991).

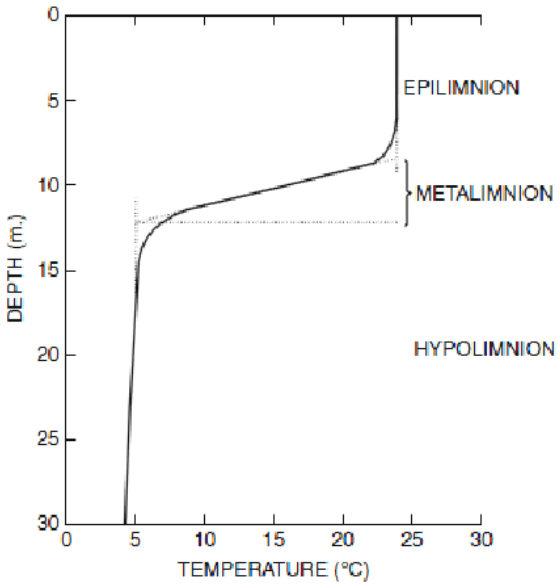

Figure 0-5: Typical thermal stratification in a deep lake. From Wetzel and Likens (1991).

Water movements

Water movements are mainly determined by the lake thermal stratification, the atmospheric forcing and the morphology of the lake basin that defines its exposure to wind. The factors influencing the mixing and transport processes in lakes are summarized in Fig. 0-6 (Imboden and Wüest, 1995).

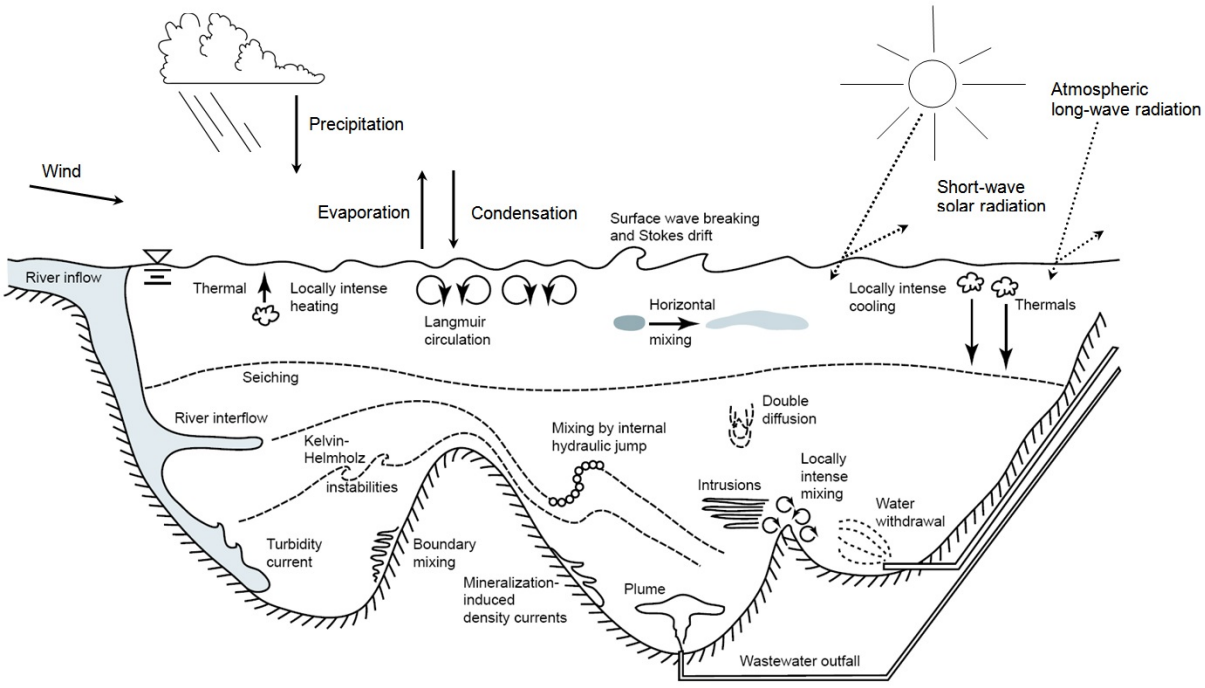

Figure 0-6: Scheme of mixing and transport processes in lakes. From Imboden and Wüest (1995).

As an example, surface waves are important mixing features within the epilimnion and provoke gas exchange with the atmosphere. Then, strong winds (above ~2 m/s) can induce Langmuir circulations. These helical vortices can provoke a deepening of the epilimnion until the barrier formed by the density gradient in the metalimnion blocks the transmission of turbulence to the hypolimnion. Moreover, wind forcing can cause displacement of the thermocline downward at the downwind end and upwelling at the upwind end of the lake. When the wind stops, the baroclinic pressure, associated with the tilted metalimnion, acts as a restoring force, inducing a long internal wave also called internal seiche. Earth's rotation may also affect internal waves when Coriolis effect on buoyancy forces is significant. This provokes the rotation of Kelvin and Poincaré waves at the basin scale. The amplitude of the thermocline displacement is maximum at the shore and decays offshore. Another important mixing mechanism is the development of a mixed layer induced by surface cooling (Figure 0-7). When a stable stratification (a) is destabilised by surface cooling that creates an unstable density profile (b), the unstable grid cells are mixed to recover stability (c).

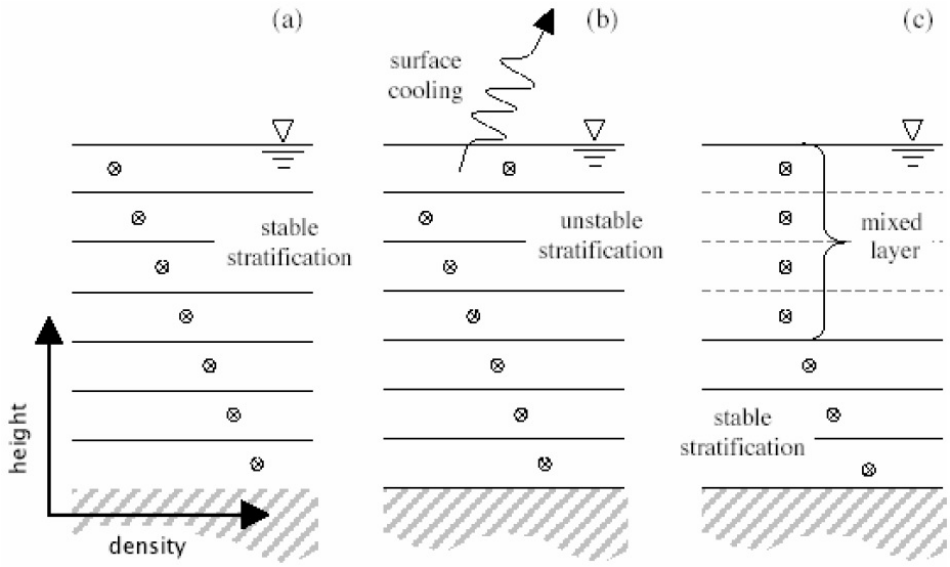

Figure 0-7: Development of a mixed layer due to surface cooling. From Hodges et al. (2000).

River inflows

River inflows are sources of nutrients, sediments and potential pollutants to lakes. The distribution pathways they will follow in the lake basin will have different impacts on the biogeochemical cycles and the ecology of the lake. The density difference between the river and the receiving lake together with the resulting mixing processes will define the intrusion pattern. An overflow will form when the river water is less dense than that of the lake. Commonly, river waters are colder and enriched in suspended matter. So, they will plunge into the lake and create a density current (i.e. underflow). Depending on dilution with the ambient water and the stratification of the lake, the river inflow can intrude the water column when it reaches the depth of neutral buoyancy and create an interflow (Figure 0-8) or follow the lake bed and possibly reach the deepest layers. Split flow can also occur when a part of the inflow intrudes in presence of a density step in the water column while the rest of the gravity current continue deeper (Cortés et al., 2015, 2014b).

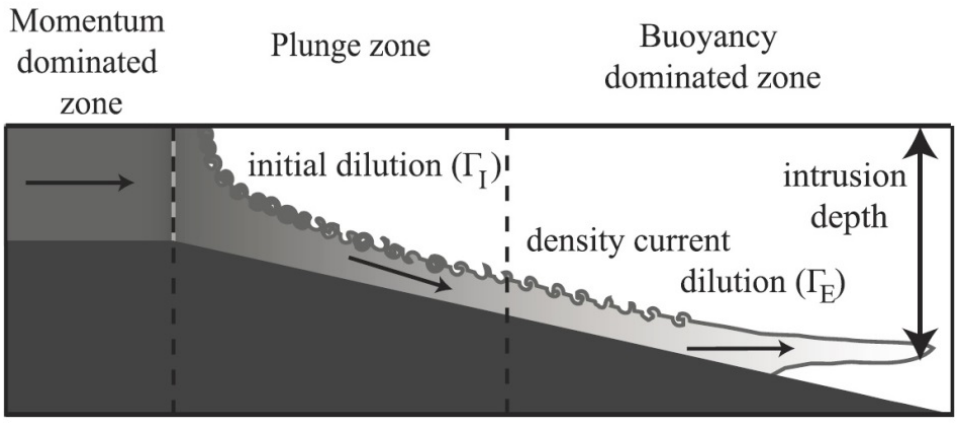

Figure 0-8: Conceptual model of a cold plunging inflow entering a stratified reservoir. From Cortés et al. (2014a).

Rueda et al. (2007) pointed out the importance of the river intrusion depth on the primary production of the lake. As illustrated in Fig. 0-9, the intrusion scenario will determine the bioavailability of the river nutrients:

1) In scenario 1, the river water intrudes in the euphotic zone, where primary production concentrates, making its nutrients directly bioavailable.
2) In scenario 2, intrusion occurs below the euphotic zone but, subsequently, it can still reach the euphotic zone either by mixing or advective processes of the lake.
3) In scenario 3, intrusion happens well below the euphotic zone so that the nutrients will not reach the upper layers until deep mixing occurs during winter period.

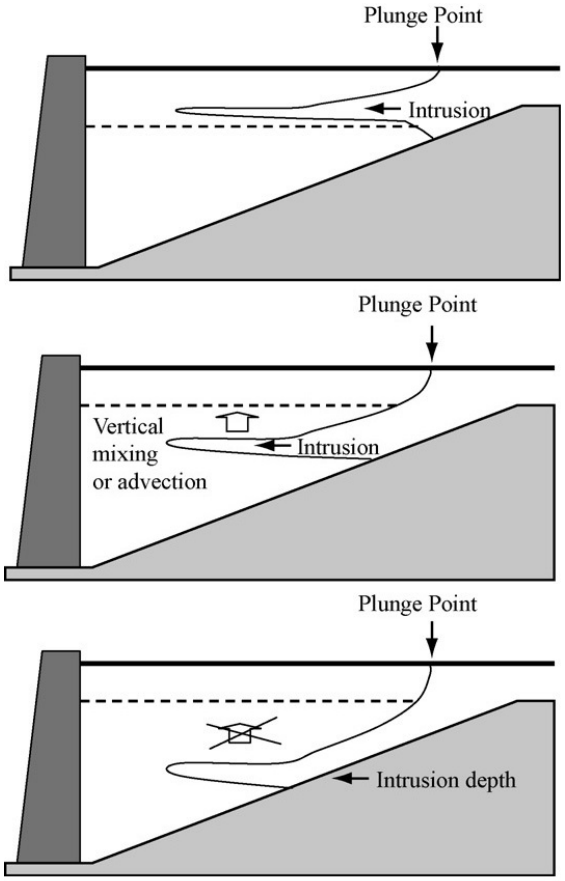

Figure 0-9: Pathways followed by a river intrusion and sources of new nutrients to the euphotic zone (limited by the dashed line). From Rueda et al. (2007).

The physics of the different river inflows has been widely studied, both in natural settings and under experimental conditions (Akiyama and Stefan, 1984; Alavian et al., 1992; Cortés et al., 2014b; Hogg, 2014; Wells and Nadarajah, 2009; Zhang et al., 2015). These studies often used different tracers to determine the transport path and the dilution rate of an inflow into a stratified reservoir. Cortés et al. (2014a), for example, demonstrated that a significant fraction of the inflow may be quickly entrained into the surface mixed layer (SML), rather than flowing to lower depths. Adding a nutrient balance, Fischer and Smith (1983) showed that about 10 % of the entering nutrients were made bioavailable to the surface water by internal wave motion. Furthermore, by coupling field experiment and numerical simulations, Marti et al. (2011) confirmed that inflow nutrients are directly bioavailable once they are intruded at the base of the SML. Instead, they intrude in deeper parts where they can then only reach the surface through a benthic boundary layer flux. Finally, Rueda et al. (2007) concluded that the biggest uncertainty on intrusion depth modelling of the interflow is the lack of our understanding of the initial

mixing within the plunge zone. As such, our capacity to estimate the impact of a river inflow on primary production is also limited.

Additionally, river underflows can be an important source of oxygen for the deep lake water. With the air temperatures rising due to climate change (IPCC, 2018), total mixing of the water column during winter turnover of deep lakes may become less frequent, hence also the re-oxygenation of their deep water. Recent studies applied climate predictions on river and lake models to determine the impact of climate change on the oxygenation of deep peri-alpine lakes by underflow (Fink et al., 2016; Råman Vinnå et al., 2018). The first one found that a change from glacial-nival regime to a nival-pluvial regime will decrease the flood frequency and, as a consequence, the occurrence of deep river underflows. The second showed that this new hydrological regime will change the seasonal variation of river SSC and so switch deep penetrating river intrusions from summer towards winter.

2.3. River mouth ecosystems

River mouths are located at the interface between lotic and lentic ecosystems. They are the results of interactions between riverine and lake inputs and the local physiographic conditions (Larson et al., 2013). These highly variable characteristics make the mixing zone dynamic and so with it, the resultant nutrient concentration gradients. These gradients are formed by a combination of conservative mixing of lake and river nutrients and processes within the river mouth that transform and retain these components. As examples of such mechanisms we can cite: i) the sedimentation and remobilization of suspended particles, ii) the incorporation of dissolved nutrients into particles via microbial growth, iii) the entrainment of dissolved nutrient and suspended particles by benthic organisms, iv) the transformation of riverine organic matter by abiotic processes such as photodegradation (Larson et al., 2016). All these processes will influence the temporal and spatial dynamic gradients in the chemical composition of the water and thus also the biogeochemical cycles of dissolved nutrients.

In general, river mouths correspond to ecosystems where a shift occurs in the main limiting factors for PP. Usually, river production is limited by light and disturbance due to current velocities and high turbidity while that of large lakes is strongly limited by nutrient concentrations. As a consequence, river mouth ecosystems provide nutrients and light and can be biologically active. This has been noted, for example, by Makarewicz et

al. (2012) and Larson et al. (2016) with Chl *a* concentrations higher in the river mouth than in the two meeting ecosystems. Thus, river mouth ecosystems can remove N and P by processing the riverine nutrients (Morrice et al., 2004; Larson et al., 2019).

A number of studies have been done in the Great Lakes of North America to evaluate the spatial influence of river plumes and the resultant nutrient loading and transformation. For example, in order to determine the link between physical-chemical conditions and phytoplankton dynamics, Schelske et al. (1980) evaluated the extent of the mixing zone at several river mouths of Lake Michigan. Morrice et al. (2004) investigated the link between hydrology and temporal dynamics of nutrients in a Lake Superior coastal wetland. They particularly noticed a shift in the limiting nutrient across the chemical gradient (from P to N). Additionally, Carlson Mazur et al. (2019) examined the influence of the hydrogeomorphic river mouth structure on mixing between the lake and the tributary. They concluded on the need of taking into account these mixing processes in a restoration perspective of these ecosystems. Finally, Jameel et al. (2018) measured the stable isotope composition of the water to determine the fraction of river water in the river mouth area and map the river plume. This approach was also used to calculate the conservative mixing proportions in comparison to the mixing proportions directly measured via nutrient concentrations as a non-conservative tracer. Seasonal differences thus allowed for estimates of the river plume dispersion patterns and associated nutrient consumption rates.

3. Study case

3.1. Rhône River

General characteristics

The Rhône River originates at the Rhône Glacier in Switzerland at an altitude of 2341 m. It flows for about 160 km through the canton of Wallis before entering Lake Geneva. The outflow of the lake becomes the French part of the Rhône River and flows over a distance of about 550 km before reaching the Mediterranean Sea. The Upper Rhône Basin is located in the southwestern part of Switzerland, in the Central Swiss Alps (Figure 0-10). It has a total surface area of 5338 km^2, and an altitudinal range of 372 to 4634 m a.s.l. (meters above sea level). The catchment is made up by 34 % of bare rock exposure, 25 % of forested terrain, 22 % of natural grassland, 9 % of glaciated surfaces or covered by perpetual snow, and 7.5 % by agricultural and urban area (Bratek et al., 2020). The hydrological regime of the catchment, typical of Alpine environments, is strongly influenced by snow and ice–melt with highest discharge in summer and lowest in winter (Figure 0-11). Mean annual discharge is 180 m^3/s.

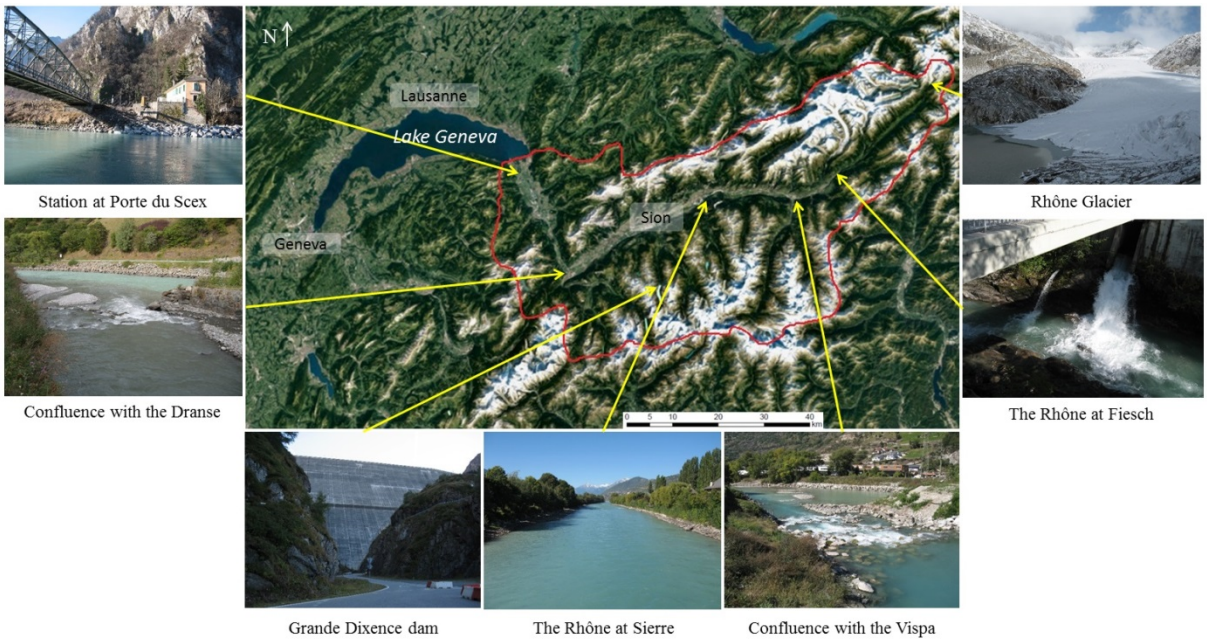

Figure 0-10: Aerial view of the Upper Rhône River catchment (limits in red).

Anthropization

The catchment has been strongly affected by anthropogenic impacts during the last century. The main course of the Rhône River has been extensively channelized for the purposes of flood protection: levees were constructed and the channel was narrowed and deepened in the periods 1863–1894 and 1930–1960 (First and Second Rhône Corrections). Due to the residual flood risk that affects the main valley, a third project was started in 2009 with the main objectives to increase the channel conveyance capacity and river ecological rehabilitation (Olivier et al., 2009). In addition, gravel mining operations are carried out along the main channel and many tributaries, eroding the base levels to the rivers in its catchment. Since the middle of the 20th century, several large hydropower dams have been built along the main tributaries of the Rhône River. The total storage capacity of these reservoirs corresponds to about 20 % of the mean annual streamflow (e.g., Loizeau and Dominik, 2000). The amount of SSC transported by the Rhône River to Lake Geneva first decreased from the 1950's with construction of dams (Loizeau and Dominik, 2000), then increased from the 1980's due to an increase of ice-melt driven by climate change (e.g., Costa et al., 2017).

Nutrient dynamics

The Upper Rhône River is considered as the main source of nutrients to Lake Geneva. A recent study evaluates that the Rhône brings 92 % of the total phosphorus (TP) and 76 % of the orthophosphate (i.e. soluble reactive phosphorus, SRP) to the lake (Sabaratnam, 2019). Since the 1970's, the SRP delivered by the Rhône decreased after measures have been taken such as treatment of phosphorus in the sewage stations of the catchment area and prohibition of phosphated detergents. It was also estimated that at least a quarter of the 43 t ($P\text{-}PO_4^{3-}$) exported per year by the Rhône comes from point sources and mainly from WWTP. It seems still possible to decrease this amount of SRP flux to the lake by improving the water treatment efficiency. Burrus et al. (1990) identified another significant source of bioavailable phosphorus coming from the spring and summer erosion of the agricultural lands of the Upper Rhone valley. This is illustrated in Fig. 0-11 with a steady low concentration of orthophosphate from late spring to early fall (close to the limit of detection) but with a significant mass flow due to the important discharge of this period.

Concerning the total mineral nitrogen input, after an increase during the 1960's the N-input has been stabilised at around 3500 tN/year for the last 40 years (Sabaratnam and Oriez, 2019). This is mainly due to unchanged agricultural practices, particularly regarding the nitrogen inputs as fertilizers. As shown in Fig. 0-11, the nitrate concentrations are low during summer because of the dilution effect but the mass flow is dominating. The silica follows the same pattern as the nitrate with the mass flow curve perfectly matching that of the discharge. Silica comes from the erosion of the crystalline rocks present in the Upper Rhône catchment.

The stable isotope composition of dissolved inorganic carbon (DIC) gives an indication on the origin of the mineral and organic carbon in the water and the biogeochemical processes that transformed the carbon into DIC. A study of Aucour et al. (1999) has examined the stable isotope composition of DIC of the Rhône River system in summer and winter and found $\delta^{13}C$ values of between –6.6 to –4.1 ‰ (n=5). Results of Favre and Piffarerio (2006) and Fontana (2008) show similar $\delta^{13}C$ values of between –6.2 to –4.9 ‰ and DIC concentrations from 40 to 70 mg/L (n=6) during different seasons. The concentrations and these relatively high $\delta^{13}C$ values for DIC are characteristic for headwaters with dominantly crystalline rocks but that also include carbonate rocks, and show a minor input of respired CO_2 (Horgby et al., 2019a, 2019b).

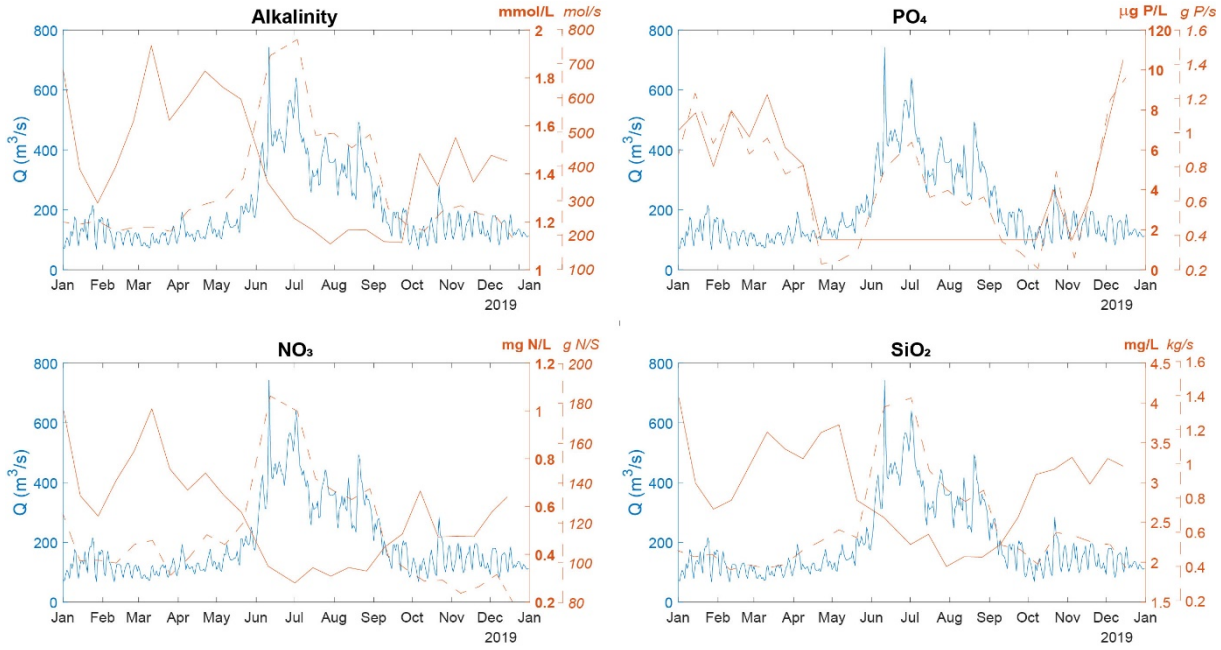

Figure 0-11: Rhône River nutrient concentration (orange solid line) and mass flow (orange dashed line). Data from OFEV/NADUF from the hydrological station of Porte du Scex located on the Rhône River 5 km upstream from its river mouth into Lake Geneva. The nutrient data are average values measured on water samples that are collected over the month proportional to the discharge. The discharge is measured continuously but the daily average discharge is presented for the year 2019 (blue line).

3.2. Lake Geneva (*Le Léman*)

General characteristics

Lake Geneva is the largest freshwater lake in Western Europe with a volume of 89 km^3, a surface area of 580 km^2 and a maximum depth of 309 m. It is a monomictic lake located between France and Switzerland at 372 m.a.s.l. It is surrounded by the Alps in the south and southeast and by the Jura Mountains in the northwest. The lake is divided into two morphologically different basins: the "Petit Lac" (small lake) and "Grand Lac" (large lake) (Figure 0-12). The "Grand Lac" is made up of: i) the "Haut Lac" in the eastern part of the basin close to the Rhône River mouth, ii) a large central abyssal plain and, iii) a progressive slope from the deepest layers of the "Grand Lac" into the "Petit Lac". The smaller basin is 76 meters deep at its maximum and extends to Geneva in the western part, where the Rhône exits the lake, 72 km from its inlet. The theoretical residence time of the lake, calculated by the ratio of its volume and the average total influx of water, is approximately 11.3 years (CIPEL, 2020). The Rhône River accounts for about 70-80 % of the input, the Dranse River from the French pre-Alps for about 5-7 %, the rivers from Jura side for about 9-11 %, the direct precipitation for 5-8 % and an unknown minor input of groundwater. In contrast to the "Petit Lac", the "Grand Lac" does not overturn every winter. With the current warming climate (IPCC, 2018), the total overturn of its water column is expected to happen less frequently (Schwefel et al., 2016). Otherwise, the lake is usually thermally stratified from spring to fall.

The water quality of Lake Geneva has been monitored since 1957 by the Commission Internationale pour la Protection des Eaux du Léman (CIPEL, 2020). One monitoring station SHL2 in the "Grand Lac" is monitored by the CIPEL, the other GE3 in the "Petit Lac" by the Canton of Geneva (Figure 0-12).

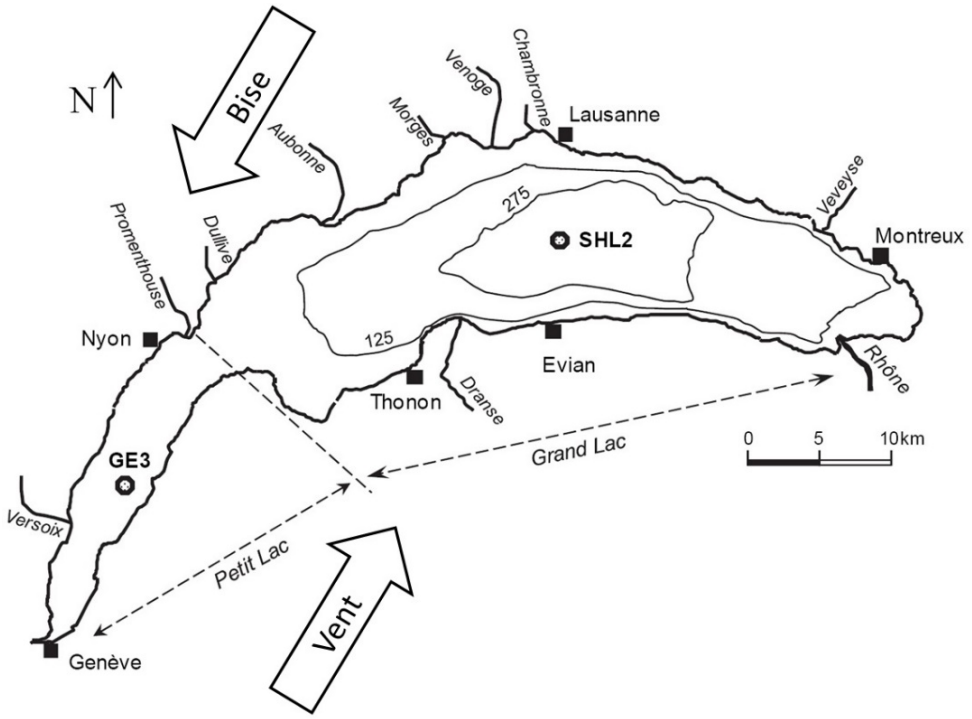

Figure 0-12: Map of Lake Geneva (Le Léman) and its main tributaries. The two dominant wind directions are indicated by arrows. From CIPEL (2020).

Hydrodynamics

Water circulation in Lake Geneva is mainly forced by wind. The strongest winds are the "Bise" from the northeast and the "Vent" from the southwest (Figure 0-12). They are both related to the passage of large-scale atmospheric pressure cells and are stronger and more frequent during winter. In summer, more frequent are land-lake breezes, thermally induced winds. These winds are generated at the basin scale and blow perpendicular to the shoreline (Lemmin and D'Adamo, 1996). The spatial variability of wind above the lake is mainly determined by topography with the eastern part being more sheltered by the Alps. The lake width is approximatively five times the internal Rossby radius (Bohle-Carbonell, 1986; Lemmin et al., 2005). Thus, basin-scale circulations of the lake are influenced by Coriolis force. Depending on these different factors, surface currents can create cyclonic and anticyclonic circulations called gyres. Lemmin and D'Adamo (1996) asserted that the coupled effect of the diurnal winds, the topography and the Earth's rotation generate a persistent cyclonic (anti-clockwise) gyre in the central part of the lake during summer. Hydrodynamic modelling of the lake's currents has been investigated with Delft3D-Flow models. The details regarding model set up, calibration and validation are provided in Razmi et al. (2013, 2014). Patterns corresponding to the two dominant wind regimes, Bise and Vent, were considered (Razmi et al., 2018). For the Bise, a basin-

wide cyclonic circulation occurs in the central and eastern part of the Grand Lac while an anticyclonic gyre forms in the western part of Grand Lac (Figure 0-13.a). With the Vent, the modelled current pattern changes with an anticyclonic gyre in the central Grand Lac and a cyclonic one in the eastern less exposed part (Figure 0-13.b). However, the anticyclonic gyre in the western part of the Grand Lac is still detected. This persistent gyre was previously observed by fishermen and described by Kreitmann (1931). Usually, these gyres are highly variable in space and time, but may last several days before breaking down into smaller gyres as a function of the dominant wind speeds and directions. In contrast to the Grand Lac, currents in the Petit Lac are predominantly westward and show less variability (Le Thi et al., 2012). Moreover, appendices of the main gyres are found in major embayments of the northern shore, in the Bays of Morges and Vidy (Razmi et al., 2017).

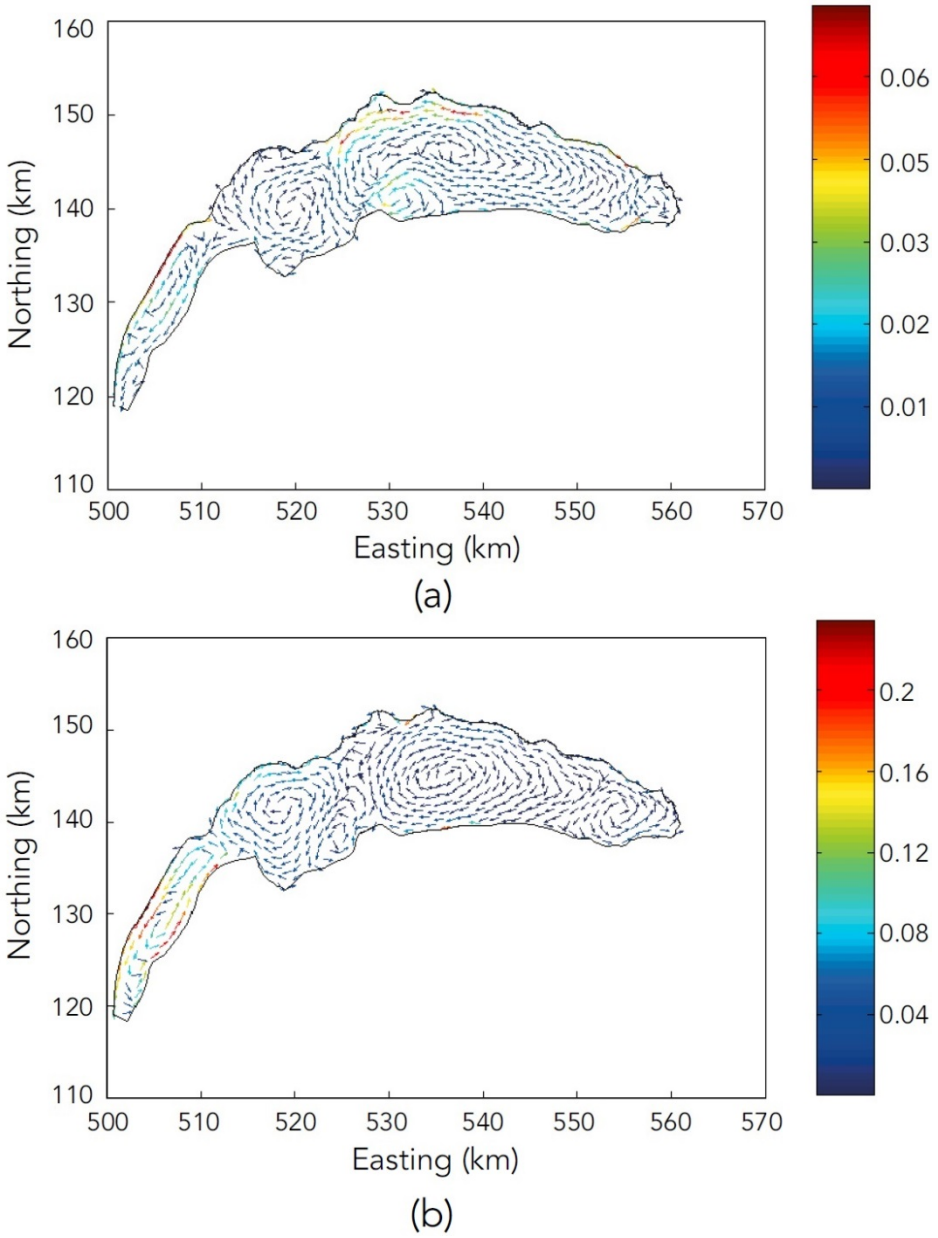

Figure 0-13: Depth-averaged, steady-state velocity vector maps in Lake Geneva. (a) "Bise" pattern (b) "Vent" pattern. The color bars show the intensity of the velocity vectors in the plot (m/s). From Razmi et al. (2018).

Lake Geneva can also react to wind stress with tilting of the thermocline that can create basin-wide internal waves when the wind stops. These internal seiches can last several days (Lemmin et al., 2005) and give rise to anticlockwise rotating Kelvin waves that contribute to vertical mixing within the lake (Bouffard and Lemmin, 2013).

Annual nutrient cycles

The cycle of the main nutrients (C, P, N, and Si) between their organic and inorganic forms is regulated by biological activity (production/consumption/decomposition). The

transformation from and to their inorganic forms is controlled by biochemical processes and the transport of organic and inorganic forms is controlled by physical processes. Altogether, it designs the biogeochemical cycle of the lake.

At the beginning of spring, if a complete overturn occurred, the nutrient distribution is homogeneous within the water column. With the ambient air temperature rising, the surface water warms up and primary production increases. Hence, the nutrient concentrations start to decrease while the oxygen concentration increases in the first meters beneath the surface. Once a thermal stratification is established, the water column is separated into physically and chemically distinct layers: a warmer epilimnion depleted in nutrients and a colder hypolimnion with relatively homogenous concentrations of the remineralized nutrients. Then, the euphotic zone corresponding to the light-abundant surface layers receiving more than 1 % of the incident light is separated from the nutrient-richer deeper layers. As illustrated in Fig. 0-14, during a year, phytoplankton communities are progressively descending to find the orthophosphate enriched layers. The nutrient depletion can thus extend down to 35-50 m depth.

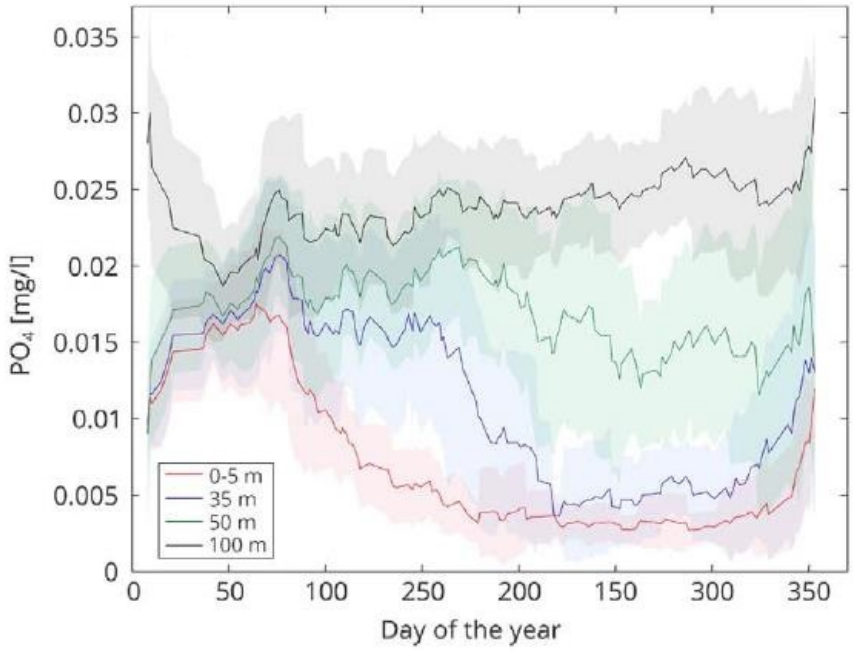

Figure 0-14: Average annual cycle of phosphate concentrations at different depths for 2002 to 2010. From Bouffard et al. (2018).

The predation of primary producers by zooplankton (i.e. grazing) peaks during the clear water phase and leads to a temporal increase of the transparency and the nutrient concentrations in the euphotic zone. It occurs usually during the month of June/July

before another primary production wave starts. In parallel, the dead organic matter settles down to the hypolimnion where it is decomposed by the bacterially induced remineralization/respiration loop that consumes the available dissolved oxygen. Hypoxia of the bottom water column can thus be induced by intense decomposition related to a high surface bioproductivity and further aggravated by a non-complete overturn during the last winter. This oxygen depletion triggers reduction of ferric iron to ferrous iron and the subsequent release of associated P. This mobilization of sedimentary P is considered as the internal phosphorus loading whereas the external loading comes from the catchment runoff. During winter, with cold temperatures and strong winds, a complete overturn of the water column can happen, and this may bring nutrients up to the surface and recharge the oxygen concentration in the deeper water column.

Eutrophication and re-oligotrophication

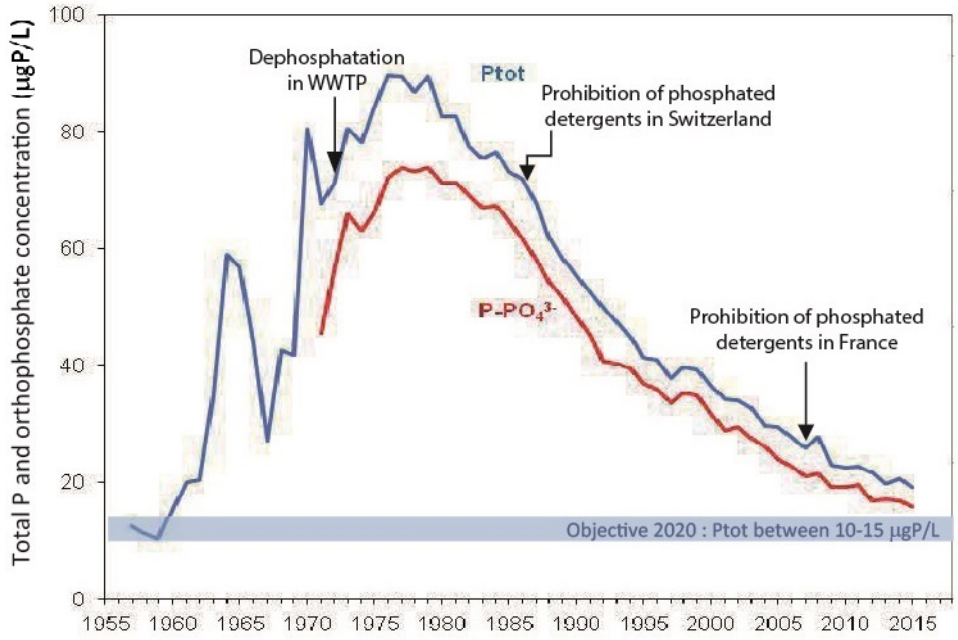

Figure 0-15: Total phosphorus and orthophosphate mean annual weighted concentrations in Lake Geneva since 1957. From CIPEL (2015).

As many lakes, *Le Léman* has faced cultural eutrophication, leading to a deterioration of its water quality during the second half of 20th century. Total P concentrations increased from 12.4 µgP/L in 1957 to 89.5 µgP/L in 1979 (Figure 0-15). As a consequence, the frequency of algal blooms, especially during summer, increased (Anneville et al., 2002) and the mean annual water transparency decreased from 10.8 m in 1957 to 7.3 m in 1979 (CIPEL, 2020). The O_2 concentrations reached critically low

levels in the deep water and were on average inferior to 3 mg/L until 2000, which barely support aerobic metabolisms. This affected all the trophic levels in the pelagic zone. From zooplankton, with eutrophic waters species like cyclopoids that dominated the community during the 1980's (Anneville et al., 2007), to fish, with the proportion of whitefish and arctic char that strongly decreased because of the lack of oxygen in the deep waters (Gerdeaux, 2004).

In order to limit the deterioration of the water quality, the CIPEL implemented phosphorus reduction policies in 1972. Additional WWTP were built and dephosphatation processes were set up. Moreover, phosphate-based detergents were progressively forbidden (Figure 0-15). These first efforts of P reduction were initially successful. Total P concentrations decreased to 16 µgP/L in 2019 (CIPEL, 2020) but still remained above the target (natural background) concentration for 2020 of 10-15 µgP/L. Since 1995, the phosphorus has been identified as limiting factor of primary production while the secondary role of silica has been recognized by influencing the phytoplankton succession (replacement of diatoms by non-siliceous species). However, nitrogen is not a main factor influencing phytoplankton growth. The concentration of nitrates increased since the 1980's (Moisset, 2017).

Nevertheless, from a biological perspective, the phytoplankton biomass remained stable (Figure 0-16) and the primary productivity even increased after the phosphorus reduction measures implemented in the 1970's (Tadonleke et al., 2009).

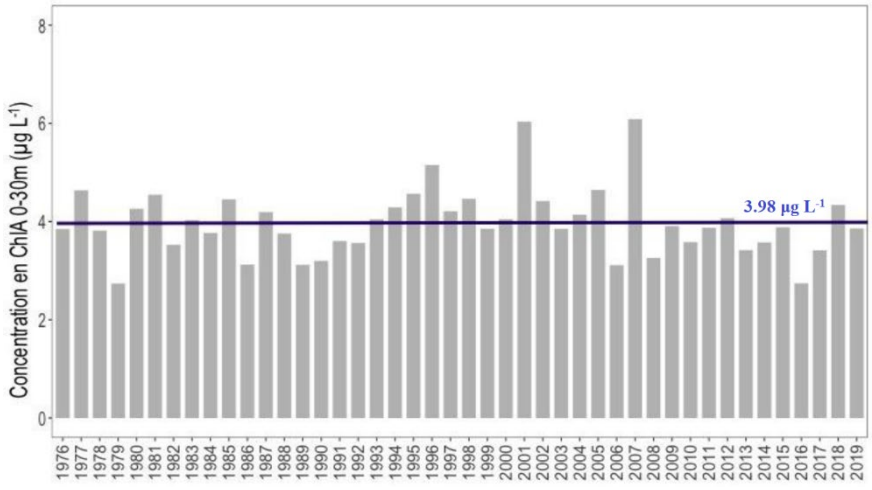

Figure 0-16: Long-term dynamic of Chl *a* concentrations in Lake Geneva (SHL2). Values are the average of the concentrations measured at every depth weighted for the layer thickness from February to November. The line indicates the average value on the entire period. From CIPEL (2020).

Indeed, the phytoplankton community evolved and adapted to this decrease of phosphorus loading as shown by the increase of the C:P ratio of the seston (Müller et al., 2019). The P depletion in the surface layers has also induced a displacement of the phytoplankton to deeper, P-enriched layers, up to 30 m, with species adapted to low light levels (Moisset, 2017). Moreover, Anneville et al. (2019) highlighted what they called the paradox of re-oligotrophication. They demonstrated that the combined effect of climate change and phosphorus reduction improved the recovery of whitefish (Anneville et al., 2017). Thus, the increased whitefish abundance resulted in higher predation on *Daphnia* (Nõges et al., 2017) and so, in a decrease of its abundance and its control on phytoplankton. Finally, as illustrated by Figure 0-17, Lake Geneva seems to be at a turning point. It has followed a horizontal trend without significant reduction of the hypolimnetic mineralization rate during last decades. It is now close to the areal P supply of 0.54 gP/m^2 identified as the threshold to trigger a decrease of oxygen consumption in the deep layers (Müller et al., 2019). Furthermore, as phosphorus was clearly identified as the most limiting nutrient in Lake Geneva today and as phosphorus concentrations are currently decreasing, it can be expected that the phytoplankton community resilience will soon be overcome, as observed in many studies (Jeppesen et al., 2005).

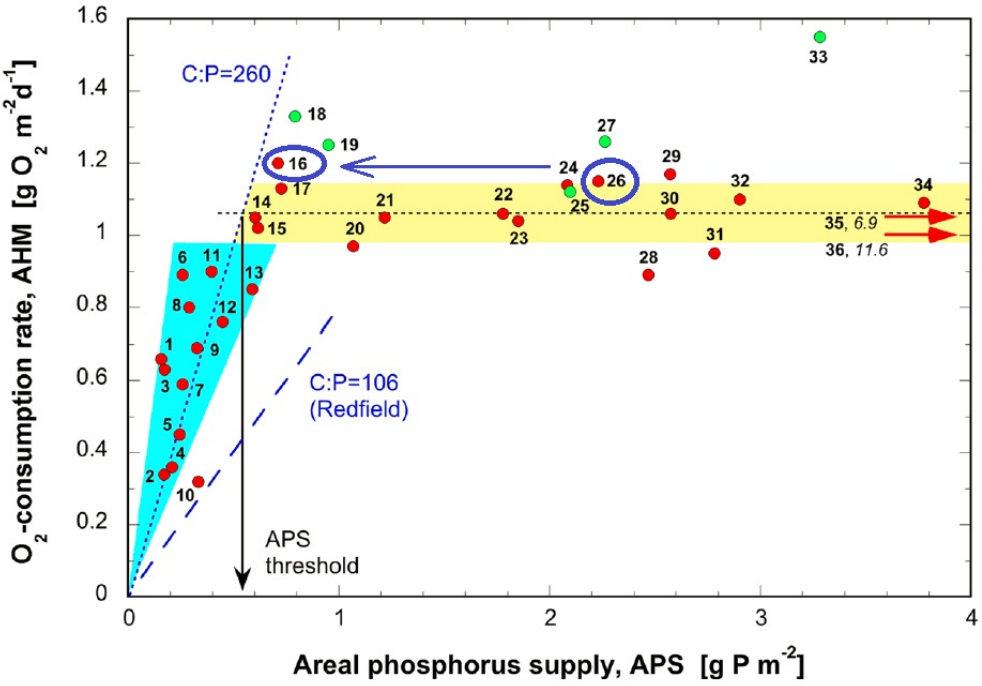

Figure 0-17: Covariation of areal hypolimnetic mineralization rate (AHM) with areal phosphorus supply per productive season (APS). Dots number 16 and 26 represent Lake Geneva during periods 2000-2010 and 1975-1985 respectively. From Müller et al. (2019).

3.3. Rhône River in Lake Geneva

The Rhône River is the main tributary to Lake Geneva as well as its main source of sediments (Kremer et al., 2015; Loizeau and Dominik, 2000), and dissolved nutrients (Sabaratnam and Oriez, 2019). As such, the Rhône plays a major role in the biogeochemical cycle of the lake. For example, Nouchi et al. (2019) demonstrated that the intrusion of the Rhône's fine particles is able to trigger whiting events (i.e. massive calcium carbonate precipitation) and showed that just one of this event can remove a quarter of the annual Ca deposit of the lake. Additionally, Bouffard and Perga (2016) discovered that the mixing of the Rhône's and the lake's organic matter can intensify the hypolimnetic respiration. This priming effect contradicts the expected oxygenation effect of the bottom water column by flood-driven turbidity currents. Moreover, some studies indicated that the Rhône River can be an important source of micropollutants to the lake (Bonvin et al., 2011; Halder et al., 2016). It is hence essential to understand the dispersion of the Rhône River within the basin and its impact on the ecology of the entire lake.

The first observation of the Rhône intrusion in *Le Léman* dates back to the 19th century by F.A. Forel (1885), who discovered underwater canyons created by gravity currents. Gorceix and Kreitmann (1930) subsequently established that the Rhône River is interflowing into the metalimnion during summer, on the basis of temperature and conductivity measurements at the location called *La Bataillère,* where the waters meet. Subsequently, several studies focussed on the Rhône's sediment dispersion using different approaches (Corella et al., 2013; Kremer et al., 2015; Lambert and Giovanoli, 1988). For example, Giovanoli (1990) determined via an ultrasonic current meter and turbidity measurements that ''interflow water masses are dissipated by horizontal spreading and entrainment of lake waters". He also determined that ''the transport path of interflows is controlled not only by density stratification and horizontal density differences but also by Coriolis force and internal currents". Loizeau (1991) confirmed the coexistence of underflows and interflows and the different sedimentation patterns associated with these flows (Figure 0-18):

1) The proximal sedimentation creates a foreset;
2) The erosion and transport processes by underflows create a canyon and a fan;
3) The transport of fine particles by interflows is deflected towards the north by Coriolis force.

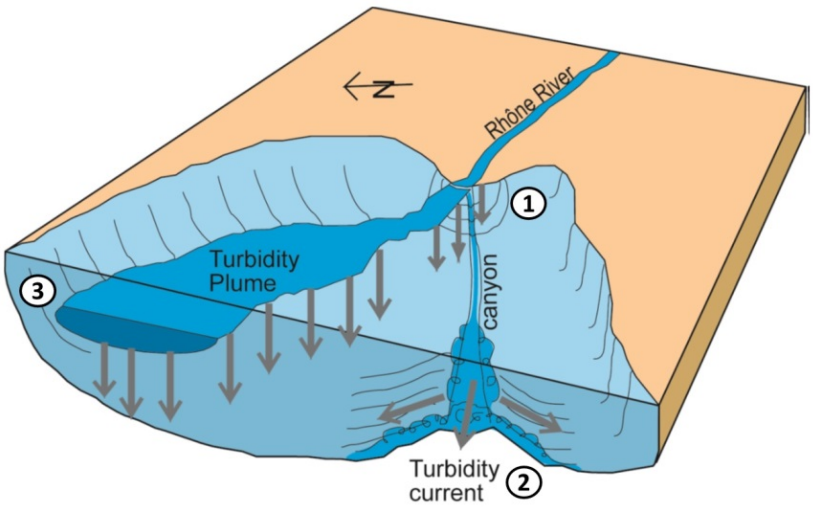

Figure 0-18: Model of the Rhône delta with the 3 sedimentation processes.
From Giovanoli (1990), modified by Loizeau (1991).

The sub-aquatic Rhône delta is a dynamic area as shown by the presence of eight paleocanyons. These meandering channels relate to the recent history of the Rhône River mouth (Sastre et al., 2010). Before the first Rhône corrections, the river mouth was composed of multiple channels entering the lake. But, since the end of the 19th century, a unique river branch brings the Rhône water to the lake (front cover picture). There is so, no more receiving basin as described by Larson et al. (2013) where riverine inputs can be deposited and metabolized. However, a project of ecological restoration aims to recover the Rhône lacustrine delta ("Un delta lacustre pour la biodiversité de l'embouchure du Rhône", Le Temps, 2017).

Concerning the Rhône water dispersion, Balvay and Ishiguro (2003) observed a Rhône interflow, using CTD profiles, at the thermocline depth being deflected around the north shore by the Coriolis force and able to reach the central part of the lake. Later, Halder et al. (2013) were able to detect with improved accuracy the interflow much further from the river mouth of the Rhône. By measuring the stable hydrogen and oxygen isotope composition of the water, they inferred the fraction of Rhône water within the interflow during summer stratification and determined an upper limit of 5 months for the travel time of the Rhône water to the Petit Lac (50 km away from the river mouth). More recently, Cimatoribus et al. (2019) presented a Lagrangian motion tracking of simulated Rhône particles using a 3D numerical model. Even though the results showed a large spatiotemporal variability of transport, they could detect preferential circulation patterns with relatively well-defined rapid transit paths (scale of several days) along the near-shore region for the upper layers of the water column and much slower particle transports

(transport rates on the scale of months) for the deeper and more central regions of the lake. The longer residence times of the water particles in the deeper parts are also related to the insulating thermal effects of the stratification and reduction of shear stress with resulting slower currents at greater depth (Michalski and Lemmin, 1995). They finally concluded on the need of experimental verification of their predictions.

4. Stable isotopes as tracers of water

The measurement of the stable isotope composition is a method widely applied to trace the elements and compounds containing the isotopes in natural settings to better understand the biogeochemical cycle. In hydrology, the hydrogen and oxygen stable isotope compositions have been widely used to determine the origin of water, its fluxes within the water cycle and the mixing processes of different water sources (e.g., McGuire and McDonnell, 2015).

4.1. Isotope definitions

Isotopes are atoms of the same element that have the same numbers of protons and electrons but different numbers of neutrons. Therefore, the various isotopes of any one element may have similar chemical behaviour (charge, bond-types in compounds, etc.) but different masses (Hoefs, 2009). The different stable isotopes of water and their natural abundances are presented in Table 0-3. Because of their mass differences, the various isotopes of an element have slightly different physico-chemical properties. For many physical, chemical, and biological processes or reactions those differences are large enough to "fractionate" or change the relative proportions of various isotopes in different molecules containing the isotopes of the element of interest. During any kind of reaction, the different molecules containing the isotopes of interest will hence compete for the different isotopes. Depending on their molecular structure and bonding characteristics, they will hence have different isotopic abundances. Fractionation is expressed by the fractionation factor α, which is the ratio of the isotope ratios for the reactant and product:

$$\alpha = \frac{R_{\text{reactant}}}{R_{\text{product}}} \qquad (1)$$

where R is the ratio of the heavy compared to the light isotope of the same element.

Table 0-3: Stable isotopes of water. From Clark and Fritz (1997)

Stable isotope	Natural abondance (%)
Oxygen	
^{16}O	99.762
^{17}O	0.038
^{18}O	0.204
Hydrogen	
^{1}H (H)	99.984
^{2}H (D)	0.015

Isotope fractionation is dependent on the temperature of the reaction and can be caused by physicochemical reactions under equilibrium conditions or non-equilibrium (kinetic) conditions, as well as by molecular diffusion (Hoefs, 2009). Equilibrium fractionation also requires a chemical equilibrium and that the reactants, as well as the products, are well mixed in the system. In this case, fractionation factors can be determined at different temperatures through experimentation or estimated by thermodynamic model calculations. In general, light isotopes are more mobile and diffuse faster compared to heavy isotopes. This is also true for the molecules containing the lighter or, respectively, the heavier isotopes. Fractionation related to diffusion is kinetic with atoms or molecules diffusing across a concentration gradient. During kinetic fractionation, the system can be far from the thermodynamic equilibrium. In this case a forward reaction can be faster, for example, compared to a slower reverse reaction. Only if the forward and reverse reactions have the same rate, an equilibrium can be achieved.

Stable isotopic compositions of low-mass elements, such as oxygen, hydrogen and carbon, are reported as "delta" values (δ) in parts per thousand (denoted as ‰) enrichments or depletions, relative to a standard of known isotopic composition:

$$\delta = \frac{R_{\text{sample}} - R_{\text{reference}}}{R_{\text{reference}}} * 1000 \qquad (2)$$

The compositions of each of the standards are hence defined to be 0 ‰. Stable oxygen and hydrogen isotopic ratios are usually reported relative to the VSMOW standard (Vienna-Standard Mean Ocean Water (Coplen, 1996). Carbon stable isotope ratios are reported relative to the VPDB (Vienna Pee Dee Belemnite) standard.

4.2. Stable isotope compositions in the water cycle

Evaporation is the primary transfer of liquid water into the atmospheric water vapor. The oceans, seas, lakes, and rivers provide nearly 90 percent of the moisture in the atmosphere via evaporation, with the remaining 10 percent being contributed by plant transpiration (e.g., Clark and Fritz, 1997; Sharp, 2007). To evaporate, a water molecule must break its hydrogen bonds with the surrounding liquid water molecules. The process is driven by the vapor pressure of water. The difference in the vapor pressures of the $H_2{}^{18}O$ and DHO isotopologues of water (isotopologue refers to the same molecule differing only in the isotopic constitution) relative to the more abundant lighter molecule $H_2{}^{16}O$ imparts disproportional enrichments of the lighter molecules into the vapour phase of water during evaporation. For example, under equilibrium conditions at 25 °C, the fractionation factors for evaporating water ($\alpha_{liquid\text{-}vapor}$) are 1.0093 for $^{18}O/^{16}O$ and 1.074 for D/H (Craig and Gordon, 1965):

$$\alpha^{18}O_{water-vapor} = \frac{(^{18}O/^{16}O)_{water}}{(^{18}O/^{16}O)_{vapor}} = \frac{1000+\delta^{18}O_{water}}{1000+\delta^{18}O_{vapor}} = 1.0093 \qquad (3)$$

$$\alpha D_{water-vapor} = \frac{(D/H)_{water}}{(D/H)_{vapor}} = \frac{1000+\delta D_{water}}{1000+\delta D_{vapor}} = 1.074 \qquad (4)$$

However, the water vapor above the oceans is not in isotopic equilibrium with the liquid water in the oceans. As a function of the relative humidity, evaporation will be driven by kinetic processes, the $^{18}O/^{16}O$ and D/H fractionation being in fact larger than at equilibrium. The extent of fractionation is influenced by the surface temperature, wind speed, salinity, i.e. all of which control the relative humidity of the air mass above the liquid surface. Moreover, the kinetic fractionation of $H_2{}^{18}O$ relative to $H_2{}^{16}O$ exceeds that of DHO relative to $HH^{16}O$, because the difference in mass between the two hydrogen isotopologues is smaller than the corresponding difference in mass of the oxygen isotopologues (Clark and Fritz, 1997).

According to the standard VSMOW, the oceans have a $\delta^{18}O$ of 0 ‰, whereas the water vapor over the oceans has a negative $\delta^{18}O$ value (Figure 0-19). The flux of moisture from the oceans and its return via rainout and runoff is, on an annual basis and global

scale, close to a dynamic equilibrium. Craig (1961) found that the $\delta^{18}O$ and δD values of meteoric waters correlate on a global scale. This linear correlation is known as the global meteoric water line (GMWL) or the local meteoric water line (LMWL). The correlation of $\delta^{18}O$ and δD values in meteoric waters is defined as follows:

$$\delta D = 8 * \delta^{18}O + 10 \text{ ‰} \qquad (5)$$

Only about 10 percent of the water evaporated from the oceans is transported over land and precipitates. As vapour leaving the surface of the ocean cools sufficiently it may condensate if the dew point is reached. That is the temperature at which humidity is 100 %. As an air mass follows a trajectory from its vapour source area to higher latitudes and over continents, it cools and loses its water vapour as precipitation, a process called "rainout" (e.g., Clark and Fritz, 1997; Hoefs, 2009). During removal of rain from a moist air mass, the residual vapor is continuously depleted in the heavy isotopes, because the rain leaving the system is enriched in ^{18}O and D (Figure 0-19).

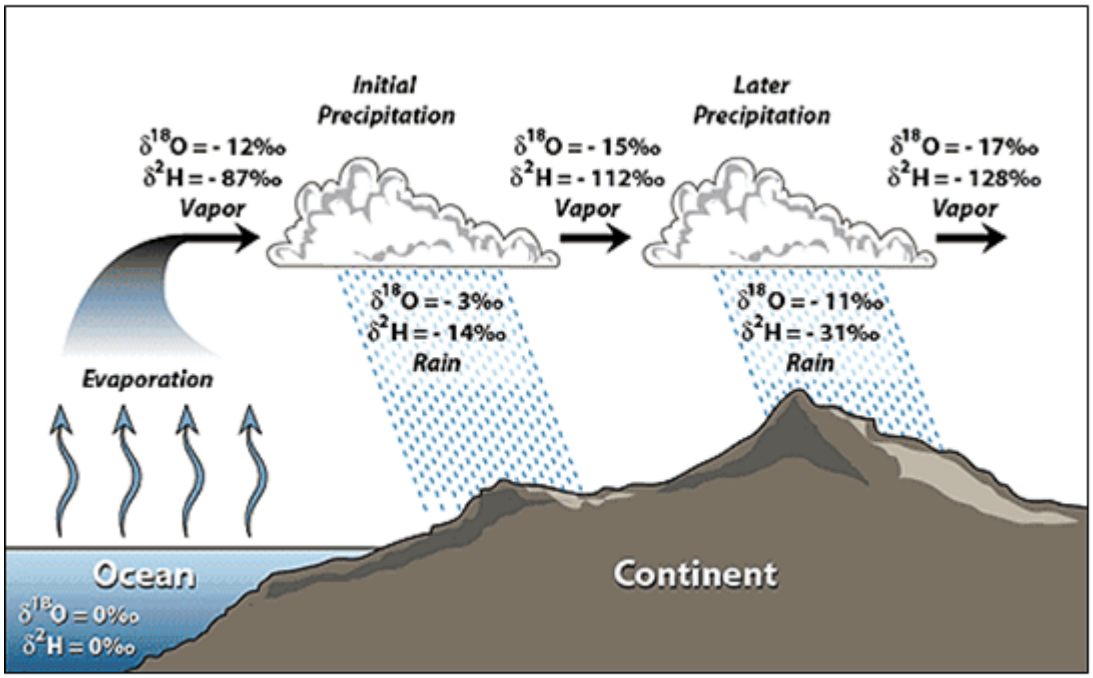

Figure 0-19: Evaporation and rainout effect on $\delta^{18}O$ and $\delta^{2}H$ values. Based on Coplen et al. (2000) and Hoefs (2009)

Therefore, the dominant control on the isotopic composition of precipitation from a given air mass is the fractionation between vapor remaining in that air mass and the liquid or ice lost as precipitation. This fractionation is similar to a distillation process and hence

often referred to as Rayleigh distillation. However, temperature also has a control on the isotopic compositions of local meteoric water, though mainly in the sense that it controls the amount of water that an air mass can hold and/or that it loses during the rain-out. While the fractionation between water vapour and the condensate increases with decreasing temperature (Sharp, 2007), this fractionating effect is small relative to the increased rainout at lower temperatures, hence the stable isotopic composition of meteoric water is more depleted at higher latitudes (latitude effect). The gross magnitude of the latitude effect in mid-latitude regions is about –0.5 ‰ per degree of latitude (Sharp, 2007). If a vapor mass moves from its oceanic source region across a continent, its isotopic composition evolves further due to topographic effects and the temperature extremes that characterize continental climates (Clark and Fritz, 1997). In Eurasia, $\delta^{18}O$ values of meteoric water decrease very regularly with distance eastward, about –3 ‰/1000 km in winter and about –1.5 ‰/1000 km in summer (Sharp, 2007). As the amplitude of seasonal variations in temperature is higher at continental sites, the variability in the isotopic composition of precipitation as a function of season is also affected.

In any region with minor relief, precipitation will occur as the air mass rises over the landscape due to thermal updrafts and the water vapour within the air mass cools adiabatically. The isotopic composition of water becomes lighter with increasing altitude, again because it is colder at higher elevations and the air masses have lost more water upon rising as they can hold less water vapour when they are cooled (altitude effect). For ^{18}O, the depletion varies between –0.15 and –0.5 ‰ per 100 m rise in altitude, with a corresponding decrease of about –1 to –4 ‰ for D (Clark and Fritz, 1997).

4.3. Stable isotope composition of water in the watershed of Lake Geneva

In Switzerland, the Swiss National Network for the Observation of Isotopes in the Water Cycle (NISOT) is monitoring since 1992 monthly tritium, D/H and $^{18}O/^{16}O$ in precipitation, surface water (rivers) and groundwater (Schürch et al., 2003). In the watershed of Lake Geneva, three stations of this network are collecting rain samples: two are located in the Upper Rhône River catchment, in Visp and Sion, and one in Nyon, at the shore of Lake Geneva (cf. locations on Figures 0-10 and 0-12). All the precipitation stations display a seasonal pattern with higher $\delta^{18}O$ values in summer and lower in winter due to a stronger fractionation between liquid and vapor of water at lower temperatures. As precipitation derives mostly from the Atlantic Ocean towards the southwest and west,

it is transported towards the interior while experiencing the continentality effect. In addition, both the Jura mountains as well as the Alps may promote an altitude effect to the precipitation and as such the $\delta^{18}O$ values for average precipitation in the Valais are lower than in Nyon. Moreover, the analysis of long-time data series has shown that the increase in mean annual air temperatures during the last decades is reflected in a slight increase in $\delta^{18}O$ values at all precipitation stations (Schotterer, 2010).

Samples from the Rhône River have been collected by the same network since the 80's at the hydrological station of Porte du Scex located 5 km upstream from Lake Geneva (cf. location on Figure 0-10). The seasonal variation in the amount of water carried by the Rhône as well as its isotopic composition are dependent on the seasonal amounts and distribution of rain and snowfall, the amount of snow and glacier melt water, as well as on the reservoir managements for hydroelectric power generation in its watershed. In fact, in contrast to the local precipitation, the river water has lower ^{18}O concentrations during the summer months compared to the winter months, which is related to larger direct contributions of higher altitude glacial melt water during summer (Halder et al., 2013). As the stable isotope composition of the precipitations is showing a trend to higher values, the $\delta^{18}O$ values of the Rhône River was also increasing from 1983 to 2009 (Schotterer, 2010). However, during the last decade, it decreased from 2012 to 2015 but increased again until 2020 (Figure 0-20). These fluctuations may be related to the melting rate variations of the glaciers.

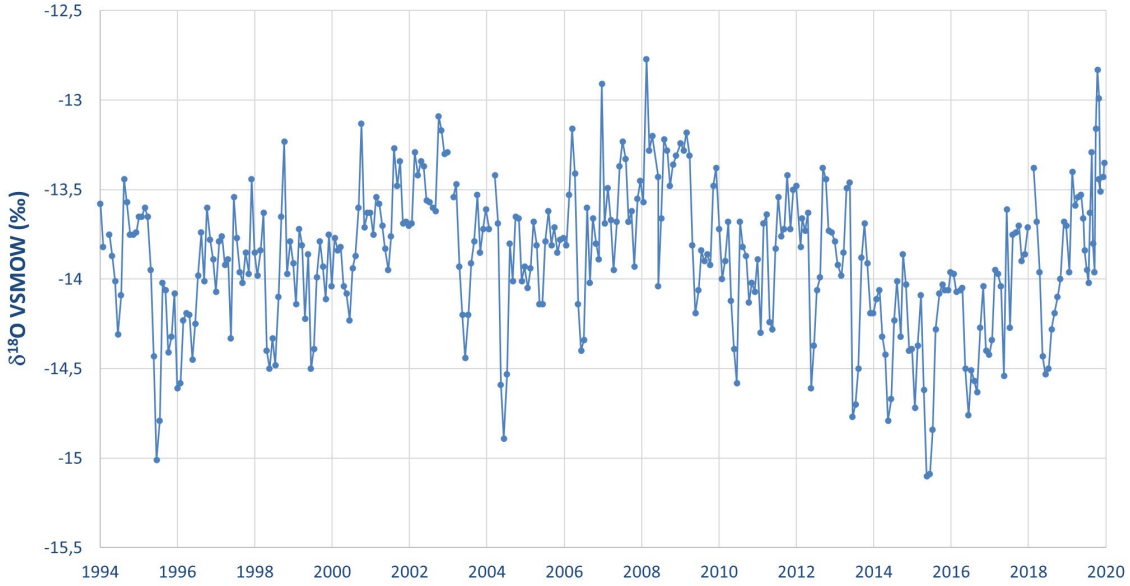

Figure 0-20: $\delta^{18}O$ fluctuations of the Rhône River at Porte du Scex (cf. Figure 0-10 for location) during the last three decades (data from OFEV/NADUF)

The stable isotope composition of the different water sources to Lake Geneva plot on the LMWL in Fig. 0-21. Halder et al. (2013) measured average values of –12.3 ‰ for $\delta^{18}O$ for homogeneous winter lake profiles. These reference values were measured after a complete winter overturn that mixed the different water inputs to the lake. On the LMWL, this values plots in between those of the Rhône River and the Jura Rivers, reflecting the mixture of these two dominant sources to the lake. The isotope composition of the lake is, at any time, distinct from its tributaries. Therefore, it is possible to trace their mixing within the lake and especially, the newly established Rhône interflow during spring and summer, particularly after a complete winter mixing. Finally, it is interesting to note that the reference value slightly changed since the study of Halder et al. (2013) and is now around -12.1 ‰ for $\delta^{18}O$. This is probably due to the evolution of the stable isotope composition of the local precipitations and of the Rhône River described above with a delayed effect caused by the important residence time of the lake (11.3 years - CIPEL, 2020).

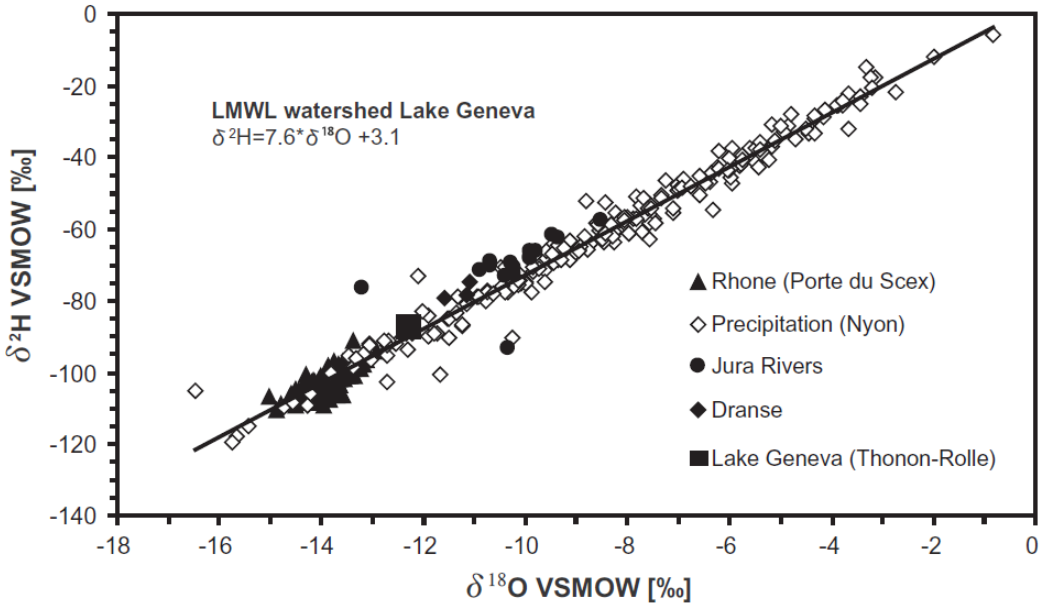

Figure 0-21: Local Meteoric Water Line of Lake Geneva watershed. From Halder et al. (2013)

5. Thesis objectives and structure

The general objective of my thesis work was to better understand the dispersion of the Rhône River water and its nutrients in Lake Geneva and the consequences on the biogeochemistry of the lake. The re-oligotrophication context and the fact that the lake has not returned to the biological conditions before the implementation of phosphorus reduction measures, led us to try to better understand the nutrient dynamics within the lake. Moreover, climate change modifies the thermal and mixing regimes of the lake (Perroud et al., 2009). As a consequence, the nutrient dynamics within the water column is perturbed by a reduced frequency of complete winter mixing (Schwefel et al., 2016), an earlier onset of stratification (Anneville et al., 2013) and consequently the establishment of a euphotic zone depleted earlier in nutrients during the year. In this context, the transport and dispersion of nutrients by the Rhône River is of prime importance in order to explain the changes in primary production.

Previous studies showed a diversity of river intrusion patterns in lakes depending on the thermal stratification of the lake, the discharge and density of the river and the morphology of the river mouth. In Lake Geneva, 3D numerical simulations highlighted the large spatio-temporal heterogeneities of Rhône River water dispersion. Furthermore, the spatial representativeness of the two monitoring stations (SHL2 and GE3) can be questioned, including a rather low density sampling calendar. Thus, a more complete spatial and temporal sampling of the lake will improve the resolution of the nutrient dynamics.

Finally, the complexities of the functioning of large sized lakes and the interdependence of physical, chemical, and biological processes may be best characterized on the basis of a multidisciplinary approach to outline the impact of the river intrusion on the primary production of the lake.

This thesis is organised into four chapters (Figure 0-22), along with their appendices, followed by a general conclusion that includes a synthesis of the results of the chapters, and proposes perspectives for future research.

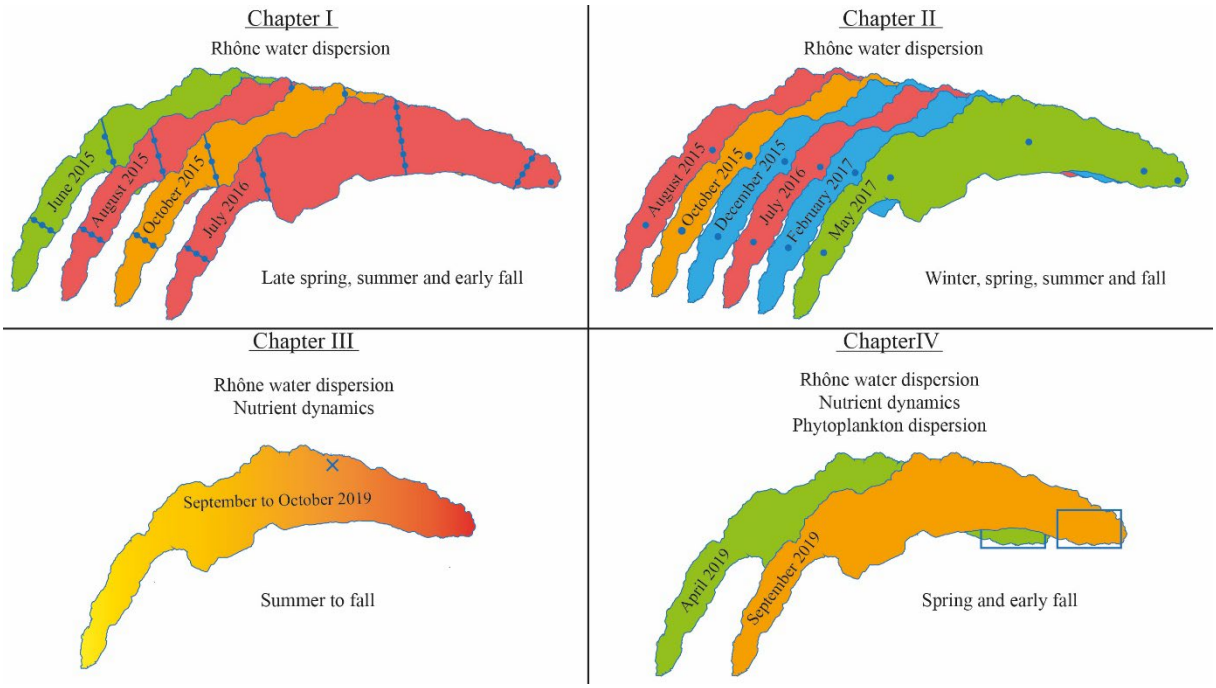

Figure 0-22: Schematic representation of the thesis chapters.

Chapter I: Rhône River dispersion in Lake Geneva during the thermal stratification period

This first chapter was published in the Journal of Great Lakes Research in June 2020 with the following reference: "Cotte, G., Vennemann, T.W., 2020. Mixing of Rhône River water in Lake Geneva: Seasonal tracing using stable isotope composition of water. J. Gt. Lakes Res. 46, 839–849". This study is based on sampling campaigns organized during 2015 and 2016 in different parts of the lake. The sampling was conducted with the help of Philippe Arpagaus (captain) from the Department F.-A. Forel for Environmental and Aquatic Sciences (DEFSE) of the University of Geneva and several other people (see Acknowledgements of the paper). Measurements and data analyses were made by Cotte G. and the manuscript was written by Cotte G. and Vennemann T.W.

Chapter II: Mixing of the Rhône River intrusion into Lake Geneva at different thermal conditions

This chapter was submitted to the Journal of Great Lakes Research in February 2021. It focusses on results of campaigns made in 2015-2016 and into 2017 in different parts of the lake. The scientific idea of this chapter is an extension of the first published chapter with additional data covering the periods of non-stratification. The sampling of the lake

was conducted with the help of Philippe Arpagaus (captain) of DEFSE and several other people (see Acknowledgements). Measurements and data analyses were made by Cotte G. and the chapter was written by Cotte G. and edited by Vennemann T.W.

Chapter III: Processes driving nutrient dispersion in Lake Geneva during the stratification period (study using the LéXPLORE platform)

In this chapter the results of a high temporal resolution sampling of the water column under the LéXPLORE platform during the months of September and October 2019 are discussed. The aim was to investigate the variations in the stratification of the lake at any one point with a high time resolution and hence conduct a continuous sampling series over an extended period. A specific pumping system was designed and built by Aurélien Ballu (IDYST, UNIL) using a submersible pump kindly borrowed to the project by Ludovic Baron (ISTE, UNIL). It was subsequently installed by Aurélien Ballu and Sébastien Lavanchy (APHYS, EPFL) at the moored platform. For the following 1.5 months Cotte G. collected and analysed the samples with the assistance in the field by several people (see Acknowledgements) and also with the kind support of Laetitia Monbaron and Thibault Lambert in the laboratories at UNIL. Jessica Chaves (UNIL) performed the isotopic analysis of the DIC with the help of Torsten Vennemann. The chapter was written by Cotte G. and edited by Vennemann T.W.

Chapter IV: Hydrodynamic, physico-chemical, and biological aspects of the transition zone between the Rhône River and Lake Geneva

A collaborative “River-Lake Transition” research project between the Ecological Engineering Laboratory (ECOL) of the EPFL (Lausanne), the Institute of Environmental Sciences (ISE) of the University of Geneva and the Institute of Earth Surface Dynamics (IDYST) of the University of Lausanne was established with the main aim of understanding the complexities and controls of phytoplankton growth in this specific estuarine area and ultimately the role of the Rhône River intrusion on the primary production of the lake. To achieve this aim a coordinated sampling strategy was elaborated by the team members involved, notably Gabriel Cotte as the principle coordinator (IDYST, UNIL), Fabio dos Santos Correia (ISE, UNIGE) and Frédéric Soulignac (ECOL, EPFL), all contributing to different aspects of the research project

within their own areas of expertise and interest. The sampling campaigns were conducted during April and September 2019 with additional assistance by Philippe Arpagaus (captain), Benjamin Daniel Graf (ECOL, EPFL) and Matthieu Fallet (MSc student at UNIL involved in the project). The nutrient, cation and anion as well as isotopic analyses were made by Gabriel Cotte and Matthieu Fallet with the help of Laetitia Monbaron and Thibault Lambert (UNIL). This chapter was written by Gabriel Cotte, Frédéric Soulignac and Fabio dos Santos Correia and edited by T.W. Vennemann and other likely co-authors/collaborators for this work.

Appendix V

In addition to the projects presented in this thesis, sampling campaigns in the Upper Rhône River watershed have been performed to sample different natural (tributaries) and anthropic (dam outputs) water inputs to the Rhône River in order to explain its important range of stable isotope composition of water before it enters the lake.

A first one has been done by Gelare Moradi and Romain Cardot (IDYST, UNIL) in December 2015. A second one has been carried out by Gabriel Cotte in March 2017 and a third one, in September 2017 by Gabriel Cotte and Christophe Borel (IDYST, UNIL). The isotopic composition of the water and of the DIC (for September 2017) have been analysed by Gabriel Cotte.

Appendices VI

During my thesis, I also contributed to the SPIKE II project during the summer of 2018, collaborating with Paolo Benettin and Andrea Rinaldi from the ECHO lab of EPFL and Jeffrey McDonnell, Magali Furlan Nehemy, Dyan Pratt, Cody Millar and Kim Janzen from the University of Saskatchewan (Canada). This project focussed on a natural laboratory-based isotopically spiked watering of a willow tree in order to experimentally determine the entire water cycle using a weighted lysimeter and isotope measurements of irrigated water, soils and plant water, as well as the analyses of water vapours. The latter was part of the UNIL collaboration and required the installation of a Picarro analyser on site. T. Vennemann and G. Cotte analysed the water vapors in this collaborative project. The results are summarized in Appendix VI.

References

Akiyama, J., Stefan, H.G., 1984. Plunging Flow into a Reservoir: Theory. Journal of Hydraulic Engineering 110, 484–499. https://doi.org/10.1061/(ASCE)0733-9429(1984)110:4(484)

Alavian, V., Jirka, G.H., Denton, R.A., Johnson, M.C., Stefan, H.G., 1992. Density Currents Entering Lakes and Reservoirs. Journal of Hydraulic Engineering 118, 1464–1489. https://doi.org/10.1061/(ASCE)0733-9429(1992)118:11(1464)

Anneville, O., Beniston, M., Gallina, N., Gillet, C., Jacquet, S., Lazzarotto, J., 2013. L'empreinte du changement climatique sur le Léman. ARCHIVES DES SCIENCES 16.

Anneville, O., Chang, C.-W., Dur, G., Souissi, S., Rimet, F., Hsieh, C., 2019. The paradox of re-oligotrophication: the role of bottom–up versus top–down controls on the phytoplankton community. Oikos 128, 1666–1677. https://doi.org/10.1111/oik.06399

Anneville, O., Dur, G., Rimet, F., Souissi, S., 2018. Plasticity in phytoplankton annual periodicity: an adaptation to long-term environmental changes. Hydrobiologia 824, 121–141. https://doi.org/10.1007/s10750-017-3412-z

Anneville, O., Ginot, V., Angeli, N., 2002. Restoration of Lake Geneva: Expected versus observed responses of phytoplankton to decreases in phosphorus. Lakes & Reservoirs: Science, Policy and Management for Sustainable Use 7, 67–80. https://doi.org/10.1046/j.1440-169X.2002.00179.x

Anneville, O., Molinero, J.C., Souissi, S., Balvay, G., Gerdeaux, D., 2007. Long-term changes in the copepod community of Lake Geneva. J Plankton Res 29, i49–i59. https://doi.org/10.1093/plankt/fbl066

Anneville, O., Vogel, C., Lobry, J., Guillard, J., 2017. Fish communities in the Anthropocene: detecting drivers of changes in the deep peri-alpine Lake Geneva. Inland Waters 7, 65–76. https://doi.org/10.1080/20442041.2017.1294350

Aucour, A.-M., Sheppard, S.M.F., Guyomar, O., Wattelet, J., 1999. Use of 13C to trace origin and cycling of inorganic carbon in the Rhoˆne river system 19.

Balvay, G., Ishiguro, N., 2003. L'écoulement des eaux du Rhône dans le lac Léman. https://doi.org/10.5169/SEALS-740434

Björk, S., 2010. The Evolution of Lakes and Wetlands, in: Eiseltová, M. (Ed.), Restoration of Lakes, Streams, Floodplains, and Bogs in Europe: Principles and

Case Studies, Wetlands: Ecology, Conservation and Management. Springer Netherlands, Dordrecht, pp. 25–35. https://doi.org/10.1007/978-90-481-9265-6_2

Boehrer, B., Schultze, M., 2008. Stratification of lakes. Rev. Geophys. 46, RG2005. https://doi.org/10.1029/2006RG000210

Bohle-Carbonell, M., 1986. Currents in Lake Geneva1: Currents in Lake Geneva. Limnol. Oceanogr. 31, 1255–1266. https://doi.org/10.4319/lo.1986.31.6.1255

Bonvin, F., Rutler, R., Chèvre, N., Halder, J., Kohn, T., 2011. Spatial and Temporal Presence of a Wastewater-Derived Micropollutant Plume in Lake Geneva. Environ. Sci. Technol. 45, 4702–4709. https://doi.org/10.1021/es2003588

Bouffard, D., Kiefer, I., Wüest, A., Wunderle, S., Odermatt, D., 2018. Are surface temperature and chlorophyll in a large deep lake related? An analysis based on satellite observations in synergy with hydrodynamic modelling and in-situ data. Remote Sensing of Environment 209, 510–523. https://doi.org/10.1016/j.rse.2018.02.056

Bouffard, D., Lemmin, U., 2013. Kelvin waves in Lake Geneva. Journal of Great Lakes Research 39, 637–645. https://doi.org/10.1016/j.jglr.2013.09.005

Bouffard, D., Perga, M.-E., 2016. Are flood-driven turbidity currents hot spots for priming effect in lakes? Biogeosciences 13, 3573–3584. https://doi.org/10.5194/bg-13-3573-2016

Bouffard, D., Wüest, A., 2018. Mixing in Stratified Lakes and Reservoirs, in: Clercx, H.J.H., Van Heijst, G.F. (Eds.), Mixing and Dispersion in Flows Dominated by Rotation and Buoyancy, CISM International Centre for Mechanical Sciences. Springer International Publishing, Cham, pp. 61–88. https://doi.org/10.1007/978-3-319-66887-1_3

Bratek, A., Emeis, K.-C., Sanders, T., Wankel, S.D., Struck, U., Möbius, J., Dähnke, K., 2020. Nitrate sources and the effect of land cover on the isotopic composition of nitrate in the catchment of the Rhône River. Isotopes in Environmental and Health Studies 56, 14–35. https://doi.org/10.1080/10256016.2020.1723580

Bruel, R., Girardclos, S., Marchetto, A., Kremer, K., Crouzet, C., Reyss, J.-L., Sabatier, P., Perga, M.-E., 2021. Reframing Lake Geneva ecological trajectory in a context of multiple but asynchronous pressures. J Paleolimnol 65, 353–368. https://doi.org/10.1007/s10933-021-00176-y

Burrus, D., Thomas, R.L., Dominik, J., Vernet, J.P., 1990. Seasonal delivery of the particulate forms of phosphorus to Lake Geneva from the upper Rhone river. Aquatic Science 52, 221–235. https://doi.org/10.1007/BF00877281

Carlson Mazur, M.L., Schaeffer, J., Granneman, J.E., Goldstrohm, N., Fitzpatrick, F.A., Larson, J.H., Reneau, P.C., Kowalski, K.P., Seelbach, P.W., 2019. Seasonal patterns in hydrochemical mixing in three Great Lakes rivermouth ecosystems. Journal of Great Lakes Research 45, 651–663. https://doi.org/10.1016/j.jglr.2019.03.009

Chevre, N., 2018. Micropollutants in Large Lakes: From Potential Pollution to Risk Assessments, 1st ed. EPFL Press. https://doi.org/10.1201/9781351240291

Cimatoribus, A.A., Lemmin, U., Barry, D.A., 2019. Tracking Lagrangian transport in Lake Geneva: A 3D numerical modeling investigation. Limnol Oceanogr 64, 1252–1269. https://doi.org/10.1002/lno.11111

Conseil scientifique de la commission internationale pour la protection des eaux du Léman contre la pollution. 2020. Rapports sur les études et recherches entreprises dans le bassin lémanique. Campagne 2019. CIPEL. Available from https://www.cipel.org/publications/rapports-scientifiques/rapport-2020-campagne-2019/

Clark, Fritz, 1997. Environmental Isotopes in Hydrogeology. CRC Press. https://doi.org/10.1201/9781482242911

Coplen, T.B., 1996. New guidelines for reporting stable hydrogen, carbon, and oxygen isotope-ratio data. Geochimica et Cosmochimica Acta 60, 3359–3360. https://doi.org/10.1016/0016-7037(96)00263-3

Coplen, T.B., Herczeg, A.L., Barnes, C., 2000. Isotope Engineering—Using Stable Isotopes of the Water Molecule to Solve Practical Problems, in: Cook, P.G., Herczeg, A.L. (Eds.), Environmental Tracers in Subsurface Hydrology. Springer US, Boston, MA, pp. 79–110. https://doi.org/10.1007/978-1-4615-4557-6_3

Corella, J.P., Arantegui, A., Loizeau, J.L., DelSontro, T., le Dantec, N., Stark, N., Anselmetti, F.S., Girardclos, S., 2013. Sediment dynamics in the subaquatic channel of the Rhone delta (Lake Geneva, France/Switzerland). Aquat Sci. https://doi.org/10.1007/s00027-013-0309-4

Cortés, A., Fleenor, W.E., Wells, M.G., de Vicente, I., Rueda, F.J., 2014a. Pathways of river water to the surface layers of stratified reservoirs. Limnol. Oceanogr. 59, 233–250. https://doi.org/10.4319/lo.2014.59.1.0233

Cortés, A., Rueda, F.J., Wells, M.G., 2014b. Experimental observations of the splitting of a gravity current at a density step in a stratified water body. J. Geophys. Res. Oceans 119, 1038–1053. https://doi.org/10.1002/2013JC009304

Cortés, A., Wells, M.G., Fringer, O.B., Arthur, R.S., Rueda, F.J., 2015. Numerical investigation of split flows by gravity currents into two-layered stratified water bodies: NUMERICAL INVESTIGATION OF SPLIT FLOWS. J. Geophys. Res. Oceans 120, 5254–5271. https://doi.org/10.1002/2015JC010722

Costa, A., Molnar, P., Stutenbecker, L., Bakker, M., Silva, T.A., Schlunegger, F., Lane, S.N., Loizeau, J.-L., Girardclos, S., 2017. Temperature signal in suspended sediment export from an Alpine catchment (preprint). Catchment hydrology/Modelling approaches. https://doi.org/10.5194/hess-2017-2

Craig, H., 1961. Isotopic Variations in Meteoric Waters. Science 133, 1702–1703. https://doi.org/10.1126/science.133.3465.1702

Craig, H., Gordon, L.I. (Eds.), 1965. Deuterium and oxygen 18 variations in the ocean and the marine atmosphere. Consiglio nazionale delle richerche, Laboratorio de geologia nucleare, Pisa.

Engel, F., Farrell, K.J., McCullough, I.M., Scordo, F., Denfeld, B.A., Dugan, H.A., de Eyto, E., Hanson, P.C., McClure, R.P., Nõges, P., Nõges, T., Ryder, E., Weathers, K.C., Weyhenmeyer, G.A., 2018. A lake classification concept for a more accurate global estimate of the dissolved inorganic carbon export from terrestrial ecosystems to inland waters. Sci Nat 105, 25. https://doi.org/10.1007/s00114-018-1547-z

Etcheverry, D. and Vennemann, T., 2009. Isotope im Grundwasser. Methoden zur Anwendung in der hydrogeologischen Praxis. Umwelt-Wissen Nr. 0930. Bundesamt für Umwelt, Bern.

Finger, D., Wüest, A., Bossard, P., 2013. Effects of oligotrophication on primary production in peri-alpine lakes: Modeling Primary Production in Lakes. Water Resour. Res. 49, 4700–4710. https://doi.org/10.1002/wrcr.20355

Fink, G., Wessels, M., Wüest, A., 2016. Flood frequency matters: Why climate change degrades deep-water quality of peri-alpine lakes. Journal of Hydrology 540, 457–468. https://doi.org/10.1016/j.jhydrol.2016.06.023

Fischer, H.B., Smith, R.D., 1983. Observations of transport to surface waters from a plunging inflow to Lake Mead1: Lake Mead transport. Limnol. Oceanogr. 28, 258–272. https://doi.org/10.4319/lo.1983.28.2.0258

Gerdeaux, D., 2004. The recent restoration of the whitefish fisheries in Lake Geneva: the roles of stocking, reoligotrophication, and climate change. Annales Zoologici Fennici 41, 181–189.

Giovanoli, F., 1990. Horizontal Transport and Sedimentation by Interflows and Turbidity Currents in Lake Geneva, in: Tilzer, M.M., Serruya, C. (Eds.), Large Lakes: Ecological Structure and Function, Brock/Springer Series in Contemporary Bioscience. Springer, Berlin, Heidelberg, pp. 175–195. https://doi.org/10.1007/978-3-642-84077-7_9

Gorceix, C., Kreitmann, L., 1930. Etude thermique de « La Bataillère » sur le Léman. rga 18, 537–551. https://doi.org/10.3406/rga.1930.4544

Halder, J., Decrouy, L., Vennemann, T.W., 2013. Mixing of Rhône River water in Lake Geneva (Switzerland–France) inferred from stable hydrogen and oxygen isotope profiles. Journal of Hydrology 477, 152–164. https://doi.org/10.1016/j.jhydrol.2012.11.026

Halder, J., Pralong, C., Bonvin, F., Lambiel, F., Vennemann, T.W., 2016. Application of $\delta^{18}O$, $\delta^{13}CDIC$, and major ions to evaluate micropollutant sources in the Bay of Vidy, Lake Geneva. Isotopes in Environmental and Health Studies 52, 94–111. https://doi.org/10.1080/10256016.2014.971786

Hodges, B.R., Imberger, J., Saggio, A., Winters, K.B., 2000. Modeling basin-scale internal waves in a stratified lake. Limnology and Oceanography 45, 1603–1620. https://doi.org/10.4319/lo.2000.45.7.1603

Hoefs, J., 2009. Stable Isotope Geochemistry, 6th ed. Springer-Verlag, Berlin Heidelberg. https://doi.org/10.1007/978-3-540-70708-0

Hogg, C.A.R., Marti, C.L., Huppert, H.E., Imberger, J., 2013. Mixing of an interflow into the ambient water of Lake Iseo. Limnol. Oceanogr. 58, 579–592. https://doi.org/10.4319/lo.2013.58.2.0579

Horgby, Å., Canadell, M.B., Ulseth, A.J., Vennemann, T.W., Battin, T.J., 2019a. High-Resolution Spatial Sampling Identifies Groundwater as Driver of CO2 Dynamics in an Alpine Stream Network. Journal of Geophysical Research: Biogeosciences 124, 1961–1976. https://doi.org/10.1029/2019JG005047

Horgby, Å., Segatto, P.L., Bertuzzo, E., Lauerwald, R., Lehner, B., Ulseth, A.J., Vennemann, T.W., Battin, T.J., 2019b. Unexpected large evasion fluxes of carbon dioxide from turbulent streams draining the world's mountains. Nature Communications 10, 4888. https://doi.org/10.1038/s41467-019-12905-z

Imboden, D. M., Wüest, A., 1995. Mixing Mechanisms in Lakes, in: Lerman, A., Imboden, Dieter M., Gat, J.R. (Eds.), Physics and Chemistry of Lakes. Springer, Berlin, Heidelberg, pp. 83–138. https://doi.org/10.1007/978-3-642-85132-2_4

Jameel, Y., Stein, S., Grimm, E., Roswell, C., Wilson, A.E., Troy, C., Höök, T.O., Bowen, G.J., 2018. Physicochemical characteristics of a southern Lake Michigan river plume. Journal of Great Lakes Research 44, 209–218. https://doi.org/10.1016/j.jglr.2018.01.003

Jenny, J.-P., Anneville, O., Arnaud, F., Baulaz, Y., Bouffard, D., Domaizon, I., Bocaniov, S.A., Chèvre, N., Dittrich, M., Dorioz, J.-M., Dunlop, E.S., Dur, G., Guillard, J., Guinaldo, T., Jacquet, S., Jamoneau, A., Jawed, Z., Jeppesen, E., Krantzberg, G., Lenters, J., Leoni, B., Meybeck, M., Nava, V., Nõges, T., Nõges, P., Patelli, M., Pebbles, V., Perga, M.-E., Rasconi, S., Ruetz, C.R., Rudstam, L., Salmaso, N., Sapna, S., Straile, D., Tammeorg, O., Twiss, M.R., Uzarski, D.G., Ventelä, A.-M., Vincent, W.F., Wilhelm, S.W., Wängberg, S.-Å., Weyhenmeyer, G.A., 2020. Scientists' Warning to Humanity: Rapid degradation of the world's large lakes. Journal of Great Lakes Research 46, 686–702. https://doi.org/10.1016/j.jglr.2020.05.006

Jenny, J.-P., Arnaud, F., Alric, B., Dorioz, J.-M., Sabatier, P., Meybeck, M., Perga, M.-E., 2014. Inherited hypoxia: A new challenge for reoligotrophicated lakes under global warming. Global Biogeochemical Cycles 28, 1413–1423. https://doi.org/10.1002/2014GB004932

Jenny, J.-P., Francus, P., Normandeau, A., Lapointe, F., Perga, M.-E., Ojala, A., Schimmelmann, A., Zolitschka, B., 2016. Global spread of hypoxia in freshwater ecosystems during the last three centuries is caused by rising local human pressure. Glob Change Biol 22, 1481–1489. https://doi.org/10.1111/gcb.13193

Jeppesen, E., Sondergaard, M., Jensen, J.P., Havens, K.E., Anneville, O., Carvalho, L., Coveney, M.F., Deneke, R., Dokulil, M.T., Foy, B., Gerdeaux, D., Hampton, S.E., Hilt, S., Kangur, K., Kohler, J., Lammens, E.H.H.R., Lauridsen, T.L., Manca, M., Miracle, M.R., Moss, B., Noges, P., Persson, G., Phillips, G., Portielje, R., Romo, S., Schelske, C.L., Straile, D., Tatrai, I., Willen, E., Winder, M., 2005. Lake responses to reduced nutrient loading - an analysis of contemporary long-term data from 35 case studies. Freshwater Biol 50, 1747–1771. https://doi.org/10.1111/j.1365-2427.2005.01415.x

Kreitmann, L., 1931. Etude des courants du lac Léman. Géocarrefour 7, 109–130. https://doi.org/10.3406/geoca.1931.3861

Kremer, K., Corella, J.P., Hilbe, M., Marillier, F., Dupuy, D., Zenhäusern, G., Girardclos, S., 2015. Changes in distal sedimentation regime of the Rhone delta system controlled by subaquatic channels (Lake Geneva, Switzerland/France). Marine Geology 370, 125–135. https://doi.org/10.1016/j.margeo.2015.10.013

Lambert, A., Giovanoli, F., 1988. Records of riverbome turbidity currents and indications of slope failures in the Rhone delta of Lake Geneva. Limnol. Oceanogr. 33, 458–468. https://doi.org/10.4319/lo.1988.33.3.0458

Larson, J.H., Evans, M.A., Fitzpatrick, F.A., Frost, P.C., Bailey, S., Kennedy, R., James, W.F., Richardson, W.B., Reneau, P.C., 2019. Water column nutrient processing rates in rivermouths of Green Bay (Lake Michigan). Biogeochemistry 142, 73–93. https://doi.org/10.1007/s10533-018-0517-z

Larson, J.H., Frost, P.C., Vallazza, J.M., Nelson, J.C., Richardson, W.B., 2016. Do rivermouths alter nutrient and seston delivery to the nearshore? Freshwater Biology 61, 1935–1949. https://doi.org/10.1111/fwb.12827

Larson, J.H., Trebitz, A.S., Steinman, A.D., Wiley, M.J., Mazur, M.C., Pebbles, V., Braun, H.A., Seelbach, P.W., 2013. Great Lakes rivermouth ecosystems: Scientific synthesis and management implications. Journal of Great Lakes Research 39, 513–524. https://doi.org/10.1016/j.jglr.2013.06.002

Lemmin, U., D'Adamo, N., n.d. Summertime winds and direct cyclonic circulation: observations from Lake Geneva. N. D 14.

Lemmin, U., Mortimer, C.H., Bäuerle, E., 2005. Internal seiche dynamics in Lake Geneva. Limnol. Oceanogr. 50, 207–216. https://doi.org/10.4319/lo.2005.50.1.0207

Loizeau, J.-L., 1991. La sédimentation récente dans le delta du Rhône, Léman: processus et évolution. University of Geneva. https://doi.org/10.13097/archive-ouverte/unige:47526

Loizeau, J.-L., Dominik, J., 2000. Evolution of the Upper Rhone River discharge and suspended sediment load during the last 80 years and some implications for Lake Geneva. Aquat. sci. 62, 54. https://doi.org/10.1007/s000270050075

Makarewicz, J.C., Lewis, T.W., Boyer, G.L., Edwards, W.J., 2012. The influence of streams on nearshore water chemistry, Lake Ontario. Journal of Great Lakes Research 38, 62–71. https://doi.org/10.1016/j.jglr.2012.02.010

Marti, C.L., Mills, R., Imberger, J., 2011. Pathways of multiple inflows into a stratified reservoir: Thomson Reservoir, Australia. Advances in Water Resources 34, 551–561. https://doi.org/10.1016/j.advwatres.2011.01.003

McGuire, K.J., McDonnell, J.J., 2015. Tracer advances in catchment hydrology. Hydrological Processes 29, 5135–5138. https://doi.org/10.1002/hyp.10740

Michalski, J., Lemmin, U., 1995. Dynamics of vertical mixing in the hypolimnion of a deep lake: Lake Geneva. Limnol. Oceanogr. 40, 809–816. https://doi.org/10.4319/lo.1995.40.4.0809

Moisset, S., 2017. Investigation of the link between phytoplankton and nutrients dynamic in Lake Geneva. University of Geneva. https://doi.org/10.13097/archive-ouverte/unige:96830

Morrice, J.A., Kelly, J.R., Trebitz, A.S., Cotter, A.M., Knuth, M.L., 2004. Temporal Dynamics of Nutrients (N and P) and Hydrology in a Lake Superior Coastal Wetland. Journal of Great Lakes Research 30, 82–96. https://doi.org/10.1016/S0380-1330(04)70379-2

Müller, B., Steinsberger, T., Schwefel, R., Gächter, R., Sturm, M., Wüest, A., 2019. Oxygen consumption in seasonally stratified lakes decreases only below a marginal phosphorus threshold. Sci Rep 9, 18054. https://doi.org/10.1038/s41598-019-54486-3

Nixon, S.W., 1995. Coastal marine eutrophication: A definition, social causes, and future concerns. Ophelia 41, 199–219. https://doi.org/10.1080/00785236.1995.10422044

Nõges, T., Anneville, O., Guillard, J., Haberman, J., Järvalt, A., Manca, M., Morabito, G., Rogora, M., Thackeray, S.J., Volta, P., Winfield, I.J., Nõges, P., 2017. Fisheries impacts on lake ecosystem structure in the context of a changing climate and trophic state. J Limnol. https://doi.org/10.4081/jlimnol.2017.1640

Nouchi, V., Kutser, T., Wüest, A., Müller, B., Odermatt, D., Baracchini, T., Bouffard, D., 2019. Resolving biogeochemical processes in lakes using remote sensing. Aquat Sci 81, 27. https://doi.org/10.1007/s00027-019-0626-3

Olivier, J.-M., Dole-Olivier, M.-J., Amoros, C., Carrel, G., Malard, F., Lamouroux, N., Bravard, J.-P., 2009. The Rhône River Basin, in: Rivers of Europe. Elsevier, pp. 247–295. https://doi.org/10.1016/B978-0-12-369449-2.00007-2

Paerl, H.W., Hall, N.S., Calandrino, E.S., 2011. Controlling harmful cyanobacterial blooms in a world experiencing anthropogenic and climatic-induced change.

Science of The Total Environment 409, 1739–1745. https://doi.org/10.1016/j.scitotenv.2011.02.001

Perroud, M., Goyette, S., Martynov, A., Beniston, M., Annevillec, O., 2009. Simulation of multiannual thermal profiles in deep Lake Geneva: A comparison of one-dimensional lake models. Limnol. Oceanogr. 54, 1574–1594. https://doi.org/10.4319/lo.2009.54.5.1574

Råman Vinnå, L., Wüest, A., Zappa, M., Fink, G., Bouffard, D., 2018. Tributaries affect the thermal response of lakes to climate change. Hydrol. Earth Syst. Sci. 22, 31–51. https://doi.org/10.5194/hess-22-31-2018

Razmi, A.M., Barry, D.A., Bakhtyar, R., Le Dantec, N., Dastgheib, A., Lemmin, U., Wüest, A., 2013. Current variability in a wide and open lacustrine embayment in Lake Geneva (Switzerland). Journal of Great Lakes Research 39, 455–465. https://doi.org/10.1016/j.jglr.2013.06.011

Razmi, A.M., Barry, D.A., Bouffard, D., Vennemann, T., Barry, C.E., Lemmin, U., 2018. Currents of Lake Geneva [WWW Document]. Micropollutants in Large Lakes: From Potential Pollution to Risk Assessments. URL https://infoscience.epfl.ch/record/252798

Razmi, A.M., Barry, D.A., Lemmin, U., Bonvin, F., Kohn, T., Bakhtyar, R., 2014. Direct effects of dominant winds on residence and travel times in the wide and open lacustrine embayment: Vidy Bay (Lake Geneva, Switzerland). Aquat Sci 76, 59–71. https://doi.org/10.1007/s00027-013-0321-8

Razmi, A.M., Lemmin, U., Bouffard, D., Wüest, A., Uittenbogaard, R.E., Barry, D.A., 2017. Gyre formation in open and deep lacustrine embayments: the example of Lake Geneva, Switzerland. Environ Fluid Mech 17, 415–428. https://doi.org/10.1007/s10652-016-9494-8

Richardson, K., Jørgensen, B.B., 2013. Eutrophication: Definition, History and Effects, in: Eutrophication in Coastal Marine Ecosystems. American Geophysical Union (AGU), pp. 1–19. https://doi.org/10.1029/CE052p0001

Rimet, F., Anneville, O., Barbet, D., Chardon, C., Crépin, L., Domaizon, I., Dorioz, J.-M., Espinat, L., Frossard, V., Guillard, J., Goulon, C., Hamelet, V., Hustache, J.-C., Jacquet, S., Lainé, L., Montuelle, B., Perney, P., Quetin, P., Rasconi, S., Schellenberger, A., Tran-Khac, V., Monet, G., 2020. The Observatory on LAkes (OLA) database: Sixty years of environmental data accessible to the public: Journal of Limnology 79. https://doi.org/10.4081/jlimnol.2020.1944

Rueda, F.J., Fleenor, W.E., de Vicente, I., 2007. Pathways of river nutrients towards the euphotic zone in a deep-reservoir of small size: Uncertainty analysis. Ecological Modelling 202, 345–361. https://doi.org/10.1016/j.ecolmodel.2006.11.006

Sas, H., 1990. Lake restoration by reduction of nutrient loading: Expectations, experiences, extrapolations. SIL Proceedings, 1922-2010 24, 247–251. https://doi.org/10.1080/03680770.1989.11898731

Sastre, V., Loizeau, J.-L., Greinert, J., Naudts, L., Arpagaus, P., Anselmetti, F., Wildi, W., 2010. Morphology and recent history of the Rhone River Delta in Lake Geneva (Switzerland). Swiss J Geosci 103, 33–42. https://doi.org/10.1007/s00015-010-0006-4

Schelske, C.L., Feldt, L.E., Simmons, M.S., 1980. Phytoplankton and physical-chemical conditions in selected rivers and the coastal zone of Lake Michigan, 1972 (No. COO-2003-36). Michigan Univ., Ann Arbor (USA). Great Lakes Research Div. https://doi.org/10.2172/5008748

Schindler, D.W., 2012. The dilemma of controlling cultural eutrophication of lakes. Proceedings of the Royal Society B: Biological Sciences 279, 4322–4333. https://doi.org/10.1098/rspb.2012.1032

Schindler, D.W., 1977. Evolution of Phosphorus Limitation in Lakes. Science 195, 260–262. https://doi.org/10.1126/science.195.4275.260

Schindler, D.W., 1974. Eutrophication and recovery in experimental lakes: implications for lake management. Science 184, 897–899. https://doi.org/10.1126/science.184.4139.897

Schmieder, K., 2004. European lake shores in danger — concepts for a sustainable development. Limnologica, Lake-shores — Ecology, Quality Assessment, Sustainable Development 34, 3–14. https://doi.org/10.1016/S0075-9511(04)80016-1

Schotterer, U., 2010. Wasserisotope in der Schweiz. Neue Ergebnisse und Erfahrungen aus dem nationalen Messnetz ISOT. GWA 10/2012, 1073-1081.

Schürch, M., Kozel, R., Schotterer, U., Tripet, J.-P., 2003. Observation of isotopes in the water cycle-the Swiss National Network (NISOT). Environmental Geology 45, 1–11. https://doi.org/10.1007/s00254-003-0843-9

Schwefel, R., Gaudard, A., Wüest, A., Bouffard, D., 2016. Effects of climate change on deepwater oxygen and winter mixing in a deep lake (Lake Geneva): Comparing

observational findings and modelling. Water Resour. Res. 52, 8811–8826. https://doi.org/10.1002/2016WR019194

Sharp, Z., 2007. Principles of stable isotope geochemistry, 1. ed. ed. Pearson/ Prentice Hall, Upper Saddle River, NJ.

Smith, V.H., 1998. Cultural Eutrophication of Inland, Estuarine, and Coastal Waters, in: Pace, M.L., Groffman, P.M. (Eds.), Successes, Limitations, and Frontiers in Ecosystem Science. Springer, New York, NY, pp. 7–49. https://doi.org/10.1007/978-1-4612-1724-4_2

Tadonleke, R.D., Lazzarotto, J., Anneville, O., Druart, J.-C., 2009. Phytoplankton productivity increased in Lake Geneva despite phosphorus loading reduction. Journal of Plankton Research 31, 1179–1194. https://doi.org/10.1093/plankt/fbp063

Thi, A.D.L., Pascalis, F.D., Umgiesser, G., Wildi, W., 2012. Structure thermique et courantologie du Léman. ARCHIVES DES SCIENCES 16.

Tranvik, L.J., Downing, J.A., Cotner, J.B., Loiselle, S.A., Striegl, R.G., Ballatore, T.J., Dillon, P., Finlay, K., Fortino, K., Knoll, L.B., Kortelainen, P.L., Kutser, T., Larsen, S., Laurion, I., Leech, D.M., McCallister, S.L., McKnight, D.M., Melack, J.M., Overholt, E., Porter, J.A., Prairie, Y., Renwick, W.H., Roland, F., Sherman, B.S., Schindler, D.W., Sobek, S., Tremblay, A., Vanni, M.J., Verschoor, A.M., Wachenfeldt, E. von, Weyhenmeyer, G.A., 2009. Lakes and reservoirs as regulators of carbon cycling and climate. Limnology and Oceanography 54, 2298–2314. https://doi.org/10.4319/lo.2009.54.6_part_2.2298

Un delta lacustre pour la biodiversité de l'embouchure du Rhône, 2017. . Le Temps.

Vadeboncoeur, Y., McIntyre, P.B., Vander Zanden, M.J., 2011. Borders of Biodiversity: Life at the Edge of the World's Large Lakes. BioScience 61, 526–537. https://doi.org/10.1525/bio.2011.61.7.7

Vonlanthen, P., Bittner, D., Hudson, A.G., Young, K.A., Müller, R., Lundsgaard-Hansen, B., Roy, D., Di Piazza, S., Largiader, C.R., Seehausen, O., 2012. Eutrophication causes speciation reversal in whitefish adaptive radiations. Nature 482, 357–362. https://doi.org/10.1038/nature10824

Wells, M., Nadarajah, P., 2009. The Intrusion Depth of Density Currents Flowing into Stratified Water Bodies. Journal of Physical Oceanography 39, 1935–1947. https://doi.org/10.1175/2009JPO4022.1

Wentzky, V.C., Tittel, J., Jäger, C.G., Rinke, K., 2018. Mechanisms preventing a decrease in phytoplankton biomass after phosphorus reductions in a German drinking water reservoir-results from more than 50 years of observation. Freshw Biol 63, 1063–1076. https://doi.org/10.1111/fwb.13116

Wetzel, R.G., Likens, G.E., 1991. Light and Temperature, in: Wetzel, R.G., Likens, G.E. (Eds.), Limnological Analyses. Springer, New York, NY, pp. 15–30. https://doi.org/10.1007/978-1-4757-4098-1_2

Withers, P.J.A., Neal, C., Jarvie, H.P., Doody, D.G., 2014. Agriculture and Eutrophication: Where Do We Go from Here? Sustainability 6, 5853–5875. https://doi.org/10.3390/su6095853

Woolway, R.I., Merchant, C.J., 2019. Worldwide alteration of lake mixing regimes in response to climate change. Nature Geoscience 12, 271–276. https://doi.org/10.1038/s41561-019-0322-x

Zhang, X., Ren, S., Lu, J., Lu, X., 2015. Effect of thermal stratification on interflow travel time in stratified reservoir. J. Zhejiang Univ. Sci. A 16, 265–278. https://doi.org/10.1631/jzus.A1400269

Chapter I

Rhône River dispersion in Lake Geneva during the thermal stratification period

Authors: Cotte Gabriel[1], Vennemann Torsten W.[2]

[1]IDYST, UNIL, Géopolis 1015 Lausanne, Gabriel.Cotte@unil.ch

[2]IDYST, UNIL, Géopolis 1015 Lausanne, Torsten.Vennemann@unil.ch

Abstract

Determining the path of river intrusions into lakes is essential, both for a better understanding of the lake circulation as well as the nutrient transport and the distribution of pollutants introduced by the rivers. The objective of this study is to understand the mixing of Rhône River water within Lake Geneva. The stable H- and O-isotope composition of water for this Alpine lake has been shown to be a powerful tool to trace the Rhône River intrusion within the lake but the details of this interflow and how it changes in space and time have not been well established yet. The present study focusses on using the isotopic tracer method in detailed cross-sections sampled at different times during the year as a tool to determine how the interflow changes with time. Different sampled cross-sections present large spatiotemporal heterogeneities of the Rhône River water dispersion. During summer and early autumn, when the lake is thermally stratified, the Rhône River is intruding in the metalimnion as an interflow and it is directed by the currents in the top layer. The stronger the thermal stratification, the more concentrated and vertically constrained will also be the Rhône interflow. Vertical and horizontal displacements of the interflow are controlled by wind-induced internal waves and the gyres within the lake established as a function of wind strengths and directions.

Keywords

Lake Geneva; Rhône River; interflow; river mixing; lake circulation; stable isotopes

1. Introduction

River inflows play a major role in the functioning of lakes. They introduce dissolved compounds, including nutrients as well as particulate matter from the watershed to the lake (Giovanoli, 1990; Loizeau and Dominik, 2000; Kremer et al., 2015) and hence are important for the ecology of the lake(Larson et al., 2013; Bouffard and Perga, 2016; Nouchi et al., 2019). Pollutants may also be introduced (Bonvin et al., 2011; Halder et al., 2016), adding another reason why their dispersion within the lake is of primordial importance. Depending on the density difference between the river and the receiving lake, several cases of dispersion can be listed. First, when the density of the tributary, controlled by the temperature, the dissolved fraction, and the suspended sediment load, is smaller than that at the lake surface, the river will float on the lake surface as an overflow. In contrast, when the river water is denser, it will create an underflow, also called gravity current. With a progressive entrainment of lake water, the river can equilibrate its density with that of the lake and create an intrusion into the water column. In a stratified lake, the river water, denser than the lake surface, will descend to potentially reach the depth of neutral buoyancy around the thermocline level and thus intrude the water column as an interflow. These different behaviours will have different impacts on the residence time of river water within the lake, the nutrient and pollutant dispersion and hence the overall health and ecology of the lake. This study focusses on the interflow of the Rhône River into Lake Geneva (local name: Lac Léman) and evaluates the displacement of this interflow within the framework of the existing knowledge on the circulation of water in this lake.

Lake Geneva is the largest freshwater lake in Western Europe with a volume of 89 km^3, a surface area of 580 km^2 and a maximum depth of 309 m. It is a monomictic lake located between France and Switzerland. Its theoretical residence time, calculated by the ratio of its volume and the total water input, is approximately 11.5 years (CIPEL, 2019). It usually presents a thermal stratification from spring to early fall. With the air temperatures rising due to climate change (IPCC, 2018), total mixing of its water column during winter turnover of the lake should be expected to happen less frequently. Surface currents within Lake Geneva are controlled by the prevailing winds, the shoreline topography and the Coriolis force and create cyclonic and anticyclonic circulations called gyres (Lemmin, 1989; Lemmin and D'Adamo, 1996). Given the variable wind directions of the dominant winds in Lake Geneva, the hydrodynamic of the lake is described to be

quite inhomogeneous, however some general circulation patterns have been documented by recent 3D hydrodynamic simulations, for example by Thi et al., (2012) and Cimatoribus et al. (2019). These studies demonstrated that during dominant wind events large-scale gyres control the circulation over most of the lake with two large gyres of an anticlockwise circulation existing in each basin (*Petit Lac* and *Grand Lac*) and one with a clockwise circulation at the interface between the two basins. These gyres are highly variable in space and time, but may last several days before breaking down into smaller gyres as a function of the dominant wind speeds and directions. Lake Geneva can also react to wind with basin-wide internal waves such as internal seiches that create downwelling towards the downwind transport direction and upwelling at the upwind side (Lemmin et al., 2005). Oscillations of water movement can be provoked in the thermocline when the wind stops and can last several days. In such a large lake, long internal waves are affected by Coriolis force and lead to anticlockwise rotating Kelvin waves (Bouffard and Lemmin, 2013). This kind of wave will increase the shear in the thermocline and so contribute to both vertical and horizontal mixing of the lake water.

The main tributary of the lake, the Rhône River, accounts for 70 % of the total water input. The river has an alpine catchment, enters in the eastern part of the lake and flows out at Geneva before continuing into France. Upstream of the lake, its hydrology is characterised by high discharge in spring and summer caused by snow and glacier melt and by a low discharge during winter. Since the 1950's, several of its tributaries are now part of the hydroelectric power scheme dams, further modifying their hydrology and that of the Rhône. During episodic high-discharge level, the Rhône inflow can sink to the bottom and flow in its lacustrine delta as a gravity current (underflow) when the river can transport a large amount of suspended sediments. More common are interflows that intrude the water column to a depth of neutral buoyancy where the density of the river water is related largely to temperature only. This neutral buoyancy is most commonly at the thermocline depth within the metalimnion during the stratification period (Halder et al., 2013). During winter, when the density of the water column is quasi-homogeneous the intrusion depth is more variable and depends on the Rhône density variations and its discharge that fluctuates with the hydroelectric dam managements upstream of the lake.

The Rhône intrusion in the lake was first described in 1885 by F.A. Forel who discovered the underwater canyons. Subsequently, several studies explored the dispersion of its water in the lake using different approaches. Giovanoli (1990), for example, determined via ultrasonic current meter and turbidity measurements that "interflow water

masses are dissipated by horizontal spreading and entrainment of lake waters". They also determined that "the transport path of interflows is controlled not only by density stratification and horizontal density differences but also by Coriolis force and internal currents". Using CTD profiles to detect the interflow, Balvay and Ishiguro (2003) observed a Rhône interflow at the thermocline depth, being deflected around the north shore by the Coriolis force and able to reach the central part of the lake. Later, Halder et al. (2013) were able to detect the interflow much further from the river mouth of the Rhône to the lake and this with improved accuracy. By measuring the stable isotope composition of the water, they inferred the fraction of Rhône water within the interflow during summer stratification and determined an upper limit of 5 months for the travel time of the Rhône water to the Petit Lac (50 km away from the river mouth). More recently, Cimatoribus et al. (2019) presented a Lagrangian motion's tracking of simulated Rhône particles using a 3D numerical model. Even though the results showed a large spatiotemporal variability of transport, they could detect preferential circulation patterns with relatively well-defined rapid transit paths (scale of several days) along the near-shore region for the upper layers of the water column and much slower particle transports (transport rates on the scale of months) for the deeper and more central regions of the lake. The longer residence times of the water particles in the deeper parts are also related to the insulating thermal effects of the stratification and reduction of shear stress with resulting slower currents at greater depth (Michalski and Lemmin, 1995).

This contribution focusses on a field approach to study the Rhône River dispersion within Lake Geneva during the stratification period. Given the good potential of tracing the Rhône interflow water through the lake via its distinct isotopic composition (Halder et al., 2013), this approach of isotopic measurements of the water is used in a more detailed study. With a seasonal tracing covering the entire basin, the data collected supports the processes responsible for the spatiotemporal heterogeneities of the Rhône River dispersion within the lake identified by the 3D numerical simulations (Cimatoribus et al., 2019). This contribution also further details the impact of the stratification on the vertical dispersion of the interflow and compares these new measurements to the effects expected from internal waves and gyral circulations on the transport dynamics of the Rhône interflow water within the lake.

2. Material and methods

2.1. Sampling strategy

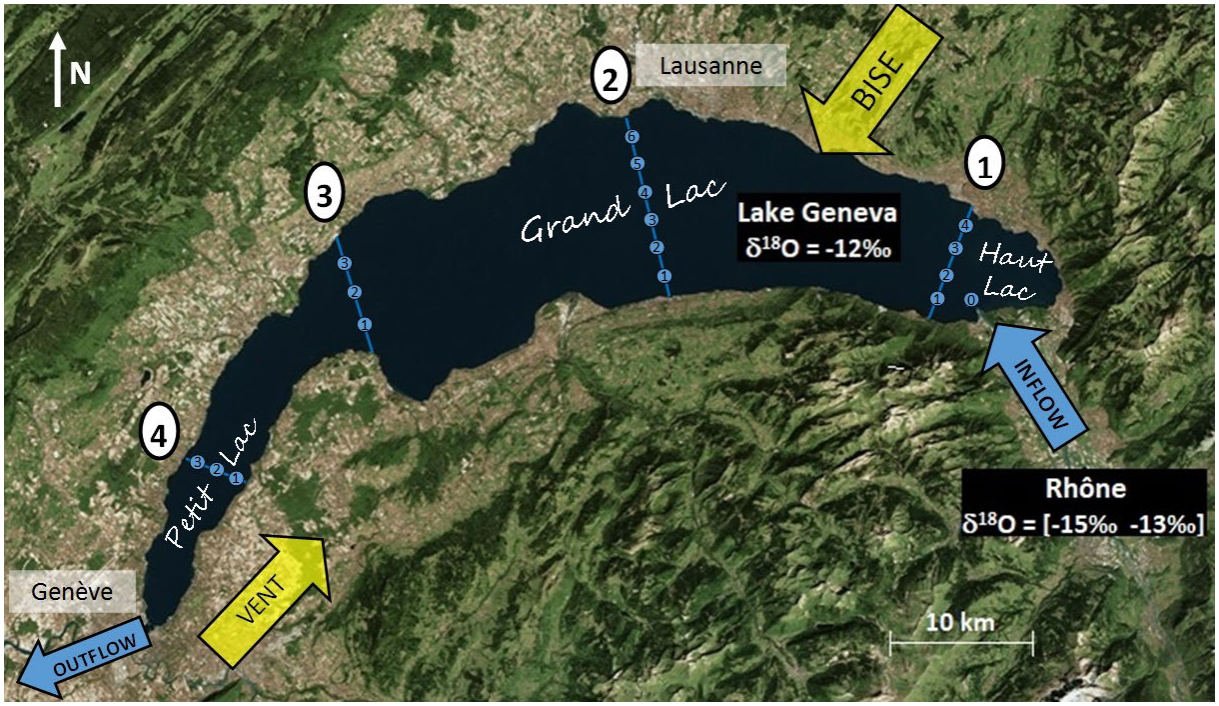

Figure 1-1: Lake Geneva aerial view. Locations of the Rhône River inflow and outflow (blue arrows) and the direction of the two main winds of the region (yellow arrows) are indicated. Blue dots represent the locations of the sampling campaign 2015–2016 along four cross-sections.

The sampling points were chosen to determine the location of the Rhône interflow in different parts of the lake. Sixteen depth profiles were sampled in four cross-sections covering the lake's length and width (Figure 1-1) in order to examine the modelled existence of four major gyres within the lake. The different locations are named by the number of the profile of the section they belong to. For example, the point 2-4 corresponds to the fourth profile of the second section. The first cross-section was located between Montreux and Saint-Gingolph in the Haut-Lac, the upstream part of the lake. Four points make up this cross-section including 1-2 located 4 km from the Rhône River mouth above the Rhône's canyon. The second cross-section was located in the middle of the Grand-Lac between Lausanne and Evian where the lake is the widest. Six points compose this section including SHL2 (2-3), the reference point for CIPEL's historical monitoring (Commission Internationale pour la Protection des Eaux du Léman) with the maximum depth (309 m). This cross-section was selected to determine the impact of the common central anticlockwise gyre on the path of the Rhône interflow. The third one is situated at the boundary between the Grand-Lac and the Petit-Lac where the bathymetry changes

from 300 m to 70 m. Three points cover this section. The fourth one is located in the middle of the Petit-Lac and made up of three points including GE3 (4-2) monitored by the Canton of Geneva. GE3 is 12 km upstream of the Rhône outlet in Geneva.

Table 1-1: Wind conditions during the month before the campaigns and Rhône and Lake's conditions during the campaigns.

Campaigns	Lake stratification (range of local stability N^2)	$Q_{Rhône}$	$T_{Rhône}$	Prevailing winds
June 2015	Strong (1.3E-3 - 7.3E-3 s^{-2})	320 m^3/s	10°C	Lake breeze: 1-3 m/s
August 2015	Strong (1.9E-3 – 6E-3 s^{-2})	270 m^3/s	10°C	Lake breeze: 1-2 m/s Bise (N-NE): 2-3 m/s
October 2015	Weakened (8.1E-6 – 1.8E-3 s^{-2})	140 m^3/s	8°C	Lake breeze: 1-4 m/s
July 2016	Strong (3.3E-4 – 4.9E-3 s^{-2})	300 m^3/s	10°C	Lake breeze: 1-3 m/s

The calendar of sampling campaigns (Table 1-1) was established in order to cover one year and sample at different seasons and hence at different thermal conditions of the lake. In this study, only the period of the year when the lake presents a thermal stratification and when the Rhône interflow is detected in the metalimnion is discussed. A total of 864 samples were collected during four distinct campaigns. Details on coordinates and sampling dates of the different profiles can be found in the Appendix I-1. Note that the July campaign corresponds to year 2016 whereas the June, August and October campaigns refer to 2015. As such, no interpretation can be done on transport continuum processes between the July campaign and the others.

The sampling campaigns were carried out using "La Licorne", the boat of the Institute F.-A. Forel of the University of Geneva that is equipped with a crane and an automatic Rosette water sampler (1018 Mini Rosette Sampling System, General Oceanics Inc.). The Rosette consists of 11 Niskin bottles (1.7 L), and was coupled to a CTD (conductivity-temperature-depth) probe (OCEAN SEVEN 316Plus CTD, IDRONAUT Srl), which was externally powered via a telemetry cable to provide real-time information on electrical conductivity, oxygen, pH, temperature and depth (pressure). A continuous CTD cast without interruptions was taken while lowering the sampling system and water samples were taken when raising the system. The data of the continuous CTD cast were used in order to determine the thermal conditions of the water column. The depths of

sampling were then chosen to determine the isotope composition of layers of different density. A sample was taken at each variation of 1 °C in the water column. Because the interflow was detected in the metalimnion (Halder et al., 2013), we sampled in more detail the layer around the thermocline. CTD data were additionally saved when the water samples were taken. The sensors accuracy, according to the manufacture, is 0.003 mS/cm for conductivity, for temperature 0.003 °C, for pressure 0.05 %, for pH 0.001 units, and for oxygen 0.01 ppm. Conductivity [κ25] is given relative to 25 °C in the result section. Physical data were processed by REDAS-5 Release 5.40 (IDRONAUT Srl). Water samples were filtered with 0.45 µm nylon filters using a peristaltic pump within days of the sampling in the laboratory. Thirty millilitres of the filtered water was stored without headspace in brown glass bottles with polyethylene-lined conical screw caps in a refrigerator at about 7 °C until measurement.

Concerning the spatial uncertainties, the drift between the theoretical and the real sampling locations was evaluated by GPS. To solve this problem and minimise the error, two rules were established. First, sampling campaigns were cancelled if the wind speed was superior to 25 m/s. Secondly, if the drift was superior to 200 m during the sampling, the profiles were repeated. An entire campaign to cover the sixteen profiles lasted for a maximum of five days. The maximum time to measure and sample a profile was one hour, in the middle of the lake where the maximum depth is recorded. Considering that the sampling was carried out during periods with moderate wind, the conditions of circulation of the lake as established gyres is expected to be stable during the campaigns and the results can be considered as quasi-synoptic. An exception is given for the July 2016 campaign where a wind event occurred between the 4th and the 6th of July.

All the CTD data and the stable isotope composition of the lake water samples collected during the four campaigns are available in Appendix I-3.

2.2. Analysis

The oxygen and hydrogen isotope compositions were analysed using a Picarro L2140i, Wavelength-Scanned Cavity Ring-Down Spectroscopy (WS-CRDS) system. For the analysis of the stable isotope compositions of water, approximately 1.7 mL of filtered water is filled into small glass vials closed with a septum screw cap. Each sample was injected eight times and an average of the last five measurements was taken to calculate the raw value. Each sequence is calibrated using three different internal standards

(ANZO, EMEB and SAAS) that were themselves calibrated against standards provided by the IAEA (International Atomic Energy Agency - VSMOW defined as 0 ‰ with VSLAP being -55.0 ‰ for $\delta^{18}O$ and 0 and -428 ‰ for $\delta^{2}H$ values; Coplen, 1996). Isotopic compositions measured are reported in the common delta-units (in permil) that represents the deviation of the isotope ratio of the sample relative to that of the international standard VSMOW (Vienna Standard Mean Ocean Water). The standard deviation of all repeated measurements of the standards and samples was better than ± 0.05 ‰ for $\delta^{18}O$ and ±0.4 ‰ for $\delta^{2}H$ values.

2.3. Calculations

A mixing model is used to calculate Rhône water fraction for each sampling location. This mixing model is based on an atomic mass balance such that:

$$\delta^{18}O_R \bullet x_R + \delta^{18}O_L \bullet x_L = \delta^{18}O_S \quad (1)$$

where $\delta^{18}O_R$ is the isotopic value of the Rhône River water. This parameter is measured once a month proportionally to the discharge by OFEV at the station Porte du Scex located 5 km upstream of the lake (Figure 1-2). x_R is the mole fraction of the Rhône water at the sampling location in the lake. $\delta^{18}O_L$ is the value of the overall mixed, unstratified lake water that is, for example, homogeneous over the whole lake after a complete overturn. This value is constant at -12.1 ‰ for $\delta^{18}O$. x_L is the mole fraction of lake water at the sampling location. $\delta^{18}O_S$ is the isotopic composition of the water at the sampling location.

Given that $x_R + x_L = 1$, the mole fraction of Rhône water at the sampling location is calculated by:

$$x_R = (\delta^{18}O_S - \delta^{18}O_L) / (\delta^{18}O_R - \delta^{18}O_L) \quad (2)$$

The value of the isotopic composition of the Rhône River water, $\delta^{18}O_R$, is determined for each campaign by the discharge-weighted average of the OFEV measurements of the last months since the stratification onset (it corresponds to the period when the Rhône

was flowing in the metalimnion). The consequent uncertainties on the Rhône fractions estimated by this method will be discussed below (Table 1-2).

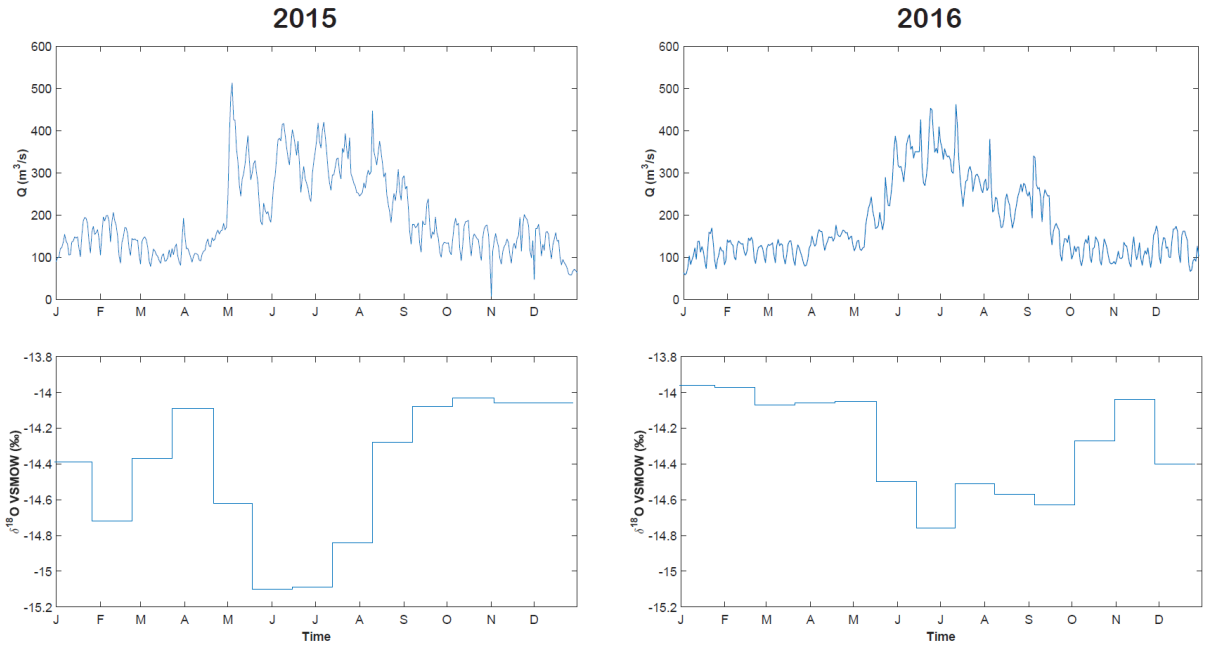

Figure 1-2: Oxygen isotope composition and daily averaged discharge of the Rhône River water during the years 2015 and 2016. Average delta values are proportional to the discharge. Isotopic composition and discharge data from OFEV/NADUF from the measurement station of Porte du Scex located 5 km upstream from the river mouth to Lake Geneva.

The uncertainty on the Rhône fraction coming from the analytic error of $\delta^{18}O_S$ (±0.05 ‰) is evaluated to ± 2 %. It is much smaller than the uncertainty linked to the seasonal variation of $\delta^{18}O_R$ (Table 1-2). Finally, the Rhône River water fractions are calculated for all the cross-sections using linear interpolation with MATLAB.

Table 1-2: Uncertainty on Rhône fractions linked to the seasonal variation of the isotopic composition of the Rhône.

Campaigns	**Months since stratification**	**$\delta^{18}O_R$ range values (‰) [min ; average ; max]**	**Uncertainties [%min ; %max]**
June 2015	4 months [03-06]	[-15.10 ; -14.74 ; -14.09]	[12.2 ; 32.4]
August 2015	6 months [03-08]	[-15.10 ; -14.75 ; -14.09]	[11.6 ; 33.2]
October 2015	8 months [03-10]	[-15.10 ; -14.64 ; -14.03]	[15.2 ; 31.8]
July 2016	4 months [03-06]	[-14.76 ; -14.46 ; -14.05]	[11.5 ; 20.8]

The software Lake Analyser (Read et al., 2011) was used to estimate the stratification strength (as measured by the Brunt-Väisälä buoyancy frequency: N^2), the thermocline depth, and the thickness of the metalimnion. To determine the upper and lower limits of

this layer, a semi-automatic approach was used. The threshold of density gradient was set to 0.005 $kg.m^{-3}.m^{-1}$ for the October campaign with the lower density gradient in order to fit with a visual estimation of the metalimnion bounds. Given the relation between the temperature of the water and its density, a factor was applied to determine the threshold used for the others campaigns. For example, for the August and July campaigns, the range of water column temperatures was from 5 to 22°C and so the factor was calculated as:

$$\alpha_{August} = [density(22°C) - density\ (5°C)] / (22 - 5) \quad (3)$$

$$\alpha_{October} = [density(13°C) - density\ (5°C)] / (13 - 5) \quad (4)$$

The ratio of α_{August} and $\alpha_{October}$ was applied to the threshold of October to determine the one of August. Therefore, the following values were retained to determine the metalimnion bounds for the different campaigns: 0.008 kg m^{-3} m^{-1} for June and 0.01 kg m^{-3} m^{-1} for August and July. Because of some occasional breakdowns in temperature profiles that could falsify the metalimnion limits calculation, a visual checking and adjustment was effected.

After all, the fractions of Rhône water in the metalimnion were calculated by averaging the interpolated values of Rhône fraction in between the average of metalimnion limits of each section.

2.4. Uncertainties and limits of the method

Considering the objective of relating the isotopic compositions of the water in the lake to the hydrodynamics of the lake circulation, it is important to note that the stable isotope compositions of water do not provide direct information on the particle ages. Even though there is a typical seasonal variation associated with the isotopic variations measured in the Rhône water (Fig. 1-2), the variable flow rates, hydro-electric schemes and including also daily variations make this seasonality difficult to detect in the Rhône water interflow though. As shown by the 3D simulations of Cimatoribus et al. (2019), "the spatial particle patterns result from the accumulation of particles having different ages". As such, the results of Rhône River fraction shown in this study represent an integral "time-signal" only, representing a cumulative history of fluid flow at any one point of sampling only. The hypotheses concerning the processes in charge of the spatial distribution are hence compared to the current circulation models for validation.

Moreover, this absence of particle age induces non negligible uncertainties on the choice of the Rhône's exact isotope composition at the time that the fractions of Rhône River water to the interflow are calculated. As illustrated in Figure 1-2, the isotopic composition of the Rhône water is varying seasonally. Time-based sampling of the Rhône water at Porte du Scex (5 km upstream the lake) during winter, spring and summer, showed important hourly variations of the isotope composition by several tenths of a permil (Figure 1-3).

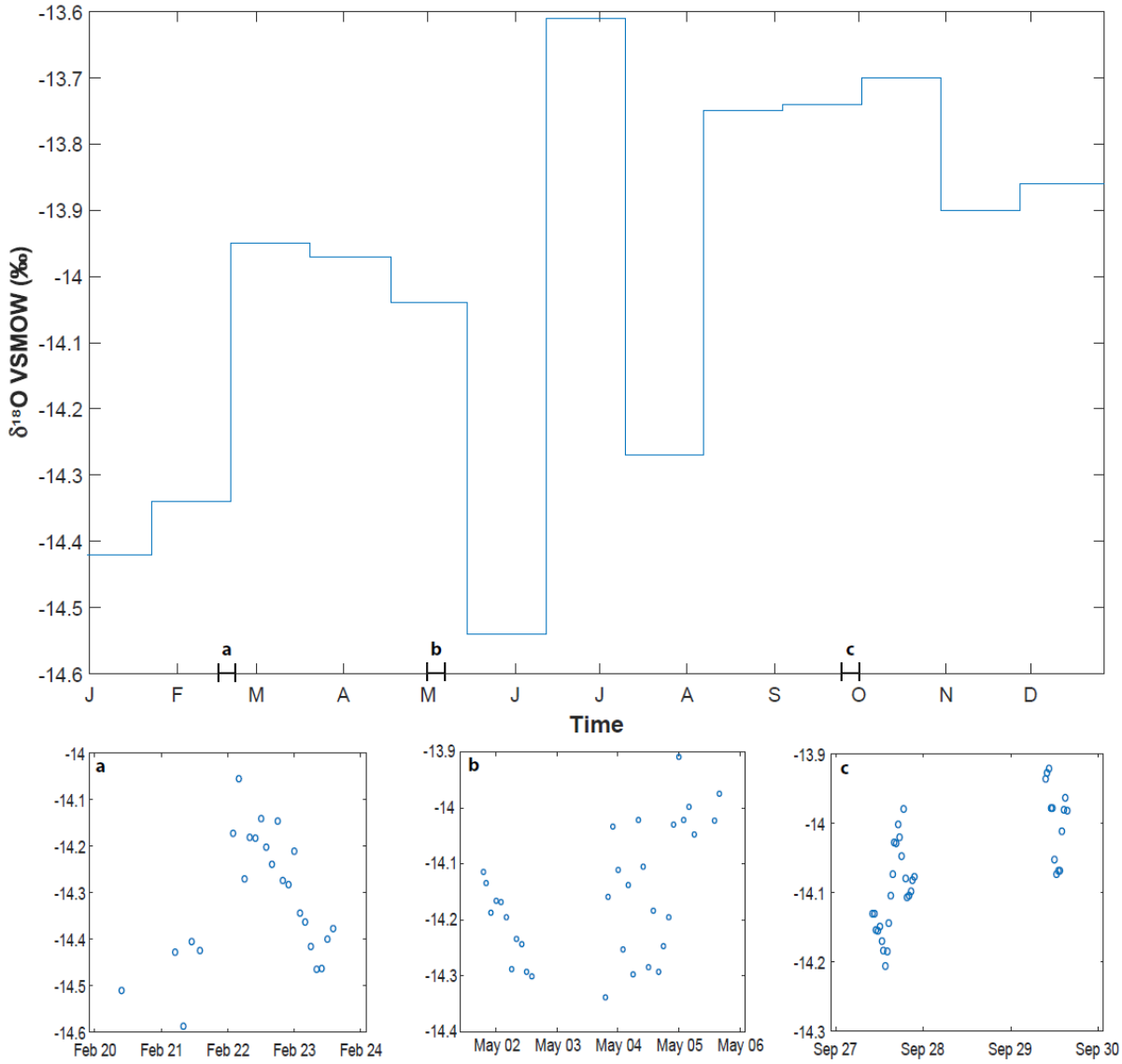

Figure 1-3: Oxygen isotope composition of the Rhône measured at the station Porte du Scex. Graph above: monthly average data of year 2017. Graphs below: hourly variations during February, May and September 2017.

These variations can be explained by the important range of isotope composition of the different water inputs to the Rhône in its Upper catchment (Appendix V). Given these

short-term variations and the larger seasonal variations, the isotopic composition of the Rhône's water is estimated as the discharge-weighted average of the months during which the stratification of the lake occurs. These variations, together with the smaller daily variations observed are incorporated as an error uncertainty on the calculated Rhône River fraction.

3. Results

Figure 1-4 and 1-5 compile all the cross-sections obtained during the four campaigns with the contoured variations of the temperature and the Rhône water fraction respectively, calculated by linear interpolation. In some profiles the Rhône River water fraction relative to the lake is lower than 0 %. This means that the lake water is enriched in heavy isotopes compared to its average composition of -12.1 ‰ for $\delta^{18}O$. This is due to direct inputs of summer precipitation and due to a small evaporative loss during the warmer months. In this section, the results are first described according to the vertical and horizontal dispersion of the Rhône water during the different seasons. The Rhône River fractions calculated for the metalimnion (Table 1-3) are presented to illustrate how the Rhône River can be transported as an interflow in this specific layer of the lake.

3.1. Vertical dispersion

It is known from the work of Halder et al. (2013) that the Rhône River can circulate as an interflow within the lake during the season of thermal stratification of the lake. CTD profiles show that during the four campaigns, the lake was stratified in temperature and hence also density, in contrast to the winter months during which the water column is homogenous in the depth range of the winter mixing. During these four campaigns carried out during summer and early fall, we can observe a metalimnion enriched in Rhône water. This specific layer varies in thickness and depth during the year.

In June 2015, the stratification was weak and the epilimnion not yet well defined. In the Haut-Lac, in cross-section 1, several layers containing Rhône water between 0 and 30 m are recognized. In section 2, as the stratification is not homogenous in all of the profiles sampled, the interflow does not have the same depth and thickness. Close to the north shore of the lake, the metalimnion is about 15 m thick and located between the surface and 17 m depth whereas in the middle of the lake, in profile 2-3, it is 5 m thick at a depth between 6 and 11 m. The thickness of the metalimnion and its depth are related to the thermal gradient that is first relatively weak and then steepens with increased stratification (Appendix I-2).

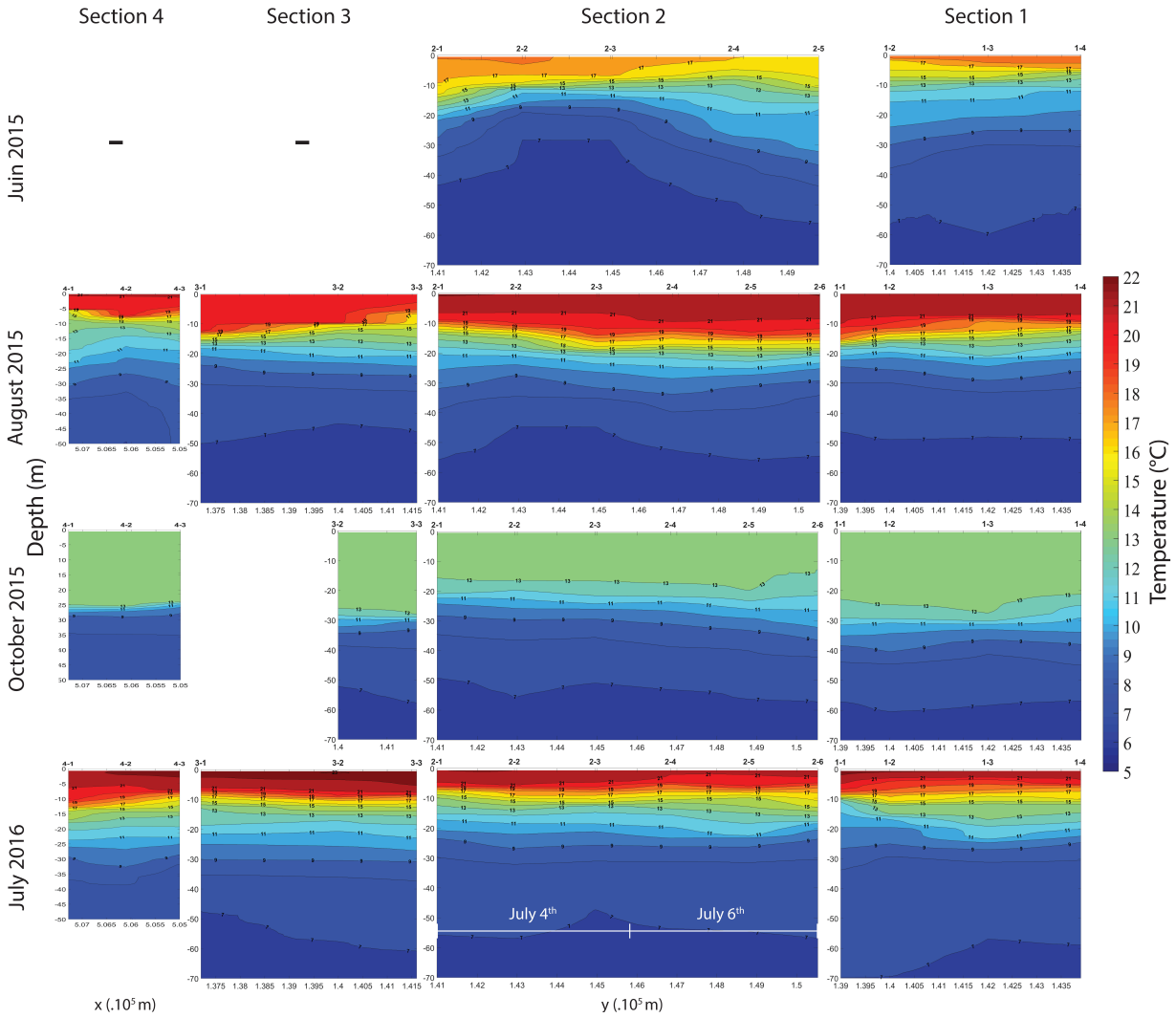

Figure 1-4: Temperature along cross-sections. Contoured variations of temperature within the first 70 m below surface, along four cross-sections (see Fig.1-1) in four seasons. The x-axis presents the position according to the Swiss coordinate system. The diagrams were established using "linear" as the method of interpolation.

The same behaviour can be noted in August 2015 in section 2 with a widening and a reduction of the width of the thermocline at the location 143 000 and 147 000 respectively (Y Swiss coordinate system), as well as in July 2016, same section, with a tightening and a widening at the location 143 000 and 149 000 respectively. This tightness of the isotherms in the middle of the lake seems to have an influence on the Rhône interflow: it is thinner where the isotherms are closely spaced.

In August 2015, the layer containing between 10 to 40 % of Rhône River water in the Grand-Lac is located at between 10 and 20 m depth. This interflow of Rhône River water follows the thermocline located at around 15 m depth in this part of the lake. It is also important to note that no isotopic anomaly related to the concentrated inflow of the Rhône River is detected in the epilmnion nor in the hypolimnion, except for the profile

number 1-4. The same pattern is observed in July 2016 with a strong thermal stratification and a thin interflow.

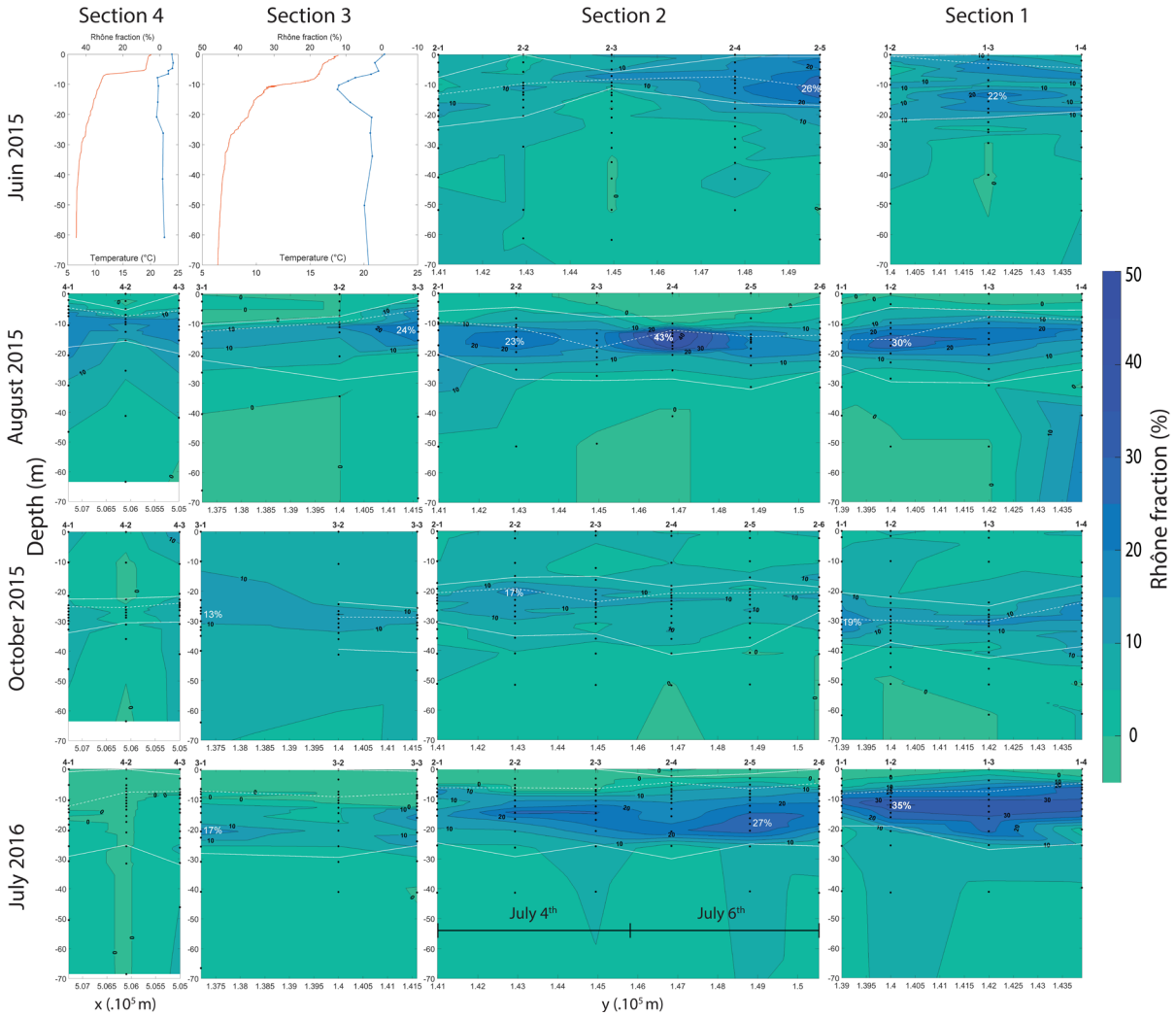

Figure 1-5: Rhône fractions along cross-sections. Contoured variations of Rhône fractions within the first 70 m below surface, along four cross-sections (see Fig.1-1) in four seasons. The black dots indicate the location of sampling points, whereas the x-axis presents the position according to the Swiss coordinate system. The diagrams were established using "linear" as the method of interpolation. The white dotted lines represent the depth of the thermocline. The white full lines represent the limits of the metalimnion. In June 2015, only profiles 3-2 and 4-2 were sampled in sections 3 and 4.

In October, when the stratification is weakened and the thermocline is deeper, the interflow is also deeper, that is at a depth of between 20 and 40 m in the Grand-Lac. While the thickness of the interflow is larger compared to June/August, it is also less concentrated in Rhône River water. It is also to be noted that in all the sections, two months after the August campaign the 10-20 m layer with up to 10-40 % of Rhône water has disappeared. In sections 1 and 2, the 0-20 m layer corresponding to the actual

epilimnion contained more than 90 % of lake water. In section 3 and 4, the epilimnion can still contain more than 10 % of Rhône water.

3.2. Horizontal dispersion

During summer and early autumn, all the metalimnion is influenced by Rhône water. All sections covering the width of the lake contain Rhône water. However, it is not distributed homogeneously. Some parts of the metalimnion are more concentrated in Rhône water than others. For example, in August and July, in the section closest to the Rhône delta, the metalimnion is more concentrated with about 30 % of a direct Rhône River contribution (profile 1-2) towards the centre of the section. In October, the pattern is less clear. Different parts of the same section have more than about 15 % of Rhône water within the metalimnion.

Section 2 shows different concentration patterns and could thus indicate preferential paths of the interflow, not necessarily the same from one month to the next, even though the depth remains fairly homogeneous. For June, August, and July 6th, the northern parts of the sections in the Grand-Lac indicate the highest concentration of Rhône River water. In contrast, during the October and July 4th campaigns, the highest concentrations were towards the southern ends of the sections. In August 2015, there are even two distinct locations along the same central section: one located in the northern part, measured at profile 2-4 with a maximum concentration of 43 % at 13.4 m depth and the other, in the southern part, at profile 2-2, with a maximum concentration of 23 % at 14.7 m depth. These two are clearly distinguished from the other profiles that have lower concentrations of Rhône water (2-1, 2-3 and 2-6). In July, there are also two distinct interflows with more than 20 % of Rhône water in separate parts of the section but at different dates and depths: in July 4th the southern interflow seems to be located at 14.6 m depth whereas the July 6th one in the northern part is at 19 m.

In section 3, in the area between the Petit and the Grand-Lac, the apparent preferential flow paths of the Rhône interflow are more variable. In August, the Rhône has a higher contribution close to the northern shore whereas during the October and July campaigns, it is present more towards the southern shore.

In the Petit-Lac, the interflow of Rhône water is less concentrated: it does not rise to more than 20 %. In this part of the lake, the Rhône water interflow appears to concentrate mainly close to the shores.

4. Discussion

4.1. Impact of the stratification

During the lake stratification period, the Rhône River is colder and hence denser than the lake's surface water. Initially it plunges and follows the lakebed as an underflow. Subsequently, depending on its density, different behaviours can occur. During episodic high discharge, when the Rhône transports important amounts of sediment, it will continue to the deeper part of the lake as an underflow (Loizeau and Dominik, 2000). Otherwise, intrusion will occur when the river and the lake equilibrate their density after progressive mixing as well as sediment loss resulting from a decreased flow of the river incursion. During the stratification period, the Rhône inflow intrudes in the metalimnion as it is colder than the epilimnion and warmer than the hypolimnion.

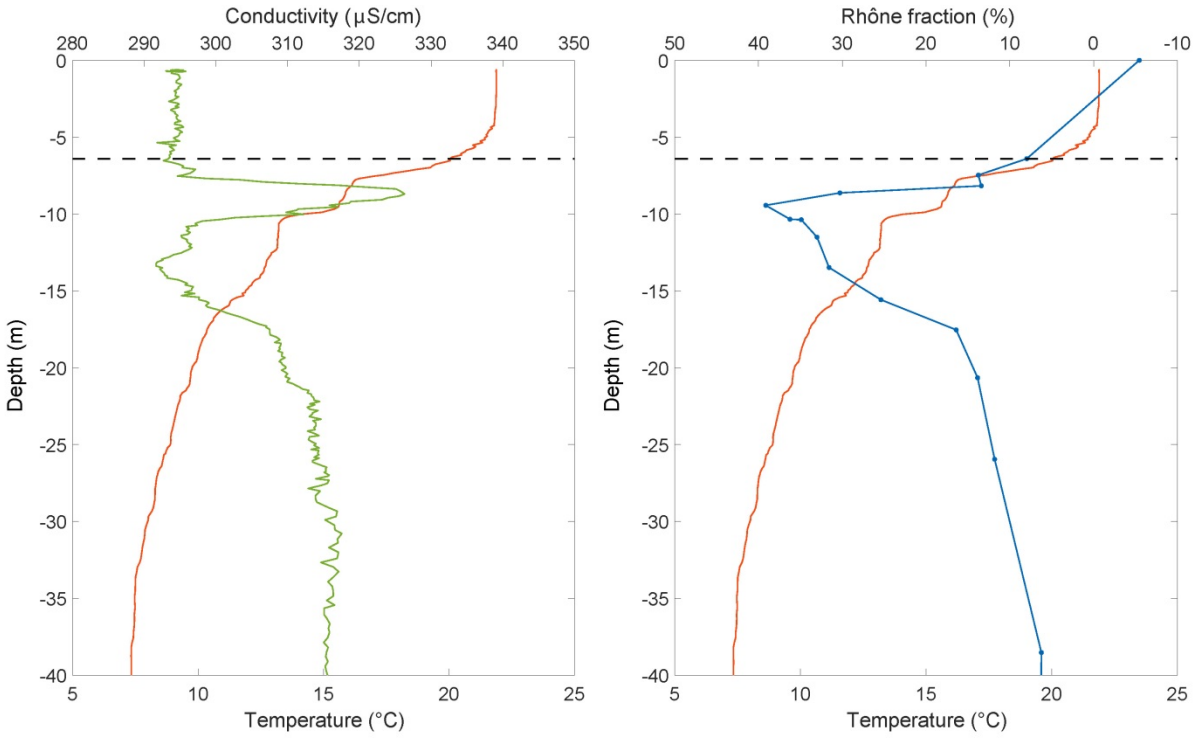

Figure 1-6: Profile 0, measured in July 2016, one km in front of the Rhône River mouth. In orange, the temperature profile. In green, the conductivity profile. In blue, the Rhône fraction profile. In black dotted line, the thermocline depth.

In Figure 1-6, in profile 0, taken 1 km in front of the Rhône River mouth, a skewed distribution of the Rhône interflow water within the lake is detected based on the conductivity measurements, but also the isotopic composition. In the upper part of the interflow, at 8 m depth, the interflow water is constrained by the thermocline above,

whereas in the lower part of the metalimnion the concentration of Rhône water is progressively decreasing. This suggests that the Rhône inflow descends below the thermocline depth when it enters. Thereafter it intrudes the water column and rises toward the thermocline where it is blocked from a further rise. Because of equal buoyancy, the interflow afterwards follows this depth of maximum local stability (the thermocline depth) throughout the Lake Geneva basin as this same distribution can be observed in other parts of the lake. However, for example in August 2015 (profiles 1-2, 2-3, 3-2), the interflow depth pattern may fluctuate depending on the thermocline depth (e.g., Halder et al., 2013). In the Haut-Lac, the maximum of Rhône water concentration is noted at 17 m depth. In the middle of the Grand-Lac, it is at 15 m. And finally, it is flowing at 11 m depth just before the Petit-Lac. This is probably due to the progressive sedimentation of the finest particles of the interflow (e.g., Giovanoli, 1990) and/or related to wind-induced surface water circulation and internal waves (see below).

On the basis of the calculations of the Rhône River interflow water fractions in the metalimnion (Table 1-3), it can be argued that the strength of the stratification has a direct control on the concentration of the Rhône River water in the interflow. The higher the local stability is (steepest thermocline), the higher will be the concentration of Rhône River water in the interflow. A strong stratification, such as in August 2015 and July 2016, will limit the vertical distribution. In fact, almost no Rhône River water is detected during these periods in the epi- and hypolimnion. As shown also by the simulations of Cimatoribus et al. (2019), this will accentuate the horizontal advection by the wind driven circulation and reduce the vertical dispersion.

Table 1-3: Rhône interflow water fractions calculated in the metalimnion and the local stability of the water column averaged on each section in brackets.

Campaigns	Section 1	Section 2	Section 3	Section 4
June 2015	13 % (2.4E-3 s^{-2})	12 % (2.0E-3 s^{-2})	-	-
August 2015	14 % (3.4E-3 s^{-2})	13 % (2.8E-3 s^{-2})	8 % (4.3E-3 s^{-2})	11 % (4.7E-3 s^{-2})
October 2015	10 % (7.3E-4 s^{-2})	8 % (5.3E-4 s^{-2})	10 % (1.1E-3 s^{-2})	5 % (1.1E-3 s^{-2})
July 2016	18 % (3.1E-3 s^{-2})	12 % (2.6E-3 s^{-2})	5 % (3.2E-3 s^{-2})	1 % (3.7E-3 s^{-2})

This trend is emphasized by the observation that the most intense stratification period (July, August and September) is preceded by the period of highest discharges (June and

July) with the highest concentration of Rhône water flowing into the metalimnion and hence the interflow.

In October, while the stratification is weakening, the Rhône River water mixes more diffusely. The Rhône River water H- and O-isotope composition also approaches that of the average lake (approximately 30 % closer: from -15 ‰ to -14 ‰ with a lake at -12 ‰) and its discharge is decreasing. The interflow amplitude hence decreases and the distribution flattens towards the deeper lake. During autumn cooling, the metalimnion becomes gradually thicker. The temperature of the Rhône is also lowering and consequently the Rhône interflow plunges towards deeper parts of the lake, together with the metalimnion widening. At the same time, the concentrated layer observed between 10 and 20 m depth in August has been continuously mixed with the lake water with the weakening of the thermal stratification during autumn.

The coupled effect of lake stratification and wind stress can induce thermocline tilting. During summer, when the lake is thermally stratified, the thermocline acts as a preferential plane for the generation and evolution of internal waves (e.g., Bouffard and Lemmin, 2013). These long internal waves, also called internal seiches, can provoke an oscillation of the thermocline, notably during calmer periods following storm events (e.g., Lemmin et al., 2005). The present results indicate that these changes in the thermocline depth also control the interflow depth of the Rhône River water. Moreover, the tightening and the widening of the isotherms create a concentration and a dilution of the Rhône River interflow, respectively. This behaviour is more evident during a strong stratification period, as has been noted during our August and July sampling campaigns, when the thermocline needs less energy to be oscillated.

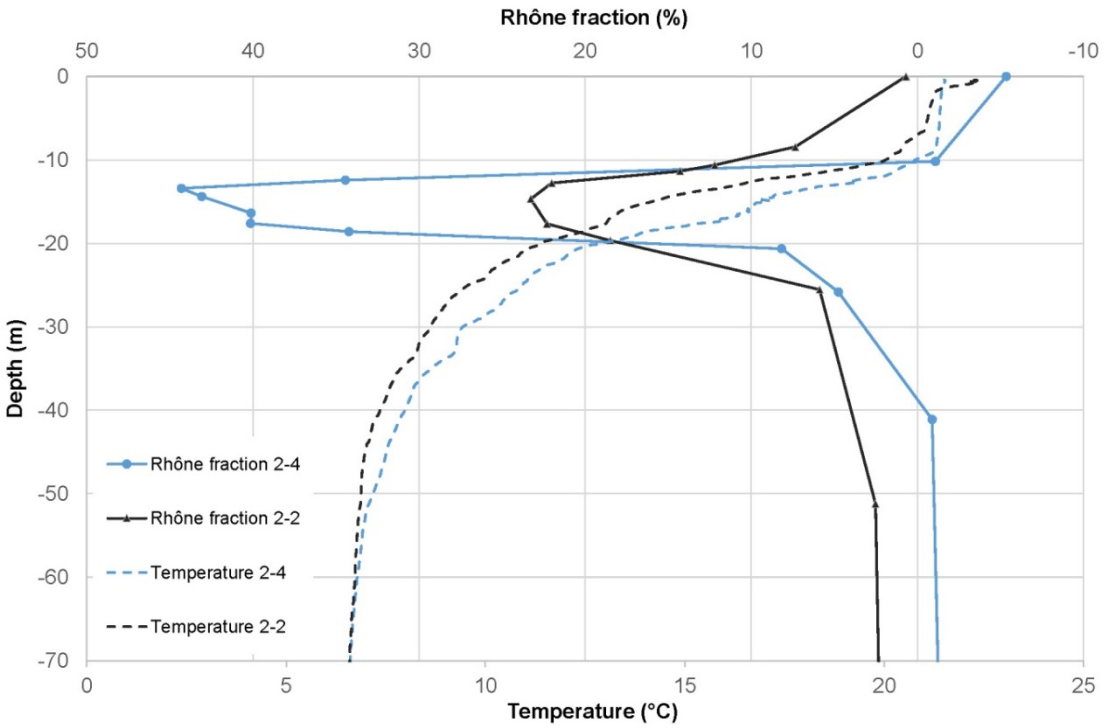

Figure 1-7: Comparison of two Rhône fraction profiles and temperature profiles of section 2 in August 2015: one (2-2) with a normal distribution, the other (2-4) with a skewed distribution.

For example, in section 2 sampled during August, the thermocline appears to be higher close the southern shore (profile 2-1 and 2-2) and the isotherms less closely spaced compared to the rest of the section. The thermal structure hence has an impact on the vertical dispersion of the interflow. As we can see in Figure 1-7, the block effect of the thermocline, well visible in profile 2-4 with a downward skewed distribution of the Rhône water, is perturbed by the higher spacing of the isotherms in profile 2-2 with an almost normal distribution (upward and downward distribution). This can be caused directly by the wind or by the propagation of internal seiches following a wind event.

Downwelling can also occur with wind forcing or internal waves as suggested by Lemmin et al. (2005). For example, in section 3 in August, an important tilting of the thermocline on the North-South axis can be observed with a subsequent higher vertical dispersion of the interflow in the northern part. This could be related to the wind or the passage of a Kelvin wave as previously described for this part of the basin by Bouffard et al. (2013). Thus, the wind induced tilting of the thermocline and internal waves also control the vertical dispersion of the Rhône interflow in the water column of the lake.

4.2. Impact of the gyres

Le Léman as a large lake presents different cyclonic and anticyclonic circulations. This gyral pattern has a strong impact on the residence time and the spatial distribution of water, nutrients and pollutants. Cimatoribus et al. (2019) illustrated "rapid transit" trajectories followed by simulated Rhône particles during the stratification period. They confirmed the presence of a consistent cyclonic gyre in the eastern central part of the Grand-Lac (Lemmin and d'Adamo, 1996). It implies a rapid westward transport from the Rhône River mouth along the northern near-shore region due to the Coriolis force. Instead of this unique large gyre, two gyres can be established with an eastern anticyclonic one bringing the Rhône River water along the southern shore and a western cyclonic one forcing the particles to cross over to the northern shore. These large gyres are highly variable in time and can break down into smaller ones inducing the spreading of the particles in the central lake area. In the Petit-Lac, models confirmed the current pattern reported by Betant and Perrenoud (1932) of a westward transport along the northern shore and a backward transport to the west along the southern shore.

Below, our measurements of the location of the Rhône River interflow within different sections of the lake are compared to those expected for the Rhône River dispersion based on the current knowledge and models for the water transport and circulation such as summarized in the work of Le Thi et al. (2012) and Cimatoribus et al. (2019).

First, some sections where no specific effects of gyres are observed can be identified. For example, in August and July, in the first section, the Rhône seems to be more concentrated in front of its mouth (profile 1-2) and homogeneously dispersed in other parts of the metalimnion. This could suggest that circulation was weak at this time in this part of the lake, allowing the Rhône to disperse itself horizontally in a uniform way.

In contrast though, most of the sections present preferential pathways characterized by horizontal dispersion heterogeneities as shown by the 3D transport models for Lake Geneva (Cimatoribus et al., 2019). In October, still in the Haut-Lac, different horizontal positions of the interflow and a higher proportion of Rhône River water detected along the southern shore are in agreement with an anticyclonic gyre in this part of the basin. In August, in the second section, the two obvious isotopic anomalies identifying the Rhône interflow support preferential paths of water transport as a consequence of a large cyclonic gyre towards the middle of the lake. This gyre transports the incoming Rhône

water westwards along the northern shore and induces a backflow eastwards along the southern shore (e.g., Lemmin and d'Adamo, 1996; Cimatoribus et al., 2019). The "backflow" part is hence less concentrated in the interflow component because of a longer travel path and hence larger entrainment of ambient lake water into the interflow. In the same section, an intermediate, transitional pathway may also be noted between the two stronger interflows. This may correspond to residual Rhône water from an older gyre or a brief perturbation of the present gyre through a change in the wind forcing.

A preferential pathway toward the northern shore is noted for July 6th and the June campaigns. Furthermore, a peculiar temperature profile was measured for section 2 in June: an upwelling of the thermocline accompanied by a tightening of the isotherms in profile 2-2 and 2-3 is noted. Such a "domed" thermocline in the middle of the lake can be due to a steady cyclonic gyre that disperses the surface water to the shores as suggested by Schwab et al. (1995). This kind of behaviour seems to have a direct impact on the Rhône water dispersion with a small upwelled interflow in the central part and a thicker one in the northern zone.

At the interface between the two basins different pathways can occur, but the transport via the gyres restrains the water to stay close to the shores. Afterward, it seems to depend on the gyre's sense of rotation that is regularly changing in this area (Le Thi et al., 2012).

In the Petit-Lac, the concentrations of Rhône interflow water do not reach more than 20 %. This is partly due to the morphologic difference between the two basins, as well as the result of the recirculation processes by the gyres in the Grand-Lac. When the water finally enters the Petit-Lac, it may circulate close to the shore, given an established cyclonic gyre that is common in this basin (Le Thi et al., 2012) and that disperses the surface water on the sides of this narrower basin.

4.3. Specific cases

July 2016 section 2

During this campaign, two interflows at different depths can be noted: one at 20 m depth close to the northern shore presenting a skewed distribution upward, and a thinner interflow blocked by the thermocline at 10 m on the southern part. This phenomenon can be explained either by the effect of a cyclonic gyre creating an interflow and a backflow

combined with a wind induced tilting of the thermocline with a downwelling effect of the northern interflow. Or it is the same and unique interflow shifted by a wind event from south to north between July 4th and July 6th, which at the same time is still descending through the water column.

October 2015 section 4

These vertical and horizontal heterogeneities noted during this campaign can be multifactorial. The presence of Rhône interflow water in the epilimnion can be explained by stronger winds in autumn able to mix the epi- and metalimnion water. The same pattern can be noted in the other sections for the same month, especially in section 3. It can also be due to the cyclonic gyre usually turning in the Petit-Lac causing the near shore dispersion of the water masses.

5. Conclusion and outlook

The new data presented here confirm that measurements of the stable isotope compositions of the lake water in depth profiles can trace the Rhône River interflow within Lake Geneva. Different sections of the lake sampled on different time-scales of days and up to months or several months apart suggest important spatiotemporal heterogeneities of the Rhône River water dispersion. The current models that calculate the circulation patterns and the dispersion of the Rhône River water within the lake can be used as a basis to interpret the measured positioning of the interflow in space and time. During the stratification period of the lake, the Rhône River is intruding in the metalimnion as an interflow and it is horizontally directed by the gyral circulations of the lake. As the gyral circulation patterns change with the prevailing meteorological conditions, so will the relative positioning of the interflow. The stronger the thermal stratification is and the longer the gyral circulation pattern remains unchanged, the more concentrated and vertically constrained will be the interflow. Well established gyres may also lead to two interflow isotopic anomalies measured in the same section at any one time. If the two anomalies are found at different depths this may be related to wind induced thermocline's inclination or gyral circulation effect. Relative differences in the concentration of the Rhône interflow water contribution in the sections may thus also

provide relative temporal information on the circulation. However, a lack of exact temporal information on the Rhône water interflow limits a more direct coupling of isotopic composition and the particle flow path modelling for water. Numerical modelling of Rhône interflow water as a function of the changing meteorological conditions can thus predict where and at what concentration the interflow may exist. Such a prediction could then be validated by a detailed "event-based" sampling campaign for isotopic measurements. As a corollary, the isotopic measurements can help to validate the hydrodynamic model with real data on the Rhône River dispersion.

A better understanding of the mixing processes and the general circulation patterns of the Rhône River interflow is of importance for interpretations of the nutrient cycle within the lake as well as the potential dispersion of dissolved pollutants (including micropollutants) introduced by the water of the Rhône River. The potential of combining measurements of pollutants within the lake with stable isotope measurements of the lake waters in order to determine the origin and hence dispersion of the pollutants has already been demonstrated by the studies of Bonvin et al. (2011) and Halder et al. (2014). Moreover, the key role of the Rhône water interflow on the nutrient cycle of the lake was also demonstrated by Bouffard and Perga (2016) and Nouchi et al. (2018). In the context of the re-oligotrophication of the lake, it would be pertinent to evaluate if the Rhône's nutrients are introduced into the photic zone principally through the influence of the interflow and how and if such an introduction may also influence the variations in the primary productivity of the lake.

Acknowledgements

A special Thank You to Philippe Arpagaus who piloted the Licorne with precision and shared his passion for the lake. Thank you also to all the sailors who helped me with the sampling: Mickael, Laetitia Monbaron, Lucie Michel, Louis Bridoux, Anaël Lehmann, Zoneibe Luz, Stéphane Mahé and Elfie Swerts. As well as to the Federal Office for the Environment of Switzerland (OFEV) that provided long term isotopic compositions of the Rhône River and precipitation from the Swiss Isotopic Network (ISOT) module of OFEV.

References

Balvay, G., Ishiguro, N., 2003. L'écoulement des eaux du Rhône dans le lac Léman. https://doi.org/10.5169/SEALS-740434

Betant, A., and G. Perrenoud, 1932. Etudes sur la partie occidentale du lac de Genève. Albert Kundig: Geneva, Switzerland.

Bonvin, F., Rutler, R., Chèvre, N., Halder, J., Kohn, T., 2011. Spatial and Temporal Presence of a Wastewater-Derived Micropollutant Plume in Lake Geneva. Environ. Sci. Technol. 45, 4702–4709. https://doi.org/10.1021/es2003588

Bouffard, D., Lemmin, U., 2013. Kelvin waves in Lake Geneva. Journal of Great Lakes Research 39, 637–645. https://doi.org/10.1016/j.jglr.2013.09.005

Bouffard, D., Perga, M.-E., 2016. Are flood-driven turbidity currents hot spots for priming effect in lakes? Biogeosciences 13, 3573–3584. https://doi.org/10.5194/bg-13-3573-2016

Cimatoribus, A.A., Lemmin, U., Barry, D.A., 2019. Tracking Lagrangian transport in Lake Geneva: A 3D numerical modeling investigation. Limnol Oceanogr 64, 1252–1269. https://doi.org/10.1002/lno.11111

Conseil scientifique de la commission internationale pour la protection des eaux du Léman contre la pollution. 2019. Rapports sur les études et recherches entreprises dans le bassin lémanique. Campagne 2018. CIPEL. Available from https://www.cipel.org/publications/rapports-scientifiques/rapport-2019-campagne-2018/

Coplen, T.B., 1996. New guidelines for reporting stable hydrogen, carbon, and oxygen isotope-ratio data. Geochimica et Cosmochimica Acta 60, 3359–3360. https://doi.org/10.1016/0016-7037(96)00263-3

Forel F-A, 1885. Les ravins sous-lacustres des fleuves glaciaires. Comptes Rendus de l'Académie des Sciences de Paris: 1-3.

Giovanoli, F., 1990. Horizontal Transport and Sedimentation by Interflows and Turbidity Currents in Lake Geneva, in: Tilzer, M.M., Serruya, C. (Eds.), Large Lakes: Ecological Structure and Function, Brock/Springer Series in Contemporary Bioscience. Springer, Berlin, Heidelberg, pp. 175–195. https://doi.org/10.1007/978-3-642-84077-7_9

Halder, J., Decrouy, L., Vennemann, T.W., 2013. Mixing of Rhône River water in Lake Geneva (Switzerland–France) inferred from stable hydrogen and oxygen isotope

profiles. Journal of Hydrology 477, 152–164. https://doi.org/10.1016/j.jhydrol.2012.11.026

Halder, J., Pralong, C., Bonvin, F., Lambiel, F., Vennemann, T.W., 2016. Application of $\delta^{18}O$, $\delta^{13}CDIC$, and major ions to evaluate micropollutant sources in the Bay of Vidy, Lake Geneva. Isotopes in Environmental and Health Studies 52, 94–111. https://doi.org/10.1080/10256016.2014.971786

IPCC, 2018. Summary for Policymakers. In: Global Warming of 1.5°C. An IPCC Special Report on the impacts of global warming of 1.5°C above pre-industrial levels and related global greenhouse gas emission pathways, in the context of strengthening the global response to the threat of climate change, sustainable development, and efforts to eradicate poverty [Masson-Delmotte, V., P. Zhai, H.-O. Pörtner, D. Roberts, J. Skea, P.R. Shukla, A. Pirani, Moufouma-Okia, C. Péan, R. Pidcock, S. Connors, J.B.R. Matthews, Y. Chen, X. Zhou, M.I. Gomis, E. Lonnoy, Maycock, M. Tignor, and T. Waterfield (eds.)]. World Meteorological Organization, Geneva, Switzerland.

Kremer, K., Corella, J.P., Hilbe, M., Marillier, F., Dupuy, D., Zenhäusern, G., Girardclos, S., 2015. Changes in distal sedimentation regime of the Rhone delta system controlled by subaquatic channels (Lake Geneva, Switzerland/France). Marine Geology 370, 125–135. https://doi.org/10.1016/j.margeo.2015.10.013

Larson, J.H., Trebitz, A.S., Steinman, A.D., Wiley, M.J., Mazur, M.C., Pebbles, V., Braun, H.A., Seelbach, P.W., 2013. Great Lakes rivermouth ecosystems: Scientific synthesis and management implications. Journal of Great Lakes Research 39, 513–524. https://doi.org/10.1016/j.jglr.2013.06.002

Lemmin, U., 1989. Dynamics of horizontal turbulent mixing in a nearshore zone of Lake Geneva: Horizontal mixing in a nearshore zone. Limnol. Oceanogr. 34, 420–434. https://doi.org/10.4319/lo.1989.34.2.0420

Lemmin, U., D'Adamo, N., n.d. Summertime winds and direct cyclonic circulation: observations from Lake Geneva. N. D 14.

Lemmin, U., Mortimer, C.H., Bäuerle, E., 2005. Internal seiche dynamics in Lake Geneva. Limnol. Oceanogr. 50, 207–216. https://doi.org/10.4319/lo.2005.50.1.0207

Loizeau, J.-L., Dominik, J., 2000. Evolution of the Upper Rhone River discharge and suspended sediment load during the last 80 years and some implications for Lake Geneva. Aquat. sci. 62, 54. https://doi.org/10.1007/s000270050075

Michalski, J., Lemmin, U., 1995. Dynamics of vertical mixing in the hypolimnion of a deep lake: Lake Geneva. Limnol. Oceanogr. 40, 809–816. https://doi.org/10.4319/lo.1995.40.4.0809

Nouchi, V., Kutser, T., Wüest, A., Müller, B., Odermatt, D., Baracchini, T., Bouffard, D., 2019. Resolving biogeochemical processes in lakes using remote sensing. Aquat Sci 81, 27. https://doi.org/10.1007/s00027-019-0626-3

Read, J.S., Hamilton, D.P., Jones, I.D., Muraoka, K., Winslow, L.A., Kroiss, R., Wu, C.H., Gaiser, E., 2011. Derivation of lake mixing and stratification indices from high-resolution lake buoy data. Environmental Modelling & Software 26, 1325–1336. https://doi.org/10.1016/j.envsoft.2011.05.006

Schwab, D.J., O'Connor, W.P., Mellor, G.L., 1995. On the Net Cyclonic Circulation in Large Stratified Lakes. J. Phys. Oceanogr. 25, 1516–1520. https://doi.org/10.1175/1520-0485(1995)025<1516:OTNCCI>2.0.CO;2

Thi, A.D.L., Pascalis, F.D., Umgiesser, G., Wildi, W., 2012. Structure thermique et courantologie du Léman. ARCHIVES DES SCIENCES 16.

Chapter II

Mixing of the Rhône River intrusion into Lake Geneva at different thermal conditions

Authors: Cotte Gabriel[1], Vennemann Torsten W.[2]

[1]IDYST, UNIL, Géopolis 1015 Lausanne, Gabriel.Cotte@unil.ch

[2]IDYST, UNIL, Géopolis 1015 Lausanne, Torsten.Vennemann@unil.ch

Abstract

After the implementation of nutrient load limitations to Lake Geneva to control the cultural eutrophication, the lake has progressed towards re-oligotrophication. However, the phytoplankton biomass remained stable. The Rhône River is the major nutrient source for the lake. Hence, it is of relevance to understand how the Rhône River actually mixes within the lake and to determine how its nutrients become bioavailable for primary producers.

The Rhône River intrudes as an interflow in the lake's metalimnion during the stratification period. However, its intrusion pattern during other periods of the year has been poorly constrained. This study uses the stable isotope composition of the water to trace the Rhône River water and determine its mixing within the lake at different thermal conditions.

The interflow is established when the thermal stratification of the lake is initiated during spring. The early weak stratification allows the intrusion to be mixed within the epilimnion of the eastern basin. The interflow reaches the far ends of Lake Geneva when the stratification is well established during early summer. At the end of summer, the metalimnion of the entire lake is enriched in Rhône River water. During fall, this layer is progressively mixed with the epilimnion at the same time as the upper layers are cooling. In winter, the Rhône River can intrude the homogeneous hypolimnion after a progressive mixing with the ambient lake during an underflow stage.

The methodological approach opens up new interpretations on the potential fertilisation effect of the Rhône River nutrients to the lake.

Keywords

Lake Geneva; Rhône River; river mixing; autumn cooling; winter intrusions; interflow onset

1. Introduction

Many lakes have faced cultural eutrophication during the second part of the 20th century worldwide (Schindler, 2012). This has led to a deterioration of their water quality. During last decades, a lot of efforts have been made to recover their ecological quality, including measures to limit the nutrient load from their watershed. However, several lakes did not follow the phytoplankton reduction pattern expected and even showed an increase in both primary production (PP) and chlorophyll *a* (Chl *a*) concentrations (Jeppesen et al., 2005; Tadonleke et al., 2009). This lake's response requires a better understanding of the processes that control the phytoplankton dynamics. Their functional structure and their seasonal variability depend on different factors essential for their growth: temperature, light, and the availability of nutrients (Reynolds, 2006). The latter is controlled by physical and biological processes. Winter mixing, for example, brings bottom nutrients to the surface where they will be used during the first spring bloom. As the stratification season passes, the euphotic zone (EZ) will be depleted and the development of phytoplankton will depend on the recycling of the organic matter and the supply of new nutrients. River inflows play a major role in the nutrient delivery to lake environments. The pathway and mixing of the river nutrients will determine their bioavailability and their biogeochemical impact on the ecosystem.

When a river enters a lake as a positively buoyant inflow, its nutrients are directly available for phytoplankton. Instead, negatively buoyant inflows can create intrusions or continue deeper as underflows. Depending on the neutral buoyancy depth compared to the euphotic zone, different scenarios can occur: 1) if the river intrudes the EZ, its nutrients are directly bioavailable; 2) if the river water intrudes below the euphotic depth, it may still reach the upper layers through mixing and advection, 3) or if the intrusion occurs well below the EZ, it may only be raised by the next winter overturn (Rueda et al., 2007). Some studies used artificial tracers to characterise the fate of a cold, plunging river in a stratified lake (Fischer and Smith, 1983; Cortés et al., 2014), while others have used natural stable isotope tracing (Halder et al., 2013; Cotte and Vennemann, 2020). In the Great Lakes, several studies evaluate the influence of streamflow on the nearshore ecosystems (Makarewicz et al., 2012; Marko et al., 2013; Jameel et al., 2018; Carlson Mazur et al., 2019) but few researches have been made on the river dispersion at the basin scale.

Lake Geneva is the largest freshwater lake in Western Europe with a volume of 89 km^3, a surface area of 580 km^2 and a maximum depth of 309 m. It is a monomictic lake located between France and Switzerland. Its theoretical residence time, calculated by the ratio of its volume and the total water input, is approximately 11.5 years (CIPEL, 2020). It usually presents a thermal stratification from spring to early fall. With air temperatures rising due to climate change (IPCC, 2018), total mixing of its water column during winter overturn of the lake is expected to happen less frequently (Perroud et al., 2009; Schwefel et al., 2016). Surface currents within Lake Geneva are controlled by the prevailing winds, the shoreline topography and the Coriolis force and create cyclonic and anticyclonic circulations called gyres (Lemmin, 1989; Lemmin and D'Adamo, 1996).

After a period of eutrophication during the 1960's and 1970's with annual average of total phosphorus reaching 90 µg P/L, Lake Geneva has been on the way of re-oligotrophication. Since the 1980's, after Swiss and French measures were taken to limit the phosphorus input into the lake, the mean concentration of total phosphorus decreased to 16 µg P/L in 2019 (CIPEL, 2020). Despite this important reduction, the amount of phytoplankton biomass measured every year has not declined (Tadonleke et al., 2009). Today, because the phosphorus becomes a limiting factor even earlier during the season, it is important to evaluate which nutrients are coming from the river, where they are transported and how they are metabolized.

This contribution examines the changes in the Rhône River dispersion within Lake Geneva throughout the year. On the basis of earlier studies that focussed on the Rhône interflow during the period of lake stratification (Halder et al., 2013; Cotte and Vennemann, 2020), this study examines more closely open questions on how this intrusion spreads throughout the lake and notably what happens to it during the non-stratified, winter period. It investigates also how the interflow takes place during spring, how it is mixed during late fall and finally whether the nutrients introduced by the Rhône are either directly or become indirectly bioavailable.

2. Material and methods

2.1. Sampling strategy

The five sampling points were chosen all along the axis of the largest depth to determine the location of the Rhône River water in different parts of the lake (Figure 2-1). Profiles 0 and 1 are located at 1 and 4 km's, respectively, from the Rhône River mouth, above the Rhône's canyon, in the eastern part called the "Haut-Lac". Profile 2 is located in the middle of the widest cross-section between Lausanne and Evian and corresponds to SHL2, the reference point for CIPEL's historical monitoring (Commission Internationale pour la Protection des Eaux du Léman) with the maximum depth (309 m). Profile 3 is situated at the boundary between the "Grand-Lac" and the "Petit-Lac" where the bathymetry changes from 300 m to 70 m. Profile 4 is located in the middle of the Petit-Lac and corresponds to GE3, the station monitored by the Canton of Geneva. It is 12 km upstream of the Rhône outlet in Geneva. These profiles were sampled over two years during six different campaigns in order to sample at different seasons and hence at different thermal conditions of the lake (Table 2-1).

Details on coordinates and sampling dates of the different profiles can be found in Appendix II-1. The sampling procedure, the spatial uncertainties and the sample preparation are described in more detail in Chapter I. The sampling locations of the May 2017 campaign are indicated in Appendix II-2 and all the CTD profiles of this campaign are available in Appendix II-3 to II-6. The Rhône River data during the February and May 2017 campaigns are available in Appendix II-7. Finally, the lake data for the June, August, October 2015 and July 2016 campaigns are available in Appendix I-3 while the lake data for the December 2015, February and May 2017 campaigns are available in Appendix II-8.

Table 2-1: Rhône and lake conditions during the campaigns.

Campaign	T_{Lake}	$T_{Rhône}$	$Q_{Rhône}$
August 2015	5.8 – 22 °C	10 °C	270 m^3/s
October 2015	5.8 – 13 °C	7.5 °C	140 m^3/s
December 2015	5.8 – 9 °C	5.3 °C	145 m^3/s
July 2016	5.8 – 22 °C	10 °C	300 m^3/s
February 2017	5.8 – 7 °C	5.8 °C	79 m^3/s
May 2017	5.8 – 11 °C	8.4 °C	95 m^3/s

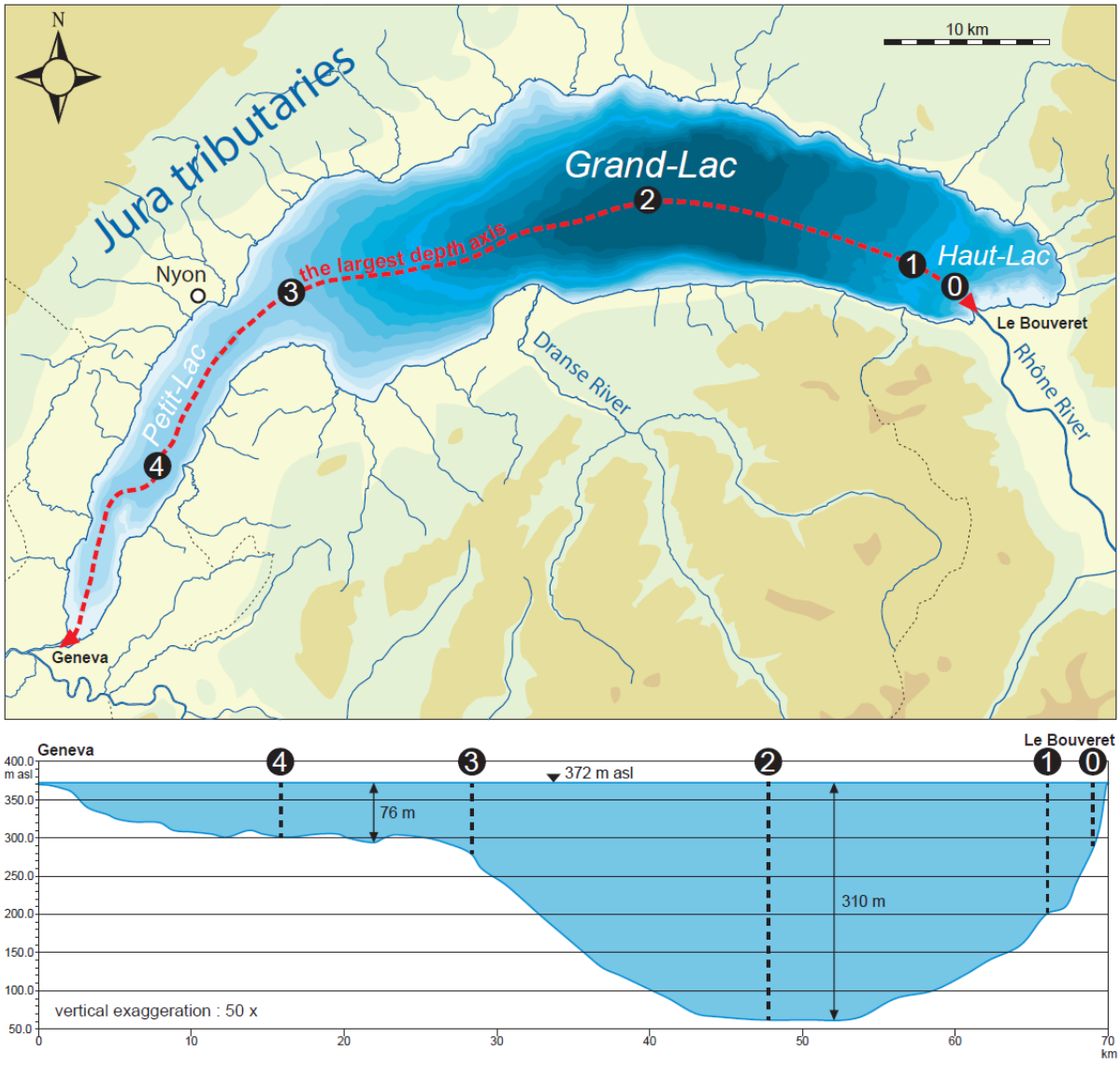

Figure 2-1: Map of Lake Geneva and location of the five sampling profiles (above). Bathymetric section of the largest depth axis (below). Modified from Pierre Corboud.

2.2. Analysis

The analysis procedure of the stable isotope composition of the water samples is detailed in Chapter I.

2.3. Calculations

Calculations of theoretical isotope compositions of the surface mixed layer (SML) have been made for some profiles to examine if they match with the measurements made. For that, mixing between different water layers and water sources has been estimated. For example, the amount of rain at the station of Nyon, a city at the interface between the Grand-Lac and the Petit-Lac (MeteoSwiss) and its isotopic composition (OFEV; Schürch et al., 2003) have been used. The stable oxygen isotope composition of different inputs of water to Lake Geneva and their contribution are presented in Table 2-2.

Table 2-2: Stable oxygen isotope composition of different water inputs to Lake Geneva. The values in bracket are the minimum, the average and the maximum of monthly average values.

Water input	**Contribution (%)**	**$\delta^{18}O_{SMOW}$ (‰)**	**Source**
Rhône River	70-80	[-14.22 ; -13.85 ; -13.65]	OFEV-Porte du Scex 2000-2017
Jura tributaries	9-11	-10.1	Favre and Piffarrerio (2006)
Dranse River	5-7	-11.3	Favre and Piffarrerio (2006)
Direct precipitation	5-8	[-11.75 ; -8.40 ; -4.69]	OFEV-Nyon 2000-2017

3. Results

Figure 2-2 compiles all the longitudinal profiles of temperature and oxygen isotope composition of water obtained during the six campaigns.

The reference value of the stable isotope composition of the lake water is chosen as the value of a homogeneous profile after a complete overturn. As the Petit-Lac mixes completely almost every winter and is not directly influenced by the Rhône River input, Profile 3 in May 2017 is taken as reference. The reference value of -12.1 ‰ is also measured in the deepest part of the lake (e.g., Profile 2 at 309 m) indicating zones not reached by the Rhône intrusion. This reference value is represented in Fig. 2-2 by a dashed blue line with the analytical error as a blue bar. It is so possible to enhance the processes responsible for enrichment or depletion in heavy isotopes within the water column.

Depletion processes

As illustrated in Table 2-2, the only source of water to the lake with depleted ^{18}O concentrations compared to the reference value of the lake is the Rhône River. As outlined already in Halder et al. (2013) and Cotte and Vennemann (2020), the values inferior to -12.1 ‰ indicate the presence of Rhône River water. This depletion is particularly marked by the low values in the metalimnion in all the profiles in August and October 2015. It is present in the four profiles 0 to 3 in July 2016, decreasing in magnitude from the river mouth. In May 2017, it is only well detectable in the Haut-Lac (Profile 0 and 1) and only as trace in the middle of the lake (Profile 2). In February for Profile 1, two distinct signals of Rhône water are measured below 100 m depth with a quasi-return to the reference value in between and at the bottom. In Profile 0, a strong depletion is noted from 80 m depth to the bottom of the lake located here at 110 m depth. The presence of Rhône water has also been measured by ^{18}O-depletions in the epilimnion and hypolimnion in profile 0 in May 2017. Finally, Rhône water is detected in the epilimnion during October and December 2015. With the weakening of the stratification the SML becomes thicker from autumn to early winter, and the influence of the Rhône interflow spreads to deeper levels.

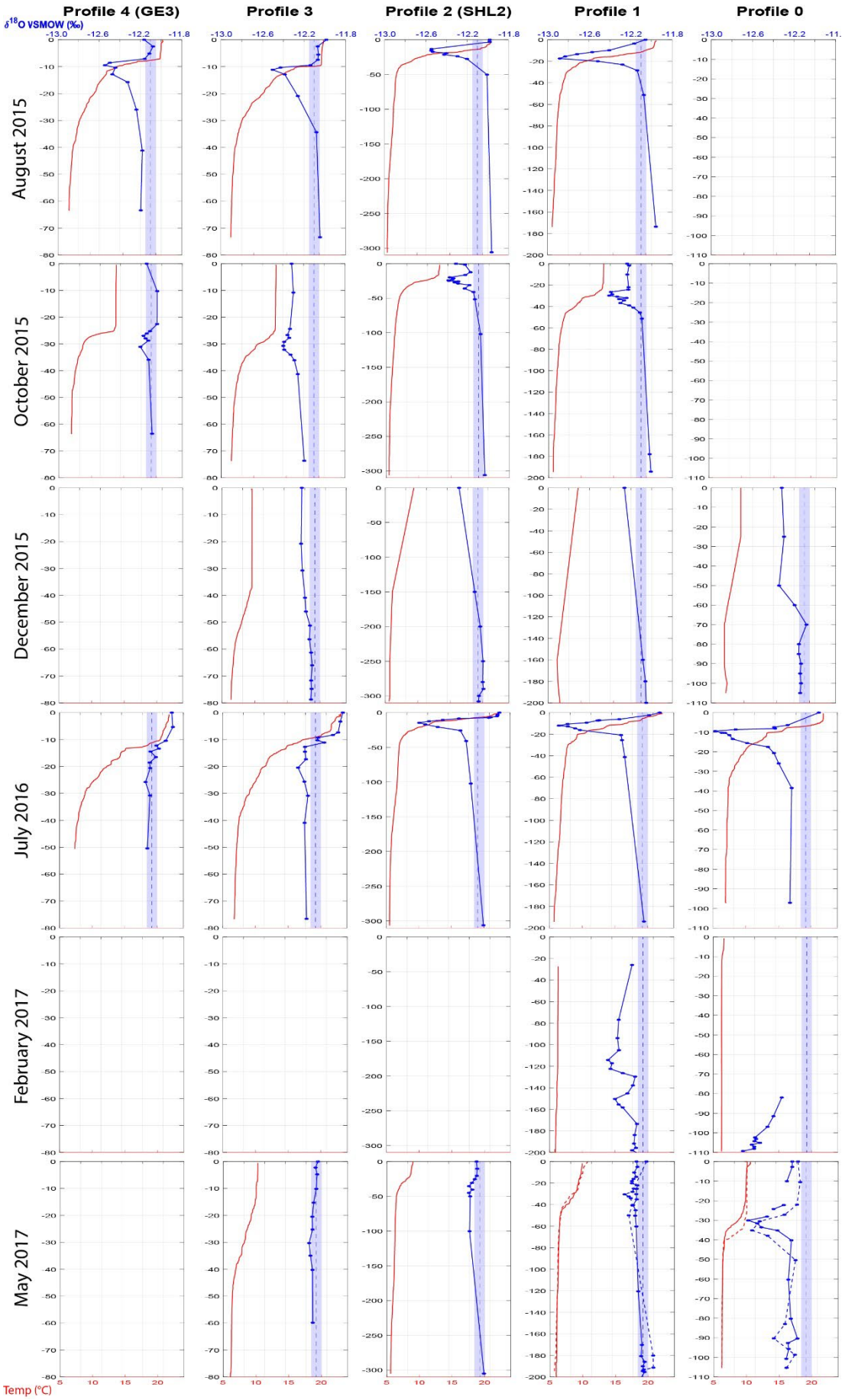

Figure 2-2: Profiles of temperature (red) and oxygen isotope composition of water (blue). The dashed blue line represents the reference value of the stable isotope composition of the lake after a complete overturn with the analytical error as blue bar.

Enrichment processes

First, some profiles, exclusively from summer campaigns, present an enrichment in heavy O-isotopes in the uppermost layers (all the profiles in July and profiles 2 and 3 in August). This can be due to the direct precipitation on the lake, enriched in heavy O-isotopes during the summer months (Table 2-2), or may be related to additional evaporation. Furthermore, the rivers entering from the Jura side may create overflows or mix directly in the shallow parts where they enter the lake.

Furthermore, some profiles present a clear SML and as such a homogenous O-isotope composition in this wind mixed layer (e.g., the first 10 m in Profile 3 in August) whereas no SML are recognized in other profiles where a progressive decrease of temperature and also of the isotope composition is measured in the epilimnion (e.g., Profile 1 and 2 in July). This can be the contribution of diffusive mixing of the summer rain water and/or the evaporated surface lake water with waters in the deeper part of the epilimnion.

Mixing calculations

Table 2-3 to 2-5 present different calculations of theoretical oxygen isotope compositions of the SML, compared to the measured value (last line in *italic*).

Table 2-3 summarizes the calculation of the effect of the rain on the isotope composition of the SML of a summer profile unreached by the Rhône interflow (Profile 4, July 2016). The amount of spring rain has been added to the lake reference value measured at the end of the winter, where its isotopic composition is its weighted average spring (March, April, May and June) composition. The good concordance between the calculated and the observed value confirms the role of the rain for the ^{18}O enrichment of the epilimnion in summer. This phenomenon can also lower the theoretically calculated average Rhône interflow water contributions by up to 9 % in this compartment.

Table 2-3: Calculation of the isotope composition of the SML in July (profile 4) with rain effect.

Source	Water level (m)	$\delta^{18}O_{SMOW}$ (‰)
Rain (Spring)	0.41	-8.16
SML Winter	10	-12.10
TOTAL	**10.4**	**-11.94**
SML July 2016 (profile 4)	*10*	*-11.93*

Table 2-4 shows the calculation of the isotopic composition of the SML in October after the progressive mixing of the upper layer by cooling and stronger wind in autumn. The difference of 0.1 ‰ can be explained by the range of values that the Rhône interflow has during summer and early fall and that depend on the input of Rhône River water and the gyres that transport it.

Table 2-4: Calculation of the isotope composition of the SML in October (profile 3) with mixing.

Source	Water level (m)	$\delta^{18}O_{VSMOW}$ (‰)
Rain (Sept. and Oct.)	0.17	-8.82
SML August 2015 (profile 3)	10	-12.08
Rhône interflow	15	-12.37
TOTAL	**25.2**	**-12.23**
SML October 2015 (profile 3)	*25*	*-12.33*

Table 2-5 illustrates the mixing of the upper layers in autumn and the resulting widening of the SML. It shows how the Rhône interflow water can be spread throughout the top layers by the effects of wind-induced mixing and lake water cooling. The horizontal mixing and the advection of less depleted water can explain the overestimation of the calculated presence of Rhône interflow water in the SML at this season.

Table 2-5: Calculation of the isotope composition of the SML in December (profile 3) with mixing.

Source	Water level (m)	$\delta^{18}O_{SMOW}$ (‰)
Rain (Nov. and Dec.)	0.09	-8.12
SML October 2015 (profile 3)	25	-12.33
Rhône interflow	12	-12.37
TOTAL	**37.1**	**-12.33**
SML December 2015 (profile 3)	*37*	*-12.23*

4. Discussion

4.1. Rhône River intrusion

As shown by Halder et al. (2013) and Cotte and Vennemann (2020), the Rhône River intrusion creates an interflow in the metalimnion during the stratification period of the lake (Fig. 2-2, August and October 2015, July 2016 and May 2017). Here, it is noted that Rhône River interflows can also occur during winter (Fig. 2-2, Profile 1 in February 2017) in deeper parts of the lake when the temperature profile is essentially homogeneous. During this period of the year, the Rhône River has the same temperature as that of the deep lake (Table 2-1). Including the suspended sediment transport of the Rhône, its density may even exceed that of the deep lake water. Moreover, the small discharge measured at this season induces a minor initial mixing with lake water, allowing the Rhône River to create gravity currents (Cortés et al., 2014). This gravity current follows the lake bed in the Rhône's canyon and by a continuous mixing equilibrates its density with the ambient water and intrudes the water column. Different hypotheses can be made on the presence of multiple intrusions: a) two different Rhône interflows that are stacked may have been temporally separated such that an initially denser interflow is intruded below a later, warmer and hence lower density flow; b) two Rhône interflows again temporarily separated but where the upper one has travelled a longer distance from the river mouth while the gyre was larger, losing more sediment and hence decreasing in density; c) the splitting of the Rhône River inflow into a first intrusion and a gravity current that creates afterwards a second intrusion (Marques, 2017); d) the same interflow was distorted by a buoyancy-driven nearshore flow, called thermal syphon (Fer, 2002), which would give a stacked appearance in 1D (personal communication, Frederic Soulignac, CIPEL).

Given the size of the lake, it takes time for the Rhône interflow to cross the Grand-Lac and enter the Petit-Lac in spring. Halder et al. (2013) estimated the minimum time to reach the second basin (55 km from the river mouth) at 5 months. The profiles of July 2016 suggest that this might be even faster. Four months after the beginning of the lake stratification, the Rhône interflow is well installed in the Grand-Lac, not yet detectable in the middle of the Petit-Lac but already present at the interface between the two basins (Profile 3). If we convert this residence time to reach the Petit-Lac to a mean current velocity, we obtain 0.5 cm/s. It is much lower than 4.2 cm/s, the mean speed measured

around 10 m depth within the central cyclonic gyre by (Lemmin and D'Adamo, 1996). This difference is probably due to the recirculation of the Rhône water in the Grand-Lac induced by the rotation of the gyres.

The results of the May campaign demonstrate an establishment of the Rhône interflow during spring. When a small stratification appears with the warming temperatures, the Rhône River starts to intrude in the metalimnion. Depending on the wind action and the resulting gyres, the interflow can reach the different parts of the lake after different transit times. For example, (Cimatoribus et al., 2019) evaluated via simulations a rapid transit time of a few days for the Rhône interflow to reach the Petit-Lac due to rapid transit pathways following the shores. However, they specified that these rapid transit pathways overlap with slower trajectories due to the intermittence of the gyres. Consequently, this delays the establishment of the Rhône interflow in the Petit-Lac as this is consistent with our measures. Profile 0 illustrates a situation with a well-established interflow just in front of the Rhône River mouth. The two different profiles at this same point show how the Rhône intrusion will faithfully follow the depth of maximum density gradient, i.e., the thermocline. At the same time, some interflow waters of the Rhône are detected in the middle of the lake (Profile 2) but not yet at the edges of the Grand-Lac (Profile 3). It is also interesting to note that the Rhône River can "split" when it is introduced into the lake at this time of the year as Rhône water is measured both in the metalimnion and in its canyon, which may have also been a temporarily separated stacking similar to that described above.

4.2. Rhône River mixing

It has been illustrated by the calculation above, that the reference value of -12.1 ‰ can shift to higher values in the epilimnion by the combined effect of rain and evaporation during summer in the upper layers of the lake (Table 2-3) and their mixing with deeper epilimnion waters. This will hide the presence of Rhône water in these parts by up to 9 % in similar meteorological conditions. Hence, this bias has to be considered for the budget of Rhône water volume in Lake Geneva and the comparisons with particle tracking simulations.

As mentioned by Rueda et al. (2007), the different pathways of an incoming river and its nutrients will impact the primary production of a lake differently. Cortés et al. (2014) demonstrated that a significant fraction of the inflow may be quickly entrained

into the SML via convective mixing of this top layer at night. Also, the initial mixing when the river enters the lake will bring river water to the top. In the case of Lake Geneva, this should also happen but with a limit of 9 % of Rhône water as measured by the O-isotopic composition in summer 2015 (see above). This would then also import river nutrients to the euphotic zone and enhance primary production. However, Rhône water has been clearly detected in the epilimnion in front of the river mouth during spring (May 2017, Profile 0). This can be provoked by two phenomena: the initial mixing and/or the entrainment of intrusion water to the top. As the young stratification established in spring is fragile, a somewhat stronger wind event can sufficiently disturb stratification and mix the river water and its nutrient throughout the SML (cf. Chapter IV). The Rhône River mouth being in the eastern part of the basin, can explain the early algal bloom usually detected in this part of the lake (e.g., Kiefer et al., 2015; Soulignac et al., 2018; Soomets et al., 2019).

Furthermore, as shown by Cotte and Vennemann (2020), the interflow deepens over autumn with the decay of the thermocline and the cooling of the Rhône River. As shown by the calculations of the SML from August to December (Table 2-4 and 2-5), the stronger winds and the air cooling during this season consequently mix the summer interflow throughout the SML. This behaviour during autumn should have a direct impact on the primary production by introducing river nutrients to the euphotic zone at a time when this zone is particularly depleted in nutrients. This mixing process may continue up until early winter, as December profiles are still depleted in the heavy O-isotopes from the surface down to 50 m depth. Therefore, we can argue that the Rhône River intrusion has the potential to sustain a late algal growth in Lake Geneva where its nutrients are still available and have not yet been metabolised.

5. Conclusion

The longitudinal profiles sampled at different thermal conditions of the lake indicate variable intrusion and mixing patterns of the Rhône River in Lake Geneva. As the stratification is established during spring, the Rhône water intrudes in the metalimnion. A part of this intrusion can be readily mixed within the epilimnion of the Haut-Lac, introducing river nutrients to the euphotic zone early in the season. Indeed, the relatively weak stratification can be easily broken by wind action on the lakes surface waters. The Rhône interflow concentrates during well-established stratification of the lake, making it distinctly visible in other, more distal parts of the lake. From summer to early fall, the Rhône water is intruding and concentrating in the metalimnion and is able to reach the Petit-Lac. Afterwards, during fall, with the deepening of the thermocline and the cooling of the top layers, the Rhône River interflow deepens and the metalimnion particularly enriched in Rhône water is progressively mixed with the epilimnion waters. Depending on the locality in the lake and the river nutrient conservation within the interflow, this mixing can induce an indirect fertilisation of the euphotic zone and sustain primary production during autumn. Then, during winter, the Rhône inflow is able to intrude the homogeneous water column after a progressive mixing with the ambient lake water. However, these winter intrusions will not provoke any fertilisation as they occur well below the euphotic zone. Instead, it will bring nutrients to the deepest part of the hypolimnion that can be remobilized during the next complete overturn. Underflows have been observed during the stratification period but they are related to flooding events when the Rhône River carries high sediment load. This has been measured in the Rhône's canyon by indirect techniques such as bottom-mounted ADCP (unpublished data, EPFL). These parts are not readily sampled because of the strong currents occurring in the Rhône delta during such event. Nevertheless, avoiding this specific condition, it is possible to evaluate the nutrient dispersion related to the Rhône intrusion in the lake and the impact on the primary production. While the present data already cover a number of different settings, the complicating wind and thermal effects in this rather large lake may allow for a much wider range of possible mixing scenarios. To have a more complete overview and quantify the Rhône River nutrient cycle within the lake, it is necessary to couple these observations with 3D numerical models (e.g., Cimatorbius et al., 2019). While hydrodynamic simulations can explain the measured data, the measurements can, in turn,

validate the model. Therefore, it would be possible to compare the nutrient input from the Rhône River to other sources and then, balance the nutrient budget of the lake.

Acknowledgements

A special Thank You to Philippe Arpagaus who piloted the Licorne with precision and shared his passion for the lake. Thank you also to all the sailors who helped me with the sampling: Arthur, Christophe Borel, Louis Bridoux, Romain Cardot, Ignes Augusta Castro Contreiras De Carvalho, Nathalie Diaz, Shannon Dyer, Micaela Faria, Thibault Lambert, Anaël Lehmann, Zoneibe Luz, Stéphane Mahé, Gelare Moradi and Elfie Swerts. As well as to the Federal Office for the Environment of Switzerland (OFEV) that provided long term H- and O-isotope compositions of the Rhône River and precipitation from the Swiss Isotopic Network (ISOT) module of OFEV.

References

Carlson Mazur, M.L., Schaeffer, J., Granneman, J.E., Goldstrohm, N., Fitzpatrick, F.A., Larson, J.H., Reneau, P.C., Kowalski, K.P., Seelbach, P.W., 2019. Seasonal patterns in hydrochemical mixing in three Great Lakes rivermouth ecosystems. J. Gt. Lakes Res. 45, 651–663. https://doi.org/10.1016/j.jglr.2019.03.009

Cimatoribus, A.A., Lemmin, U., Barry, D.A., 2019. Tracking Lagrangian transport in Lake Geneva: A 3D numerical modeling investigation. Limnol. Oceanogr. 64, 1252–1269. https://doi.org/10.1002/lno.11111

Conseil scientifique de la commission internationale pour la protection des eaux du Léman contre la pollution. 2020. Rapports sur les études et recherches entreprises dans le bassin lémanique. Campagne 2019. CIPEL. Available from https://www.cipel.org/publications/rapports-scientifiques/rapport-2020-campagne-2019/.

Coplen, T.B., 1996. New guidelines for reporting stable hydrogen, carbon, and oxygen isotope-ratio data. Geochim. Cosmochim. Acta 60, 3359–3360. https://doi.org/10.1016/0016-7037(96)00263-3

Cortés, A., Fleenor, W.E., Wells, M.G., de Vicente, I., Rueda, F.J., 2014. Pathways of river water to the surface layers of stratified reservoirs. Limnol. Oceanogr. 59, 233–250. https://doi.org/10.4319/lo.2014.59.1.0233

Cotte, G., Vennemann, T.W., 2020. Mixing of Rhône River water in Lake Geneva: Seasonal tracing using stable isotope composition of water. J. Gt. Lakes Res. 46, 839–849. https://doi.org/10.1016/j.jglr.2020.05.015

Favre, L. and Piffarrerio, R., 2006. Un bilan isotopique et chimique du Lac Léman en 2005. Isotopes de l'oxygène, de l'hydrogène et du carbone, ainsi que les concentrations du DIC, des nitrates et des orthophosphates. Master thesis, Institut de Minéralogie et Géochimie, Université de Lausanne.

Fer, I., 2002. Winter cascading of cold water in Lake Geneva. J. Geophys. Res. 107, 3060. https://doi.org/10.1029/2001JC000828

Fischer, H.B., Smith, R.D., 1983. Observations of transport to surface waters from a plunging inflow to Lake Mead1: Lake Mead transport. Limnol. Oceanogr. 28, 258–272. https://doi.org/10.4319/lo.1983.28.2.0258

Halder, J., Decrouy, L., Vennemann, T.W., 2013. Mixing of Rhône River water in Lake Geneva (Switzerland–France) inferred from stable hydrogen and oxygen isotope profiles. J. Hydrol. 477, 152–164. https://doi.org/10.1016/j.jhydrol.2012.11.026

Jameel, Y., Stein, S., Grimm, E., Roswell, C., Wilson, A.E., Troy, C., Höök, T.O., Bowen, G.J., 2018. Physicochemical characteristics of a southern Lake Michigan river plume. J. Gt. Lakes Res. 44, 209–218. https://doi.org/10.1016/j.jglr.2018.01.003

Jeppesen, E., Sondergaard, M., Jensen, J.P., Havens, K.E., Anneville, O., Carvalho, L., Coveney, M.F., Deneke, R., Dokulil, M.T., Foy, B., Gerdeaux, D., Hampton, S.E., Hilt, S., Kangur, K., Kohler, J., Lammens, E.H.H.R., Lauridsen, T.L., Manca, M., Miracle, M.R., Moss, B., Noges, P., Persson, G., Phillips, G., Portielje, R., Romo, S., Schelske, C.L., Straile, D., Tatrai, I., Willen, E., Winder, M., 2005. Lake responses to reduced nutrient loading - an analysis of contemporary long-term data from 35 case studies. Freshw. Biol. 50, 1747–1771. https://doi.org/10.1111/j.1365-2427.2005.01415.x

Kiefer, I., Odermatt, D., Anneville, O., Wüest, A., Bouffard, D., 2015. Application of remote sensing for the optimization of in-situ sampling for monitoring of phytoplankton abundance in a large lake. Sci. Total Environ. 527–528, 493–506. https://doi.org/10.1016/j.scitotenv.2015.05.011

Lemmin, U., 1989. Dynamics of horizontal turbulent mixing in a nearshore zone of Lake Geneva: Horizontal mixing in a nearshore zone. Limnol. Oceanogr. 34, 420–434. https://doi.org/10.4319/lo.1989.34.2.0420

Lemmin, U., D'Adamo, N., 1996. Summertime winds and direct cyclonic circulation: observations from Lake Geneva. N D 14.

Makarewicz, J.C., Lewis, T.W., Boyer, G.L., Edwards, W.J., 2012. The influence of streams on nearshore water chemistry, Lake Ontario. J. Gt. Lakes Res. 38, 62–71. https://doi.org/10.1016/j.jglr.2012.02.010

Marko, K.M., Rutherford, E.S., Eadie, B.J., Johengen, T.H., Lansing, M.B., 2013. Delivery of nutrients and seston from the Muskegon River Watershed to near shore Lake Michigan. J. Gt. Lakes Res. 39, 672–681. https://doi.org/10.1016/j.jglr.2013.08.002

Marques, G.M., 2017. Flow splitting in numerical simulations of oceanic dense-water outflows. Ocean Model. 19.

Perroud, M., Goyette, S., Martynov, A., Beniston, M., Annevillec, O., 2009. Simulation of multiannual thermal profiles in deep Lake Geneva: A comparison of one-

dimensional lake models. Limnol. Oceanogr. 54, 1574–1594. https://doi.org/10.4319/lo.2009.54.5.1574

Reynolds, C.S., 2006. The Ecology of Phytoplankton [WWW Document]. Camb. Core. https://doi.org/10.1017/CBO9780511542145

Rueda, F.J., Fleenor, W.E., de Vicente, I., 2007. Pathways of river nutrients towards the euphotic zone in a deep-reservoir of small size: Uncertainty analysis. Ecol. Model. 202, 345–361. https://doi.org/10.1016/j.ecolmodel.2006.11.006

Schindler, D.W., 2012. The dilemma of controlling cultural eutrophication of lakes. Proc. R. Soc. B Biol. Sci. 279, 4322–4333. https://doi.org/10.1098/rspb.2012.1032

Schürch, M., Kozel, R., Schotterer, U., Tripet, J.-P., 2003. Observation of isotopes in the water cycle-the Swiss National Network (NISOT). Environ. Geol. 45, 1–11. https://doi.org/10.1007/s00254-003-0843-9

Soomets, T., Kutser, T., Wüest, A., Bouffard, D., 2019. Spatial and temporal changes of primary production in a deep peri-alpine lake. Inland Waters 9, 49–60. https://doi.org/10.1080/20442041.2018.1530529

Soulignac, F., Danis, P.-A., Bouffard, D., Chanudet, V., Dambrine, E., Guénand, Y., Harmel, T., Ibelings, B.W., Trevisan, D., Uittenbogaard, R., Anneville, O., 2018. Using 3D modeling and remote sensing capabilities for a better understanding of spatio-temporal heterogeneities of phytoplankton abundance in large lakes. J. Gt. Lakes Res. 44, 756–764. https://doi.org/10.1016/j.jglr.2018.05.008

Tadonleke, R.D., Lazzarotto, J., Anneville, O., Druart, J.-C., 2009. Phytoplankton productivity increased in Lake Geneva despite phosphorus loading reduction. J. Plankton Res. 31, 1179–1194. https://doi.org/10.1093/plankt/fbp063

Chapter III

Processes driving nutrient dispersion in Lake Geneva during the stratification period (study using the LéXPLORE platform)

Authors: Cotte Gabriel[1], Vennemann Torsten W.[2]

[1]IDYST, UNIL, Géopolis 1015 Lausanne, Gabriel.Cotte@unil.ch

[2]IDYST, UNIL, Géopolis 1015 Lausanne, Torsten.Vennemann@unil.ch

Abstract

The ecosystem of Lake Geneva has been perturbed by cultural eutrophication. In addition, climate change influences the recovery of the bioproductivity by changing its thermal structure and hence, the mixing regime and nutrient dynamics. As such, it is important to determine the processes driving the nutrient dynamics in the context of the re-oligotrophication of the lake. In this study, three processes have been proposed as hypotheses of the major controls on nutrient concentrations of the euphotic zone of the lake. The first concerns the Rhône River, the main tributary and nutrient input to the lake. It is hypothesised that the Rhône River, transported as an interflow during the stratification period, carries nutrients to the Grand-Lac, the main basin of Lake Geneva. The second hypothesis is the vertical advection of nutrient-enriched deeper waters to the nutrient-depleted epilimnion. The third supports an influence of the water column metabolism via the photosynthesis/respiration processes, and where this can be estimated through the use of the oxygen saturation as a proxy.

In order to have a high temporal resolution of the nutrient dynamics, we used the recently established research platform LéXPLORE located close to Pully within Lake Geneva. This platform offers an easy access to the pelagic zone and is equipped with a wide range of sensors that monitor the hydrodynamic and metabolic processes of the lake at this site. The metalimnion has been regularly sampled during September and October 2019 to determine the nutrient concentrations and the Rhône River water fractions, as inferred by the stable isotope composition of the water.

The study period covers important heterogeneities with regard to the thermal and hydrodynamic conditions of the lake. The vertical advection has been identified as a major control of the nutrient dynamics with upwelling and downwelling of water induced by the rotation of the gyre or the direct wind forcing. As the core zone of the Rhône interflow is located directly below the thermocline, a coupled upwelling of silica enriched water from the deeper layers and from the Rhône River has been measured during an upwelling of the thermocline. However, the bioproductivity signal was difficult to assess during agitated periods as the dissolved oxygen saturation is directly correlated to the vertical motions. However, biological recycling of the mineralised nutrients has been observed during calmer periods. Thereby, a higher resolution of the nutrient dynamics

coupled to the actual monitoring of water quality of the lake is relevant in order to distinguish the overall processes driving the nutrient dispersion.

Keywords

LéXPLORE; nutrient dynamics; upwelling; river interflow; metabolism; nutrient depletion

1. Introduction

In the context of the re-oligotrophication scheme of Lake Geneva, its phosphorus concentrations have been considerably reduced from 90 µgP/L in 1979 to 16 µgP/L in 2019 (CIPEL, 2020). However, despite these restrictions, the phytoplankton biomass remained stable (Anneville and Pelletier, 2000; Tadonleke et al., 2009). The phytoplankton community adapted to this shift of trophic state by changing its seasonal dynamics of species assemblages (Anneville et al., 2018). The P-depletion in the surface layers has also induced a displacement of the phytoplankton to deeper, P enriched layers, up to 30 m, with species adapted to low light levels (Moisset, 2017). Additionally, the coupled effect of climate change is assumed to accentuate the non-recovery tendency. Indeed, the climate warming increases the water temperature and extends the growing season with a longer stratification period (Anneville et al., 2013). It also impacts the mixing regime by modifying the thermal structure (Perroud et al., 2009; Perroud and Goyette, 2012). Consequently, the nutrient dynamics within the water column are perturbed by a reduced frequency of complete winter mixing, an earlier stratification onset and, as a result, an euphotic zone depleted in nutrients earlier during the year.

Hence, it is relevant to determine the origin of the nutrients and their distribution in space and time throughout the lake to better assess their metabolization by primary producers. The objective of this study is to determine the different processes driving the nutrient dynamics within Lake Geneva during its stratification period. The hypotheses on these main processes include:

- H1: As the Rhône River is the main external source of nutrients to the lake (Sabaratnam and Oriez, 2019), the horizontal advection of the Rhône nutrients via the interflow phenomenon is expected (Cotte and Vennemann, 2020). The Rhône water fraction measured by the isotopic composition of the water is then used as a proxy for the net water flux from the Rhône, as this is a conservative tracer for the mixing process, while the nutrients may not be conservative.

- H2: During the stratification period of the lake, the thermocline acts as a barrier between the epilimnion depleted in nutrients due to photosynthetic uptake and the hypolimnion enriched in nutrients by the remineralization processes. Enriched water can then be upwelled to upper layers by vertical motions (Bouffard et al., 2018; Lemmin et al., 2005). The thermocline excursion is then chosen as a proxy of the second hypothesized process, i.e. the vertical advection of nutrient-enriched deeper water.

- H3: As photosynthesis transforms the dissolved inorganic nutrients into organic matter and produces dissolved oxygen (DO), respiration releases these nutrients and consumes oxygen. The oxygen saturation of the water is used as proxy of the metabolism selected as third hypothesized process here.

In addition to their sensitivity to climate change (e.g., Zhong et al., 2016), large lakes are complex ecosystems where it is challenging to distinguish the physical, chemical and biological processes occurring simultaneously. In order to have a high temporal resolution of the nutrient dynamics, we used the recently established research platform LéXPLORE located close to Pully within Lake Geneva (www.lexplore.info). This platform provides an easy access to the pelagic zone of the lake and gives the opportunity to regularly sample the water column. Moreover, a whole set of parameters are monitored continuously to assess the hydrodynamic and metabolic processes of the lake.

In this study, we first determine the relationship between the different processes supposed to control the nutrient dynamics. For specific pre-defined periods of the measurements, hypotheses are made on the processes at work regarding the changes in the nutrient concentrations. Nutrient concentration models will then be applied to test these hypotheses for a specific event.

2. Material and methods

2.1. Sampling strategy

LéXPLORE is a scientific platform located on Lake Geneva (Swiss coordinates: X 540292 / Y 150176). It is anchored at 570 m from the northern coast at a lake depth of 110 m, 20 km northwestward of the Rhône River mouth (Figure 3-1). During 6 weeks, an ISCO autosampler connected to a submerged pump was installed at the platform (Figure 3-2). This system collected 120 samples from mid-September to the end of October 2020 at the averaged thermocline depth where the Rhône River interflow was previously detected (Cotte and Vennemann, 2020). From September 13th to October 7th, the pump was continuously pumping at 18 m depth. It was subsequently lowered to 22 m depth until October 25th in order to follow the autumn deepening of the thermocline. The ISCO Avalanche autosampler, equipped with 14 bottles of 1 L, was programmed to sample every 3 hours with the samples stored at 5 °C. Samples were collected and filtered with 0.7 µm nylon filters using an electric pump maximum 3 days after their sampling and then, stored at -18 °C until the nutrient analysis were done. Split samples for the stable isotope analysis were refrigerated at 5 °C prior to analysis, performed within a week of sampling.

To evaluate the preservation of the samples stored in the autosampler, a control sample was taken whenever the next sampling sequence was started and this sample was directly filtered and stored in the fridge while the same water was stored in the ISCO bottle for 2 days before the same treatment and final analysis. The replicate analyses had relative errors not exceeding 10 % (except for the orthophosphates), which validates that the samples were preserved in their original state (Table 3-1).

Additionally, regular water samples have been taken at 15 depths along the water column at LéXPLORE by the APHYS team (EPFL). The analyses of the different forms of P and N have been performed at EAWAG (Appendix III-1).

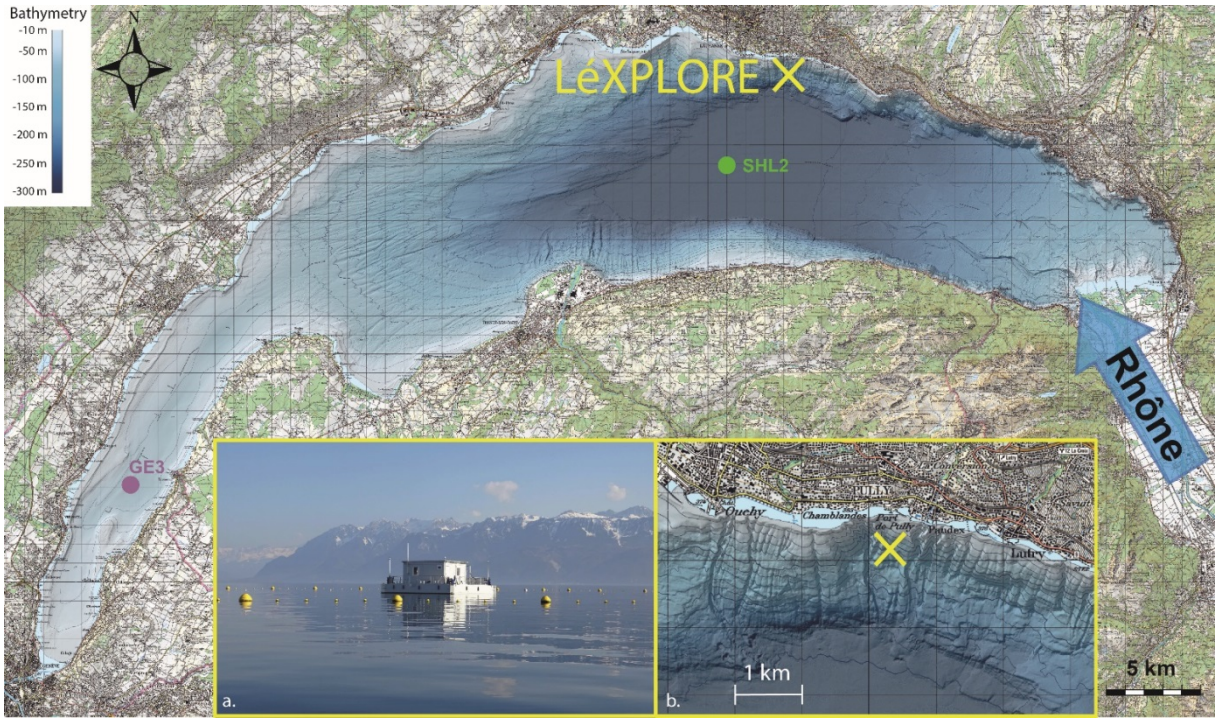

Figure 3-1: Map of Lake Geneva showing the location of the LéXPLORE platform as a yellow cross. The Rhône River inflow is indicated by a blue arrow. The green and purple dots represent the locations of the two permanent monitoring stations within Lake Geneva.
Insets: a. Image of the platform. b. Larger scale map of the area around the platform.

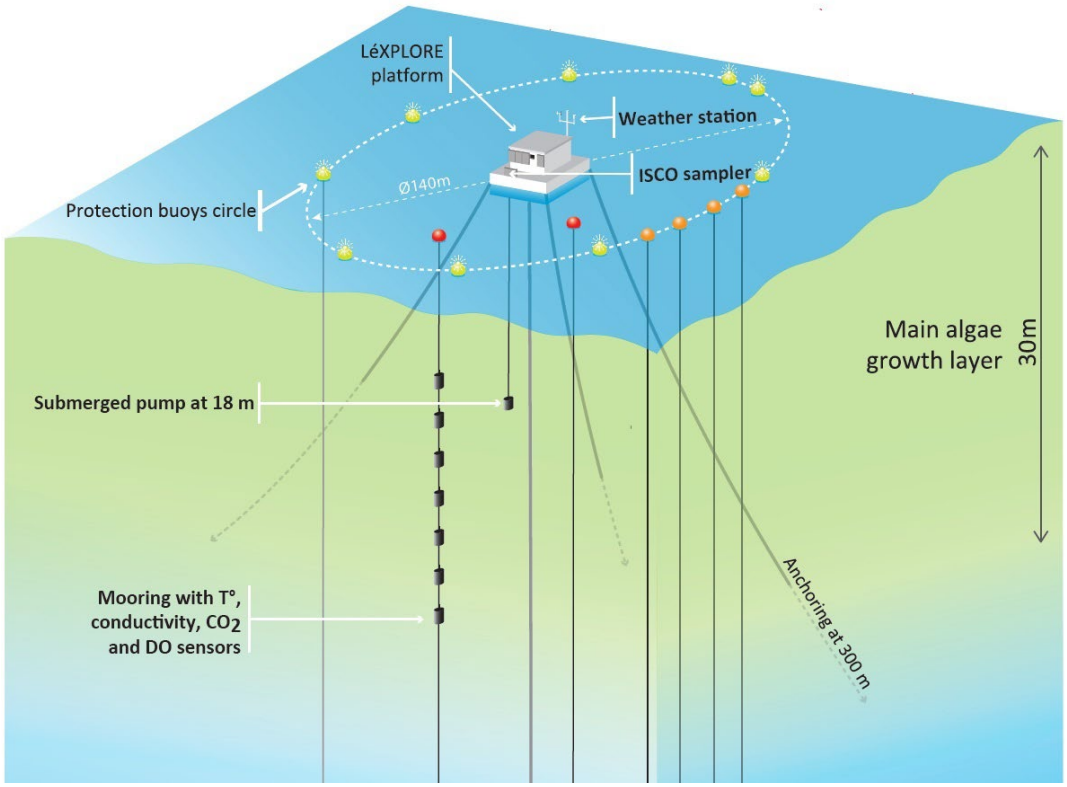

Figure 3-2: LéXPLORE platform scheme (copyright: LéXPLORE platform).

Table 3-1: Compositions for the control sample and the sample stored in the ISCO sampler. The compositions (in bold) are given with their analytical error below (normal font)

Samples	$\delta^{18}O$ VSMOW	δD VSMOW	$\delta^{13}DIC$ VPDB	DIC (mg/L)	PO_4^{3-} (µg P/L)	NO_3^- (mg N/L)	SiO_2 (mg/L)
Control sample	**-12.36 ‰**	**-91.0 ‰**	**-6.78 ‰**	**82.7**	**1.6**	**0.43**	**0.47**
	0.04	0.1	0.07	0.2	0.1	0.01	0.00
Stored sample	**-12.38 ‰**	**-90.8 ‰**	**-6.37 ‰**	**80.9**	**2.0**	**0.41**	**0.48**
	0.02	0.28	0.07	0.2	0.1	0.02	0.01
Difference	-0.02 ‰	0.16 ‰	0.40 ‰	-1.8	0.4	-0.02	0.01
Relative error	**0.1 %**	**-0.2 %**	**-6.0 %**	**-2.2 %**	**24.1 %**	**-4.4 %**	**2.3 %**

2.2. Analysis

Stable isotopes of water

The oxygen and hydrogen isotope compositions were analysed using a Picarro L2140i and a method identical to that described in Cotte and Vennemann (2020).

DIC concentration and its isotopic composition

The isotopic composition of DIC has proven to be a marker of the biogeochemical processes in water column of Lake Geneva (e.g., Halder et al., 2013). During the stratification period, the top layers are progressively enriched in ^{13}C by the diffusion of atmospheric CO_2 into and throughout the epilimnion and the metalimnion of the water column which is driven by photosynthetic uptake of CO_2. Consequently, a progressive ^{13}C depletion with depth that depends on the thermal stratification and mixing processes is observed in the metalimnion. The $\delta^{13}C_{DIC}$ can thus be used as an indicator of the vertical advection processes.

The carbon isotope composition of DIC was analyzed using a Gasbench II coupled to a ThermoFinnigan DeltaPlus XL isotope ratio mass spectrometer (IRMS). Measurements were made according to the method of Spötl and Vennemann (2003) but where the aqueous solution (0.8 to 1.5 ml) was injected into vials containing 10 drops of H_3PO_4 (85 %) and flushed with He prior to injection. The raw value was calibrated using an internal laboratory standard (Carrara Marble, $\delta^{13}C_{DIC}$ = 2.05 ‰ VPDB). Isotopic ratios

measured are reported in the common δ-units as permil deviation of the isotope ratio of the sample relative to that of the standard, Vienna Peedee Belemnite (VPDB). An average of the last nine out of ten measurement peaks was used to calculate the raw value. The standard deviation of all samples as well as standard measurements was within ±0.08 ‰ (1σ) for $\delta^{13}C_{DIC}$ values. DIC concentration was determined using the second sample peak intensity (total intensity measured by IRMS for m/z = 44, 45, and 46) versus weights from the standard carbonates as a calibration. The analytical error was estimated by the standard deviation of the six standards analysed within the sequence.

Nutrient concentration

The orthophosphate ($P\text{-}PO_4^{3-}$) concentrations were measured spectrophotometrically using the molybdenum blue method (Murphy and Riley, 1962) at 882 nm on a UV-visible spectrometer (Perkin Elmer). The analytical error was estimated by the standard deviation of the standards analysed as triplicates. The detection limit is 1 μg ($P\text{-}PO_4^{3-}$)/L.

Nitrate concentrations were measured by liquid ion-chromatography (ICS-1100 of Dionex). Each sequence was calibrated using five standards. A sequence consisted of duplicate samples, internal standards and blanks. The analytical error for each sample was estimated by the standard deviation of the duplicates. The detection limit is 0.07 mg ($N\text{-}NO_3^-$)/L.

The silica concentrations were measured spectrophotometrically using a SmartChem 200 (AMS Alliance). Duplicates of samples were analysed with internal standards and blanks. The standard deviation of the duplicates was used to evaluate the analytical error. The detection limit is 0.1 mg SiO_2/L.

2.3. High frequency data set

Wind speed and direction were measured during the sampling period by a Campbell Meteostation installed on the platform (Figure 3-2).

Current velocities were measured by a downward looking ADCP RDI 300 kHz installed in the platform's moon pool managed by the APHYS team (EPFL).

Several parameters were recorded at high frequency at fixed depth all along a mooring chain (Figure 3-2) managed by the APHYS team (EPFL) and the LAKES group of IDYST (UNIL). Temperature was monitored at 13 depths between 0.5 and 30 m with

Minilog-II-T sensors (VEMCO, resolution 0.01°C). DO data were collected at 6 depths between 0.5 and 30 m with MiniDOt sensors. A gap in these data occurring from October 8th to 23rd is due to maintenance of the mooring.

Table 3-2: Metadata collected at LéXPLORE platform

Data	Location	Frequency	Utility
Wind speed and direction	Meteostation	10 min	Wind forcing
Temperature	Mooring 0-30 m	1 min	Thermocline depth (vertical advection)
Current velocity	ADCP	10 min	Horizontal advection
DO	Mooring 0-30 m	5 min	Metabolism
$\delta^{18}O$ and $\delta^{2}H$ of H_2O	Submerged pump	120 samples over 6 weeks	Rhône River fraction
DIC and $\delta^{13}C_{DIC}$	Submerged pump	120 samples over 6 weeks	Vertical advection
Nutrients (P, N and Si)	Submerged pump	120 samples over 6 weeks	Nutrient dynamics

2.4. Calculations

Thermocline

The thermocline depth was calculated as the depth with the highest temperature gradient within the water column for the entire sampling period. The thermocline depth is expressed as negative value.

Isotope mixing model

A mixing model is used to calculate the Rhône water fraction for each sampling location. This mixing model is based on an atomic mass balance such that:

$$\delta^{18}O_R \bullet x_R + \delta^{18}O_L \bullet x_L = \delta^{18}O_S \quad (1)$$

Given that $x_R + x_L = 1$, the mole fraction of Rhône water at the sampling time is calculated by:

$$x_R = (\delta^{18}O_S - \delta^{18}O_L) / (\delta^{18}O_R - \delta^{18}O_L) \quad (2)$$

where $\delta^{18}O_R$ is the isotopic value of the Rhône River water. The $\delta^{18}O_R$ is measured once a month proportionally to the discharge by OFEV (Swiss Federal Office of Environment) at Porte du Scex located 5 km upstream of the lake (Figure 3-3). The value of the isotopic composition of the Rhône River water $\delta^{18}O_R$ is determined by the discharge-weighted average of the OFEV measurements of the last months since the stratification onset (it corresponds to the period when the Rhône was flowing in the metalimnion). The uncertainty on the Rhône fraction based on the analytic error for $\delta^{18}O_S$ of ± 0.05 ‰ is evaluated to ± 2 %. It is smaller than the uncertainty linked to the seasonal variation of $\delta^{18}O_R$ though (discussed in Cotte and Vennemann, 2020). x_R is the mole fraction of the Rhône water at the sampling time. $\delta^{18}O_L$ is the value of the mixed, unstratified lake water column that is, for example, homogeneous over the whole lake after a complete overturn. This value is -12.15 ‰, as determined by the isotopic composition of the lake at 103 m depth under the platform during the stratification period, which we assumed not to have been impacted by the Rhône River water or other river inputs closer to the platform. x_L is the mole fraction of lake water at the sampling time. $\delta^{18}O_S$ is the isotopic composition of the water measured for the sample collected.

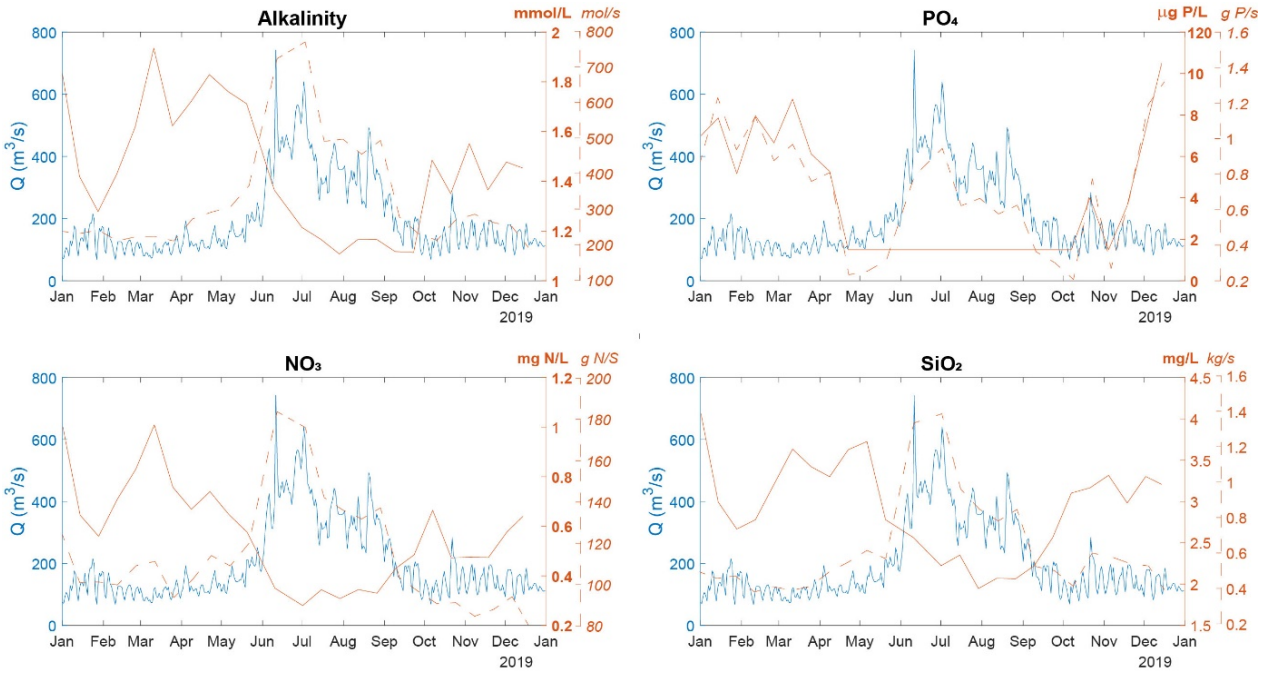

Figure 3-3: Rhône River nutrient concentration (orange solid line) and mass flow (orange dashed line). Data from OFEV/NAQUA from the hydrological station of Porte du Scex located on the Rhône River 5 km upstream from its river mouth into Lake Geneva. The nutrient data are average values measured on water samples that are collected over the month proportional to the discharge. The discharge is measured continuously but the daily average discharge is presented for the year 2019 (blue line).

2.5. Study approach

First, different focal periods among the entire study period were selected depending on the evolution of the physical characteristics of the water column. Secondly, linear regression analysis between parameters hypothesized as drivers of the nutrient dynamics is used to test their independence for each focal period (Rhône River water fraction, thermocline depth as proxy of the vertical advection, and oxygen saturation as proxy of the metabolism). Third, linear regression analysis between these parameters and the nutrient concentrations for each focal period are used to test the hypotheses on the processes driving the nutrient dynamics. Finally, these hypotheses are verified by applying models of nutrient concentration for a specific event. All the statistical analyses have been performed using MATLAB.

Nutrient concentration models

In order to verify the hypotheses on the processes in charge of the nutrient dynamics, nutrient concentration models have been established.

The first model (M1), the *Rhône River Mixing Model,* calculates the possible horizontal advection of nutrient from the Rhône River interflow via the Rhône fractions measured at the sampling point:

$$C_M = x_R \bullet C_R + (1 - x_R) \bullet C_L \quad (3)$$

where C_R is the average of the Rhône River nutrient concentrations measured in August and September by OFEV at Porte du Scex (Figure 3-3). Integration of the concentrations for these two months accounts for the variable transit time of the Rhône River interflow from its mouth to the platform (Cimatoribus et al., 2019). C_L is the averaged nutrient concentration of the 10 first meters of the water column measured by the CIPEL at the central monitoring station SHL2 during the study period (Appendix III-2). This nutrient depleted layer during stratification is above the Rhône interflow at this period (Cotte and Vennemann, 2020).

The second one (M2) is a *Vertical Advection Model* to evaluate the possible range of nutrient concentrations when deeper enriched water is upwelled to the sampling point:

$$C_M = a \bullet h + C_S \quad (4)$$

where C_M is the calculated nutrient concentration at the sampling point after the upwelling event. C_S is the nutrient concentration measured at the sampling point before the upwelling event (i.e., before the rise of the thermocline). The vertical nutrient gradient *a* is calculated by performing a simple linear regression on the averaged depth profiles of nutrient concentration measured at the monitoring station SHL2 by CIPEL during the study period (Appendix III-2). The gradient *a* corresponds to the regression coefficient of the linear regression. Only the 10-30 m layer is considered for this calculation as it corresponds to the part of the water column where the thermocline is detected. And *h* is the height of the upwelling measured by the evolution of the thermocline depth during the upwelling event.

3. Results

3.1. Temporal context

The time series of the high frequency data of wind, currents, thermal structure, conductivity and dissolved oxygen are presented in Figure 3-4 (4a to 4e). In view of the heterogeneities of these parameters during the study period, three focal periods have been defined to present and discuss the results:

- P1: a "Summer Period" from September 13th to 17th (16 samples)
- P2: a "Windy Period" from October 1st to 7th (29 samples)
- P3: an "Autumn Period" from October 23rd to 26th (15 samples)

The "Summer Period" (P1) is characterized by a strong thermal stratification with surface water reaching 20 °C. The wind conditions were calm with a maximum velocity of 3 m/s. Before this period, from September 10th to 13th, the thermocline descends from 5 to 22 m (Figure 3-4c). This displacement suggests the rotation of a cyclonic gyre in the central lake that dispersed the central surface water toward the shores when the conditions are simulated by Meteolakes (Baracchini et al., 2020 – Appendix III-3a). This is supported by the westward currents recorded by the ADCP data (the 12th at 20-25 m depth – Figure 3-4b). During the 13th of September, the water column is recovering from this downwelling and stabilizes with the thermocline at around 15 m depth.

The second focal period is more agitated with wind peaks reaching speeds of 8 m/s. These repeated peaks generate oscillations of the thermocline during two weeks and alternately eastward and westward currents. The wind induced motions provoke an important upwelling on the 6th of October, as indicated by a rise of the thermocline from 24 to 11 m depth (Figure 3-4c). This date is selected as a sub-period to determine the impact of such phenomena on the nutrient dynamics.

The third period is more representative of the autumn conditions with a weaker stratification, a surface mixed layer thicker than 15 m and a deeper thermocline but with calmer conditions than the previous period. A downwelling event is, however, noted during the 24th of October, which may again be related to the establishment of a central cyclonic gyre (Appendix III-3b).

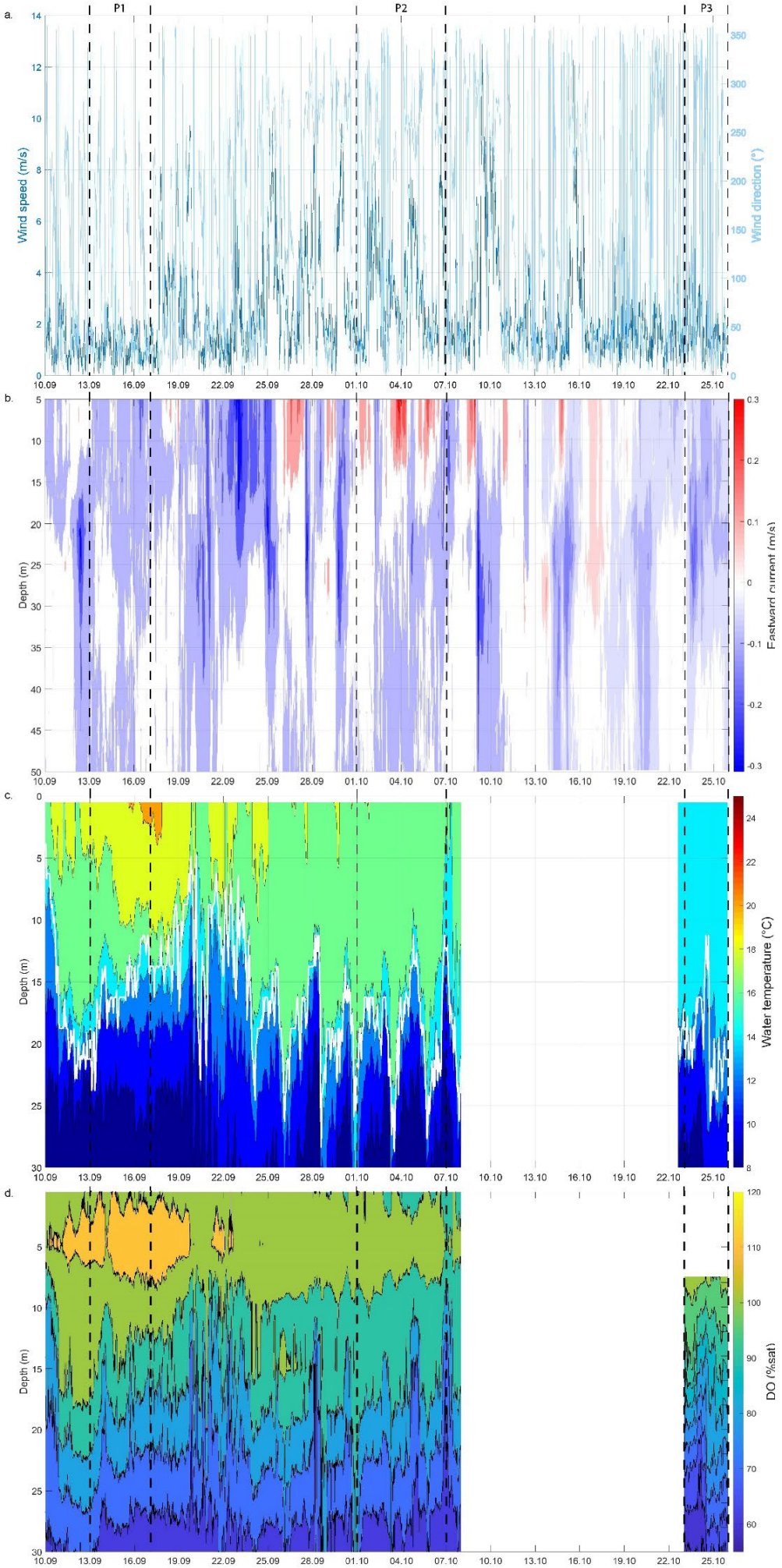

Figure 3-4: Time series of wind speed and direction (a), currents (b), temperature (c) and oxygen saturation (d). Three focal periods are indicated by black dashed lines (P1, P2, and P3), the thermocline (in c) by a white line.

3.2. Correlation between processes

Rhône River fractions are highly variable in time from 0 to 25 % during the study period (all measurements of the isotopic compositions of water and the related Rhône River fractions are given in Appendix III-4). As shown by the time series (Figure 3-5a) and the boxplots (Figure 3-6), the Rhône River water fractions are synchronously varying with the thermocline depth. The highest fractions are measured during a period of stable conditions and especially during the first period with the strongest stratification whereas the smallest fractions correspond to the second period with the most important wind induced movements.

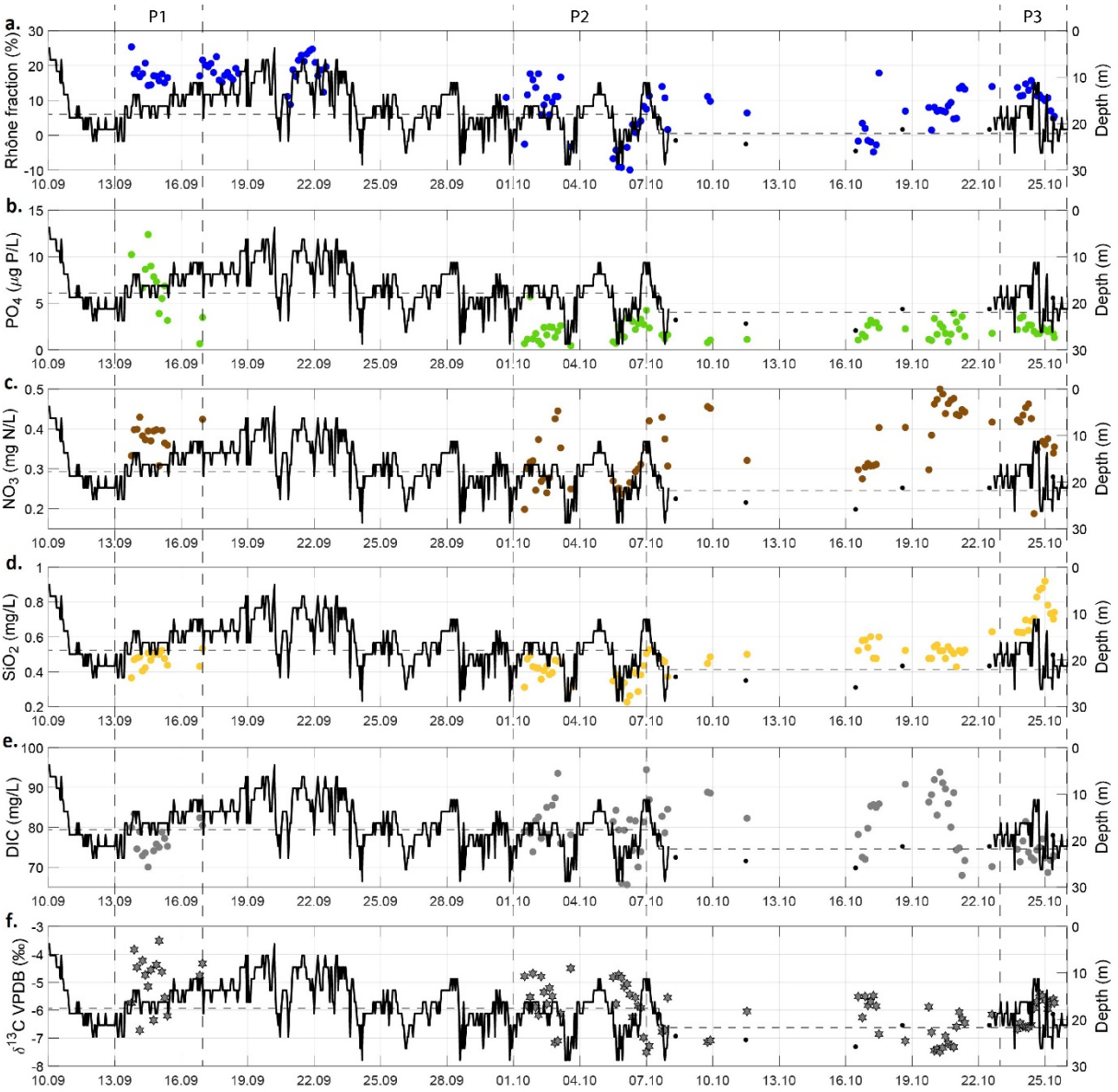

Figure 3-5: Time series of Rhône River water fraction (a), nutrient concentrations (b, c and d), DIC concentration (e) and isotopic composition of DIC (f) (all on the left axis). The thermocline depth is shown as the solid black line and the pump depth, 18 and 22 m, as the dashed line (right axis).

The Rhône fractions are linked to the thermocline excursions, especially during the "Windy Period" (P2) and the upwelling event on October 6th, as noted in Table 3-3 with a high coefficient of determination (R^2 = 0.42 and 0.66 respectively with p-values < 0.001). As shown by Fig. 3-7, the Rhône River fraction depends on the thermocline depth in relation to the pump location. When the thermocline is located above the pump, the Rhône fractions are significantly higher compared to when it is below the pump.

Table 3-3: Results of linear regressions between different parameters identified as proxy of the nutrient dynamic processes for the three focal periods and the 6th of October. Reported are the equations of the linear models (Estimate +SE), the coefficients of determination R^2, the degrees of freedom (df) and the significance levels (p-values). Indicated in bold are the significant correlations with p-value <0.001, in green, the positive correlations and, in red, the negative.

Periods	Dependent variable	Explanatory variable	Estimate (SE)	df	R^2	p-value
Period 1	Rhône fraction	Eastward current	86.4 (18.8)	15	0.326	0.021
	Rhône fraction	Thermocline depth	0.59 (27)	15	0.149	0.140
	DO % sat.	**Thermocline depth**	**-1.01 (74)**	**95**	**0.534**	**<0.001**
	DO % sat.	Rhône fraction	-0.55 (99)	15	0.163	0.121
Period 2	Rhône fraction	Eastward current	37.6 (5.1)	28	0.047	0.256
	Rhône fraction	**Thermocline depth**	**1.36 (30.5)**	**28**	**0.421**	**<0.001**
	DO % sat.	**Thermocline depth**	**-1.12 (65.5)**	**147**	**0.545**	**<0.001**
	DO % sat.	Rhône fraction	-0.14 (87)	28	0.052	0.235
October 6th	Rhône fraction	Eastward current	-86.5 (-4.2)	13	0.306	0.040
	Rhône fraction	**Thermocline depth**	**1.16 (21.8)**	**13**	**0.658**	**<0.001**
	DO % sat.	**Thermocline depth**	**-1.50 (54.4)**	**39**	**0.925**	**<0.001**
	DO % sat.	**Rhône fraction**	**-0.84 (83)**	**13**	**0.73**	**<0.001**
Period 3	Rhône fraction	Eastward current	-15 (10)	14	0.022	0.601
	Rhône fraction	Thermocline depth	0.33 (17.4)	14	0.204	0.091
	DO % sat.	**Thermocline depth**	**-0.67 (62.6)**	**71**	**0.222**	**<0.001**
	DO % sat.	Rhône fraction	-1.05 (88)	14	0.360	0.018

As we can see for all the periods, the oxygen saturation is negatively correlated with the thermocline depth. Indeed, when upper layers are downwelled to deeper layers, they introduce oxygen and vice versa. As such, the oxygen saturation cannot be used as a proxy of in-situ bioproductivity if the vertical motions are important.

3.3. Nutrient concentrations

Nutrient concentrations (PO_4^{3-}, NO_3^- and SiO_2) are also variable with time as illustrated in Figure 3-5 (data are available in Appendix III-5). Differences are particularly noteworthy from one period to another (boxplots in Figure 3-6 and time series of each focal period in Appendices III-7 to III-9).

For the orthophosphate relatively high concentrations were measured during the first period with 10 µg P/L on average, reaching 34 µg P/L on September 14th. It then decreases to around 2 µg P/L for the two other periods as it is measured for the first 50 m by the EPFL profiles (Appendix III-1). Moreover, orthophosphate concentration seems to be slightly higher during the night and lower during the day during the entire study period (ANOVA test: F = 3.45, p-value = 0,067), likely related to a diurnal cycle of photosynthesis/respiration (Figure 3-5b). This trend appears clearly on October 16th/17th and from October 19th to 21st (ANOVA test: F = 6.73, p-value = 0,017) during a relatively calm period as shown by the current velocities (Figure 3-4b). Unfortunately, no DO data were available at this period due to mooring maintenance. If we refer to the correlation factors (Table 3-4), orthophosphate concentration is weakly and negatively correlated to the DO during the third period ($R^2 = 0.47$, p-value < 0.005).

Nitrate concentration shows some important variations during the second, wind agitated period, with concentrations from 0.11 to 0.45 mg N/L. The concentration of nitrate is positively correlated to the Rhône fraction ($R^2 = 0.81$, p-values < 0.001) and to the thermocline depth ($R^2 = 0.74$, p-values < 0.001) for the specific upwelling event of the 6th of October (Table 3-4).

Silica concentration presents the highest values during the third period when the pump was fixed at 22 m depth with 0.74 mg/L on average. Silica is strongly correlated to both the Rhône fraction ($R^2 = 0.61$, p-values < 0.001) and the thermocline depth ($R^2 = 0.53$, p-values < 0.001) during the second period and to the DO ($R^2 = 0.58$, p-values < 0.001) during the third (Table 3-4).

The DIC concentrations are the most important and variable during the Windy Period (P2 – Figure 3-5e) but no significant correlation with selected processes have been noticed. In contrast, its isotopic composition shows significant negative correlation with the thermocline depth during the second period, especially during the 6th of October ($R^2 = 0.67$, p-values < 0.001). It is also positively correlated to the DO ($R^2 = 0.87$, p-values

< 0.001) during the Autumn Period (P3). However, the highest values (the heaviest) are measured during the Summer Period (P1 – Figure 3-6h).

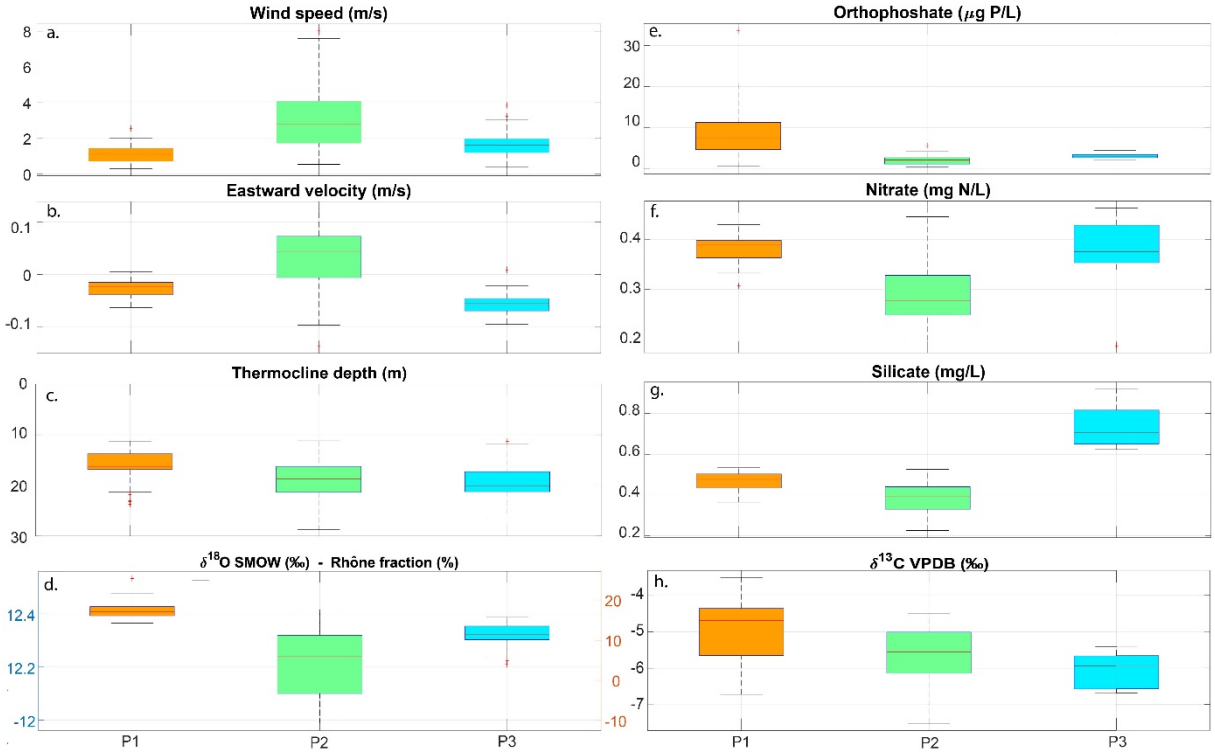

Figure 3-6: Box plots of the different parameters clustered for the three focal periods P1, P2, and P3. On each box, the central red mark indicates the median, and the blue bottom and top edges of the box indicate the 25th and 75th percentiles, respectively.

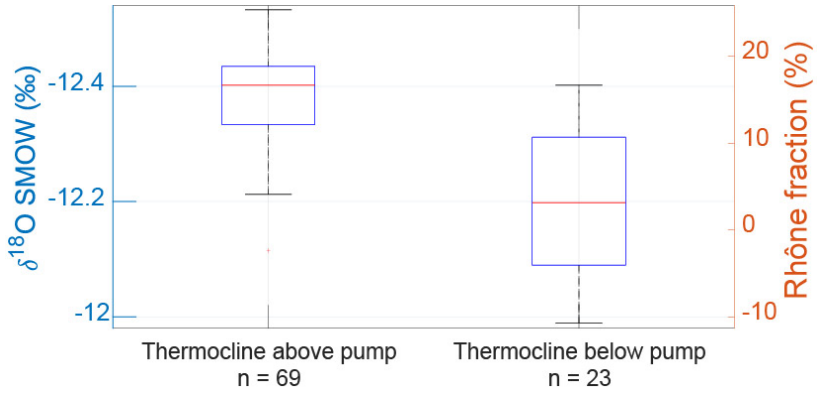

Figure 3-7: The stable isotope composition of water derived Rhône fractions measured when the thermocline is located above the submerged pump are significantly higher than when it is below (ANOVA test: F = 75.9 and p-value = 1.4E-13).

Table 3-4: Results of linear regressions between nutrient concentrations and fraction of Rhône River water, thermocline depth and dissolved oxygen saturation for the three focal periods and the 6th of October. Reported are the equations of the linear models (Estimate +SE), the coefficients of determination R^2, the degrees of freedom (df) and the significance levels (p-values). Indicated in bold are the significant correlations with p-value <0.001, in green, the positive correlations and, in red, the negative.

Explanatory variable	Dependent variable	**Period 1** (df = 15)			**Period 2** (df = 28)			**October 6th** (df = 13)			**Period 3** (df = 14)		
		Estimate (SE)	R^2	p-value	Estimate (SE)	R^2	p-value	Estimate (SE)	R^2	p-value	Estimate (SE)	R^2	p-value
Rhône fraction	PO_4^{3-}	0.002 (9.7)	0	0.998	0.02 (2.0)	0.032	0.352	0.065 (2.5)	0.220	0.091	0.074 (1.4)	0.144	0.163
	NO_3^-	0 (0.4)	0.001	0.89	0.004 (0.28)	0.352	0.002	**0.007 (0.30)**	**0.811**	**<0.001**	0.005 (0.3)	0.050	0.461
	SiO_2	-0.007 (0.6)	0.200	0.082	**0.007 (0.36)**	**0.614**	**<0.001**	0.009 (0.37)	0.554	0.002	-0.007 (0.81)	0.049	0.430
	DIC	0.319 (71.4)	0.060	0.361	0.21 (78.8)	0.081	0.135	0.34 (79)	0.101	0.268	0.28 (70.6)	0.090	0.276
	δ^{13}_{DIC}	-0.009 (-4.8)	0	0.922	-0.05 (-5.5)	0.239	0.007	**-0.11 (-5.9)**	**0.793**	**<0.001**	-0.09 (-5)	0.380	0.014
Thermocline depth	PO_4^{3-}	-0.06 (8.8)	0	0.958	0.04 (2.9)	0.020	0.465	0.051 (3.4)	0.065	0.378	0.031 (2.9)	0.049	0.427
	NO_3^-	0.005 (0.4)	0.077	0.297	0.007 (0.4)	0.235	0.014	**0.009 (0.48)**	**0.744**	**<0.001**	-0.004 (0.31)	0.049	0.469
	SiO_2	0.002 (0.5)	0.009	0.731	**0.013 (0.64)**	**0.531**	**<0.001**	**0.014 (0.63)**	**0.681**	**<0.001**	-0.013 (0.49)	0.328	0.026
	DIC	0.67 (87.6)	0.114	0.200	0.66 (92.3)	0.177	0.023	0.74 (93)	0.238	0.077	0.07 (75.1)	0.011	0.715
	δ^{13}_{DIC}	0.10 (-3.4)	0.039	0.464	**-0.12 (-7.9)**	**0.336**	**<0.001**	**-0.14 (-8.6)**	**0.671**	**<0.001**	-0.06 (-7.1)	0.252	0.056
Dissolved Oxygen (% sat.)	PO_4^{3-}	-0.90 (90.2)	0.185	0.096	-0.08 (9.2)	0.146	0.041	-0.07 (8.6)	0.269	0.058	-0.077 (8.1)	0.476	0.004
	NO_3^-	-0.003 (0.6)	0.151	0.136	-0.007 (0.89)	0.286	0.006	**-0.007 (0.9)**	**0.807**	**<0.001**	-0.008 (0.95)	0.330	0.040
	SiO_2	0.002 (0.28)	0.030	0.524	-0.006 (0.92)	0.206	0.013	-0.009 (1.1)	0.566	0.002	**0.013 (-0.29)**	**0.583**	**<0.001**
	DIC	-0.29 (103)	0.093	0.250	-0.47 (120)	0.157	0.033	-0.52 (122)	0.230	0.083	-0.24 (92.4)	0.205	0.090
	δ^{13}_{DIC}	-0.02 (-2.9)	0.009	0.729	**-0.11 (-15)**	**0.549**	**<0.001**	**0.11 (-15)**	**0.784**	**<0.001**	**0.08 (-12)**	**0.872**	**<0.001**

3.4. Models on October 6th

The day of October 6th is selected to apply the models of nutrient concentration as it presents a well identifiable upwelling event. The Rhône fractions and the thermocline level progressively rise from 0 to 11 % and from 24 m to 11 m deep respectively (Appendix III-8).

The significant positive correlations of nitrate and silica concentrations with the Rhône water fractions during this event support the hypothesis H1 that horizontal advection from the Rhône River influences the distribution of the nutrients in the water column. The mixing model supports this hypothesis with good correspondence between the modelled and measured data for the silica but not for the nitrate (Figure 3-8a and 3-8b respectively). Moreover, these two nutrients show significant positive correlations with the thermocline depth, which supports the second hypothesis H2 of vertical advection of enriched water. It is supported by the good correspondence between the measured silica concentrations and the ones calculated by the vertical advection model (Figure 3-8a). The modelled nitrate concentrations also show a rising trend, supporting this hypothesis (Figure 3-8b). Additionally, it is validated by the observed increase of the DIC concentration and the significant negative correlation between its isotope composition and the thermocline depth. The low values, until -7.5 ‰ at the maximum of the upwelling, are characteristics of the composition of the deep layers of the lake not impacted by bioproductivity, CO_2 diffusion and carbonate precipitation in the epilimnion (Halder et al., 2013).

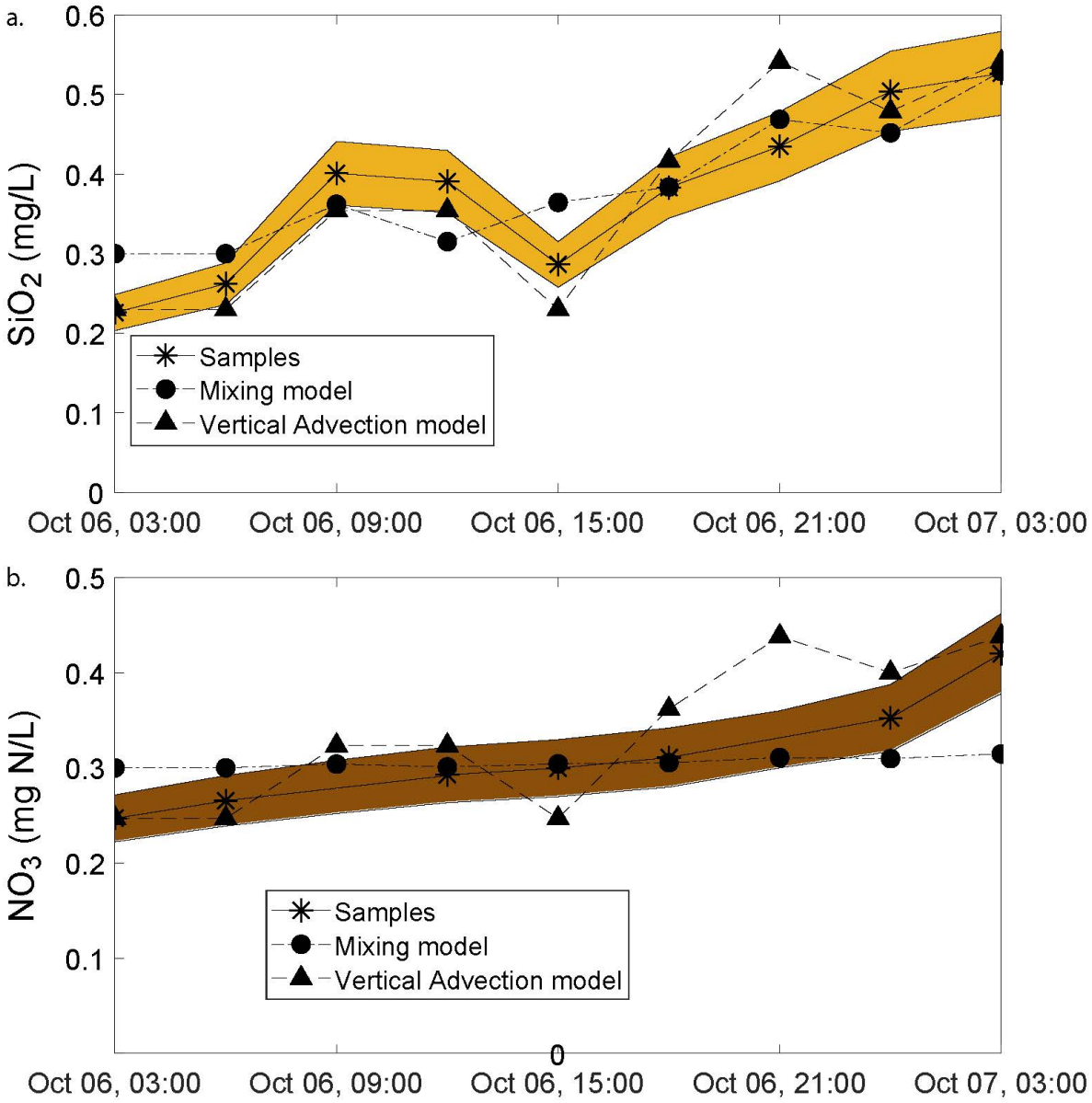

Figure 3-8: Measured and modelled data of silica concentrations (a) and nitrate concentrations (b) during the upwelling event of October 6th. The measured data are represented by stars with +/- 10 % limits in colour. Mixing model data and vertical advection model data are shown as circles and triangles respectively.

4. Discussion

4.1. Rhône interflow dynamics

During the stratification period, the Rhône River intrusion occurs in the metalimnion of Lake Geneva. Most of the interflow is then located below the thermocline as this point of highest density gradient blocks its upward vertical diffusion (Cotte and Vennemann, 2020). This is confirmed by the higher calculated Rhône River water fraction when the thermocline is located above the depth of the pump intake (Figure 3-7). However, albeit smaller, Rhône water fractions are also measured when the thermocline is situated below the pump. This can be explained by a widening of the isotherms inducing a higher vertical dispersion of the Rhône interflow as observed by Cotte and Vennemann (2020). These perturbations of the water column stability can be provoked by wind induced hydrodynamic processes such as Kelvin waves (Bouffard and Lemmin, 2013). A more pronounced stratification results in a more concentrated metalimnion in Rhône River water (Cotte and Vennemann, 2020). This is shown here by the highest Rhône River water fractions measured during the Summer Period. With the weakening of the stratification, the Rhône interflow is dispersed and progressively mixed in the surface mixed layer (cf. Chapter II) and is thus less concentrated around the thermocline, as observed during the Autumn Period.

Horizontally, the Rhône interflow advection by the wind induced circulation is accentuated by the strength of the stratification (Cimatoribus et al., 2019). However, the measured Rhône River fractions do not correlate with the horizontal currents, even during periods with a stable thermocline (Period 1, Table 3-3). This is related to the gyral circulations of the lake. These gyres can create a rapid transit path along the northern shore when a cyclonic gyre sets up at the basin scale. Instead, smaller gyres can appear and disperse more widely the Rhône interflow water (Cimatoribus et al., 2019). Thus, currents from the eastern part of the lake do not necessarily receive water from the Rhône rivermouth. During the stratification period, the metalimnion is continuously supplied with Rhône River water but the exact locations of this interflow are governed by the recirculation in the basin depending on the direction of rotation of the gyres. As a consequence, the recirculation rates control the transit times of the Rhône River interflow and with that the flux of the nutrients received from the Rhône River. In addition, given

the variable nutrient concentrations of the Rhône itself, a high Rhône River fraction does not necessarily result in a significant input of nutrients from the Rhône.

4.2. Nutrient dynamics processes

The first period is the most stable, characterized by a pronounced stratification and hence also low vertical and horizontal motions (Figure 3-4). This results in a stable thermocline and relatively homogeneous nutrient concentrations at any one depth (Figure 3-6). An exception is given by the orthophosphate that reaches high concentrations of 34 µg P/L on the 14th of September but then decreases to baseline values of 2-3 µg P/L only. As the platform is close to the shore (570 m), this might also be a local focussed outwash due to an accidental input of excess phosphorus in the coastal zone.

The Second Period is clearly the most agitated, with changing strengths and directions of wind causing important horizontal and vertical water movements (Figure 3-4). The associated large displacements of the thermocline also displace the chemocline and may also lead to important upwelling of deep water enriched in nitrate and silica as seen on the 6th of October. This event provokes also the vertical advection of the core zone of the Rhône interflow that brings residual silica from the river. Indeed, the diatom biomass (i.e. species metabolising silica) decreased from more than 3000 µg/L in spring to about 1000 µg/L in autumn (CIPEL, 2020) reducing the biological silica uptake. However, the upwelling is not enough to bring water enriched in orthophosphate up to the pump depth; the thermocline having a maximum depth of 29 m while the orthophosphate depletion extends down to 50 m.

The third period is less agitated but still has displacements of the thermocline from about 16 to 23 m depth on the 24th of October (Appendix III-9) related to the anticlockwise rotation of the central gyre (Appendix III-3b). This downwelling, similarly to the one occurring on the 3rd of October (P2), is accompanied by a slight decrease in orthophosphate (from 2.7 to 1.9 µg P/L on average), nitrate (from 0.44 to 0.36 mg N/L in average), as well as an increase of $\delta^{13}C_{DIC}$ (from -6.5 to -5.6 ‰ on average). However, these changes occur just ahead of the downwelling event. Indeed, an increase of DO (from 70 to 80 % sat. in average) also occurs about 6 hours before the decrease of the thermocline (Appendix III-9). This suggests an increase in photosynthesis and consumption of dissolved nutrients just before the more agitated episode.

4.3. Nutrient bioavailability

These variable concentrations of nutrient measured at a fixed depth clearly demonstrate the important nutrient dynamics of the lake's water column. These horizontal and vertical movements of the Rhône River interflow and its charge of nutrients will hence also influence the overall primary production of the lake. This is expected to particularly affect this period of the year as the epilimnion and metalimnion are generally depleted in nutrients towards the end of the growing season. For instance, if we refer to the fertilisation processes by a river intrusion described by Rueda et al. (2007), a direct fertilisation of the Rhône River can be considered at this time of the year when it is observed as an interflow in the metalimnion. Moreover, by intruding the water column just below the thermocline, it can fertilise the upper layers of the metalimnion when wind-induced upwelling raises the thermocline. However, the spatial extent of such effects will depend, as discussed before, on the transit path of the interflow that is controlled by the main circulation pattern of the lake (Cimatoribus et al., 2019). The primary production and hence the uptake of nutrients on the interflow pathway will also define the nutrient conservation (Mackay et al., 2011). In this study, the nutrient input from the Rhône River to this part of the lake has been significantly measured only for the silica. Hence, the Rhône interflow phenomenon may have an impact on the diatom community of the Grand-Lac, the main basin of Lake Geneva, at this time of the year.

The vertical motions within the water column hence can be noted to be important factors of the nutrient dynamics within Lake Geneva. By upwelling enriched-nutrient water or downwelling nutrient-depleted water, the bioavailability of the nutrients for the primary producers will fluctuate in concert (Pannard et al., 2011). Thus, the vertical oscillations produced by direct wind forcing or internal waves may modify the distribution of phytoplankton (Serra et al., 2007).

Finally, the internal metabolic processes within the bioproductive zone will also influence the nutrient dynamics. However, their impact is hard to quantify as the proxies of this metabolism (DO and $\delta^{13}C_{DIC}$) are highly correlated with the lake's hydrodynamic (Table 3-3). Nevertheless, some evidence of such processes is detectable in our data during calm periods. The diurnal cycle of energy availability and thus slight increase and decrease of orthophosphate concentration during night and day respectively, indicates an efficient recycling of the recently remineralized nutrients by the primary producers. Moreover, the consumption of orthophosphate and nitrate in parallel of the enrichment in

^{13}C of the DIC observed in the middle of the 24th of October supports an increase in photosynthetic activity.

5. Conclusion

The new data presented here show nutrient concentrations that are highly variable in space and time within Lake Geneva's water column during the stratification period. The nutrient dynamics is controlled by the hydrodynamics of the lake. Indeed, the local forces of the gyral motions of water and the direct impact of wind forcing on the thermocline location induce vertical as well as horizontal displacements of the nutrients. In addition, the Rhône River water reaches the central northern part of the lake via its pronounced interflow. Depending on the variable nutrient concentrations of the Rhône River, its interflow pathway and the biological uptake within the interflow itself, the Rhône nutrients can fertilise the lake to a lesser or stronger degree. As the Rhône interflow is focussed just below the thermocline, vertical advections of Rhône nutrients and also nutrient-richer deeper water from hypolimnion can be uplifted during an upwelling event. This coupled transport brings nutrients up to the euphotic zone and can hence make them bioavailable. Then, the efficiency of primary producers to uptake the remineralized P has been revealed. It is particularly notable in this context of re-oligotrophication of the lake and at this time of the year with particularly low orthophosphate concentrations in the top-layers.

However, as commonly noted for large lakes, these processes controlling the nutrient concentrations in the water column mostly occur simultaneously. The parameters used as proxies of these processes showing strong interdependence, it makes their different contributions hardly quantifiable. A higher sampling frequency could allow to deconvolute the different physical, chemical and biological processes occurring to different time-scales. For example, a spectral analysis of a denser nutrient signal should allow to estimate the metabolic rate and distinguish it from the vertical and horizontal advection. To increase the temporal resolution of nutrient data, direct onsite analysis can be imagined with the conception of a chemical laboratory on the platform. Furthermore, another interesting opportunity would be to use the currently on site Thetis autonomous profiler to evaluate the Rhône interflow inputs. Actually, the Thetis allows to get high frequency data of the top 50 m of Lake Geneva near the LéXPLORE platform (https://www.epfl.ch/labs/aphys/index-html/news/thetis-letters/). By checking the correspondence between its backscattering signal and the Rhône water input using the stable isotope composition of the water, its signal could be used as proxy of the Rhône interflow. It would be of interest to quantify and compare the Rhône River interflow and

the upwelling inputs of nutrient to the euphotic zone over the scale of the whole growing season.

The detailed time-series analyses of this study also reiterate the rather poor spatial and temporal representativeness of the monitoring station SHL2. As it is located in the middle of the lake, it is not influenced in the same way by the wind induced motions and the Rhône input compared to the coastal areas. A coupled monitoring of this central point and at the location of the LéXPLORE platform would offer a good opportunity to determine the link between the hydrodynamic and the ecological processes of the larger lake.

Finally, this study demonstrates that a good assessment of the water quality of a lake the size of Lake Geneva requires detailed monitoring of both rivers and others surface water inputs, as well as monitoring the upwelling of deeper waters and the metabolic processes within the active zone of primary production.

Acknowledgements

Thank you to the steering committee of the platform for accepting my project. A special thanks to Aurelien Ballu (IDYST, UNIL) and Sébastien Lavanchy (APHYS, EPFL) for their technical supervision and for the installation of the pumping system at the platform. Thank you to Ludovic Baron (ISTE, UNIL) who kindly borrowed the submersible pump to the project. Thank you to Matthieu Fallet, Pascal Perolo, Nathalie Diaz, Benjamin Lehmann, Jessica Chaves, Annelore Bessat and Martin Calianno who helped me with the sampling. Finally, thank you to Laetitia Monbaron and Thibault Lambert for their support in the laboratories and to Jessica Chaves (UNIL) who performed the DIC analysis.

References

Anneville, O., Beniston, M., Gallina, N., Gillet, C., Jacquet, S., Lazzarotto, J., 2013. L'empreinte du changement climatique sur le Léman. ARCHIVES DES SCIENCES 16.

Anneville, O., Dur, G., Rimet, F., Souissi, S., 2018. Plasticity in phytoplankton annual periodicity: an adaptation to long-term environmental changes. Hydrobiologia 824, 121–141. https://doi.org/10.1007/s10750-017-3412-z

Anneville, O., Pelletier, J.P., 2000. Recovery of Lake Geneva from eutrophication: quantitative response of phytoplankton. fal 148, 607–624. https://doi.org/10.1127/archiv-hydrobiol/148/2000/607

Baracchini, T., Wüest, A., Bouffard, D., 2020. Meteolakes: An operational online three-dimensional forecasting platform for lake hydrodynamics. Water Research 172, 115529. https://doi.org/10.1016/j.watres.2020.115529

Bouffard, D., Kiefer, I., Wüest, A., Wunderle, S., Odermatt, D., 2018. Are surface temperature and chlorophyll in a large deep lake related? An analysis based on satellite observations in synergy with hydrodynamic modelling and in-situ data. Remote Sensing of Environment 209, 510–523. https://doi.org/10.1016/j.rse.2018.02.056

Bouffard, D., Lemmin, U., 2013. Kelvin waves in Lake Geneva. Journal of Great Lakes Research 39, 637–645. https://doi.org/10.1016/j.jglr.2013.09.005

Cimatoribus, A.A., Lemmin, U., Barry, D.A., 2019. Tracking Lagrangian transport in Lake Geneva: A 3D numerical modeling investigation. Limnol Oceanogr 64, 1252–1269. https://doi.org/10.1002/lno.11111

Conseil scientifique de la commission internationale pour la protection des eaux du Léman contre la pollution. 2020. Rapports sur les études et recherches entreprises dans le bassin lémanique. Campagne 2019. CIPEL.

Cotte, G., Vennemann, T.W., 2020. Mixing of Rhône River water in Lake Geneva: Seasonal tracing using stable isotope composition of water. Journal of Great Lakes Research 46, 839–849. https://doi.org/10.1016/j.jglr.2020.05.015

Lemmin, U., Mortimer, C.H., Bäuerle, E., 2005. Internal seiche dynamics in Lake Geneva. Limnol. Oceanogr. 50, 207–216. https://doi.org/10.4319/lo.2005.50.1.0207

Mackay, E.B., Jones, I.D., Folkard, A.M., Thackeray, S.J., 2011. Transition zones in small lakes: the importance of dilution and biological uptake on lake-wide heterogeneity. Hydrobiologia 678, 85–97. https://doi.org/10.1007/s10750-011-0825-y

Moisset, S., 2017. Investigation of the link between phytoplankton and nutrients dynamic in Lake Geneva. Thèse de doctorat. University of Geneva. https://doi.org/10.13097/archive-ouverte/unige:96830

Pannard, A., Beisner, B.E., Bird, D.F., Braun, J., Planas, D., Bormans, M., 2011. Recurrent internal waves in a small lake: Potential ecological consequences for metalimnetic phytoplankton populations: Vertical internal modes in a small lake. Limnol. Oceanogr. 1, 91–109. https://doi.org/10.1215/21573698-1303296

Perroud, M., Goyette, S., 2012. Interfacing a one-dimensional lake model with a single-column atmospheric model: 2. Thermal response of the deep Lake Geneva, Switzerland under a 2 × CO2 global climate change. Water Resources Research 48. https://doi.org/10.1029/2011WR011222

Perroud, M., Goyette, S., Martynov, A., Beniston, M., Annevillec, O., 2009. Simulation of multiannual thermal profiles in deep Lake Geneva: A comparison of one-dimensional lake models. Limnol. Oceanogr. 54, 1574–1594. https://doi.org/10.4319/lo.2009.54.5.1574

Rueda, F.J., Fleenor, W.E., de Vicente, I., 2007. Pathways of river nutrients towards the euphotic zone in a deep-reservoir of small size: Uncertainty analysis.Ecological Modelling 202, 345–361. https://doi.org/10.1016/j.ecolmodel.2006.11.006

Serra, T., Vidal, J., Casamitjana, X., Soler, M., Colomer, J., 2007. The role of surface vertical mixing in phytoplankton distribution in a stratified reservoir. Limnol. Oceanogr. 52, 620–634. https://doi.org/10.4319/lo.2007.52.2.0620

Spötl, C., Vennemann, T.W., 2003. Continuous-flow isotope ratio mass spectrometric analysis of carbonate minerals. Rapid Communications in Mass Spectrometry 17, 1004–1006. https://doi.org/10.1002/rcm.1010

Tadonleke, R.D., Lazzarotto, J., Anneville, O., Druart, J.-C., 2009. Phytoplankton productivity increased in Lake Geneva despite phosphorus loading reduction. Journal of Plankton Research 31, 1179–1194. https://doi.org/10.1093/plankt/fbp063

Zhong, Y., Notaro, M., Vavrus, S.J., Foster, M.J., 2016. Recent accelerated warming of the Laurentian Great Lakes: Physical drivers. Limnology and Oceanography 61, 1762–1786. https://doi.org/10.1002/lno.10331

Chapter IV

Hydrodynamic, physico-chemical, and biological aspects of the transition zone between the Rhône River and Lake Geneva

Authors: Cotte Gabriel[1], Frédéric Soulignac[2], Fabio dos Santos Correia[3], Matthieu Fallet[1], Bastiaan Willem Ibelings[3], Ulrich Lemmin[2], Andrew D. Barry[2], and Torsten W. Vennemann[1]

[1]IDYST, UNIL, Géopolis, 1015 Lausanne, Gabriel.Cotte@unil.ch
[2]ECOL, EPFL, Route Cantonale, 1015 Lausanne, Frederic.Soulignac@epfl.ch
[3]ISE, UNIGE, Uni Carl Vogt, 1205 Genève, Fabio.DosSantosCorreia@unige.ch

Abstract

Lake Geneva is in a process of re-oligotrophication with phosphorous concentrations decreasing last decades. However, the phytoplankton biomass measured in the lake remained stable. Today, the effect of climate change is impacting the nutrient dynamics of the lake and it is expected that the only source of nutrients to the euphotic zone will come from the watershed. As the Rhône River has been identified as the main phosphorus input to the lake, it is important to assess its influence on the dispersion of phosphorous in the lake and then on primary production. This study focused on the transition zone between the Rhône River and Lake Geneva with the aim of better understanding the complexities and controls of phytoplankton growth in this area. Two field campaigns were carried out and the water samples collected from longitudinal and transversal transects were analysed for both nutrient and phytoplankton concentrations, and the fraction of Rhône River water was determined by the stable isotope composition of the water. The results indicate gradients in P and Si which are related to the Rhône intrusion. Furthermore, the Rhône River mouth area appears to be a dynamic zone that punctually present optimal condition for phytoplankton growth. In April, a wind event homogenised the early, weak stratification of the lake, mixed the Rhône-derived nutrients and drop the turbidity within the euphotic zone, increasing by 44 % the phytoplankton biovolume. In September, out of the turbid and turbulent near field of the river mouth, the Rhône interflow located just below the thermocline generated a local deep chlorophyll maximum.

Keywords

Lake Geneva; Rhône River mouth; hydrodynamics; nutrient gradient; phytoplankton; lake-river mixing

1. Introduction

After a period of eutrophication during the 1960's and 1970's with annual average total phosphorus concentrations reaching 90 µg P/L, Lake Geneva is in a process of re-oligotrophication. Since the 1980's, Swiss and French measures have been taken to limit the phosphorus input into the lake. Hence, the mean concentration of total phosphorus decreased to about 16 µgP/L in 2019 (CIPEL, 2020). Despite this important reduction, the amount of phytoplankton biomass measured every year has not declined (Tadonleke et al., 2009; Rimet et al., 2020). This initiated a range of studies to determine the evolution of the phytoplankton community through time (Anneville et al., 2002, 2018) and to better understand the spatio-temporal heterogeneities of algal growth in the lake (Soulignac et al., 2018). It has been shown that the phosphorus became the limiting nutrient driving primary production from 1995 onwards (Moisset, 2017). Additionally, climate change provokes an extension of the growing season with an advanced stratification onset and earlier algal blooms in spring (Anneville et al., 2018). Moreover, climate warming is expected to reduce the frequency of the complete lake overturn occurring at the end of winter that bring bottom nutrients to the surface water (Perroud et al., 2009). Consequently, it is expected that the main nutrients input to the euphotic zone of the lake will come from its watershed (Anneville et al., 2013). It is then important to further evaluate the riverine inputs of the nutrients, their transport and their subsequent distribution in the lake, in order to help understand their metabolization and hence their role in the primary production of the lake.

The Rhône River is the principal tributary to Lake Geneva, both in terms of discharge of water and sediment load. It represents 77 % of the annual dissolved inorganic phosphorus input from the rivers to the lake (24 t in 2018, CIPEL 2019). Therefore, it influences the physical and chemical properties of the lake and also its ecological functioning (Bouffard and Perga, 2016; Nouchi et al., 2019). The Rhône River mouth is located in the eastern part of Lake Geneva, called the Haut-Lac. It has been discovered that the Rhône River water is transported as an interflow through the entire basin during the stratification period of the lake (Halder et al., 2013). This interflow occurs at the thermocline depth and its transport is driven by the circulation gyres of the lake (Cotte and Vennemann, 2020).

While the primary production and the biodiversity of the phytoplankton are regularly monitored in Lake Geneva, this is only done at two stations: SHL2 in middle and at the

deepest point of the lake, and GE3 in the smaller Lake Geneva basin (CIPEL reports 1969 to 2020). As these profiles represent only the central points within the two lake basins (Kiefer et al., 2015), much less is known about the river-lake transition zones. Not only may these zones represent much more complex phytoplankton dynamics, but given the importance of the Rhône River for the overall water balance, this transition zone also can be expected to play a major role in the ecology of the lake as a whole (Soomets et al., 2019).

The river-lake transition zone was hence examined at the Rhône River mouth with the aim of understanding the complexities and controls of phytoplankton growth in this specific deltaic ecosystem. Specific research questions asked include:

1) Is there a chemical gradient related to the Rhône River intrusion in the river-lake transition zone?
2) Which hydrodynamic processes at the river mouth, if any, are contributing to change the conditions for phytoplankton growth?
3) Is there a biological gradient, hence is there a specific "ecocline" present in this transition zone?

Preliminary field measurements made during July 2018 in the area of the river mouth showed a high concentration of chlorophyll *a* (Chl *a*) and phytoplankton (measured using respectively a Fluoroprobe and a CytoBuoy) close to the river mouth suggesting an optimal zone for the phytoplankton growth (Correia et al., in preparation). Field experiments in the transition zone within a 2 km radius from the river mouth revealed complex hydrodynamics in this region, involving also the introduction and subsequent loss of suspended sediments at the river-lake transition (Piton et al., in preparation). These initial measurements hence support the existence of an ecocline defined by the Rhône River intrusion. Moreover, we presume the hydrodynamic processes occurring at the river mouth induced by the Rhône River intrusion are able to produce vortex effects and so, upwelling of nutrient-rich bottom waters, remobilising nutrients for phytoplankton. Finally, we expect a higher abundance of phytoplankton due to a - hypothetical - optimal zone where an equilibrium occurs between the nutrients transported by the Rhône River and the other limiting factors within the lake, such as sunlight (low turbidity), low flow speed and temperature.

2. Material and methods

2.1. Sampling strategy

Fieldwork was planned to include two different seasons: the first campaign was organised in April during the spring phytoplankton bloom, which also represents the period of the first onset of the thermal stratification of Lake Geneva, and a second campaign in September at the end of summer covering a period of stronger stratification with an euphotic zone more depleted in dissolved nutrients. Two transects were sampled per campaign, each campaign covering two days with one transect per day (Figure 4-1). The transversal transect (T1) was located in the near field which is defined as the area where the Rhône interflow current velocity is still measurable with a typical background current in the lake of 10 cm/s. The second, longitudinal transect (T2) is located on the river-lake continuum. The suffixes A for April and S for September were added to the transect names to differentiate the campaigns (e.g., T1-A, T1-S). Details on coordinates and sampling dates of the different stations can be found in Appendix IV-1.

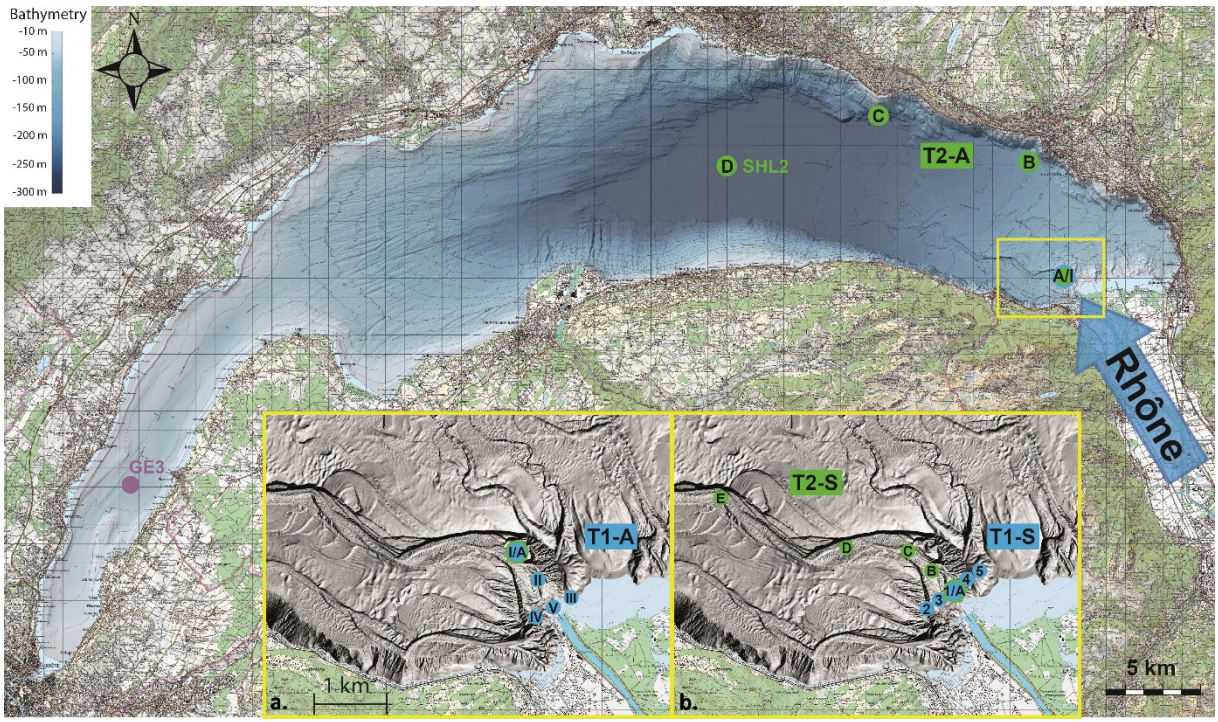

Figure 4-1: Bathymetric map of Lake Geneva and sampling stations of transect 2 in April (A to D) (main map). The Rhône River inflow is indicated by a blue arrow. SHL2 and GE3 are the two permanent monitoring stations within Lake Geneva. Larger scale maps of the Rhône River mouth area show the sampling stations of transect 1 in April (I to V) (insert a) and sampling stations of transect 1 (1 to 5) and 2 (A to E) in September (insert b).

On the 2nd of April 2019, the T2-A stations were chosen as a function of the hydrodynamic forecast of the online model meteolakes.ch (Baracchini et al., 2020). These simulations indicated a cyclonic gyre in the main basin deflecting the water towards the northern shore (Appendix IV-2). One station was then placed one km in front of the Rhône River mouth (A) and two along the northern shore (B - 5 km and C - 14 km from the river mouth). An additional sampling station was placed 22 km from the river mouth, towards the middle of the lake (D), still on the supposed path of the Rhône interflow transported by the cyclonic gyre, but also corresponding to the location of SHL2, the CIPEL's monitoring station (Rimet et al., 2020). On the 4th of April, because no trace of interflow was detected at 5 km from the river mouth (profile GC11 – Appendix IV-3), the T1-A stations I to V were placed closer to the river mouth.

On the 24th of September 2019, sampling covered the stations 1 to 5 for T1-S and on the 26th of September the stations A to E for T2-S (Figure 4-1). Continuous vertical profiles of current velocity and direction were measured along the rectilinear ADCP transect 1 corresponding to T1-S, by using a Teledyne Marine Workhorse Sentinel ADCP on the 24th of September, and along the circular ADCP transects 2 to 5 on the 26th of September (Figure 4-2). The ADCP was mounted facing downwards on a small catamaran, and the catamaran was towed by the boat *Elodea* (ECOL laboratory – EPFL) that progressed at its minimal speed of approximately 0.7 m/s. The bin size was set to 1 m and the number of bins to 100. The ADCP measurements were used to track the river interflow along its development from the river mouth into the lake (Figure 4-2). When considering the horizontal direction, the station 1 is located in the middle of the river interflow along the rectilinear ADCP transect 1 at 400 m from the river mouth. The stations 2 and 5 are located outside of the river interflow at the west and at the east, respectively. The station 3 is located in the middle of stations 2 and 1, and station 4 is in between stations 1 and 5. The stations A to C are located in the centre of the river interflow at 400, 800 and 1200 m from the river mouth, respectively. The station D defines the limit of the near field area at 2 km and the station E is the background station located 4 km from the river mouth.

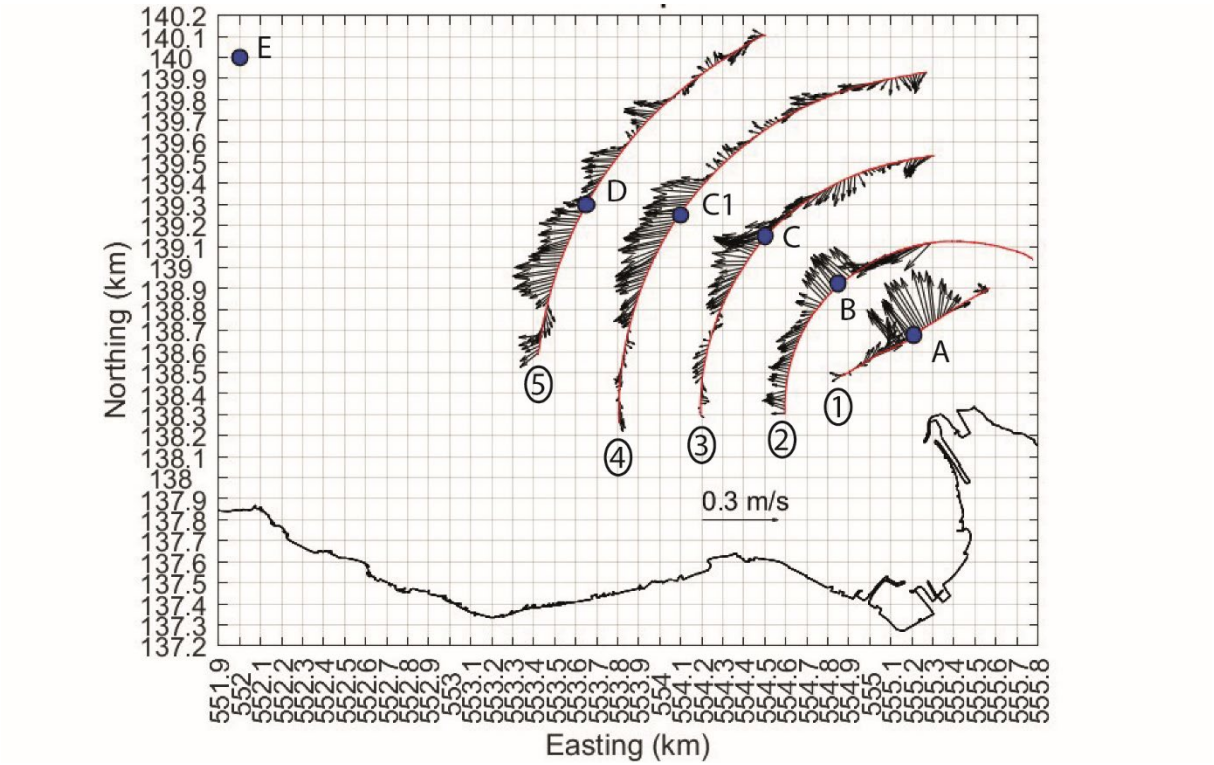

Figure 4-2: Quiver plots of measured current velocity at 25 m depth in the Rhône River mouth area at the ADCP transects 1 to 5 on the 26th of September. The sampling stations of T2-S (A to E) are indicated by blue dots. The black line at the bottom indicates the shore line.

Samples for the chemical and biological measurements were taken using the boat *La Licorne* (Department F.-A. Forel – UNIGE), equipped with an automatic Rosette water sampler (1018 Mini Rosette Sampling System, General Oceanics Inc.). The Rosette consists of 11 Niskin bottles (1.7 L), and was coupled to a CTD (conductivity-temperature-depth) probe (OCEAN SEVEN 316Plus CTD, IDRONAUT Srl), which was externally powered via a telemetry cable to provide real-time information on electrical conductivity, oxygen, pH, temperature and depth (pressure). A continuous CTD cast without interruptions was taken while lowering the sampling system and water samples were taken when raising the system. In order to compare the different profiles, a systematic depth sampling was choosen for the depth locations. Ten of the eleven bottles of the Rosette were used for this sampling (1, 2.5, 5, 7.5, 10, 15, 20, 30, 100 m, bottom) and the remaining bottle to sample a possible peak of turbidity in the middle of the interflow. CTD data were saved when the water samples were taken. The sensor precisions are 0.003 mS/cm for conductivity, 0.003 °C for temperature, 0.05 % for the depth (pressure), 0.001 units for pH, and 0.01 ppm for oxygen measurements. Conductivity [κ25] is given relative to 25 °C in the result section. Physical data were processed by REDAS-5 Release 5.40 (IDRONAUT Srl). For the biological analysis,

aliquots of 5 ml were directly taken from raw water samples and fixed with 200 µL of glutaraldéhyde (Vaulot et al., 1989). No duplicates were taken. For the chemical analysis, water samples were filtered with 0.45 µm nylon filters using a peristaltic pump and stored at 5 °C directly on board. Upon return to the laboratory, samples were stored at -18 °C until the major ion analysis was done. Split samples for the stable isotope analysis were refrigerated at 5 °C prior to analysis, performed within a week of sampling. Finally, an ISCO automatic sampler was installed at the hydrologic station of Porte du Scex, located 5 km upstream of the Rhône River mouth, which sampled the waters on a daily basis in parallel to the sampling campaigns to determine the daily fluctuations of the stable isotope composition of the river water. Finally, grab river samples were taken at the river mouth with a bucket from the river surface every sampling day to evaluate the nutrient input from the Rhône watershed.

2.2. Analysis

Stable isotopes of water

The oxygen and hydrogen isotope compositions were analysed using a Picarro L2140i following the method described in Cotte and Vennemann (2020).

Nutrient concentrations

The orthophosphate ($P\text{-}PO_4^{3-}$) concentrations were measured spectrophotometrically using the molybdenum blue method (Murphy and Riley, 1962) at 882 nm on a UV-visible spectrometer (Perkin Elmer). The analytical error was estimated by the standard deviation of the standards analysed as triplicates. The detection limit is 1 µg ($P\text{-}PO_4^{3-}$)/L.

Nitrate concentrations were measured by liquid ion-chromatography (ICS-1100 of Dionex). Each sequence was calibrated using five standards. A sequence consisted of duplicate samples, internal standards and blanks. The analytical error for each sample was estimated by the standard deviation of the duplicates. The detection limit is 0.07 mg ($N\text{-}NO_3^-$)/L.

The silica concentrations were measured spectrophotometrically using a SmartChem 200 (AMS Alliance). Duplicates of samples were analysed with internal standards and blanks. The standard deviation of the duplicates was used to evaluate the analytical error. The detection limit is 0.1 mg SiO_2/L.

All the chemical analysis results are presented in Appendix IV-4.

Phytoplankton biovolume

A CytoSense scanning flow cytometer (CytoBuoy, The Netherlands) was configured with a smart-trigger level of 20 mV for red fluorescence (FLR, targeted to count only the particles having chlorophyll) at a flow rate of 4.1 µL/s for 15 min maximum; the pump switched off once 15 000 particles had been analysed. After a testing phase, data were treated with *CytoClus 4 software* to remove electronic noise and any debris such as particulate organic matter. Groups were clustered according to the size of the cell and the predominant fluorescence emitted by the cell. The size groups were the following: pico- [0,3] ; nano- [3,20] ; micro- [20,200] µm. The "nano-group" was divided into 3 subgroups: nano- [3,5] ; [5,10] ; [10,20] µm. The fluorescence groups were both red fluorescence (FLR) and orange fluorescence (FLO), corresponding to different phytoplankton functional types. The measurements used for analyses included the concentration of phytoplankton [individuals/µL], the number of cells, the length of forward scatter (FWS in µm), and the mean of the total fluorescence emissions (mV/µL).

2.3. Monitoring data

Meteorological data are available from Le Bouveret, the harbour next to the Rhône River mouth (MeteoSwiss); Rhône river discharge, temperature, turbidity and water quality data are available for the hydrological station Porte du Scex (Swiss Federal Office of the Environment, OFEV), and vertical profiles of physico-chemical parameters at the monitoring station SHL2 for the 1st of April and the 24th of September (CIPEL/INRA, Rimet et al., 2020).

2.4. Calculations

Isotope mixing model

A mixing model is used to calculate the Rhône water fraction for each sampling location. This mixing model is based on an atomic mass balance such that:

$$\delta^{18}O_R \bullet x_R + \delta^{18}O_L \bullet x_L = \delta^{18}O_S \quad (1)$$

Given that $x_R + x_L = 1$, the mole fraction of Rhône water at the sampling time is calculated by:

$$x_R = (\delta^{18}O_S - \delta^{18}O_L) / (\delta^{18}O_R - \delta^{18}O_L) \quad (2)$$

where $\delta^{18}O_R$ is the isotopic composition of the Rhône River water. This parameter is measured once a month proportionally to the discharge by OFEV (Swiss Federal Office of Environment) at the station Porte du Scex located 5 km upstream of the lake. It was also measured from our ISCO samples to evaluate the daily fluctuations during the campaigns (Appendix IV-5). $\delta^{18}O_R$ is calculated as the average of the daily measurements of the corresponding sampling day. $\delta^{18}O_S$ is the isotopic composition of the water measured at the sampling location. The uncertainty on the Rhône fraction related to the analytic error of $\delta^{18}O_S$ (±0.05 ‰) is evaluated to ± 2 %. $\delta^{18}O_L$ is the value of the mixed, unstratified lake water column that is, for example, homogeneous over the whole lake after a complete overturn. This value is constant at -12.1 ‰ for $\delta^{18}O$.

Water column stability

The software Lake Analyser (Read et al., 2011) was used to estimate the stratification strength (as measured by the Brunt-Väisälä buoyancy frequency: N^2), the thermocline depth, and the thickness of the metalimnion for the profiles of the September campaign showing a clear stratification.

Clusterisation and statistical analysis

In order to determine the impact of the Rhône water intrusion on the chemical composition and primary production of the surrounding lake water, clusters of sampling points into lake zones have been defined.

A first cluster, used for the April campaign, determines three categories relative to the Rhône water fraction (Figure 4-3):

- An ambient zone, outside of the river plume, defined by the absence of Rhône River water (less than 2 %, the uncertainty on the Rhône River water fraction)

- A transition zone between the Rhône interflow and the ambient lake with a Rhône River water fraction between 2 and 10 %
- A core zone of the Rhône interflow with Rhône River water fraction higher than 10 %

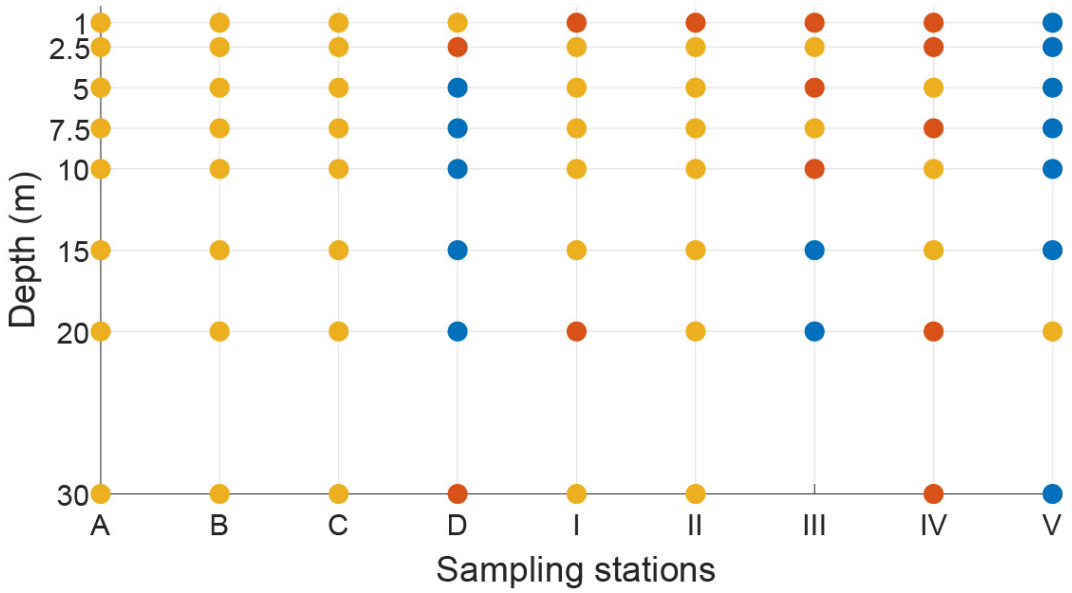

Figure 4-3: April clustering of sampling points into lake zones relative to the Rhône River fraction. The ambient zone is in yellow (less than 2 % of Rhône River water), the transition zone in red (between 2 and 10 %) and the core zone in blue (more than 10 %). Location of sampling stations is indicated on the maps shown in Figure 4-1.

In September, a second cluster determines four categories relative to the Rhône water fraction and the detection of Rhône interflow current velocity, i.e. velocity higher than the typical background current in the lake of 10 cm/s (Figure 4-4):

- An ambient zone without Rhône interflow current velocity nor Rhône water (v-/w-)
- A zone with Rhône interflow current velocity but no Rhône water detected (v+/w-)
- A zone without Rhône interflow current velocity but with Rhône water (v-/w+)
- A last zone with both detected (v+/w+)

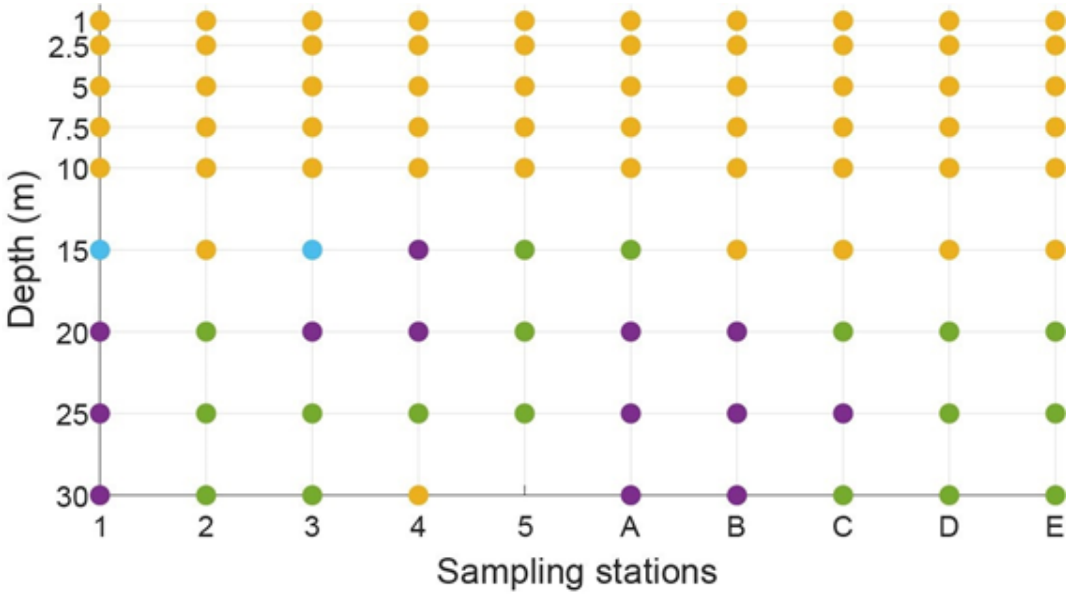

Figure 4-4: September clustering relative to the Rhône River fraction and the Rhône interflow current velocity. The ambient zone is in yellow (v-/w- = no velocity and no Rhône water), the zone v+/w- is in light blue, the zone v-/w+ is in green and the zone v+/w+ is in purple. Location of sampling stations is indicated on the maps shown in Figure 4-1.

Statistical analysis of the variance (ANOVA) was performed to detect significant differences between the clusters. Linear regression analysis was carried out to determine potential nutrient gradients within the river-lake transition zone. The fraction of Rhône water was used as an explanatory variable and the nutrient concentrations as response variables. All the statistical analysis were performed using MATLAB with a significance level of $\alpha = 0.01$.

3. Results

3.1. Meteorological, river and lake conditions

April conditions

Meteorological conditions (Appendixes IV-6 and IV-7): the weather conditions were quite different between the two sampling days in April. The 2nd of April was marked by high temperature and atmospheric pressure (median values of 10.5 °C and 967 hPa respectively), while the 4th of April had low temperature and atmospheric pressure (2 °C and 959 hPa). Wind conditions were calm during the sampling days but a short period of strong wind was noted in between these two sampling days. On the 3rd of April, a north-west wind blew for several hours reaching 14 m/s and provoking surface lake currents stronger than 20 cm/s (Appendix IV-8).

River conditions (boxplots in Figure 4-5 – time series in Appendix IV-9): Because of a cold front passing through the event, the Rhône River temperature strongly decreased between the 2nd and 4th of April, from 7.4 to 5.2 °C (median values). The discharge changed from 125 to 205 m^3/s and the conductivity decreased from 355 to 295 µS/cm.

Lake conditions at SHL2 (Appendixes IV-10 and IV-11): On the 1st of April, the lake had a weak spring thermal stratification with surface water reaching 10 °C (deep waters constant at 5.8 °C). No surface mixed layer was detected but a shallow thermocline at 2.5 m depth was already established. The concentration of orthophosphates was low in the upper 30 m with an average of 3 µg P/L. Given the monitoring profiles taken during the previous winter (Appendix IV-12), only a partial overturn of the lake water occurred, with the lake mixing down to 135 m, compared to a full depth of 309 m (CIPEL, 2020). This limits the input of orthophosphates through upwelling from the deep waters. During this period, the phytoplankton community was dominated by diatom species like *Asterionella formosa* and *Ulnaria delicatissima var. angustissima.*

September conditions

Meteorological conditions (Appendixes IV-13 and IV-14): the wind direction had the same pattern for the two sampling days with winds from the south during the night, changing to a south-westerly during the day. The wind speed decreased slightly between

the two sampling days. The median values of the wind speed were 2 and 1.5 m s^{-1} on 24th and 26th September, respectively.

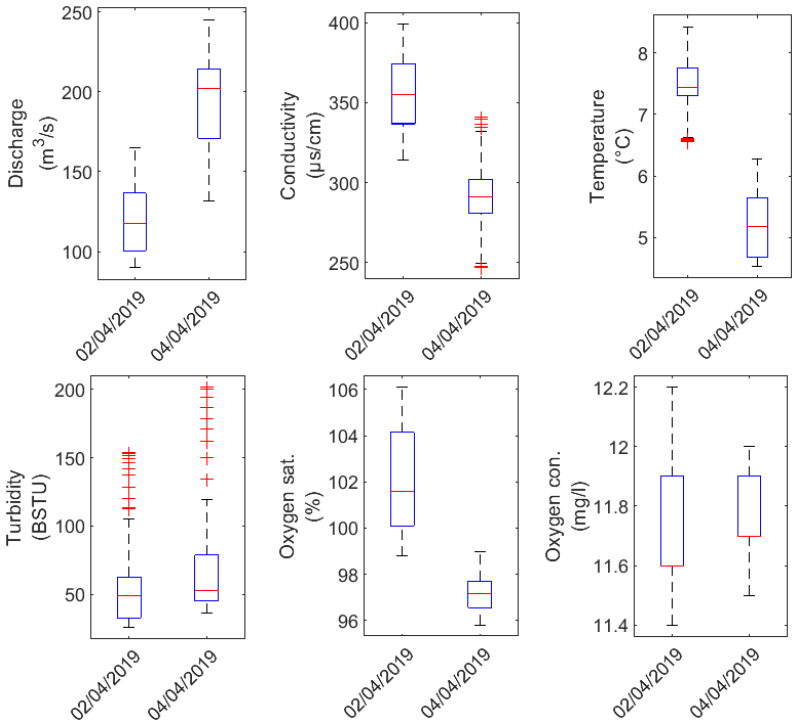

Figure 4-5: Boxplot of river parameters during the April 2019 sampling campaign from measurements on a 10-minutes basis. On each box, the central mark indicates the median, and the bottom and top edges of the box indicate the 25th and 75th percentiles, respectively.

River conditions (boxplots in Figure 4-6 – time series in Appendix IV-15): The river discharge was relatively constant from the 24th to the 26th of September. The median values of the discharge were 195 and 197 m^3/s on the 24th and 26th, respectively. On the 24th September, the river temperature was 8.14 °C ± 0.27, which is lower than the lake surface mixed layer temperature measured at SHL2. On the 26th of September, the river temperature was also lower than that of the lake surface mixed layer but a rapid increase of river temperature occurred in the morning, at approximately 6 a.m. The temperature reached a peak of 10.08 °C at 10 a.m. and returned to a stable level around 8 °C.

Lake conditions at SHL2 (Appendixes IV-16 and IV-17): The lake was stratified at that time of the year. The temperature was 17.8 °C in the surface mixed layer and decreased below 7 m to 5.9 °C in the hypolimnion. A peak of turbidity (2.28 FTU) was located around 14 m depth. It correlated with high concentration of particulate organic carbon, nitrogen and phosphorus. Biological observations show that this peak corresponded to *Planktothrix rubescens*, a filamentous cyanobacterium.

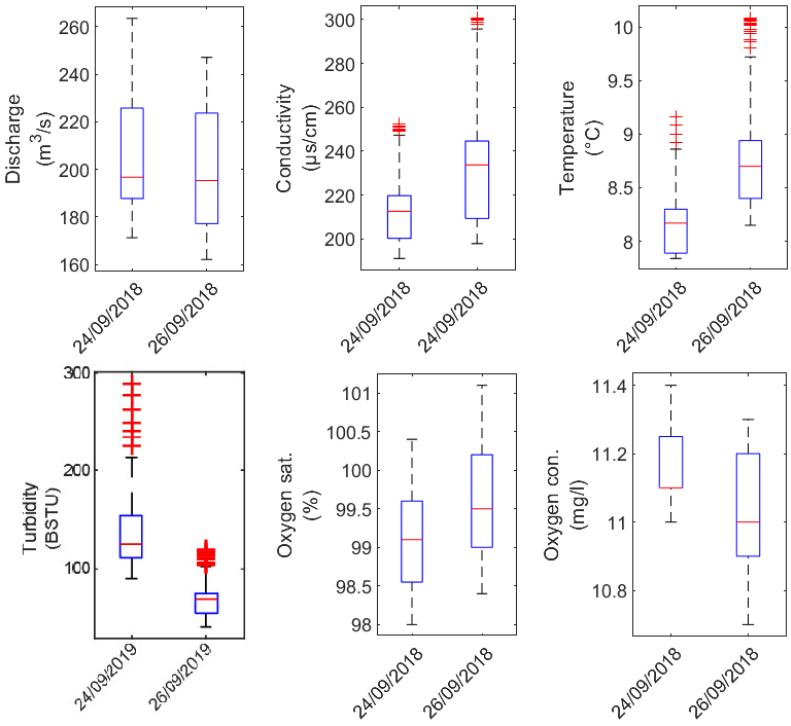

Figure 4-6: Boxplot of river parameters during the September 2019 sampling campaign from measurements on a 10-minutes basis. On each box, the central mark indicates the median, and the bottom and top edges of the box indicate the 25th and 75th percentiles, respectively.

3.2. Rhône River tracing

CTD profiles of the different transects are available in Appendix IV-18 and IV-19.

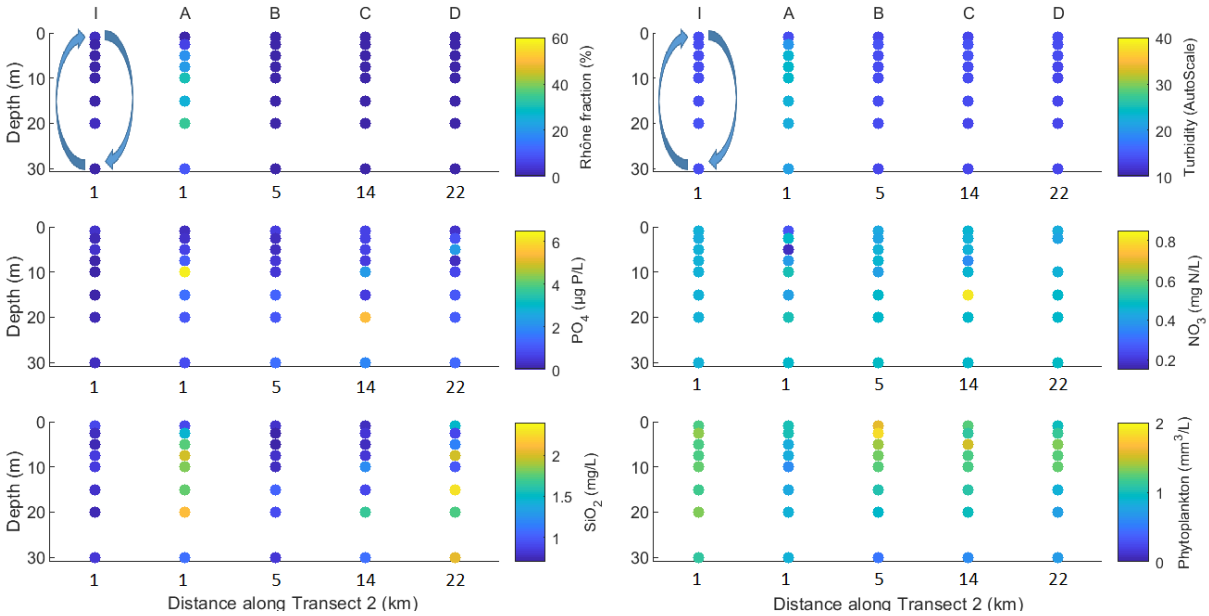

Figure 4-7: Profiles of transect T2-A of April 2nd and profile I of April 4th (profile A after wind event of April 3rd). The blue arrows indicate the wind-induced mixing extent of the water column.

In April, no significant difference from the reference isotope composition of the lake water was detected at the three profiles sampled in the Grand-Lac (profiles B, C and D). Meanwhile, a substantial interflow of Rhône River water was detected in the Haut-Lac between 3 and 30 m depth (profile A) both in terms of stable isotope composition of water, conductivity and turbidity (Figure 4-7). The next sampling day, after the strong north-west wind event, the interflow was detected between 55 and 80 m depth at the same station (profile I – Figure 4-8). At the station closer to the river mouth (0.5 x closer; profile II), no significant isotope anomaly was measured but a turbidity signal is measured at the bottom of the canyon. No interflow water of the Rhône was detected at the western profile IV while turbid Rhône water was measured in the eastern shallow area of profile III. Finally, at the location called *La Bataillère* (profile V), turbid and cold Rhône water was observed floating on the lake water (Figure 4-9 and Appendix IV-18).

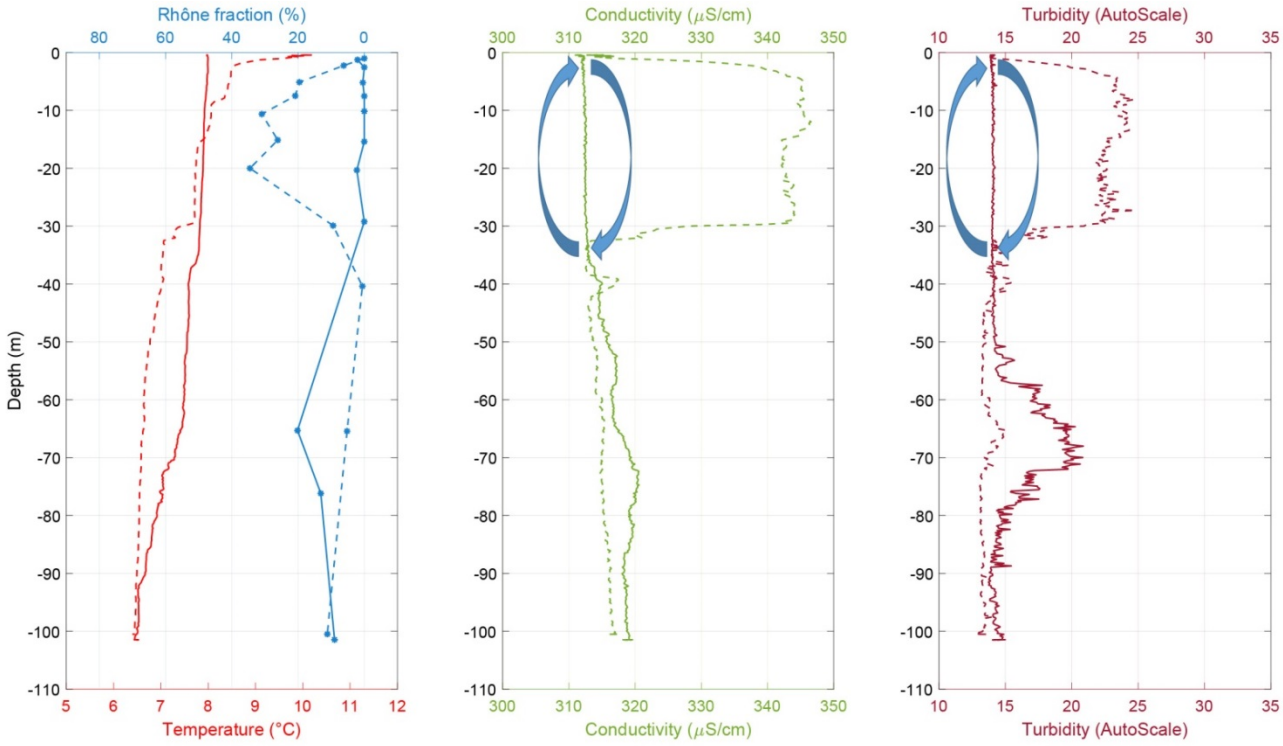

Figure 4-8: Water mixing by the wind event of the 3rd of April. Profile A (before wind event) shown as a dashed line and profile I (after wind event) as a continuous line. The blue arrows indicate the wind-induced mixing extent of the water column.

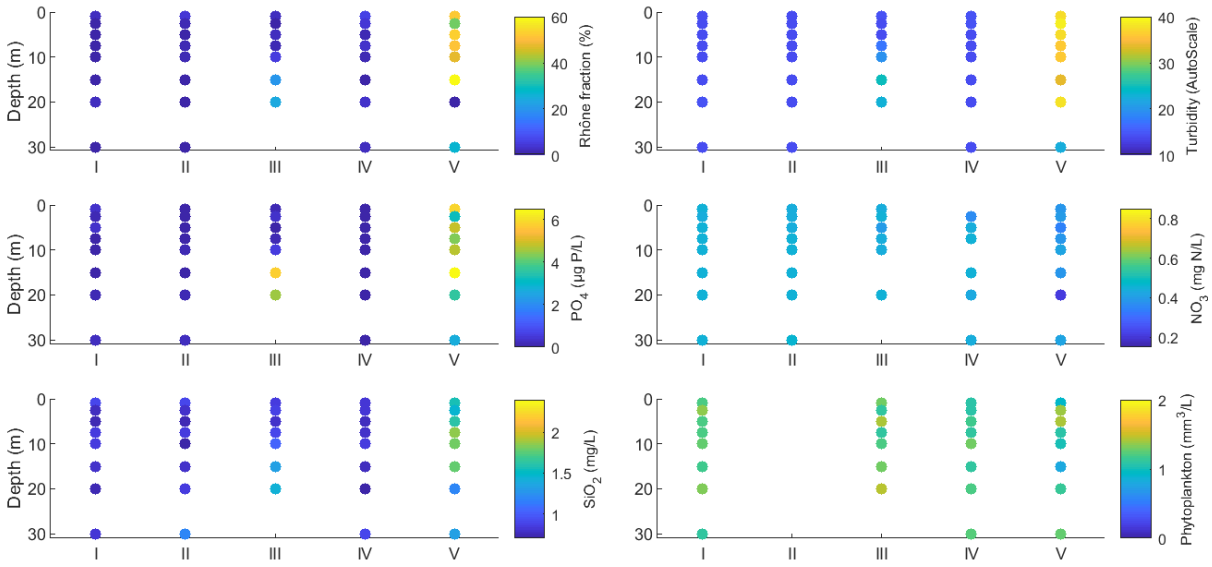

Figure 4-9: Profiles of transect T1-A of April 4th.

In September, a Rhône River interflow was detected all along the transversal transect T1-S between 20 and 30 m depth in terms of stable isotope composition of water, turbidity and negative anomaly of conductivity (Figure 4-10). It was centred at 20 m depth below the averaged thermocline depth detected at 15 m on the CTD profiles of transect T1-S (Appendix IV-20). While in terms of normal velocities, it was only detected at the stations 1, 3 and 4. If we look at the vertical velocities, it's interesting to note ascendant currents of about 10 cm/s located above the right canyon wall, from 12 m deep to the surface (Figure 4-11). On the river to open lake transect T2-S, the Rhône interflow was concentrated at around 30 % in its core zone in the near field area (profiles A, B and C) and around 20 % outside (profiles D and E – Figure 4-12). The core zone was located at about 25 m depth, still below the thermocline detected at about 20 m depths (Appendix IV-20). Due to an increase of Rhône conductivity during the 26th of September, the interflow anomaly of conductivity was less marked. In terms of turbidity, the intrusion was well marked. Moreover, turbidity was measured at the bottom of the canyon at profiles A, B, C, and D, along with lower $\delta^{18}O$ values (Appendix IV-19).

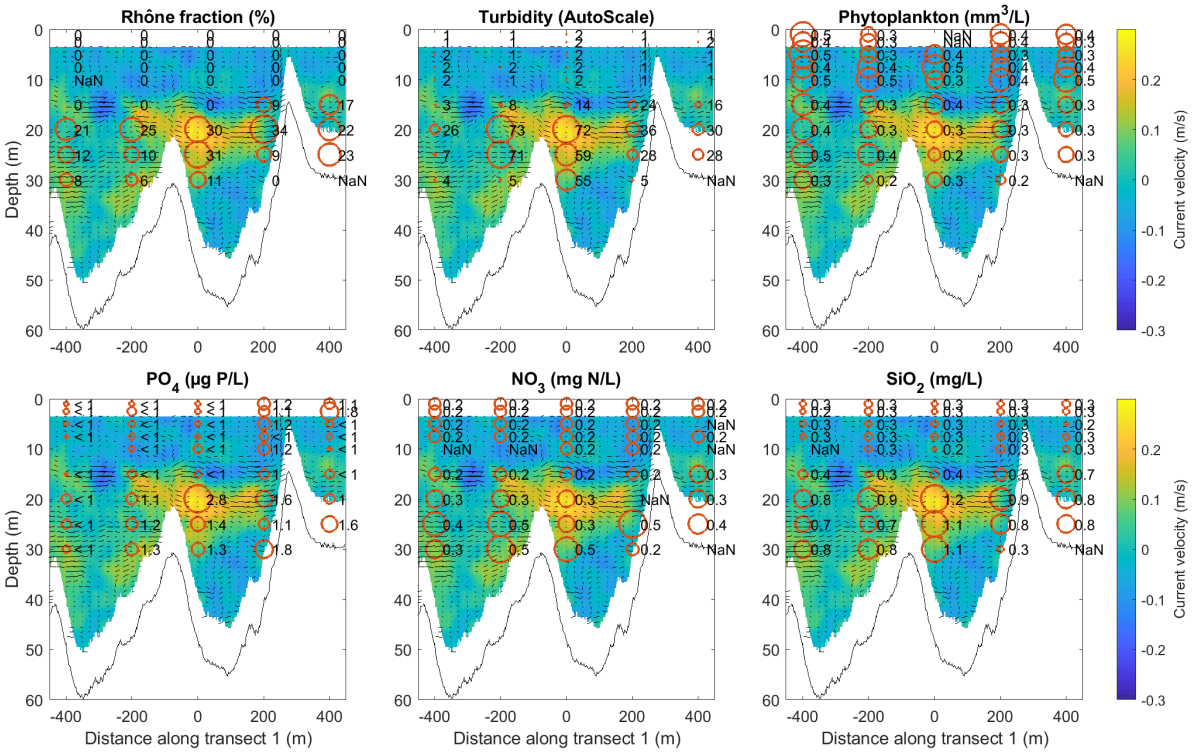

Figure 4-10: Vertical profiles at the stations of transect T1-S (from left to right : 2 – 3 – 1 – 4 – 5) with values of parameters indicated by red circles and the normal component of the velocity current indicated by the background colormap. The black line at the bottom indicates the lake's bottom.

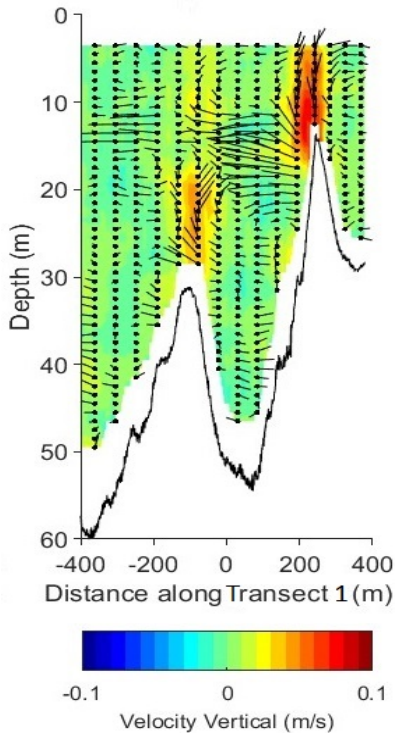

Figure 4-11: Transect T1-S with the vertical component of the velocity current indicated by the background colormap. The black line at the bottom indicates the lake's bottom.

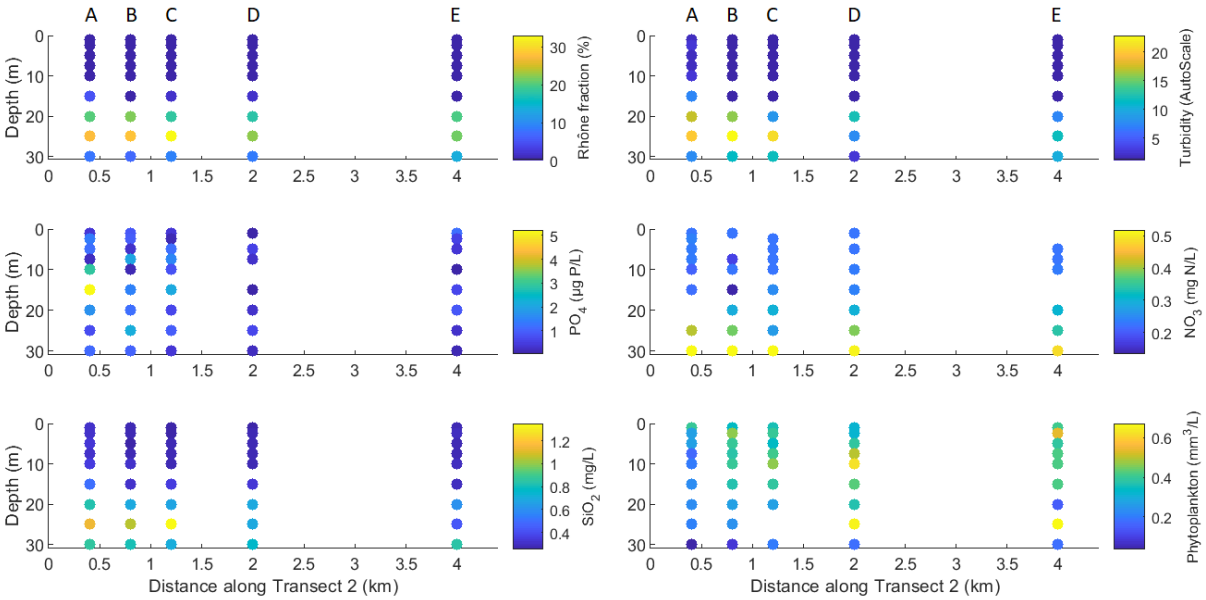

Figure 4-12: Depth profiles at the stations of transect T2-S (from left to right : A – B – C – D – E). The limit of the near field was detected at station D by ADCP profiling (see Figure 4-2).

3.3. Nutrient concentrations

There was a net input of orthophosphates from the river to the lake during the two seasons (Figures 4-13 and 4-14). Even with an important variation of the phosphate concentration within the Rhône waters, there were significant differences between the river, the core and the transition zone concentrations (tests ANOVA in Appendix IV-21). It is important to note that the lake concentration of phosphorous was already low in April and was at the same level during September (around 1 µg P/L), whereas the Rhône concentration was on average twice as high in spring compared to early fall (7.6 vs 3.6 µg P/L). In April, the Rhône nitrate concentration had a small dilution effect on the lake nitrate levels, with averages 0.36 mg N/L and 0.45 mg N/L respectively. In September the nitrate concentration was higher in the Rhône (0.32 mg N/L) compared to that in the lake (0.22 mg N/L) but, by looking at the depth profiles (Figures 4-10 and 4-12), such higher concentrations in the interflow were mainly due to the depth gradient of nitrate (Figure 4-18). The silica concentration also showed an important depth gradient with an increase with depth at the beginning of autumn due to the biological uptake by diatiom species all along the growing season. The river input of silica was however higher than the silica concentration of the ambient lake at the interflow depth, hence correlating with the Rhône River fraction ($R^2 = 0.79$, *p-value* < 0.001 – Figure 4-18). In transect T2-S, the influence of the river intrusion in the water column was visible in terms of the isotopic

composition of water and the silica concentration. Both diminished with distance from the river mouth and with consequent mixing with ambient water (Figure 4-12).

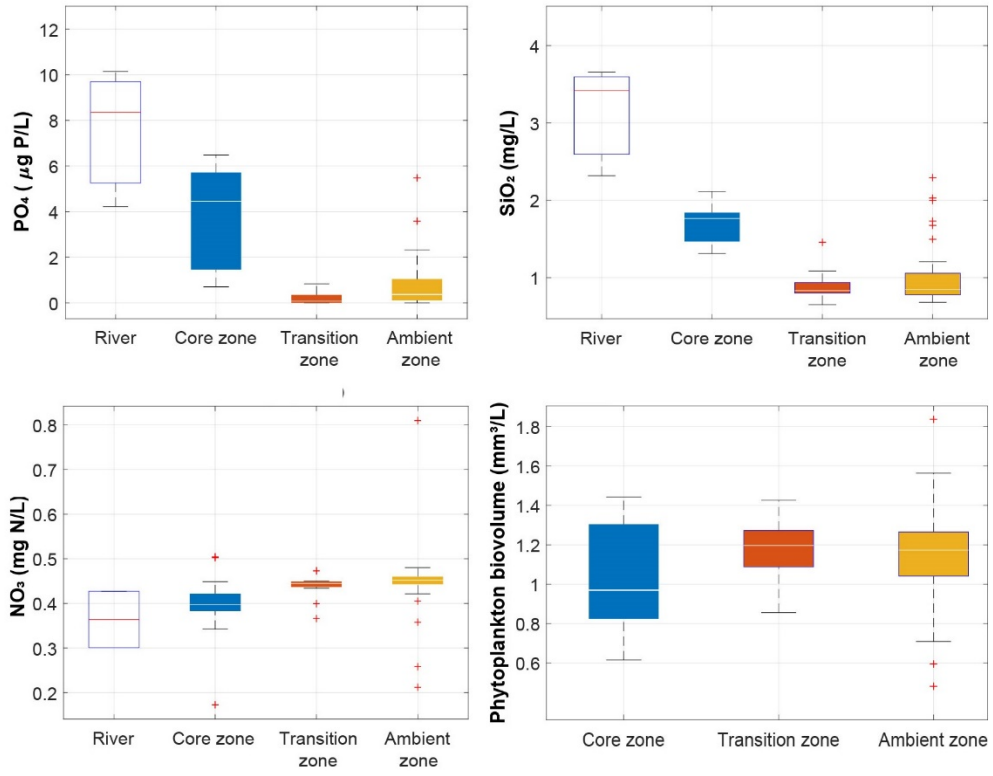

Figure 4-13: Boxplots of concentrations relative to April clusters(n_{River} = 3, $n_{Core\ zone}$ = 14, $n_{Transition\ zone}$ = 13, $n_{Ambient\ zone}$ = 44). On each box, the central mark indicates the median, and the bottom and top edges of the box indicate the 25th and 75th percentiles, respectively.

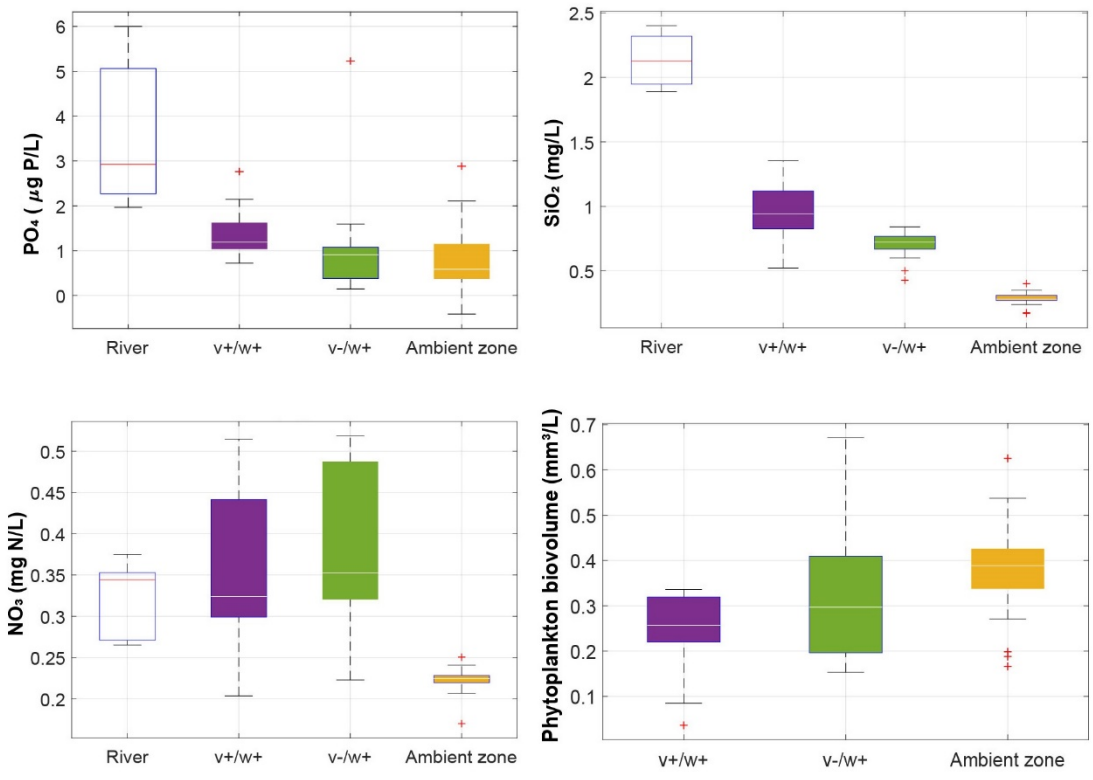

Figure 4-14: Boxplots of concentrations relative to September clusters (n_{River} = 5, $n_{v+/w+}$ = 13, $n_{v-/w+}$ = 18, $n_{Ambient\ zone}$ = 55). On each box, the central mark indicates the median, and the bottom and top edges of the box indicate the 25th and 75th percentiles, respectively.

3.4. Phytoplankton biovolume

Phytoplankton biovolumes showed the same pattern for the two seasons: the core zone of the interflow with the strongest current and the highest turbidity had the lowest biovolume, followed by the transition zone and the ambient zone (Figures 4-13 and 4-14). But there was a difference in scale: in April the algal biovolume is almost three times higher compared to September, with averages of 1.15 mm^3/L vs 0.39 mm^3/L in the ambient zone for April and September, respectively.

Concerning the biovolume of phytoplankton relative to the distance from the Rhône inflow, the minimum was located close to the river mouth, at station A, on the 2nd of April, with a profile average of 0.86 mm^3/L. Then, it reaches a maximum of 1.22 mm^3/L at profile B, 5 km from the river mouth, before decreasing to 1.04 mm^3/L in the middle of the lake (profile D – Figure 4-15). On the 4th of April, after the wind-induced mixing of the water column, the phytoplankton biovolume increased by 44 % at station A/I. Moreover, it seems to be homogenised in the Haut-Lac with concentrations averaging 1.22 mm^3/L at stations I, III and IV and vertical standard deviations that decreased at station I. Meanwhile, the values at station V, just in front of the Rhône, remained low with an average of 1.13 mm^3/L.

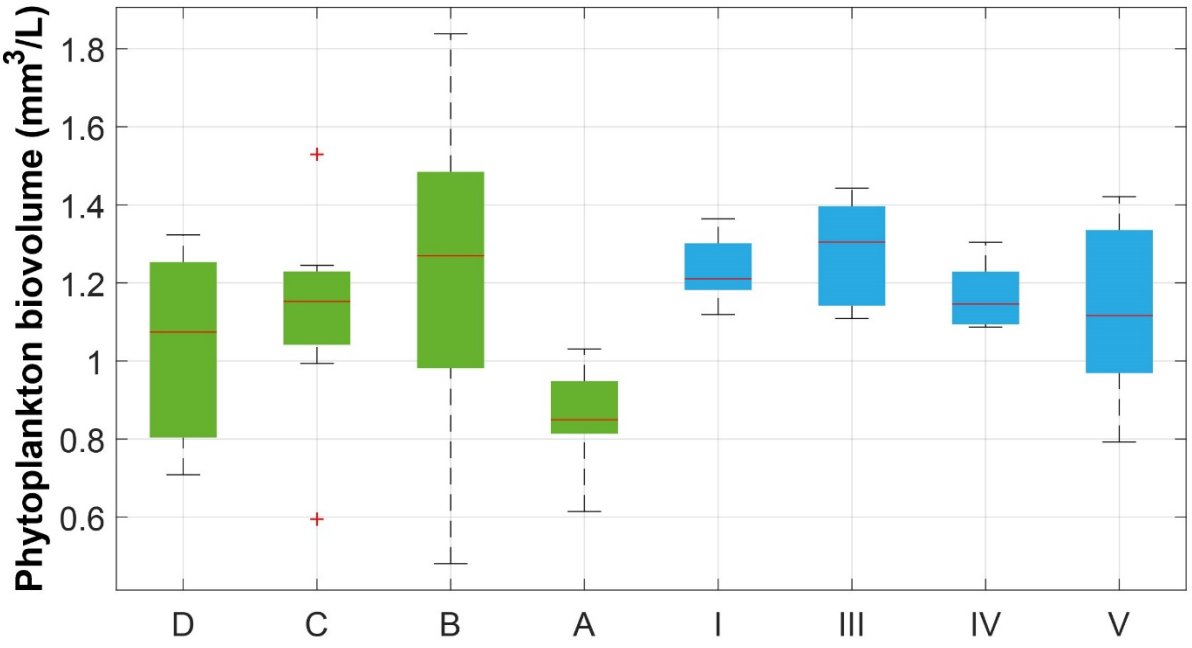

Figure 4-15: Boxplots of phytoplankton biovolume relative to April stations of T2-A (A to D) and T1-A (I to V). On each box, the central mark indicates the median, and the bottom and top edges of the box indicate the 25th and 75th percentiles, respectively.

On the 24th of September, the phytoplankton dispersion was vertically heterogeneous in front of the river mouth (T1-S – Figure 4-10) with low values below the thermocline and slightly more elevated in the epilimnion, averaging 0.31 and 0.39 mm^3/L respectively. Horizontally, the phytoplankton biovolumes were higher at station 2 with an average of 0.44 mm^3/L compared to the other stations of T1-S with an average of 0.34 mm^3/L (Figure 4-16). The vertical profile at station 2 also showed the less intense turbidity plume on transect T1-S (Figure 4-10). On the 26th, the biovolumes decreased at all depths of station 1/A. Biovolumes were especially low at station A in front of the Rhône with an average of 0.22 mm^3/L. Then, it increased progressively with the distance from the river mouth to reach an average of 0.40 mm^3/L at station E located at 4 km (Figure 4-16). At 25 m depth, at the depth of the core zone of the interflow, the biovolumes were relatively low in the near field (stations A and B) with an average of 0.22 mm^3/L, but then increased by a factor of 3 outwards with maxima of 0.66 mm^3/L and 0.67 mm^3/L at station D and E, respectively (Figure 4-12). These maxima were also 64 % higher than the averaged biovolume between 0 and 20 m deep at the same stations.

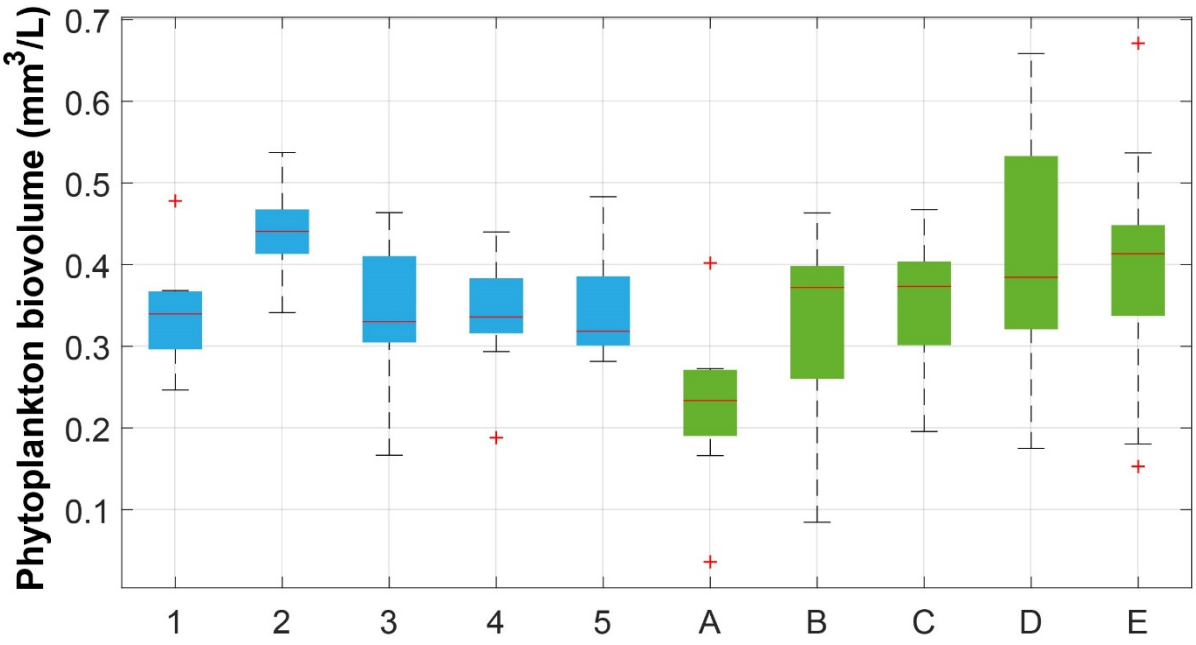

Figure 4-16: Boxplots of phytoplankton biovolume relative to September stations of T1-S (1 to 5) and T2-S (A to E). On each box, the central mark indicates the median, and the bottom and top edges of the box indicate the 25th and 75th percentiles, respectively.

4. Discussion

4.1. Rhône River intrusion

The conductivity of the Rhône River is variable depending on its discharge and seasonally variable conditions in its catchment. In spring and summer, when the Rhône River is mainly fed by snow and glacial melt waters, the dissolved major ions transported by the Rhône (80 % of carbonate ions, sulphate ions and associated Ca) are diluted by the higher discharge. Often short-term changes in major ion concentrations may also be caused by the operation of dams for the generation of hydropower in the catchment of the upper Rhône. Consequently, a positive or a negative anomaly in conductivity can be detected in the lake at the location of the Rhône River interflow within one week or even a single day, as noted during the April campaign. In September, the conductivity of the Rhône was measured to be lower than that of the lake (230 compared to 260-300 µS/cm), thus resulting in a negative anomaly at the interflow depth. Therefore, conductivity alone and its relative change cannot be used to detect the Rhône water interflow or identify a chemical gradient related to the interflow only. However, orthophosphates and silica concentrations in April, and silica concentrations in September indicated a significant nutrient gradient induced by the Rhône intrusion (Figures 4-17 and 4-18).

In terms of turbidity, the Rhône River plume was well detectable in and out of the near field area. The turbidity signal corresponded to the presence of the interflow, likely supported by higher flow velocities within the interflow, clearly noted in the transversal transect (T1-S – Figure 4-10). Then, the turbidity had maximum values in the near field but decreased with distance out of this zone (T2-S – Figure 4-12). However, a turbidity anomaly could still be measured at the background station E. As noted already by Giovanoli (1990), the fine fraction of the sediments as well as likely additional authigenic minerals can stay in suspension within the Rhône River interflow.

Moreover, the turbidity measured at the bottom of the canyon at stations A, B, C, and D (Appendix IV-19), along with lower $\delta^{18}O$ values, suggests a stacking of an interflow and an underflow. This may represent two different periods of Rhône River injection with different densities, or perhaps a splitting of the river inflow into two: an interflow concentrated in river water that intrudes at the density step of the thermocline and a gravity current that follows the bottom of the canyon (Cortés et al., 2014a).

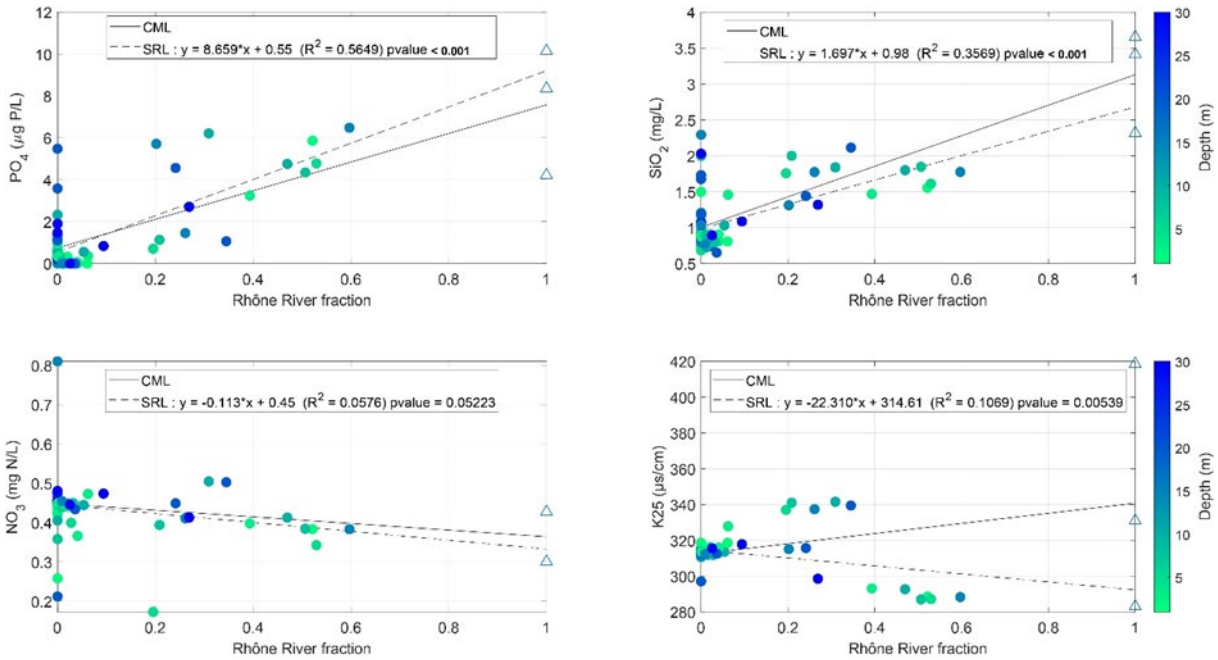

Figure 4-17: Conservative Mixing Line (CML) between lake and river endmembers, and Sample Regression Line (SRL) with the measured concentrations in the river mouth area (April). Lake and river samples are indicated by circles and triangles respectively. Reported are the equation of the linear model for the SRL, the coefficients of determination R^2 and the significance level (p-values).

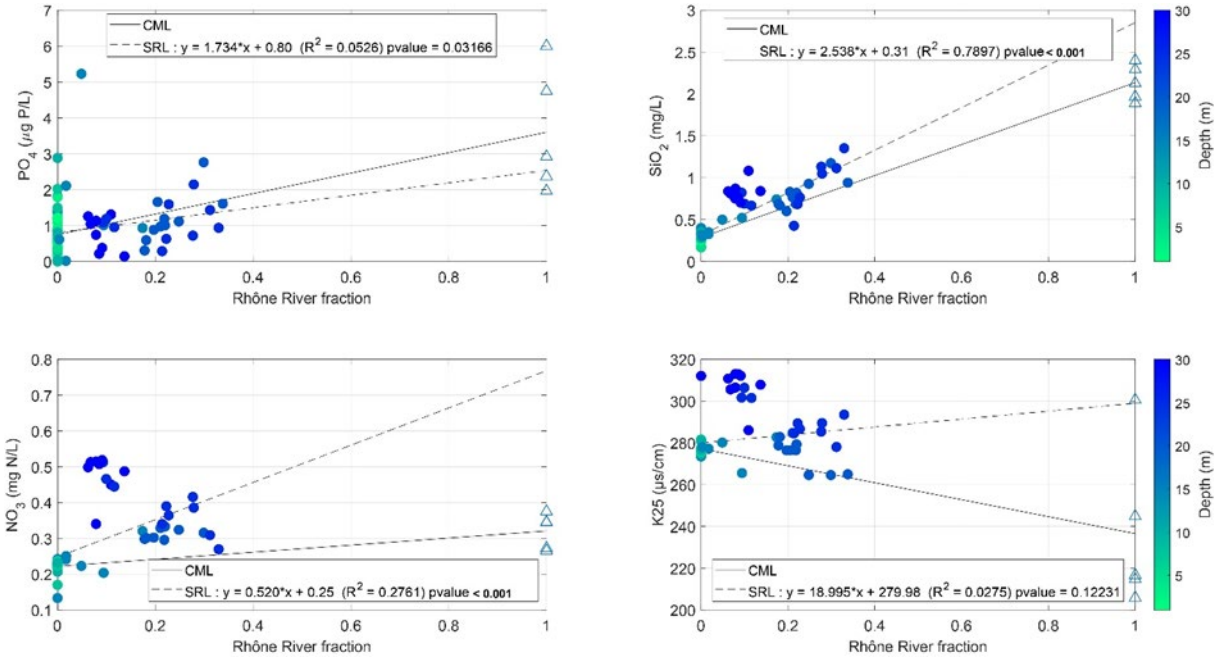

Figure 4-18: Conservative Mixing Line (CML) between lake and river endmembers, and Sample Regression Line (SRL) with the measured concentrations in the river mouth area (September). Lake and river samples are indicated by circles and triangles respectively. Reported are the equation of the linear model for the SRL, the coefficients of determination R^2 and the significance level (p-values).

Furthermore, some vertical profiles in the near field (at stations 2 and 5 in T1-S – Figure 4-10) indicated the presence of Rhône River water even where no changes in velocity were measurable. This can be explained by the variable hydrodynamics within this area. Depending on the discharge of the river, its density and the lake currents, the interflow can establish itself at a restricted depth close to the entry point, but subsequently change its location as these parameters fluctuate on relatively short time scales (e.g., Soulignac et al., in preparation). Out of the near field area (stations D and E of T2-S – Figure 4-12), the river momentum does not control the interflow dispersion anymore. The interflow, stabilised in a specific layer within the metalimnion in terms of its buoyancy, is then directed by the currents of the lake (Cimatoribus et al., 2019; Cotte and Vennemann, 2020). Alternatively, a reversed situation may also be noted, such as when a velocity difference is measured for a certain layer but where this layer may not contain any measurable Rhône River water (e.g., blue dots in Figure 4-4). This might be the result of a "piston effect" where the currents from the river intrusion may actually push ambient lake water.

Previous studies demonstrated the capacity of the stable isotope composition of water to trace the Rhône River interflow within the entire lake (Cotte and Vennemann, 2020; Halder et al., 2013). In the present study, no trace of the Rhône interflow water was detected over the measured vertical profiles outside of the river mouth area in April. The condition for the interflow to reach further into the lake, i.e. a strong stratification, was not yet established. Consequently, the Rhône River nutrients stay in the Haut-Lac and are preferentially mixed in the surface mixed layer of this part of the lake when wind events occur at this season (see below). Or alternatively, the Rhône River may intrude deeper in the hypolimnion when the thermal stratification is weakened as seen after the wind event in April or during winter season (cf. Chapter II).

4.2. The river mouth: a dynamic area

Some hydrodynamic processes able to change the Rhône intrusion pattern have been detected. These can potentially change the chemical and biological gradients and make the river mouth area highly dynamic.

First, the wind event of the 3rd of April homogenised the water column to 35 m depth and hence mixed the Rhône interflow of the 2nd of April with ambient lake water (Figure 4-8). It was noted with the measurement on the 4th of April (Figure 4-7), that the Rhône

signal in terms of isotope composition, turbidity and nutrient concentration has disappeared from the top 30 m. In addition, the newly established density gradient and thermocline which briefly established itself at 70 m depth, forced the Rhône to intrude the water column well below the euphotic zone. However, at this depth no significant Rhône nutrient input was detected because the nutrient concentrations in these layers of the lake already corresponding to those of the Rhône.

Secondly, some vortexes of ascent currents were measured as expected in the transversal sections in September (Figure 4-11). They might be the result of the Rhône interflow encountering the canyon walls, in this case the right side in the direction of the flow. However, no significant upwelling of nutrients was detected as the water layer affected was too shallow and poor in nutrients.

Finally, as it was observed for the April campaign during a period of weak stratification, the river intrusion depth can quickly change even during a period of strong stratification. Indeed, in September, despite a lower density during the 26th compared to the 24th (higher temperature and lower sediment load – Figure 4-6), the Rhône intruded 5 m deeper, following the deepening of the thermocline occurring in between the two sampling days. With relatively homogenous meteorological conditions during these two days (Appendix IV-14), these results show how the river intrusion depth is influenced by the lake stratification (e.g., Cimatoribus et al., 2019; Cotte and Vennemann, 2020).

4.3. A punctual optimal zone for phytoplankton

During April, the early thermal stratification allowed the Rhône nutrients to be transported as an interflow into the shallow metalimnion. However, the presence of an opaque turbidity plume in the river mouth area related to the Rhône water intrusion (station A – Figure 8) blocked the sunlight penetration and inhibited the phytoplankton photosynthesis. After the wind induced mixing of the water column and the deepening of the Rhône intrusion, the turbidity dropped in the top 30 m allowing the phytoplankton to grow by 44 % (station I compared to station A – Figure 15) while it stayed relatively low in the turbid plunge zone (station V). In September, a significant input of P and Si was measured, but no fertilisation effect was observed in the river mouth near field (T1-S – Figure 10). Similarly, the phytoplankton development was limited by the sediment plume of the Rhône interflow and its important current velocity. Instead, out of this turbulent and turbid near field, at the Rhône intrusion depth, we observed a strong increase of

phytoplankton biovolume by a factor of 3 (T2-S – Figure 12). As claimed by Cortés et al. (2014b), river intrusions occurring in the metalimnion can fuel algal growth and lead to the development of a deep chlorophyll maximum.

Using remote sensing, Kiefer et al. (2015) and Soomets et al. (2019) measured respectively a higher Chl *a* concentration and a higher PP in the eastern part of Lake Geneva and hypothesized a relation with the proximity of the Rhône input. Moreover, Kiefer et al. (2015) measured the highest variability of Chl *a* in this area around the Rhône inflow especially in spring. Our results suggest that these observations can be explained by the highly variable Rhône River intrusion pattern. During our study, we showed that the turbidity plume induced by the Rhône interflow may limit phytoplankton growth underneath in the near field area. Then, if the river intrusion depth change or we move out of this near field, phytoplankton development can be enhanced. Finally, our results reveal that an ecocline can develop in the transition zone between the Rhône River and Lake Geneva where an equilibrium occurs between the river limiting factors (temperature, light and low flow velocities) and those that are limiting phytoplankton development in the lake (nutrient concentrations, P and Si) but it is temporally and spatially dynamic depending on the meteorological, hydrological and lake conditions.

Using satellite images and a hydrodynamic model, Soulignac et al. (2018) indicated an earlier onset of phytoplankton development in spring 2011 in the Haut-Lac compared to the rest of the lake. They argued that this sheltered area may favour an earlier stratification and hence improved access to light, leading to an earlier onset of the spring bloom. We can add that the Rhône River nutrients start to intrude in the metalimnion in this part of the lake at the beginning of spring. Then, as we measured it, a subsequent wind event can disrupt the weak stratification, mix the Rhône interflow and its nutrients into the euphotic surface layer and limit further transport. As a consequence, the Rhône nutrients stay in the Haut-Lac and this eastern part of the lake (station I – Figure 15), except the turbid near field area (stations A and V), appears to be an optimal zone for phytoplankton compared to the central lake (station D).

5. Conclusion

A significant chemical gradient related to the Rhône River intrusion and subsequent dispersion of the interflow was measured during the two campaigns in the eastern part of Lake Geneva. Additionally, punctual optimal conditions for primary production were identified in this area.

Vertical vortexes have been measured in the close near field area but their action is limited to the upper 10-15 m of the surface waters, no upwelling of higher nutrient waters have been detected. However, the river mouth area was identified as a highly dynamic zone. Indeed, the variable Rhône River intrusion pattern related to the meteorological and hydrological conditions, as well as the lake stratification, change the characteristic of the observed ecocline.

In early spring, the thermal stratification was too weak to allow the Rhône River interflow to reach the central part of the lake. Despite a net input of phosphorus, the phytoplankton growth was limited by the turbid Rhône River plume at the river mouth. However, a sudden wind event mixed the top 30 m of the water column, dropped the turbidity, provoking an increase of 44 % of the phytoplankton biovolume. Moreover, the deep intrusion of river nutrients in September seems to maintain an autumnal phytoplankton growth when the euphotic surface layer is depleted in nutrients. These fertilisation effects were measured in the region surrounding the sediment plume of the Rhône where the phytoplankton growth is inhibited. Therefore, the Haut-Lac, except this turbid and turbulent near field, appears as a dynamic zone that can present punctually optimal conditions for phytoplankton.

As a consequence, these results question the representativeness of the existing two monitoring stations. As argued by Kiefer et al. (2015), the river-lake transition zones have to be taken into account for a lake ecosystem monitoring. Our study confirms that the influence of the river interflow on primary production should be considered to understand the trophic evolution of the lake.

Complete lake overturns in winter are expected to occur less frequently in future due to climate change (Perroud et al., 2009). As measured during the winter of 2019, partial mixing of the water column limits the upwelling of nutrient-richer water. In this context, the Rhône River interflow and the related nutrient supply to the euphotic zone have a more notable impact on the primary production of the lake. This fertilization effect is more important earlier in the growing season in absence of a prior complete overturn.

Enhanced primary production in front of transition zones has already been noted for small lakes (Mackay et al., 2011; Vidal Hurtado et al., 2007). This multidisciplinary study confirms this process in a large lake in the context of its re-oligotrophication.

Acknowledgements

Thank you to Marie-Elodie Perga, Nicolas Escoffier, Orlane Anneville, Andrew Barry, Ulrich Lemmin, Robert Eduard Uittenbogaard, Bastiaan Ibelings and Torsten Vennemann for their advices in the design of this project. A special Thank You to Philippe Arpagaus who piloted the Licorne with precision and shared his passion for the lake. Thank you to Matthieu Fallet who has been involved in the project as MSc student at UNIL. Thank you to Loriann Chevalier and Marie Coudene who helped to prepare and performed the April campaign. Thank you to Kylian, Léo, Chris, Olu, Franziska, David and Hauren for their help during the sampling campaign of September.

References

Anneville, O., Beniston, M., Gallina, N., Gillet, C., Jacquet, S., Lazzarotto, J., 2013. L'empreinte du changement climatique sur le Léman. Arch. Sci. 16.

Anneville, O., Dur, G., Rimet, F., Souissi, S., 2018. Plasticity in phytoplankton annual periodicity: an adaptation to long-term environmental changes. Hydrobiologia 824, 121–141. https://doi.org/10.1007/s10750-017-3412-z

Anneville, O., Ginot, V., Angeli, N., 2002. Restoration of Lake Geneva: Expected versus observed responses of phytoplankton to decreases in phosphorus. Lakes Reserv. Sci. Policy Manag. Sustain. Use 7, 67–80. https://doi.org/10.1046/j.1440-169X.2002.00179.x

Baracchini, T., Wüest, A., Bouffard, D., 2020. Meteolakes: An operational online three-dimensional forecasting platform for lake hydrodynamics. Water Res. 172, 115529. https://doi.org/10.1016/j.watres.2020.115529

Bouffard, D., Perga, M.-E., 2016. Are flood-driven turbidity currents hot spots for priming effect in lakes? Biogeosciences 13, 3573–3584. https://doi.org/10.5194/bg-13-3573-2016

Cimatoribus, A.A., Lemmin, U., Barry, D.A., 2019. Tracking Lagrangian transport in Lake Geneva: A 3D numerical modeling investigation. Limnol. Oceanogr. 64, 1252–1269. https://doi.org/10.1002/lno.11111

Conseil scientifique de la commission internationale pour la protection des eaux du Léman contre la pollution. 2019. Rapports sur les études et recherches entreprises dans le bassin lémanique. Campagne 2018. CIPEL. Available from https://www.cipel.org/publications/rapports-scientifiques/rapport-2019-campagne-2018/.

Conseil scientifique de la commission internationale pour la protection des eaux du Léman contre la pollution. 2020. Rapports sur les études et recherches entreprises dans le bassin lémanique. Campagne 2019. CIPEL. Available from https://www.cipel.org/publications/rapports-scientifiques/rapport-2020-campagne-2019/

Cortés, A., Rueda, F.J., Wells, M.G., 2014a. Experimental observations of the splitting of a gravity current at a density step in a stratified water body. J. Geophys. Res. Oceans 119, 1038–1053. https://doi.org/10.1002/2013JC009304

Cortés, A., Fleenor, W.E., Wells, M.G., de Vicente, I., Rueda, F.J., 2014b. Pathways of river water to the surface layers of stratified reservoirs. Limnol. Oceanogr. 59, 233–250. https://doi.org/10.4319/lo.2014.59.1.0233

Cotte, G., Vennemann, T.W., 2020. Mixing of Rhône River water in Lake Geneva: Seasonal tracing using stable isotope composition of water. J. Gt. Lakes Res. 46, 839–849. https://doi.org/10.1016/j.jglr.2020.05.015

Giovanoli, F., 1990. Horizontal Transport and Sedimentation by Interflows and Turbidity Currents in Lake Geneva, in: Tilzer, M.M., Serruya, C. (Eds.), Large Lakes: Ecological Structure and Function, Brock/Springer Series in Contemporary Bioscience. Springer, Berlin, Heidelberg, pp. 175–195. https://doi.org/10.1007/978-3-642-84077-7_9

Halder, J., Decrouy, L., Vennemann, T.W., 2013. Mixing of Rhône River water in Lake Geneva (Switzerland–France) inferred from stable hydrogen and oxygen isotope profiles. J. Hydrol. 477, 152–164. https://doi.org/10.1016/j.jhydrol.2012.11.026

Kiefer, I., Odermatt, D., Anneville, O., Wüest, A., Bouffard, D., 2015. Application of remote sensing for the optimization of in-situ sampling for monitoring of phytoplankton abundance in a large lake. Sci. Total Environ. 527–528, 493–506. https://doi.org/10.1016/j.scitotenv.2015.05.011

Mackay, E.B., Jones, I.D., Folkard, A.M., Thackeray, S.J., 2011. Transition zones in small lakes: the importance of dilution and biological uptake on lake-wide heterogeneity. Hydrobiologia 678, 85–97. https://doi.org/10.1007/s10750-011-0825-y

Moisset, S., 2017. Investigation of the link between phytoplankton and nutrients dynamic in Lake Geneva. Thèse de doctorat. University of Geneva. https://doi.org/10.13097/archive-ouverte/unige:96830

Nouchi, V., Kutser, T., Wüest, A., Müller, B., Odermatt, D., Baracchini, T., Bouffard, D., 2019. Resolving biogeochemical processes in lakes using remote sensing. Aquat. Sci. 81, 27. https://doi.org/10.1007/s00027-019-0626-3

Perroud, M., Goyette, S., Martynov, A., Beniston, M., Annevillec, O., 2009. Simulation of multiannual thermal profiles in deep Lake Geneva: A comparison of one-dimensional lake models. Limnol. Oceanogr. 54, 1574–1594. https://doi.org/10.4319/lo.2009.54.5.1574

Read, J.S., Hamilton, D.P., Jones, I.D., Muraoka, K., Winslow, L.A., Kroiss, R., Wu, C.H., Gaiser, E., 2011. Derivation of lake mixing and stratification indices from

high-resolution lake buoy data. Environ. Model. Softw. 26, 1325–1336. https://doi.org/10.1016/j.envsoft.2011.05.006

Rimet, F., 2013. The phytoplankton of Lake Geneva. Campagne 2012. Commission Internationale pour la Protection des Eaux du Léman, pp. 82–93.

Rimet, F., Anneville, O., Barbet, D., Chardon, C., Crépin, L., Domaizon, I., Dorioz, J.-M., Espinat, L., Frossard, V., Guillard, J., Goulon, C., Hamelet, V., Hustache, J.-C., Jacquet, S., Lainé, L., Montuelle, B., Perney, P., Quetin, P., Rasconi, S., Schellenberger, A., Tran-Khac, V., Monet, G., 2020. The Observatory on LAkes (OLA) database: Sixty years of environmental data accessible to the public: J. Limnol. 79. https://doi.org/10.4081/jlimnol.2020.1944

Rueda, F.J., Fleenor, W.E., de Vicente, I., 2007. Pathways of river nutrients towards the euphotic zone in a deep-reservoir of small size: Uncertainty analysis. Ecol. Model. 202, 345–361. https://doi.org/10.1016/j.ecolmodel.2006.11.006

Soomets, T., Kutser, T., Wüest, A., Bouffard, D., 2019. Spatial and temporal changes of primary production in a deep peri-alpine lake. Inland Waters 9, 49–60. https://doi.org/10.1080/20442041.2018.1530529

Soulignac, F., Danis, P.-A., Bouffard, D., Chanudet, V., Dambrine, E., Guénand, Y., Harmel, T., Ibelings, B.W., Trevisan, D., Uittenbogaard, R., Anneville, O., 2018. Using 3D modeling and remote sensing capabilities for a better understanding of spatio-temporal heterogeneities of phytoplankton abundance in large lakes. J. Gt. Lakes Res. 44, 756–764. https://doi.org/10.1016/j.jglr.2018.05.008

Tadonleke, R.D., Lazzarotto, J., Anneville, O., Druart, J.-C., 2009. Phytoplankton productivity increased in Lake Geneva despite phosphorus loading reduction. J. Plankton Res. 31, 1179–1194. https://doi.org/10.1093/plankt/fbp063

Vaulot, D., Courties, C., Partensky, F., 1989. A simple method to preserve oceanic phytoplankton for flow cytometric analyses. Cytometry 10, 629–635. https://doi.org/10.1002/cyto.990100519

Vidal Hurtado, J., Casamitjana, X., Universitat de Girona, Departament de Física, 2007. Basin-scale hydrodynamics in a Mediterranean reservoir, implications for the phytoplankton dynamics. Universitat de Girona, Girona.

Conclusion

1. Synthesis

The aim of this thesis was to study the dispersion of the Rhône River in Lake Geneva and to determine its impact on the biogeochemistry of the lake in the context of its re-oligotrophication. A number of field campaigns during different seasons and in different parts of the lake were conducted in order to strategically sample the lake. The methodological approach combines: 1) stable isotope tracing of the Rhône water at the basin scale at different thermal conditions, 2) studies of the nutrient dynamics in the lake during the stratification period and its relationship to the Rhône River interflow, 3) a multidisciplinary approach to assess the fertilisation effect of the Rhône River in the lake.

The following findings synthetize the results of this work (Figure 5-1).

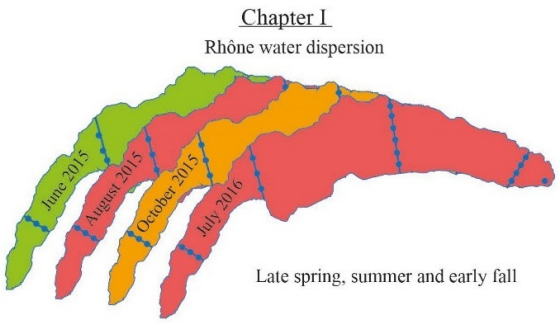

The Rhône River interflow during the stratification period

1) Vertical dispersion

- In the metalimnion below the thermocline

- The stronger the stratification is, the more concentrated and vertically constrained is the interflow

- Vertical displacement with thermocline tilting

- In autumn, the interflow widens and progressively plunges together with the thermocline towards larger depths

2) Horizontal dispersion

- Directed by the gyres of the lake

- Detected in all profiles throughout the lake

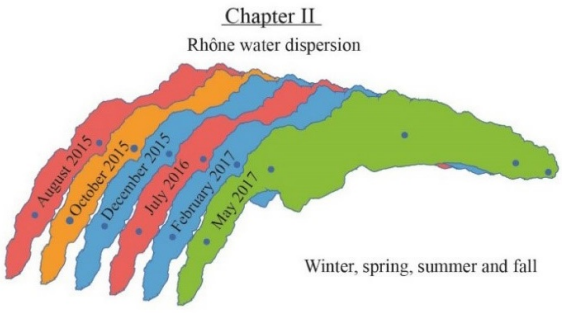

Different intrusion patterns with different thermal conditions

1) Spring

- The interflow establishes in the Haut-Lac with the onset of the stratification

- It requires a well-established stratification to reach the central lake otherwise it can be mixed within the epilimnion

2) Autumn

- The metalimnion enriched in Rhône water in summer is progressively mixed with the epilimnion

3) Winter

- Intrusions can occur without stratification according to the thermal mixing with the ambient lake water

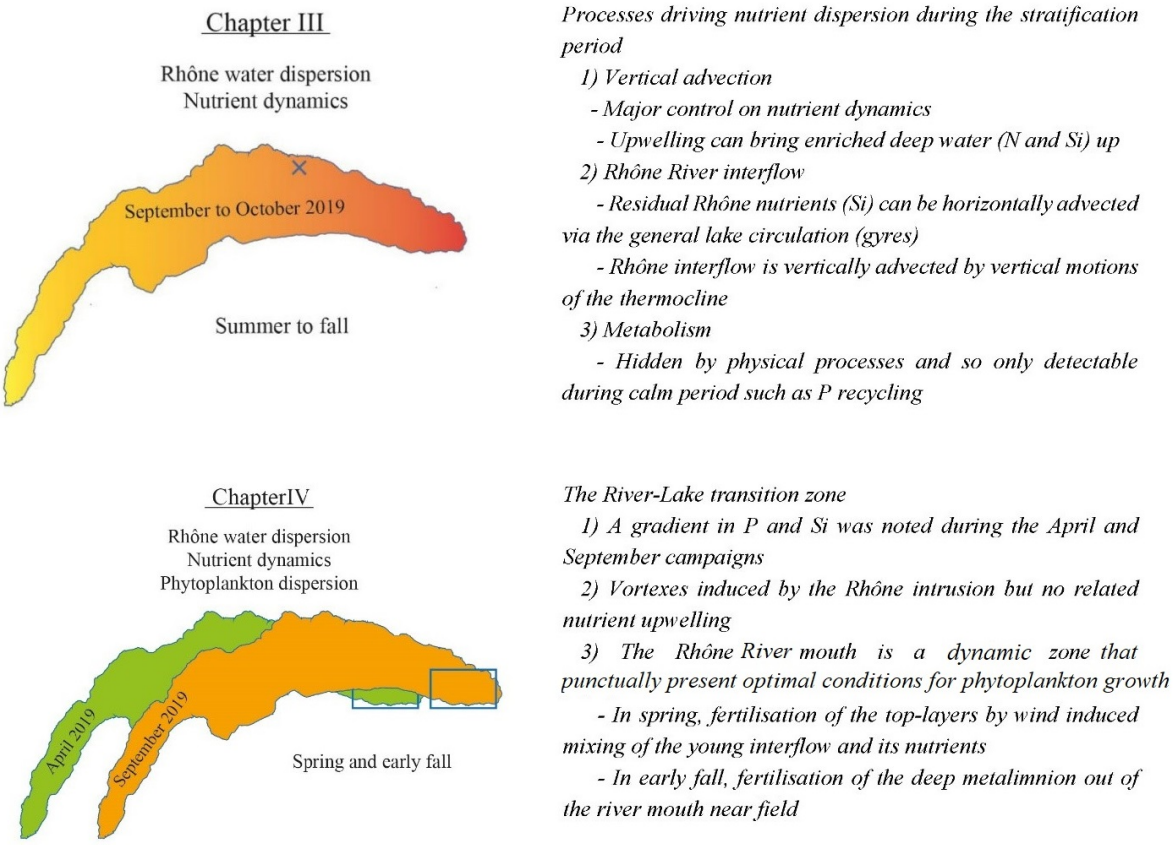

Figure 5-1: Main results of each thesis chapter.

1.1. Tracing of the Rhône River intrusion into Lake Geneva

The reference isotopic composition of the lake water is dictated by mixing of the different water inputs to the lake and the lake overturns during the winter. As demonstrated by Halder et al. (2013), the distinct isotopic composition of the Rhône River compared to the reference value of the lake allows the Rhône intrusion to be traced. The stable isotope composition of the water can then be used as a conservative tracer for the Rhône interflow within the lake. The results of this study indicate that the metalimnion throughout the lake is finally influenced by the Rhône interflow at the end of the stratification period (Cotte and Vennemann, 2020). However, not all the anomalies in conductivity measured in the metalimnion are necessarily related to the Rhône water. Indeed, some anomalies in conductivity as well as the Rhône interflow are located at the thermocline depth where other processes occur. As Lake Geneva is considered to be a "transformer lake" (*cf.* Engel et al., 2018), its conductivity profile is the result of several processes occurring in the epilimnion and the metalimnion (photosynthesis/respiration, CO_2 diffusion, carbonate precipitation, other river influence…). Moreover, the

conductivity is not conservative and together with the variability of the Rhône River conductivity with time, makes this parameter unsuitable to trace the Rhône River water. However, the turbidity is an interesting proxy to localise the Rhône interflow in the Haut-Lac. The turbidity of the Rhône is related to its fine-grained sediment charge and this too is readily dispersed over a considerable area (e.g., Giovanoli, 1990). In contrast to the isotopic composition though, the turbidity is also not necessarily conservative as its position around the thermocline depth is a function of the the settling of other particles out of the Rhône interflow. In the end, only the stable isotope composition of the water appears to be a truly conservative tracer of the Rhône water. Nevertheless, here too some precautions must be taken as mixing effects with ^{18}O-enriched surface waters (rain water and water enriched by evaporation) can cancel the influence of the isotopically light Rhône water, reducing its influence by up to 9 % according to the precipitation rate of year 2015. As no trace of Rhône water was detected during summer 2015 in the epilimnion (no isotopic value inferior to the reference value of the lake), we can argue that this compartment of the lake did not receive more than 9 % of Rhône water during this season. Furthermore, the general circulation of the lake illustrated by the basin-scale gyres implies an important recirculation of the water. Stable isotope compositions of the water are also limited in terms of a temporal evolution of the interflow. To help understand the flow path of the Rhône water more precisely and with a higher temporal resolution requires 3D models of particle tracking. Such models can, in contrast be verified using the point-in time approach given through the sampling and isotopic analyses of the water column.

1.2. Dynamics of the Rhône River intrusion into Lake Geneva over the course of a year

In spring, usually in March, the thermal stratification sets up at first in the eastern part of the lake (the Haut-Lac) where the Rhône River mouth is located (Soulignac et al., 2018). The thermal structure of the lake as such is favourable for the injection of the alpine river water around the depth of the maximum density gradient established in the lake at this time. The river and its nutrients define an interflow in the shallow metalimnion. The early stratification is, however, fragile and is readily interrupted by wind forcing. Consequently, such an event induces a mixing of the nutrient charge of the Rhône intrusion within the epilimnion prior to plunging of the interflow to deeper levels at the newly established thermocline. As the interflow requires a well-established stratification,

it takes several weeks to reach the central lake. During its passage to the central parts though, the interflow-related mixing preferentially fertilises the eastern part of the lake. Besides the conditions for an early stratification, it can explain the enhanced primary production usually observed in spring in the Haut-Lac. Furthermore, the increasing discharge of the Rhône because of increased snow melt at this season translates into a reinforced initial mixing between lake and river waters at the plunge state (e.g., Cortés et al., 2014). This can also explain the presence of Rhône water detected in the epilimnion of the river mouth area in May.

In summer, when the thermal stratification is well established in the lake, the colder Rhône River entering the lake first plunges then, intrudes the lake's water column. The interflow then rises toward the thermocline depth with the loss of its coarse sediments and the progressive mixing with the ambient lake waters. Afterwards, it is blocked from a further rise by the thermocline as suggested by the skewed distribution of the Rhône interflow. Over the summer, the metalimnion layer is continuously flushed by the Rhône interflow reaching an average of about 10 % of Rhône River water. The stronger is the stratification, the most concentrated is the interflow. Moreover, at this season, the Rhône interflow is dispersed throughout the entire basin by the general circulation of the lake. It can reach the Petit-Lac in less than four months. It also recirculates according to the gyral motions. The initial mixing, reinforced due to the high discharge levels induced by further snow and glacial melt waters, creates two patches of Rhône River water release into the lake: a major as an interflow, and another weaker injection in the epilimnion. The latter is, however, not exceeding 9 % of Rhône water during summer 2015, as explained in the previous part. A direct fertilisation of the deep metalimnion related to the Rhône interflow is then reported during this season. Furthermore, when episodic flood events happen, a high sediment load of the Rhône River may also generate underflows and hence also limit the fertilisation of the euphotic zone. Finally, splitting of the river inflow with a major part as an interflow and a minor part as a turbidity current has been also noticed during this season.

During autumn, cooler air temperatures and the stronger winds can cool surface waters sufficiently to mix epilimnion and metalimnion waters. The progressive erosion of the stratification and the related plunge of the thermocline induce a deeper Rhône intrusion. The decrease of the discharge volume and of the isotopic difference between the Rhône and the lake weakens the recognition of the interflow. The metalimnion enriched in Rhône River water is then progressively mixed with the epilmnion. With this

mixing, Rhône River water is detected in the epilmnion until further mixing with the isotopically heavier waters eliminates the trace of the Rhône River water. At this time of the year, because the intrusion occurs below the euphotic zone, upwelling and progressive mixing allow the nutrient-enriched Rhône River water to reach the surface. An indirect fertilisation effect is hence induced by the river nutrients.

In winter, the lake temperature profile is quasi-homogeneous and the Rhône discharge is lowered. A small fraction of Rhône River water is introduced in the top-layers by the reduced initial mixing. The major volume of the Rhône River then plunges down into the canyon as an underflow. After a progressive mixing with ambient water of the lake, it may introduces as a weak interflow into the deeper water column. The intrusions measured at this season were particularly deep (below 100 m) and were not necessarily related to the small temperature gradient that can persist at this season. These circumstances do not provoke any fertilisation but the nutrients introduced to the deep layers can be remobilised during the next complete overturn.

Table 5-1 summarizes the physical characteristics of the Rhône interflow, the Rhône River and the lake stratification during the sampling campaigns, except the December campaign when no interflow was detected.

1.3. Nutrient dynamics and primary production

The vertical advection of nutrient-richer deep water has been identified as major control of the nutrient dispersion (N and Si) in the top-layers during the stratification period at the LéXPLORE platform. Moreover, the metabolic processes in the lake influence first the uptake, then the release of nutrients (P and N), and has been detected during periods of low vertical and horizontal advections. In addition, the Rhône intrusion has been proven to be a significant input of nutrients (P and Si) to the euphotic layer of the Haut-Lac, enhancing phytoplankton growth in this part of the lake. This observation is particularly evident in spring after a winter without a complete overturn as in 2019, inducing an euphotic layer rapidly depleted in nutrients by the vernal bloom. If the hydrodynamic model predictions are correct and climate change reduces the periodicity of complete overturns, the upper epilimnion layers would be depleted in their nutrient content, while only the phosphorus inputs would come from the watershed. The Rhône River intrusion would then play a major role for the primary production of the lake.

Instead, the deeper layers continuously enriched in nutrients by remineralisation processes and phosphorus mobilization from the sediment would constitute an important stock that can be mobilised during the next complete overturn and provoke an important fertilisation of the lake.

Furthermore, it has been shown that hydrodynamic processes play an important role on the nutrient dynamics and also on the primary production of the lake. Indeed, the wind-induced mixing of the Rhône intrusion and its nutrients within the top-layers and the consequent drop of the turbidity, stimulated the primary production at this profile measured in the Haut-Lac in April 2019. The thermocline excursion, whether provoked by the direct forcing of the wind action, internal waves, or the gyres' rotation, can induce a displacement of the limit between the depleted and the enriched layer in nutrients, and a vertical advection of the Rhône interflow and its residual nutrients.

Finally, the Haut-Lac, the eastern part of the lake receiving the Rhône's nutrients, has been identified as a dynamic zone that can punctually present optimal conditions for phytoplankton growth. Indeed, an ecocline develops where an equilibrium occurs between the nutrients transported by the Rhône River and the other limiting factors within the lake, such as sunlight (low turbidity), low flow speed and temperature.

Table 5-1: Stratification, Rhône interflow and hydrological characteristics during the eight sampling campaigns. The stratification characteristics (*) are given for the middle of the lake (SHL2) or the most offshore station (February 2017 and September 2019). The maximum detection distance of the interflow ($^{\Delta}$) is given in comparison with the maximum sampling distance from the Rhône River mouth.

Campaign	June 2015	August 2015	October 2015	July 2016	February 2017	May 2017	April 2019	September 2019
Thickness of SML (m)*	7	10	16	5	130	20	0	17
SML temperature (°C)*	17	21	13	21	6.3	9	-	17
Buoyancy frequency N^2 (s^{-2})*	$2.0\ 10^{-3}$	$2.8\ 10^{-3}$	$5.3\ 10^{-4}$	$2.6\ 10^{-3}$	-	$1.3\ 10^{-4}$	$3.2\ 10^{-4}$	$1.9\ 10^{-3}$
Interflow depth (m)	10-17	12-17	23-32	12-20	60-160	25-40	5-30	20-25
Interflow thickness (m)	2.5-30	10-20	16-28	13-20	40-60	8-25	30	7-17
Isotherm location of the interflow (°C)	10-14	13-16	10-11.5	11-13.5	6.1-6.2	7-9	7.5-9	9-17
Rhône fraction (%)	12-27	14-43	4-20	7-36	3-10	4-25	30	20-30
Maximum detection distance (km)$^{\Delta}$	42/55	55/55	55/55	42/55	5/5	22/42	1/22	4/4
Rhône discharge (m^3/s)	320	270	140	300	79	95	100-200	180-220
Rhône temperature (°C)	10	10	7.5	10	5.8	8.4	5-8	8-9

2. Perspectives

The Rhône River dispersion and its fertilisation effect in Lake Geneva have different implications in several research studies. Here, some perspectives are proposed for possible future investigations.

2.1. Carbon cycle in Lake Geneva

Lake Geneva has been identified as a source of CO_2 to the atmosphere ("CARBOGEN project", LAKES team, IDYST, UNIL, 2020). The major carbon input to the lake comes from carbonate weathering in its catchment and is imported mainly as DIC via the Rhône River. It has been demonstrated that the whiting events (i.e. calcite precipitation) occurring in the lake (Figure 5-2) can be triggered by the Rhône intrusion (Nouchi et al., 2019). It has been hypothesised that the Rhône particles carried by the river interflow can serve as nucleation cells for this process. In addition, it has been shown that primary production creates favourable conditions for such an event by increasing the pH of the water. The present work has demonstrated that the Rhône can be a major driver of the phytoplankton activity in the Haut-Lac. Hence, we can argue that the Rhône is playing a double role in this sequence by triggering the whiting and by its fertilisation effect.

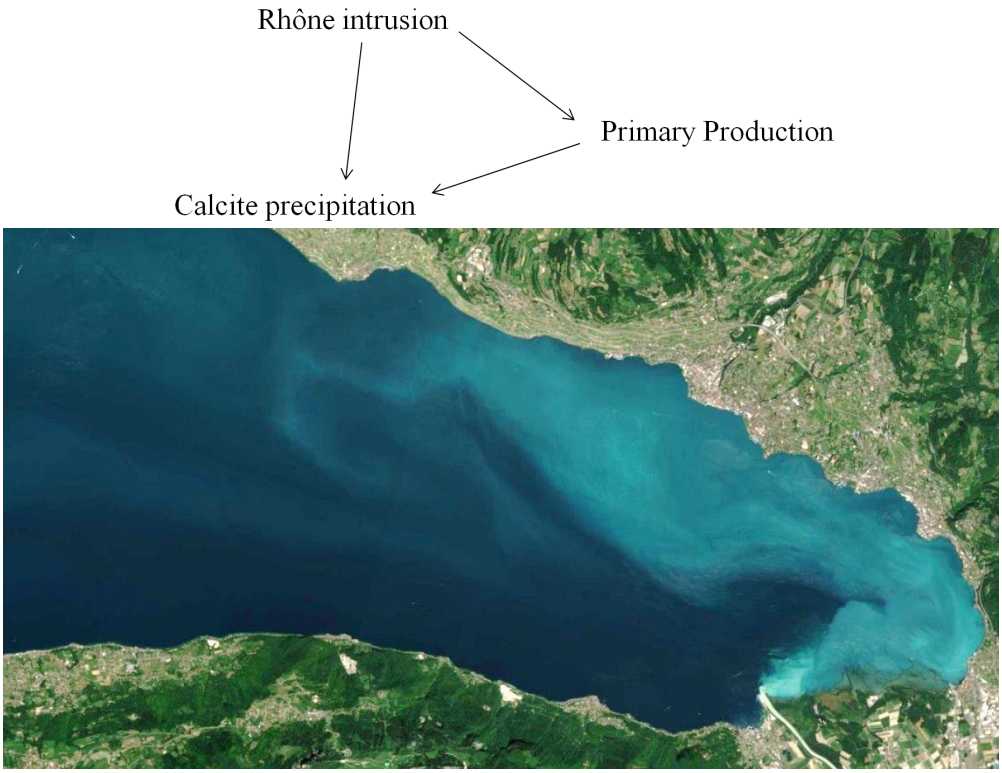

Figure 5-2: Whiting event of the 19th of June 2017 (Sentinel 2).

An individual whiting event has been evaluated to remove about ¼ of the annual Ca deposition (Nouchi et al., 2019). Moreover, another project studied the dissolved organic matter (DOM) degradation in the mixing zone between the Rhône River and Lake Geneva through laboratory incubations (Lambert and Perga, 2019). A higher respiration was found in the mixed water compared to the individual waters and was related to interactions between the different microbial communities. The Rhône River intrusion hence plays an important role in the biogeochemical processes of the lake. A coupling of the methods (remote sensing, bioassays, isotope tracing…) appears to be required to better assess its dispersion pattern, and ultimately to determine the carbon fluxes within the lake.

2.2. Phosphorus cycle in Lake Geneva

After the measures taken to reduce the P-input to the lake, phosphorus has been determined to strongly control phytoplankton growth since 2007 (Moisset, 2017). As such, it is important to assess its dynamics in order to help understand the trophic evolution of the lake.

In this thesis, the Rhône River interflow has been identified as a significant source of orthophosphate to the euphotic zone of the lake, enhancing primary production on its pathway. This impact was clearly identifiable during a growing season taking place after a winter without a complete overturn of the water column. Hence, if these overturns are expected to occur less frequently due to climate warming, as predicted by the hydrodynamic models (Anneville et al., 2013), the phosphorus input from the Rhône River will play a major role in the phytoplankton dynamic of the lake. In this perspective, it would be relevant to evaluate the different P-inputs to the lake and compare the internal loads, including the winter mixing and the P-mineralisation within the water column, and the external load, mainly represented by the Rhône River (Sabaratnam, 2019). Moreover, to get a clear overview of the nutrient dynamics during the stratification period, it will be pertinent to quantify and compare the P-inputs to the euphotic zone from the Rhône River interflow, as well as from the upwelling of the deeper, nutrient-enriched layers of the lake. The first is introduced continuously during summer, except during flooding events, and the latter is provoked by strong wind agitation of surface waters. Both can happen simultaneously as shown in this thesis. In the end, this kind of study requires 3D

hydrodynamic modelling with particle tracking to provide an overview of the lake's processes anytime and anywhere.

In order to complete the phosphorus cycle and clearly assess the drivers of primary production, all the trophic chain levels have to be considered. Indeed, top-down (e.g., Anneville et al., 2019) and bottom-up effects (e.g., Van Donk et al., 2008) can act simultaneously in lakes under the coupled-effect of re-oligotrophication and climate change. Moreover, a high resolution of the nutrient dynamics is needed to quantify the metabolic processes, such as P-recycling of the biota, occurring with low DIP concentrations. For that purpose, the LéXPLORE platform offers a perfect tool to study these processes (www.lexplore.info/). For instance, coupling the optical backscattering signal of the Thetis autonomous profiler (www.epfl.ch/labs/aphys/index-html/news/thetis-letters/) with the isotope tracing of the Rhône River would enable to validate the presence of the Rhône interflow in the signal and thus would monitor the Rhône nutrients input with the Thetis. Indeed, the optical backscattering at 700 nm is a proxy of the fine particles floating in the water column. With the isotopic composition of some water samples, it would be possible to relate these particles to those transported by the Rhône interflow.

2.3. 3D modelling of the lake

Considering the complexity of the large lake systems (hydrodynamic, transport, mixing, nutrient and phytoplankton dynamics…), a better understanding of the processes requires 3D modelling. For example, the river intrusion dispersion is highly variable in space and time depending on the river and lake densities, the river discharge and the currents within the lake. To precisely assess its impact on the primary production and improve the 3D ecological models of the lake, a robust dispersion modelling is necessary. For example, as highlight by Rueda et al. (2007), the river intrusion depth in relation to the euphotic zone determines the bioavailability of its nutrients. Accordingly, coupling a 1D intrusion model (Akiyama and Stefan, 1984) to a 3D particle tracking modelling (Cimatoribus et al., 2019) would allow for an improved assessment of the river intrusion dynamics. It remains to be seen what the computational requirements for such an approach would be.

Furthermore, a coupled approach based on both time-specific isotope measurements and 3D particle tracking modelling would help to improve the knowledge on the

dispersion and mixing of the Rhône River within the lake. Following a first validation of the hydrodynamic model with temperature profiles, the relative age of the water through the interflow can be assessed by particle tracking simulations. As the isotope composition of the Rhône River varies seasonally, this step would allow for a more robust estimate of the Rhône water fraction via the isotope mixing model. Comparison to the simulated particle concentrations should thus validate the model. Finally, the validated 3D model can be used to explain the hydrodynamic processes affecting the Rhône dispersion, such as the gyral motions of the lake and the internal waves related to the action of the prevailing winds.

Additionally, sampling campaigns using model predictions of the river dispersion would allow to determine the chemical and biological gradients related to rapid versus slow transit river pathways and with that the extent of the fertilisation effect. Such a coupled approach would be useful to determine the pathway of the river intrusion and predict its impact on the biogeochemical cycles of the lake.

2.4. Evolution of the Upper Rhône River catchment

With climate warming and local anthropogenic modifications, the Upper Rhône catchment is currently experiencing notable changes. For instance, the shift from a glacial-nival regime to a nival-pluvial regime due to climate change would modify the sediment mobilisation in the watershed. Actually, an increase of the discharge during winter and a decrease during summer, already initiated by the dam's construction, would increase the SSC during winter and decrease it during summer. This, in turn, would switch deep penetrating river intrusions from summer towards winter (Råman Vinnå et al., 2018). With a lower occurrence of a complete overturn of the lake, it would supply river nutrients to the deepest layers of the lake and create intense algal bloom once remobilized during an overturn to the upper euphotic layer.

Additionally, the ecological restoration of confluences of the Rhône and some of its tributaries planned in the third Rhône's correction (Rey et al., 2008) would modify the mobilisation of sediments and nutrients. By breaking the river embankments, it will offer new connections between the river and the fluvial plain and enhance the rate of sediment deposition. This would change the nutrient dynamics in the Rhône River and thus, the nutrient delivery to the lake.

This evolution of the Rhône nutrient dynamics can be monitored by the installation of autosamplers at the different hydrological stations along the Rhône River at different seasons. Due to the large range in elevation, the Upper Rhône catchment offers an interesting place for an isotopic tracing of the different water inputs (cf. Appendix V). It would be possible, for example, to trace the different nutrient sources and to determine the influence of the dam inputs. The capacity to distinguish the different sources via isotopic mixing models remains to be ascertained.

Finally, the project of ecological restoration of the lacustrine Rhône delta (Figure 5-3) would also modify the nutrient dynamics to the lake ("Un delta lacustre pour la biodiversité de l'embouchure du Rhône", Le Temps, 2017). The conversion of the actual unique river canal into multiple branches would likely induce the recovery of a receiving basin as described by Larson et al. (2013). It would then offer potential for the Rhône sediments to settle and for its nutrients to be uptaken by the new vegetation. This new geomorphologic feature will change the river water trajectory and the resulting mixing with the lake water. It would then generate new intrusion patterns like possibly multiple intrusions. These changes of the hydrodynamics and nutrient mobilisations in the new river mouth ecosystem would also be of interest to study.

Figure 5-3: The Rhône delta after the ecological restoration project planned by the Canton de Vaud (CGI, Etat de Vaud).

References

Akiyama, J., Stefan, H.G., 1984. Plunging Flow into a Reservoir: Theory. Journal of Hydraulic Engineering 110, 484–499. https://doi.org/10.1061/(ASCE)0733-9429(1984)110:4(484)

Anneville, O., Beniston, M., Gallina, N., Gillet, C., Jacquet, S., Lazzarotto, J., 2013. L'empreinte du changement climatique sur le Léman. ARCHIVES DES SCIENCES 16.

Anneville, O., Chang, C.-W., Dur, G., Souissi, S., Rimet, F., Hsieh, C., 2019. The paradox of re-oligotrophication: the role of bottom–up versus top–down controls on the phytoplankton community. Oikos 128, 1666–1677. https://doi.org/10.1111/oik.06399

CARBOGEN – LAKES: Past, present and future of alpine lakes, 2020. URL https://wp.unil.ch/lakes/research/carbogen/

Cimatoribus, A.A., Lemmin, U., Barry, D.A., 2019. Tracking Lagrangian transport in Lake Geneva: A 3D numerical modeling investigation. Limnol Oceanogr 64, 1252–1269. https://doi.org/10.1002/lno.11111

Cortés, A., Fleenor, W.E., Wells, M.G., de Vicente, I., Rueda, F.J., 2014. Pathways of river water to the surface layers of stratified reservoirs. Limnol. Oceanogr. 59, 233–250. https://doi.org/10.4319/lo.2014.59.1.0233

Cotte, G., Vennemann, T.W., 2020. Mixing of Rhône River water in Lake Geneva: Seasonal tracing using stable isotope composition of water. Journal of Great Lakes Research 46, 839–849. https://doi.org/10.1016/j.jglr.2020.05.015

Engel, F., Farrell, K.J., McCullough, I.M., Scordo, F., Denfeld, B.A., Dugan, H.A., de Eyto, E., Hanson, P.C., McClure, R.P., Nõges, P., Nõges, T., Ryder, E., Weathers, K.C., Weyhenmeyer, G.A., 2018. A lake classification concept for a more accurate global estimate of the dissolved inorganic carbon export from terrestrial ecosystems to inland waters. Sci Nat 105, 25. https://doi.org/10.1007/s00114-018-1547-z

Giovanoli, F., 1990. Horizontal Transport and Sedimentation by Interflows and Turbidity Currents in Lake Geneva, in: Tilzer, M.M., Serruya, C. (Eds.), Large Lakes: Ecological Structure and Function, Brock/Springer Series in Contemporary

Bioscience. Springer, Berlin, Heidelberg, pp. 175–195. https://doi.org/10.1007/978-3-642-84077-7_9

Halder, J., Decrouy, L., Vennemann, T.W., 2013. Mixing of Rhône River water in Lake Geneva (Switzerland–France) inferred from stable hydrogen and oxygen isotope profiles. Journal of Hydrology 477, 152–164. https://doi.org/10.1016/j.jhydrol.2012.11.026

Lambert, T., Perga, M.-E., 2019. Non-conservative patterns of dissolved organic matter degradation when and where lake water mixes. Aquat Sci 81, 64. https://doi.org/10.1007/s00027-019-0662-z

Larson, J.H., Trebitz, A.S., Steinman, A.D., Wiley, M.J., Mazur, M.C., Pebbles, V., Braun, H.A., Seelbach, P.W., 2013. Great Lakes rivermouth ecosystems: Scientific synthesis and management implications. Journal of Great Lakes Research 39, 513–524. https://doi.org/10.1016/j.jglr.2013.06.002

Moisset, S., 2017. Investigation of the link between phytoplankton and nutrients dynamic in Lake Geneva. University of Geneva. https://doi.org/10.13097/archive-ouverte/unige:96830

Nouchi, V., Kutser, T., Wüest, A., Müller, B., Odermatt, D., Baracchini, T., Bouffard, D., 2019. Resolving biogeochemical processes in lakes using remote sensing. Aquat Sci 81, 27. https://doi.org/10.1007/s00027-019-0626-3

Råman Vinnå, L., Wüest, A., Zappa, M., Fink, G., Bouffard, D., 2018. Tributaries affect the thermal response of lakes to climate change. Hydrol. Earth Syst. Sci. 22, 31–51. https://doi.org/10.5194/hess-22-31-2018

Rey Y., Nicoud S., Romailler G. & Bureau d'études Impact SA, 2008, Rapport d'impact sur l'environnement – 1re étape du Plan d'aménagement de la 3e correction du Rhône publié pour information publique. Canton du Valais.

Rueda, F.J., Fleenor, W.E., de Vicente, I., 2007. Pathways of river nutrients towards the euphotic zone in a deep-reservoir of small size: Uncertainty analysis. Ecological Modelling 202, 345–361. https://doi.org/10.1016/j.ecolmodel.2006.11.006

Sabaratnam and Oriez, 2019, Assessment of the input from the tributaries into the Lake Geneva and into the Rhône downstream Geneva, Rapport CIPEL, Campagne 2018, 117-135

Soulignac, F., Danis, P.-A., Bouffard, D., Chanudet, V., Dambrine, E., Guénand, Y., Harmel, T., Ibelings, B.W., Trevisan, D., Uittenbogaard, R., Anneville, O., 2018. Using 3D modeling and remote sensing capabilities for a better understanding of

spatio-temporal heterogeneities of phytoplankton abundance in large lakes. Journal of Great Lakes Research 44, 756–764. https://doi.org/10.1016/j.jglr.2018.05.008

Un delta lacustre pour la biodiversité de l'embouchure du Rhône, Boris Busslinger, 7 septembre 2017, Le Temps. https://www.letemps.ch/suisse/un-delta-lacustre-biodiversite-lembouchure-rhone

Van Donk, E., Hessen, D.O., Verschoor, A.M., Gulati, R.D., 2008. Re-oligotrophication by phosphorus reduction and effects on seston quality in lakes. Limnologica 38, 189–202. https://doi.org/10.1016/j.limno.2008.05.005

Appendix I

(Chapter I)

Appendix I-1: Positions according to the Swiss coordinate system (CH1903/LV03) and sampling dates of the profiles.

Profile	X (m)	Y (m)	June 2015	August 2015	October 2015	July 2016
0	554725	139048	-	-	-	july 5th 10 am
1-4	553093	143886	june 11th 3 pm	august 27th 10 am	october 28th 10 am	july 5th 3 pm
1-3	552500	142000	june 11th 12 am	august 27th 11 am	october 28th 11 am	july 5th 2 pm
1-2	552000	140000	june 11th 2 pm	august 27th 12 am	october 28th 12 am	july 5th 12 am
1-1	551600	139000	-	august 27th 1 pm	october 28th 1 pm	july 5th 11 am
2-6	533485	149721	june 12th 10 am	-	-	-
2-5	534021	147776	june 12th 12 am	-	-	-
2-6	533211	150533	-	august 28th 1 pm	october 29th 2 pm	july 6th 12 am
2-5	533739	148805	-	august 28th 12 am	october 29th 1 pm	july 6th 11 am
2-4	534284	146841	-	august 28th 11 am	october 29th 12 am	july 6th 10 am
2-3	534700	144950	june 12th 1 pm	august 28th 10 am	october 29th 11 am	july 4th 5 pm
2-2	535089	142929	june 12th 3 pm	august 27th 3 pm	october 29th 10 am	july 4th 4 pm
2-1	535388	140987	june 11th 6 pm	august 27th 4 pm	october 28th 3 pm	july 4th 3 pm
3-3	514000	141600	-	august 25th 12 am	october 26th 11 am	july 8th 4 pm
3-2	515000	140000	june 23rd 12 am	august 25th 11 am	october 26th 12 am	july 8th 3 pm
3-1	516700	137200	-	august 25th 10 am	october 26th 1 pm	july 8th 2 pm
4-3	505000	129000	-	august 25th 4 pm	october 26th 4 pm	july 8th 12 am
4-2	506100	128040	june 23rd 2 pm	august 25th 3 pm	october 26th 3 pm	july 8th 11 am
4-1	507282	127980	-	august 25th 2 pm	october 26th 2 pm	july 8th 10 am

Appendix I-2: Lake Analyser calculations. The Brunt-Väisälä buoyancy frequency (N^2) is expressed in s^{-2} while the top and lower limits of the metalimnion (metaT and metaB), the thickness of the metalimnion (h(meta)) and the thermocline depth (thermD) are expressed in meters.

	June 2015					August 2015					October 2015					July 2016				
	N^2	metaT	thermD	metaB	h(meta)	N^2	metaT	thermD	metaB	h(meta)	N^2	metaT	thermD	metaB	h(meta)	N^2	metaT	thermD	metaB	h(meta)
0	-	-	-	-	-	-	-	-	-	-	-	-	-	-	-	4.9E-03	2.5	6.5	23.0	20.5
1-1	-	-	-	-	-	3.9E-03	8.7	15.5	24.1	15.4	5.6E-04	20.7	29.6	43.8	23.1	4.3E-03	0.0	8.4	19.1	19.1
1-2	1.5E-03	0.5	0.5	22.0	21.5	2.5E-03	4.6	15.3	29.6	25.0	7.5E-04	22.5	30.0	37.4	15.0	2.4E-03	0.0	7.5	19.1	19.1
1-3	1.8E-03	0.0	3.2	21.0	21.0	3.8E-03	5.6	7.6	30.0	24.4	1.2E-03	25.3	30.4	42.6	17.3	2.0E-03	0.0	7.6	27.0	27.0
1-4	4.0E-03	0.0	4.5	19.0	19.0	3.4E-03	5.5	8.7	25.6	20.1	4.3E-04	17.9	24.0	38.8	20.9	3.5E-03	0.0	4.8	25.1	25.1
2-1	1.6E-03	7.6	13.3	24.1	16.5	3.8E-03	6.0	9.4	20.2	14.2	8.2E-04	18.0	20.7	30.5	12.4	3.3E-04	0.0	6.2	24.6	24.6
2-2	3.6E-03	0.0	9.7	20.7	20.7	2.9E-03	4.7	11.4	28.7	24.1	5.1E-04	15.5	19.1	35.2	19.7	3.7E-03	0.0	6.2	29.3	29.3
2-3	2.3E-03	5.9	8.3	11.3	5.3	2.5E-03	7.9	18.3	29.2	21.2	2.8E-04	15.1	23.8	34.5	19.3	2.7E-03	0.0	6.5	25.2	25.2
2-4	1.4E-03	0.6	7.3	16.1	15.5	2.4E-03	7.5	12.4	28.7	21.1	6.2E-04	18.7	20.8	41.5	22.8	2.9E-03	2.5	4.5	29.9	27.4
2-5	1.3E-03	0.6	11.1	16.9	16.2	3.6E-03	5.5	14.5	32.1	26.7	5.1E-04	16.4	20.7	38.7	22.2	2.8E-03	1.6	6.6	25.0	23.4
2-6	-	-	-	-	-	1.9E-03	3.8	14.0	26.1	22.4	4.6E-04	18.7	20.5	42.0	23.3	3.1E-03	0.0	4.7	25.7	25.7
3-1	-	-	-	-	-	4.0E-03	10.3	12.6	22.2	11.9	-	-	-	-	-	3.2E-03	0.0	7.1	28.0	28.0
3-2	2.3E-03	0.0	9.2	15.3	15.3	6.0E-03	7.6	9.5	28.9	21.4	8.1E-04	23.6	28.6	39.5	15.8	2.8E-03	0.0	9.1	29.4	29.4
3-3	-	-	-	-	-	2.8E-03	1.2	5.5	26.0	24.8	1.3E-03	25.7	28.7	40.6	14.9	3.6E-03	0.6	8.0	25.4	24.9
4-1	-	-	-	-	-	6.0E-03	1.6	4.8	18.0	16.4	1.5E-03	22.5	25.1	33.8	11.3	4.5E-03	0.9	12.4	29.1	28.3
4-2	7.3E-03	0.0	5.5	15.8	15.8	5.5E-03	5.5	7.6	16.0	10.5	1.8E-03	22.3	25.3	30.4	8.1	2.1E-03	0.0	7.7	25.3	25.3
4-3	-	-	-	-	-	2.6E-03	0.0	5.7	20.2	20.2	8.1E-06	21.6	23.9	30.2	8.6	4.4E-03	1.9	7.4	31.9	30.0

Appendix I-3: CTD data (depth, temperature, conductivity, oxygen concentration, oxygen saturation and pH) and stable isotope composition of the lake water samples for the four sampling campaigns.

Profile	Sampling date	Depth (m)	T (°C)	K25 (µS/cm)	O_2 (mg/L)	O_2 (% sat.)	pH	**$\delta^{18}O$ VSMOW**	std. dev.	**δD VSMOW**	std. dev.
June 2015											
1-4	11.06.2015	0.0		0				**-12.17**	0.06	**-94.1**	0.6
1-4	11.06.2015	2.1	17.9	294	11.2	118	8.6	**-12.29**	0.13		
1-4	11.06.2015	5.3	17.5	294	10.9	115	8.6	**-12.40**	0.14	**-88.2**	0.8
1-4	11.06.2015	7.4	12.7	299	11.5	109	8.5	**-12.55**	0.15	**-89.2**	0.7
1-4	11.06.2015	10.4	11.8	306	11.0	102	8.3	**-12.28**	0.10		
1-4	11.06.2015	11.7	11.0	308	10.4	94	8.1	**-12.38**	0.03	**-91.7**	0.7
1-4	11.06.2015	14.1	10.6	309	10.2	92	8.0	**-12.45**	0.15	**-90.3**	1.2
1-4	11.06.2015	16.1	10.4	311	9.5	85	8.0	**-12.31**	0.12		
1-4	11.06.2015	18.3	10.0	304	9.3	82	8.0	**-12.57**	0.14	**-90.7**	1.3
1-4	11.06.2015	20.5	9.4	311	9.1	80	7.9	**-12.30**	0.10		
1-4	11.06.2015	25.6	8.5	313	9.2	79	7.9	**-12.26**	0.08	**-94.7**	1.0
1-4	11.06.2015	31.0	8.0	315	9.4	79	7.9	**-12.28**	0.11		
1-4	11.06.2015	41.4	7.2	317	9.7	81	7.9	**-12.16**	0.08	**-93.7**	0.6
1-4	11.06.2015	52.0	6.9	317	10.0	83	7.9	**-12.22**	0.10	**-93.4**	0.7
1-4	11.06.2015	82.8	6.5	316	10.3	84	8.0	**-12.29**	0.12	**-92.3**	1.3
1-4	11.06.2015	121.9	6.3	318	9.8	80	7.9	**-12.26**	0.10	**-93.4**	0.7
1-4	11.06.2015	163.6	5.9	318	8.5	69	7.9	**-12.09**	0.14	**-91.5**	1.4
1-4	11.06.2015	203.4	5.6	324	7.3	58	7.8	**-11.94**	0.09	**-93.8**	0.7
1-3	11.06.2015	0.0						**-12.32**	0.04	**-94.6**	0.7
1-3	11.06.2015	1.7	18.5	288	10.7	115	8.6	**-12.48**	0.06	**-96.3**	0.8
1-3	11.06.2015	4.4	15.3	291	11.6	116	8.5	**-12.58**	0.06	**-96.1**	0.8
1-3	11.06.2015	8.6	13.0	302	11.5	110	8.5	**-12.36**	0.08	**-95.4**	0.4
1-3	11.06.2015	10.6	12.2	303	10.9	102	8.4	**-12.34**	0.07	**-95.4**	0.6
1-3	11.06.2015	13.3	10.8	300	9.4	85	8.1	**-12.69**	0.11	**-96.4**	1.5
1-3	11.06.2015	15.6	10.3	308	9.2	83	8.0	**-12.51**	0.10	**-95.0**	0.9
1-3	11.06.2015	18.0	9.8	308	9.1	80	7.9	**-12.59**	0.10	**-94.9**	1.1
1-3	11.06.2015	19.4	9.4	313	8.9	78	7.9	**-12.43**	0.11	**-93.8**	1.1
1-3	11.06.2015	22.5	9.2	313	9.8	85	7.9	**-12.31**	0.08	**-94.3**	0.8
1-3	11.06.2015	25.1	8.4	315	8.9	76	7.9	**-12.14**	0.04	**-94.9**	0.8
1-3	11.06.2015	25.9	8.6	313	9.9	85	7.9	**-12.28**	0.06	**-94.0**	0.6
1-3	11.06.2015	29.5	7.8	315	9.2	78	7.9	**-12.06**	0.04	**-94.9**	0.3
1-3	11.06.2015	40.1	7.1	316	9.5	79	7.9	**-12.04**	0.09	**-94.2**	0.8
1-3	11.06.2015	40.1	7.1	316	9.6	79	7.9	**-12.09**	0.09	**-93.4**	0.6
1-3	11.06.2015	81.2	6.7	317	10.0	82	8.0	**-12.12**	0.09	**-94.0**	0.6
1-3	11.06.2015	122.6	6.3	317	9.7	78	7.9	**-12.10**	0.07	**-94.1**	0.7
1-3	11.06.2015	174.3	5.9	322	8.1	65	7.8	**-12.10**	0.04	**-92.6**	0.8
1-2	11.06.2015	0.0						**-12.41**	0.15	**-89.2**	0.9
1-2	11.06.2015	2.9	16.4	300	10.4	107	8.6	**-12.33**	0.22		
1-2	11.06.2015	4.7	16.1	300	10.5	107	8.6	**-12.00**	0.11	**-85.5**	0.7
1-2	11.06.2015	8.0	13.3	304	10.6	101	8.5	**-12.27**	0.13	**-86.2**	1.1
1-2	11.06.2015	10.1	12.8	306	10.9	103	8.4	**-12.40**	0.09	**-90.6**	0.6
1-2	11.06.2015	12.9	12.1	307	10.3	96	8.3	**-12.28**	0.10	**-90.1**	0.7
1-2	11.06.2015	14.9	11.3	310	10.0	91	8.2	**-12.28**	0.20	**-86.4**	1.0
1-2	11.06.2015	18.0	10.8	309	9.8	89	8.1	**-12.39**	0.08	**-90.9**	0.9
1-2	11.06.2015	20.9	10.3	312	9.6	86	8.0	**-12.40**	0.11	**-90.8**	0.9
1-2	11.06.2015	23.6	10.2	311	9.3	83	8.0	**-12.27**	0.15	**-87.4**	0.7
1-2	11.06.2015	24.9	9.7	313	9.5	84	8.0	**-12.31**	0.08	**-88.0**	1.7
1-2	11.06.2015	28.6	9.3	312	9.2	80	7.9	**-12.30**	0.07	**-89.1**	1.0
1-2	11.06.2015	31.6	8.9	313	9.3	81	7.9	**-12.32**	0.15	**-89.6**	0.8
1-2	11.06.2015	40.2	7.8	316	9.6	81	7.9	**-12.31**	0.14	**-88.9**	1.2
1-2	11.06.2015	49.7	7.4	317	9.8	82	7.9	**-12.15**	0.06	**-88.8**	1.1
1-2	11.06.2015	81.7	6.6	317	10.5	86	8.0	**-12.20**	0.20	**-86.4**	1.2
1-2	11.06.2015	142.7	6.1	319	9.6	78	7.9	**-12.33**	0.13	**-86.8**	1.8
1-2	11.06.2015	178.3	5.9	322	8.5	68	7.8	**-12.23**	0.07	**-87.0**	1.0
2-6	12.06.2015	0.0						**-12.55**	0.09	**-92.7**	0.4
2-6	12.06.2015	2.5	16.1	292	11.4	116	8.5	**-12.66**	0.05	**-92.2**	0.3

Profile	Sampling date	Depth (m)	T (°C)	K25 (µS/cm)	O_2 (mg/L)	O_2 (% sat.)	pH	**$\delta^{18}O$ VSMOW**	std. dev.	**δD VSMOW**	std. dev.
2-6	12.06.2015	4.9	15.9	292	11.5	116	8.5	**-12.59**	0.11	**-92.5**	0.2
2-6	12.06.2015	7.7	15.7	291	11.4	116	8.4	**-12.76**	0.10	**-92.7**	0.5
2-6	12.06.2015	9.9	14.8	291	11.4	113	8.4	**-12.78**	0.12	**-93.0**	0.5
2-6	12.06.2015	12.1	13.0	296	11.5	109	8.3	**-12.77**	0.08	**-93.2**	0.5
2-6	12.06.2015	13.8	12.4	298	11.4	107	8.3	**-12.76**	0.09	**-93.0**	0.3
2-6	12.06.2015	15.9	11.2	304	10.8	99	8.1	**-12.64**	0.04	**-92.2**	0.4
2-6	12.06.2015	18.7	10.9	306	10.8	98	8.0	**-12.39**	0.08	**-91.9**	0.2
2-6	12.06.2015	20.7	10.8	306	10.8	98	8.0	**-12.42**	0.08	**-91.6**	0.3
2-6	12.06.2015	26.3	10.6	310	10.5	95	8.0	**-12.30**	0.08	**-91.1**	0.3
2-6	12.06.2015	30.9	9.8	310	10.2	90	7.9	**-12.29**	0.04	**-90.8**	0.4
2-6	12.06.2015	36.1	8.9	314	10.4	90	7.9	**-12.16**	0.06	**-90.3**	0.2
2-6	12.06.2015	51.4	7.0	316	10.9	90	7.9	**-12.10**	0.07	**-89.3**	0.2
2-6	12.06.2015	61.6	6.8	316	11.2	92	7.9	**-12.12**	0.09	**-89.9**	0.3
2-6	12.06.2015	81.9	6.5	317	11.5	94	7.9	**-12.09**	0.05	**-89.8**	0.3
2-6	12.06.2015	122.6	6.2	318	10.9	88	7.9	**-12.14**	0.06	**-89.8**	0.4
2-6	12.06.2015	163.8	5.9	322	9.4	76	7.8	**-12.11**	0.04	**-89.2**	0.1
2-5	12.06.2015	0.0						**-12.40**	0.12	**-91.5**	0.3
2-5	12.06.2015	2.6	16.5	293	11.2	115	8.5	**-12.49**	0.06	**-92.0**	0.1
2-5	12.06.2015	5.5	15.8	290	11.1	112	8.4	**-12.48**	0.03	**-92.3**	0.2
2-5	12.06.2015	7.3	13.2	299	11.5	110	8.4	**-12.48**	0.06	**-92.3**	0.4
2-5	12.06.2015	8.6	12.9	300	11.5	110	8.4	**-12.47**	0.11	**-92.0**	0.1
2-5	12.06.2015	9.6	12.6	301	11.3	106	8.3	**-12.54**	0.03	**-92.2**	0.3
2-5	12.06.2015	11.1	12.3	297	11.0	103	8.2	**-12.59**	0.11	**-93.2**	0.4
2-5	12.06.2015	12.8	12.0	300	10.8	101	8.2	**-12.57**	0.05	**-92.8**	0.2
2-5	12.06.2015	16.0	11.3	311	10.6	97	8.1	**-12.44**	0.10	**-91.6**	0.4
2-5	12.06.2015	18.0	10.8	307	10.5	95	8.0	**-12.42**	0.04	**-91.4**	0.3
2-5	12.06.2015	21.1	10.3	309	10.2	91	8.0	**-12.26**	0.04	**-90.6**	0.3
2-5	12.06.2015	23.9	9.4	312	10.3	90	7.9	**-12.19**	0.05	**-90.0**	0.2
2-5	12.06.2015	28.1	9.2	313	10.1	88	7.9	**-12.22**	0.06	**-89.9**	0.4
2-5	12.06.2015	30.9	8.4	315	10.1	87	7.9	**-12.19**	0.05	**-89.9**	0.3
2-5	12.06.2015	36.1	7.8	316	10.2	86	7.9	**-12.22**	0.07	**-89.5**	0.3
2-5	12.06.2015	41.5	7.3	317	10.3	86	7.8	**-12.27**	0.04	**-89.5**	0.2
2-5	12.06.2015	51.9	6.9	317	10.6	88	7.9	**-12.19**	0.07	**-89.6**	0.3
2-5	12.06.2015	71.6	6.6	317	11.2	91	7.9	**-12.14**	0.05	**-89.5**	0.2
2-5	12.06.2015	102.5	6.3	317	10.9	88	7.9	**-12.20**	0.07	**-89.3**	0.2
2-5	12.06.2015	143.5	6.0	320	9.7	78	7.9	**-12.13**	0.06	**-89.1**	0.2
2-5	12.06.2015	184.2	5.7	323	8.2	66	7.8	**-12.01**	0.08	**-88.5**	0.2
2-5	12.06.2015	258.7	5.4	327	6.0	48	7.7	**-12.01**	0.10	**-88.3**	0.3
2-3	12.06.2015	0.0						**-12.39**	0.11	**-91.5**	0.4
2-3	12.06.2015	2.1	17.5	294	11.9	125	8.6	**-12.28**	0.05	**-90.8**	0.3
2-3	12.06.2015	4.9	17.1	291	11.9	124	8.6	**-12.35**	0.09	**-91.3**	0.1
2-3	12.06.2015	7.1	15.8	290	11.6	117	8.5	**-12.58**	0.03	**-92.6**	0.3
2-3	12.06.2015	9.3	13.3	295	12.4	119	8.4	**-12.39**	0.08	**-91.1**	0.4
2-3	12.06.2015	10.4	12.5	304	12.5	118	8.5	**-12.20**	0.06	**-90.1**	0.5
2-3	12.06.2015	11.4	11.6	306	12.6	116	8.5	**-12.24**	0.09	**-90.2**	0.3
2-3	12.06.2015	12.7	11.2	310	12.6	115	8.4	**-12.19**	0.11	**-90.5**	0.3
2-3	12.06.2015	13.6	10.6	311	12.2	110	8.4	**-12.19**	0.09	**-90.0**	0.1
2-3	12.06.2015	15.6	9.4	313	11.1	98	8.1	**-12.11**	0.07	**-90.1**	0.2
2-3	12.06.2015	18.1	9.0	314	10.7	93	8.0	**-12.10**	0.09	**-90.0**	0.1
2-3	12.06.2015	21.0	8.5	314	10.7	92	7.9	**-12.20**	0.08	**-89.9**	0.3
2-3	12.06.2015	26.1	7.4	316	10.3	86	7.8	**-12.20**	0.09	**-89.9**	0.1
2-3	12.06.2015	31.1	7.1	318	10.2	85	7.8	**-12.11**	0.11	**-89.7**	0.2
2-3	12.06.2015	35.9	6.9	316	10.7	88	7.9	**-12.08**	0.09	**-89.7**	0.3
2-3	12.06.2015	41.3	6.8	315	10.9	90	7.9	**-12.08**	0.04	**-89.6**	0.2
2-3	12.06.2015	51.8	6.6	316	11.1	90	7.9	**-12.09**	0.08	**-90.0**	0.4
2-3	12.06.2015	61.8	6.6	316	11.0	90	7.9	**-12.16**	0.06	**-89.7**	0.2
2-3	12.06.2015	82.3	6.4	317	10.9	89	7.9	**-12.20**	0.05	**-89.6**	0.2
2-3	12.06.2015	123.1	6.2	318	10.6	86	7.9	**-12.21**	0.10	**-89.6**	0.3
2-3	12.06.2015	164.1	6.0	317	8.9	72	7.9	**-12.12**	0.03	**-89.6**	0.2
2-3	12.06.2015	204.7	5.6	323	7.9	63	7.8	**-12.08**	0.05	**-88.9**	0.3
2-3	12.06.2015	305.5	5.4	332	4.4	35	7.7	**-12.05**	0.04	**-89.1**	0.2
2-2	12.06.2015	0.0						**-12.21**	0.06	**-89.9**	0.2

Profile	Sampling date	Depth (m)	T (°C)	K25 (µS/cm)	O_2 (mg/L)	O_2 (% sat.)	pH	**$\delta^{18}O$ VSMOW**	std. dev.	**δD VSMOW**	std. dev.
2-2	12.06.2015	2.5	18.1	296	11.9	126	8.6	**-12.21**	0.10	**-89.6**	0.4
2-2	12.06.2015	5.8	17.5	297	11.9	125	8.6	**-12.22**	0.02	**-89.8**	0.2
2-2	12.06.2015	9.3	15.9	298	12.4	125	8.6	**-12.25**	0.04	**-90.3**	0.1
2-2	12.06.2015	10.3	15.2	298	12.4	124	8.6	**-12.41**	0.04	**-90.6**	0.2
2-2	12.06.2015	11.3	12.7	305	12.7	120	8.5	**-12.41**	0.06	**-90.9**	0.2
2-2	12.06.2015	12.6	11.5	308	12.8	117	8.4	**-12.32**	0.03	**-90.8**	0.1
2-2	12.06.2015	13.4	10.9	309	11.9	108	8.3	**-12.31**	0.05	**-90.7**	0.1
2-2	12.06.2015	15.0	9.9	311	10.9	97	8.1	**-12.31**	0.05	**-90.7**	0.2
2-2	12.06.2015	17.6	8.4	315	10.4	89	7.9	**-12.33**	0.04	**-90.4**	0.2
2-2	12.06.2015	20.5	7.8	315	10.4	88	7.8	**-12.28**	0.08	**-90.1**	0.2
2-2	12.06.2015	30.7	7.0	317	10.9	90	7.9	**-12.23**	0.05	**-90.0**	0.4
2-2	12.06.2015	51.7	6.6	316	11.2	92	7.9	**-12.23**	0.08	**-89.7**	0.2
2-2	12.06.2015	61.3	6.6	317	11.2	91	7.9	**-12.22**	0.04	**-89.9**	0.3
2-2	12.06.2015	81.7	6.4	317	11.0	89	7.9	**-12.29**	0.05	**-89.9**	0.2
2-2	12.06.2015	122.9	6.1	319	10.3	83	7.9	**-12.22**	0.08	**-89.9**	0.3
2-2	12.06.2015	153.8	5.9	321	9.4	76	7.8	**-12.20**	0.04	**-89.1**	0.2
2-2	12.06.2015	204.8	5.6	324	7.8	62	7.8	**-12.15**	0.06	**-88.7**	0.2
2-1	11.06.2015	0.0						**-12.31**	0.05	**-90.1**	0.3
2-1	11.06.2015	2.6	17.6	295	12.2	128	8.6	**-12.27**	0.05	**-90.1**	0.5
2-1	11.06.2015	5.8	17.4	295	12.1	127	8.6	**-12.23**	0.05	**-90.0**	0.3
2-1	11.06.2015	12.1	16.9	296	12.0	125	8.6	**-12.21**	0.06	**-89.9**	0.2
2-1	11.06.2015	14.8	15.0	300	12.3	122	8.5	**-12.29**	0.06	**-90.3**	0.1
2-1	11.06.2015	16.9	13.1	305	12.1	115	8.5	**-12.39**	0.05	**-90.5**	0.2
2-1	11.06.2015	18.5	12.0	308	11.4	106	8.3	**-12.36**	0.07	**-90.6**	0.5
2-1	11.06.2015	20.5	10.3	312	10.3	92	8.0	**-12.35**	0.06	**-90.9**	0.2
2-1	11.06.2015	22.4	9.7	312	10.0	88	7.9	**-12.34**	0.04	**-90.6**	0.3
2-1	11.06.2015	25.1	9.1	313	9.9	86	7.9	**-12.35**	0.05	**-90.4**	0.2
2-1	11.06.2015	31.2	8.2	314	9.9	84	7.9	**-12.32**	0.03	**-90.2**	0.1
2-1	11.06.2015	41.0	7.0	316	10.3	85	7.9	**-12.22**	0.03	**-89.6**	0.3
2-1	11.06.2015	51.8	6.8	316	10.7	88	7.9	**-12.24**	0.04	**-89.8**	0.3
2-1	11.06.2015	81.8	6.5	317	10.6	87	8.0	**-12.25**	0.03	**-89.8**	0.3
2-1	11.06.2015	122.8	6.1	320	9.4	76	7.9	**-12.22**	0.04	**-89.6**	0.2
2-1	11.06.2015	145.0	5.9	321	8.7	69	7.9	**-12.24**	0.03	**-89.4**	0.4
2-1	11.06.2015	176.8	5.6	325	7.9	63	7.8	**-12.15**	0.03	**-89.3**	0.2
3-2	23.06.2015	0.0						**-12.08**	0.04	**-88.8**	0.2
3-2	23.06.2015	2.8	15.8	298	11.1	113	8.6	**-12.15**	0.05	**-90.4**	0.3
3-2	23.06.2015	5.6	15.6	299	11.1	112	8.5	**-12.12**	0.06	**-90.1**	0.3
3-2	23.06.2015	6.7	15.5	298	10.7	108	8.5	**-12.18**	0.05	**-90.1**	0.3
3-2	23.06.2015	7.8	15.3	299	11.1	111	8.5	**-12.28**	0.08	**-90.1**	0.1
3-2	23.06.2015	8.9	14.4	301	10.1	99	8.4	**-12.33**	0.09	**-90.4**	0.3
3-2	23.06.2015	10.3	11.8	306	9.8	90	8.1	**-12.40**	0.05	**-90.2**	0.4
3-2	23.06.2015	11.7	10.6	308	9.2	83	7.9	**-12.41**	0.08	**-90.5**	0.2
3-2	23.06.2015	15.9	9.6	312	9.2	81	7.8	**-12.32**	0.01	**-90.0**	0.5
3-2	23.06.2015	21.0	8.9	314	9.2	80	7.8	**-12.17**	0.07	**-89.6**	0.3
3-2	23.06.2015	26.2	7.8	316	9.7	82	7.9	**-12.18**	0.03	**-89.4**	0.2
3-2	23.06.2015	33.9	7.1	317	10.2	84	7.9	**-12.17**	0.07	**-89.2**	0.3
3-2	23.06.2015	50.2	6.7	316	10.8	89	7.9	**-12.22**	0.08	**-89.1**	0.3
3-2	23.06.2015	71.9	6.4	317	11.0	89	8.0	**-12.19**	0.06	**-89.2**	0.3
4-2	23.06.2015	0.0						**-11.93**	0.04	**-88.9**	0.2
4-2	23.06.2015	2.9	19.3	295	10.7	116	8.6	**-11.92**	0.03	**-88.5**	0.3
4-2	23.06.2015	4.7	18.7	296	11.0	118	8.5	**-11.93**	0.03	**-88.6**	0.3
4-2	23.06.2015	5.5	17.1	296	11.2	116	8.5	**-11.98**	0.05	**-89.5**	0.3
4-2	23.06.2015	6.5	13.1	304	11.4	108	8.3	**-11.98**	0.13	**-90.2**	0.5
4-2	23.06.2015	7.8	11.3	309	11.1	102	8.1	**-12.13**	0.04	**-90.7**	0.2
4-2	23.06.2015	10.5	10.7	310	10.1	91	8.0	**-12.12**	0.05	**-90.3**	0.2
4-2	23.06.2015	15.9	9.7	313	9.8	86	7.9	**-12.13**	0.07	**-90.0**	0.4
4-2	23.06.2015	20.8	9.1	313	9.8	85	7.9	**-12.14**	0.12	**-90.6**	0.9
4-2	23.06.2015	26.2	8.2	316	10.3	88	7.9	**-12.05**	0.06	**-89.5**	0.3
4-2	23.06.2015	41.4	6.9	318	11.0	90	7.9	**-12.06**	0.04	**-89.4**	0.2
4-2	23.06.2015	60.8	6.5	319	11.0	90	8.0	**-12.04**	0.04	**-89.5**	0.2
August 2015											
1-4	27.08.2015	0.0						**-12.08**	0.11	**-91.2**	0.5

Profile	Sampling date	Depth (m)	T (°C)	K25 (µS/cm)	O_2 (mg/L)	O_2 (% sat.)	pH	**$\delta^{18}O$ VSMOW**	std. dev.	**δD VSMOW**	std. dev.
1-4	27.08.2015	2.2	21.2	267	10.2	115	8.6	**-12.03**	0.05	**-89.5**	0.1
1-4	27.08.2015	7.8	21.0	266	10.2	114	8.6	**-12.22**	0.07	**-90.7**	0.1
1-4	27.08.2015	9.7	18.1	271	10.7	114	8.3	**-12.42**	0.06	**-92.6**	0.3
1-4	27.08.2015	11.8	17.5	271	9.6	101	8.0	**-12.61**	0.03	**-93.4**	0.1
1-4	27.08.2015	12.5	16.7	274	9.7	100	8.3	**-12.59**	0.07	**-93.4**	0.4
1-4	27.08.2015	14.4	13.1	293	7.6	73	7.8	**-12.57**	0.06	**-93.2**	0.4
1-4	27.08.2015	16.5	12.1	301	7.1	66	7.8	**-12.38**	0.04	**-92.3**	0.3
1-4	27.08.2015	18.7	11.0	309	6.6	60	7.8	**-12.37**	0.04	**-91.9**	0.4
1-4	27.08.2015	20.9	9.9	313	6.5	58	7.8	**-12.28**	0.07	**-90.8**	0.4
1-4	27.08.2015	25.7	9.0	316	7.3	63	7.8	**-12.17**	0.02	**-89.8**	0.2
1-4	27.08.2015	31.3	8.1	317	8.2	70	7.8	**-12.07**	0.01	**-90.0**	0.4
1-4	27.08.2015	40.8	7.4	317	9.0	75	7.8	**-12.49**	0.09	**-91.7**	0.2
1-4	27.08.2015	82.2	6.5	318	10.3	84	7.9	**-12.58**	0.09	**-91.4**	0.3
1-4	27.08.2015	204.1	5.7	325	6.4	51	7.8	**-12.30**	0.13	**-89.9**	0.5
1-3	27.08.2015	0.0						**-12.04**	0.05	**-89.7**	0.4
1-3	27.08.2015	3.3	21.1	266	10.0	113	8.7	**-12.01**	0.06	**-89.4**	0.3
1-3	27.08.2015	7.9	20.0	268	10.3	113	8.5	**-12.38**	0.06	**-92.0**	0.2
1-3	27.08.2015	10.0	17.8	267	10.0	106	8.4	**-12.54**	0.05	**-93.0**	0.2
1-3	27.08.2015	13.2	16.4	268	9.6	98	8.1	**-12.70**	0.05	**-93.9**	0.4
1-3	27.08.2015	15.2	14.1	278	8.5	82	8.0	**-12.73**	0.03	**-93.7**	0.4
1-3	27.08.2015	17.1	13.3	285	8.0	77	7.9	**-12.60**	0.06	**-93.2**	0.3
1-3	27.08.2015	20.4	11.0	305	6.8	62	7.8	**-12.51**	0.05	**-92.6**	0.2
1-3	27.08.2015	25.3	9.5	317	6.8	60	7.8	**-12.28**	0.05	**-90.6**	0.1
1-3	27.08.2015	30.7	8.5	318	7.7	66	7.9	**-12.21**	0.04	**-89.9**	0.3
1-3	27.08.2015	51.3	6.9	318	9.7	80	7.9	**-12.09**	0.06	**-89.6**	0.2
1-3	27.08.2015	178.8	5.7	324	7.4	59	7.9	**-12.02**	0.03	**-88.9**	0.3
1-2	27.08.2015	0.0						**-12.06**	0.06	**-89.0**	0.3
1-2	27.08.2015	3.5	21.2	266	10.0	113	8.7	**-12.16**	0.03	**-89.8**	0.4
1-2	27.08.2015	9.8	19.5	271	10.4	114	8.6	**-12.41**	0.07	**-91.3**	0.3
1-2	27.08.2015	11.5	19.4	268	10.2	112	8.5	**-12.57**	0.05	**-91.5**	0.6
1-2	27.08.2015	13.4	17.6	260	9.1	96	8.3	**-12.72**	0.06	**-92.0**	0.1
1-2	27.08.2015	15.5	15.2	270	8.6	85	8.0	**-12.83**	0.04	**-93.4**	0.4
1-2	27.08.2015	17.4	12.6	284	7.5	71	7.9	**-12.88**	0.04	**-93.4**	0.3
1-2	27.08.2015	20.0	10.4	309	6.8	61	7.8	**-12.52**	0.03	**-91.4**	0.3
1-2	27.08.2015	23.1	9.1	315	7.5	66	7.9	**-12.28**	0.06	**-89.7**	0.2
1-2	27.08.2015	28.5	8.3	316	8.7	74	7.9	**-12.14**	0.08	**-89.5**	0.4
1-2	27.08.2015	51.3	6.8	317	9.8	81	7.9	**-12.07**	0.06	**-89.1**	0.3
1-2	27.08.2015	173.6	5.7	325	6.8	55	7.9	**-11.96**	0.05	**-87.8**	0.2
1-1	27.08.2015	0.0						**-12.12**	0.06	**-89.9**	0.6
1-1	27.08.2015	3.1	21.4	266	9.9	112	8.7	**-11.98**	0.08	**-89.7**	0.1
1-1	27.08.2015	10.4	19.7	266	10.0	110	8.5	**-12.19**	0.06	**-90.7**	0.5
1-1	27.08.2015	13.4	17.9	270	9.3	99	8.2	**-12.57**	0.08	**-93.1**	0.4
1-1	27.08.2015	16.5	14.4	276	8.1	80	8.0	**-12.57**	0.06	**-93.7**	0.3
1-1	27.08.2015	19.2	11.0	290	8.8	80	7.9	**-12.58**	0.08	**-93.3**	0.3
1-1	27.08.2015	21.4	9.9	302	7.6	67	7.9	**-12.33**	0.04	**-91.7**	0.2
1-1	27.08.2015	31.3	7.5	316	9.3	78	7.9	**-12.16**	0.08	**-90.0**	0.4
1-1	27.08.2015	41.0	7.1	317	9.5	79	7.9	**-12.06**			
1-1	27.08.2015	184.1	5.7	325	6.9	55	7.9	**-11.95**			
2-6	28.08.2015	0.0						**-11.99**	0.02	**-88.8**	0.3
2-6	28.08.2015	9.6	19.9	270	10.0	111	8.6	**-12.26**	0.05	**-90.6**	0.5
2-6	28.08.2015	11.8	19.1	272	9.9	108	8.4	**-12.34**	0.05	**-91.1**	0.1
2-6	28.08.2015	13.8	17.8	275	9.4	99	8.2	**-12.39**	0.03	**-91.9**	0.2
2-6	28.08.2015	15.7	15.7	281	8.9	90	8.0	**-12.46**	0.10	**-92.8**	0.3
2-6	28.08.2015	17.5	14.4	285	7.9	77	7.9	**-12.59**	0.03	**-93.0**	0.1
2-6	28.08.2015	19.7	12.2	296	6.9	65	7.8	**-12.48**	0.07	**-93.1**	1.2
2-6	28.08.2015	20.7	11.6	301	6.7	62	7.8	**-12.47**	0.09	**-92.0**	0.2
2-6	28.08.2015	22.8	10.6	309	6.6	60	7.8	**-12.34**	0.04	**-90.9**	0.2
2-6	28.08.2015	24.8	10.1	313	6.6	58	7.8	**-12.25**	0.06	**-90.4**	0.2
2-6	28.08.2015	31.5	8.3	318	7.6	65	7.8	**-12.15**	0.05	**-89.5**	0.2
2-6	28.08.2015	91.0	6.4	316	10.0	81	8.0	**-12.11**	0.03	**-88.9**	0.2
2-5	28.08.2015	0.0						**-12.04**	0.02	**-88.9**	0.3
2-5	28.08.2015	8.4	20.7	267	10.3	115	8.6	**-12.11**	0.07	**-89.4**	0.2

Profile	Sampling date	Depth (m)	T (°C)	K25 (µS/cm)	O_2 (mg/L)	O_2 (% sat.)	pH	**$\delta^{18}O$ VSMOW**	std. dev.	**δD VSMOW**	std. dev.
2-5	28.08.2015	13.8	18.1	268	10.1	107	8.4	**-12.61**	0.05	**-92.7**	0.6
2-5	28.08.2015	14.8	16.8	274	10.1	104	8.3	**-12.55**	0.03	**-92.8**	0.3
2-5	28.08.2015	15.5	16.6	276	10.1	104	8.3	**-12.60**	0.05	**-92.5**	0.1
2-5	28.08.2015	16.1	16.3	275	10.1	103	8.2	**-12.60**	0.08	**-92.6**	0.2
2-5	28.08.2015	16.6	15.8	277	9.4	95	8.0	**-12.56**	0.08	**-92.2**	0.1
2-5	28.08.2015	18.5	13.8	284	7.7	75	7.9	**-12.60**	0.05	**-92.4**	0.3
2-5	28.08.2015	20.9	12.5	299	7.1	67	7.8	**-12.53**	0.02	**-92.0**	0.3
2-5	28.08.2015	24.2	11.1	311	6.5	59	7.8	**-12.33**	0.05	**-90.9**	0.2
2-5	28.08.2015	31.3	9.1	319	7.0	61	7.8	**-12.17**	0.05	**-89.4**	0.3
2-5	28.08.2015	204.0	5.7	324	7.2	57	7.9	**-11.96**	0.06	**-87.9**	0.3
2-4	28.08.2015	102.4	6.3	317	10.3	84	8.0	**-12.06**	0.05	**-89.4**	0.1
2-4	28.08.2015	41.1	7.7	320	8.2	69	7.9	**-12.08**	0.04	**-90.0**	0.2
2-4	28.08.2015	25.8	10.5	312	6.5	58	7.8	**-12.22**	0.07	**-91.0**	0.3
2-4	28.08.2015	20.6	11.9	298	6.8	63	7.9	**-12.31**	0.04	**-92.0**	0.3
2-4	28.08.2015	18.6	13.6	285	7.4	72	7.9	**-12.98**	0.04	**-94.4**	0.4
2-4	28.08.2015	17.6	14.7	276	8.8	87	8.0	**-13.13**	0.07	**-94.7**	0.4
2-4	28.08.2015	16.4	15.3	273	9.3	93	8.1	**-13.13**	0.01	**-94.4**	0.1
2-4	28.08.2015	14.4	16.9	275	11.0	114	8.4	**-13.21**	0.06	**-94.3**	0.3
2-4	28.08.2015	13.4	17.5	273	11.4	119	8.5	**-13.24**	0.05	**-94.4**	0.3
2-4	28.08.2015	12.4	18.8	270	11.2	121	8.5	**-12.98**	0.08	**-93.1**	0.2
2-4	28.08.2015	10.2	20.4	269	10.2	113	8.6	**-12.07**	0.09	**-90.1**	0.4
2-4	28.08.2015	0.0						**-11.96**	0.08	**-89.9**	0.1
2-3	28.08.2015	0.0						**-11.98**	0.07	**-89.5**	0.3
2-3	28.08.2015	3.2	21.3	267	10.3	116	8.6	**-11.98**	0.04	**-90.0**	0.3
2-3	28.08.2015	13.4	17.4	274	10.2	107	8.2	**-12.55**	0.03	**-93.1**	0.3
2-3	28.08.2015	15.7	16.6	275	9.1	94	8.0	**-12.55**	0.06	**-93.4**	0.3
2-3	28.08.2015	17.4	13.2	287	7.8	75	7.9	**-12.53**	0.07	**-93.5**	0.2
2-3	28.08.2015	19.5	12.2	296	7.3	69	7.8	**-12.40**	0.06	**-92.5**	0.3
2-3	28.08.2015	21.5	11.3	304	6.9	63	7.8	**-12.42**	0.04	**-91.9**	0.2
2-3	28.08.2015	23.8	10.2	313	6.4	57	7.8	**-12.29**	0.05	**-91.4**	0.1
2-3	28.08.2015	27.6	9.6	317	6.7	59	7.8	**-12.20**	0.03	**-90.8**	0.3
2-3	28.08.2015	50.3	6.7	319	9.8	81	7.9	**-12.01**	0.05	**-89.7**	0.4
2-3	28.08.2015	306.0	5.4	334	2.5	20	7.8	**-11.96**	0.06	**-88.8**	0.2
2-2	27.08.2015	0.0						**-12.12**	0.03	**-89.2**	0.2
2-2	27.08.2015	8.4	20.3	268	10.6	118	8.6	**-12.29**	0.05	**-90.0**	0.4
2-2	27.08.2015	10.6	19.4	269	10.9	119	8.6	**-12.41**	0.07	**-90.9**	0.3
2-2	27.08.2015	11.3	19.0	271	10.8	117	8.5	**-12.47**	0.04	**-91.1**	0.2
2-2	27.08.2015	12.8	16.9	274	9.9	102	8.2	**-12.67**	0.03	**-92.2**	0.4
2-2	27.08.2015	14.7	14.0	285	8.4	82	7.9	**-12.70**	0.07	**-92.4**	0.1
2-2	27.08.2015	17.6	12.5	291	7.3	69	7.8	**-12.67**	0.08	**-92.1**	0.4
2-2	27.08.2015	19.7	12.0	302	7.6	71	7.9	**-12.58**	0.09	**-91.3**	0.4
2-2	27.08.2015	25.5	9.6	317	6.8	59	7.8	**-12.25**	0.03	**-90.1**	0.3
2-2	27.08.2015	51.2	6.8	317	9.5	78	7.9	**-12.16**	0.09	**-88.6**	0.1
2-2	27.08.2015	309.7	5.4	335	2.4	19	7.7	**-12.10**	0.10	**-88.8**	2.0
2-1	27.08.2015	0.0						**-12.18**	0.03	**-90.1**	0.4
2-1	27.08.2015	2.9	21.3	267	10.4	117	8.7	**-12.11**	0.06	**-89.3**	0.2
2-1	27.08.2015	8.4	20.8	267	10.7	120	8.7	**-12.19**	0.05	**-89.5**	0.2
2-1	27.08.2015	9.8	20.4	269	10.5	117	8.6	**-12.17**	0.04	**-89.7**	0.4
2-1	27.08.2015	10.3	19.6	268	10.4	114	8.4	**-12.50**	0.04	**-91.4**	0.4
2-1	27.08.2015	12.4	15.9	280	9.8	99	8.1	**-12.54**	0.05	**-92.2**	0.3
2-1	27.08.2015	17.5	12.4	298	6.9	64	7.8	**-12.58**	0.03	**-92.1**	0.3
2-1	27.08.2015	20.7	10.9	307	6.9	62	7.8	**-12.50**	0.08	**-91.6**	0.4
2-1	27.08.2015	25.7	10.0	312	6.8	60	7.8	**-12.43**	0.05	**-90.5**	0.2
2-1	27.08.2015	51.3	7.2	319	8.7	72	7.9	**-12.19**	0.06	**-89.3**	0.4
2-1	27.08.2015	174.3	5.9	322	8.1	65	7.9	**-12.10**	0.05	**-88.9**	0.3
3-3	25.08.2015	0.0						**-12.14**	0.05	**-89.7**	0.1
3-3	25.08.2015	2.4	20.0	272	1.8	2	8.5	**-12.17**	0.04	**-89.9**	0.4
3-3	25.08.2015	3.9	19.7	273	1.8	2	8.5	**-12.30**	0.05	**-90.6**	0.3
3-3	25.08.2015	5.8	18.1	275	1.7	2	8.4	**-12.57**	0.03	**-92.1**	0.2
3-3	25.08.2015	6.8	16.8	280	1.6	2	8.3	**-12.57**	0.09	**-92.4**	0.5
3-3	25.08.2015	8.4	16.6	284	1.6	2	8.1	**-12.53**	0.02	**-92.3**	0.4
3-3	25.08.2015	10.6	15.2	285	1.5	2	8.0	**-12.74**	0.01	**-94.0**	0.4

Profile	Sampling date	Depth (m)	T (°C)	K25 (µS/cm)	O_2 (mg/L)	O_2 (% sat.)	pH	**$\delta^{18}O$ VSMOW**	std. dev.	**δD VSMOW**	std. dev.
3-3	25.08.2015	12.7	14.4	280	1.5	1	8.0	**-12.74**	0.06	**-93.0**	0.3
3-3	25.08.2015	15.6	13.4	284	51.6	496	8.0	**-12.63**	0.04	**-92.9**	0.1
3-3	25.08.2015	20.6	11.1	308	42.0	382	7.9	**-12.10**	0.07	**-90.2**	0.2
3-3	25.08.2015	41.2	7.1	320	53.9	446	8.0	**-12.21**	0.08	**-89.6**	0.1
3-3	25.08.2015	68.6	6.6	319	60.2	492	8.0	**-12.21**	0.05	**-89.4**	0.3
3-2	25.08.2015	0.0						**-11.98**	0.03	**-89.6**	0.2
3-2	25.08.2015	2.5	20.5	269	1.8	2	8.6	**-12.07**	0.03	**-89.0**	0.1
3-2	25.08.2015	5.5	20.4	269	1.8	2	8.5	**-12.06**	0.03	**-89.2**	0.4
3-2	25.08.2015	7.5	20.3	269	1.8	2	8.4	**-12.07**	0.08	**-89.0**	0.3
3-2	25.08.2015	9.5	19.9	268	1.8	2	8.1	**-12.14**	0.07	**-89.0**	0.3
3-2	25.08.2015	10.3	16.2	284	1.6	2	8.0	**-12.43**	0.08	**-91.4**	0.3
3-2	25.08.2015	11.1	16.0	283	1.6	2	7.9	**-12.50**	0.05	**-91.7**	0.4
3-2	25.08.2015	12.9	14.3	290	1.5	1	7.9	**-12.38**	0.03	**-91.4**	0.5
3-2	25.08.2015	20.9	11.0	310	1.2	1	7.9	**-12.26**	0.02	**-90.4**	0.2
3-2	25.08.2015	34.4	7.7	321	0.9	1	8.0	**-12.08**	0.07	**-89.3**	0.3
3-2	25.08.2015	73.4	6.5	318	0.8	1	8.0	**-12.04**	0.03	**-89.0**	0.2
3-1	25.08.2015	0.0						**-11.99**	0.05	**-89.5**	0.2
3-1	25.08.2015	2.5	20.6	269	1.8	2	8.6	**-12.11**	0.06	**-89.9**	0.4
3-1	25.08.2015	5.6	20.5	269	1.8	2	8.6	**-12.04**	0.03	**-89.5**	0.2
3-1	25.08.2015	9.8	20.3	270	1.8	2	8.4	**-12.09**	0.02	**-90.0**	0.2
3-1	25.08.2015	12.6	17.7	280	1.7	2	8.1	**-12.38**	0.04	**-91.9**	0.2
3-1	25.08.2015	14.5	16.0	284	1.6	2	7.9	**-12.48**	0.05	**-92.2**	0.4
3-1	25.08.2015	16.6	12.6	301	1.3	1	7.8	**-12.40**	0.05	**-91.9**	0.2
3-1	25.08.2015	21.0	9.4	317	1.1	1	7.9	**-12.29**	0.02	**-90.7**	0.5
3-1	25.08.2015	26.4	8.8	318	1.0	1	7.9	**-12.22**	0.03	**-90.3**	0.5
3-1	25.08.2015	40.4	7.3	319	0.9	1	7.9	**-12.04**	0.06	**-89.3**	0.3
3-1	25.08.2015	66.0	6.6	320	0.8	1	8.0	**-11.95**	0.01	**-89.1**	0.4
4-3	25.08.2015	0.0						**-12.12**	0.04	**-89.6**	0.3
4-3	25.08.2015	2.3	20.6	270	9.5	106	8.5	**-12.17**	0.05	**-89.8**	0.3
4-3	25.08.2015	4.9	19.0	274	9.2	100	8.2	**-12.22**	0.06	**-90.0**	0.4
4-3	25.08.2015	6.6	16.9	283	9.2	95	8.0	**-12.41**	0.03	**-91.8**	0.3
4-3	25.08.2015	8.8	15.3	289	7.9	79	8.0	**-12.52**	0.04	**-92.4**	0.2
4-3	25.08.2015	11.0	14.3	292	7.3	71	7.9	**-12.54**	0.08	**-92.2**	0.4
4-3	25.08.2015	12.2	13.9	295	7.1	69	7.9	**-12.51**	0.06	**-92.1**	0.2
4-3	25.08.2015	15.7	12.0	304	6.6	62	7.9	**-12.51**	0.05	**-91.7**	0.3
4-3	25.08.2015	21.0	10.5	313	6.1	55	7.9	**-12.41**	0.05	**-91.4**	0.4
4-3	25.08.2015	41.8	8.3	322	6.8	58	8.0	**-12.23**	0.04	**-90.2**	0.4
4-2	25.08.2015	0.0						**-12.16**	0.07	**-89.5**	0.2
4-2	25.08.2015	2.5	20.8	269	9.6	107	8.6	**-12.08**	0.02	**-89.7**	0.2
4-2	25.08.2015	5.1	20.7	268	9.4	105	8.5	**-12.11**	0.08	**-89.6**	0.3
4-2	25.08.2015	7.1	19.3	273	8.7	94	8.1	**-12.16**	0.06	**-90.1**	0.2
4-2	25.08.2015	8.5	15.2	289	7.4	74	7.9	**-12.50**	0.07	**-92.2**	0.3
4-2	25.08.2015	9.5	14.2	295	6.9	68	7.9	**-12.54**	0.05	**-92.0**	0.2
4-2	25.08.2015	10.4	12.6	304	6.8	64	7.9	**-12.44**	0.06	**-91.6**	0.4
4-2	25.08.2015	12.8	11.7	308	6.3	58	7.9	**-12.47**	0.07	**-91.5**	0.6
4-2	25.08.2015	15.8	10.8	313	6.2	56	7.9	**-12.32**	0.07	**-91.4**	0.5
4-2	25.08.2015	26.0	8.7	320	6.6	57	7.9	**-12.24**	0.04	**-90.2**	0.3
4-2	25.08.2015	41.2	7.2	320	7.8	65	8.0	**-12.18**	0.06	**-89.6**	0.4
4-2	25.08.2015	63.4	6.7	321	8.0	66	8.0	**-12.20**	0.04	**-89.5**	0.3
4-1	25.08.2015	0.0						**-12.10**	0.03	**-89.9**	0.3
4-1	25.08.2015	2.1	20.8	269	9.0	101	8.5	**-12.16**	0.09	**-89.8**	0.1
4-1	25.08.2015	4.2	19.8	273	9.2	101	8.4	**-12.29**	0.12	**-90.0**	0.2
4-1	25.08.2015	5.3	18.5	278	9.3	100	8.3	**-12.28**	0.07	**-90.1**	0.4
4-1	25.08.2015	6.5	15.3	290	8.0	80	8.0	**-12.56**	0.04	**-92.1**	0.1
4-1	25.08.2015	7.5	14.2	293	7.4	73	7.9	**-12.53**	0.05	**-91.8**	0.3
4-1	25.08.2015	10.7	13.2	300	7.1	68	7.9	**-12.58**	0.11	**-91.9**	0.4
4-1	25.08.2015	20.8	11.3	309	6.2	57	7.9	**-12.50**	0.04	**-91.5**	0.3
4-1	25.08.2015	30.9	8.6	320	6.5	56	8.0	**-12.32**	0.05	**-89.9**	0.3
4-1	25.08.2015	46.5	7.4	320	7.2	60	8.0	**-12.23**	0.05	**-89.5**	0.3
October 2015											
1-4	28.10.2015	0.0						**-12.23**		**-90.6**	
1-4	28.10.2015	2.8	13.4	284	10.7	102	8.4				

Profile	Sampling date	Depth (m)	T (°C)	K25 (µS/cm)	O_2 (mg/L)	O_2 (% sat.)	pH	**$\delta^{18}O$ VSMOW**	std. dev.	**δD VSMOW**	std. dev.
1-4	28.10.2015	10.6	13.4	285	10.5	101	8.4	**-12.19**	0.10	**-90.7**	0.4
1-4	28.10.2015	15.3	13.3	285	10.4	100	8.3	**-12.21**	0.06	**-90.6**	0.5
1-4	28.10.2015	18.6	13.3	286	9.7	93	8.2	**-12.29**	0.08	**-90.7**	0.2
1-4	28.10.2015	20.7	13.0	288	9.3	89	8.1	**-12.30**	0.07	**-91.3**	0.4
1-4	28.10.2015	22.7	12.7	291	8.6	81	8.0	**-12.43**	0.04	**-91.6**	0.3
1-4	28.10.2015	24.9	12.0	297	8.5	79	7.9	**-12.51**	0.04	**-91.9**	0.2
1-4	28.10.2015	26.8	11.5	296	8.3	76	7.9	**-12.52**	0.05	**-92.2**	0.3
1-4	28.10.2015	28.5	11.3	301	7.4	68	7.8	**-12.51**	0.04	**-92.2**	0.2
1-4	28.10.2015	30.8	10.6	306	6.9	62	7.7	**-12.44**	0.07	**-91.7**	0.2
1-4	28.10.2015	33.5	10.2	310	6.8	61	7.7	**-12.34**	0.09	**-91.3**	0.2
1-4	28.10.2015	35.7	9.7	311	6.8	60	7.7	**-12.39**	0.03	**-91.2**	0.4
1-4	28.10.2015	37.9	9.2	316	7.0	61	7.7	**-12.37**	0.13	**-90.6**	0.2
1-4	28.10.2015	39.9	8.8	318	7.3	63	7.7	**-12.37**	0.04	**-90.5**	0.2
1-4	28.10.2015	42.0	8.3	318	7.7	66	7.8	**-12.36**	0.10	**-90.4**	0.2
1-4	28.10.2015	44.0	8.1	319	8.0	68	7.8	**-12.25**	0.07	**-90.5**	0.4
1-4	28.10.2015	46.0	7.8	320	8.7	73	7.8	**-12.21**		**-89.9**	
1-4	28.10.2015	51.5	7.1	319	9.3	77	7.8	**-12.03**		**-89.6**	
1-4	28.10.2015	61.3	6.9	318	10.1	83	7.9	**-12.23**		**-90.0**	
1-4	28.10.2015	204.4	5.7	327	7.9	63	7.8	**-11.93**		**-89.0**	
1-3	28.10.2015	0.0						**-12.19**	0.10	**-91.1**	0.4
1-3	28.10.2015	2.3	13.4	286	10.5	101	8.3	**-12.22**	0.11	**-90.6**	0.4
1-3	28.10.2015	10.4	13.3	286	10.5	101	8.3	**-12.18**	0.10	**-90.7**	0.2
1-3	28.10.2015	24.0	13.2	287	10.0	96	8.2	**-12.28**	0.04	**-91.0**	0.1
1-3	28.10.2015	26.5	13.1	288	9.4	89	8.1	**-12.27**	0.07	**-91.0**	0.2
1-3	28.10.2015	28.0	12.7	291	9.1	86	8.0	**-12.29**	0.12	**-91.4**	0.2
1-3	28.10.2015	28.8	12.2	295	7.7	72	7.9	**-12.44**	0.07	**-92.1**	0.3
1-3	28.10.2015	29.9	11.2	303	8.1	74	7.9	**-12.47**	0.04	**-91.9**	0.1
1-3	28.10.2015	31.0	10.7	298	7.5	67	7.8	**-12.54**	0.07	**-92.4**	0.4
1-3	28.10.2015	31.9	10.5	306	6.2	55	7.7	**-12.40**	0.09	**-91.5**	0.3
1-3	28.10.2015	34.5	9.9	315	6.4	56	7.7	**-12.30**	0.03	**-90.9**	0.4
1-3	28.10.2015	36.9	9.2	316	7.0	61	7.7	**-12.22**	0.07	**-90.6**	0.3
1-3	28.10.2015	39.0	8.4	318	7.2	62	7.7	**-12.19**	0.06	**-90.4**	0.4
1-3	28.10.2015	40.7	8.2	319	7.6	65	7.8	**-12.23**	0.05	**-90.4**	0.2
1-3	28.10.2015	46.2	7.5	320	8.6	72	7.8	**-12.18**	0.09	**-90.0**	0.4
1-3	28.10.2015	51.5	7.2	320	9.1	75	7.8	**-12.21**	0.07	**-89.9**	0.4
1-3	28.10.2015	61.6	6.9	318	9.9	81	7.9	**-12.09**	0.07	**-89.6**	0.4
1-3	28.10.2015	193.6	5.7	326	7.9	63	7.9	**-11.98**	0.13	**-89.1**	0.2
1-2	28.10.2015	0.0						**-12.24**	0.09	**-90.5**	0.4
1-2	28.10.2015	1.7	13.5	285	10.5	101	8.4	**-12.22**	0.07	**-90.7**	0.1
1-2	28.10.2015	10.1	13.4	285	10.4	100	8.3	**-12.24**	0.05	**-90.7**	0.3
1-2	28.10.2015	22.1	13.1	289	9.2	88	8.1	**-12.22**	0.03	**-90.8**	0.2
1-2	28.10.2015	24.2	12.7	291	9.2	87	8.0	**-12.23**	0.08	**-91.2**	0.3
1-2	28.10.2015	26.5	12.3	290	8.6	80	8.0	**-12.39**	0.07	**-91.4**	0.4
1-2	28.10.2015	28.6	11.5	298	7.8	72	7.9	**-12.38**	0.07	**-91.9**	0.4
1-2	28.10.2015	29.8	11.2	303	6.5	59	7.8	**-12.41**	0.05	**-91.9**	0.3
1-2	28.10.2015	30.8	10.5	312	6.5	58	7.8	**-12.33**	0.06	**-91.0**	0.1
1-2	28.10.2015	32.0	10.3	313	6.3	56	7.7	**-12.24**	0.06	**-90.8**	0.1
1-2	28.10.2015	33.1	10.0	315	6.4	57	7.7	**-12.32**	0.08	**-90.9**	0.2
1-2	28.10.2015	34.3	10.0	315	6.5	57	7.7	**-12.27**	0.08	**-91.1**	0.4
1-2	28.10.2015	36.8	9.6	314	6.4	57	7.7	**-12.30**	0.04	**-90.8**	0.2
1-2	28.10.2015	38.9	9.1	318	6.7	58	7.7	**-12.22**	0.06	**-90.7**	0.2
1-2	28.10.2015	41.0	8.8	319	6.7	58	7.7	**-12.18**	0.07	**-90.1**	0.2
1-2	28.10.2015	45.7	7.6	319	8.4	70	7.8	**-12.11**	0.05	**-89.8**	0.4
1-2	28.10.2015	51.3	7.2	319	9.0	74	7.8	**-12.09**	0.05	**-89.8**	0.3
1-2	28.10.2015	177.9	5.8	324	8.7	69	7.9	**-12.02**	0.09	**-88.8**	0.3
1-2	28.10.2015	194.2	5.7	324	8.0	64	7.9	**-12.01**	0.05	**-89.1**	0.2
1-1	28.10.2015	0.0						**-12.18**	0.07	**-90.7**	0.1
1-1	28.10.2015	2.1	13.5	285	10.5	101	8.4	**-12.22**	0.06	**-90.7**	0.3
1-1	28.10.2015	10.3	13.4	285	10.4	100	8.3	**-12.23**	0.09	**-90.5**	0.3
1-1	28.10.2015	20.5	13.1	288	9.6	92	8.2	**-12.32**	0.03	**-90.8**	0.4
1-1	28.10.2015	23.8	12.8	289	9.6	91	8.1	**-12.45**	0.06	**-92.0**	0.2
1-1	28.10.2015	26.8	12.3	287	8.6	80	8.0	**-12.48**	0.03	**-92.7**	0.4

Profile	Sampling date	Depth (m)	T (°C)	K25 (µS/cm)	O_2 (mg/L)	O_2 (% sat.)	pH	**$\delta^{18}O$ VSMOW**	std. dev.	**δD VSMOW**	std. dev.
1-1	28.10.2015	29.0	11.4	296	9.0	82	7.9	**-12.53**	0.03	**-92.7**	0.4
1-1	28.10.2015	31.3	10.8	293	8.8	80	7.9	**-12.57**	0.03	**-93.0**	0.5
1-1	28.10.2015	33.0	10.4	295	7.0	63	7.8	**-12.57**	0.05	**-92.7**	0.2
1-1	28.10.2015	35.0	9.4	315	6.5	57	7.7	**-12.38**	0.08	**-91.3**	0.2
1-1	28.10.2015	36.9	9.2	318	6.5	57	7.7	**-12.31**	0.05	**-90.7**	0.1
1-1	28.10.2015	39.0	8.5	319	7.2	61	7.7	**-12.13**	0.09	**-90.2**	0.2
1-1	28.10.2015	40.8	8.0	319	7.7	65	7.8	**-12.15**	0.08	**-89.6**	0.2
1-1	28.10.2015	46.1	7.5	319	8.5	71	7.8	**-12.12**	0.09	**-90.2**	0.4
1-1	28.10.2015	51.5	7.1	319	9.2	76	7.8	**-12.18**	0.05	**-89.9**	0.3
1-1	28.10.2015	61.8	6.8	319	9.9	81	7.9	**-12.17**	0.03	**-89.9**	0.3
1-1	28.10.2015	183.8	5.8	324	8.4	67	7.9	**-12.05**	0.10	**-89.0**	0.4
2-6	29.10.2015	0.0						**-12.31**	0.05	**-90.9**	0.3
2-6	29.10.2015	2.4	13.2	287	10.3	98	8.2	**-12.20**	0.05	**-90.7**	0.3
2-6	29.10.2015	10.0	13.0	288	9.5	91	8.1	**-12.20**	0.06	**-90.9**	0.4
2-6	29.10.2015	15.5	12.6	292	8.9	84	8.0	**-12.38**	0.04	**-91.2**	0.4
2-6	29.10.2015	18.7	12.5	295	8.5	80	7.9	**-12.27**	0.04	**-91.1**	0.3
2-6	29.10.2015	21.6	11.9	302	-0.1	-1	7.9	**-12.37**	0.08	**-91.6**	0.4
2-6	29.10.2015	23.6	11.6	300	-0.1	-1	7.9	**-12.32**	0.04	**-91.6**	0.2
2-6	29.10.2015	25.2	11.3	300	-0.1	-1	7.9	**-12.28**	0.03	**-91.5**	0.3
2-6	29.10.2015	26.7	10.8	302	-0.1	-1	7.8	**-12.31**	0.08	**-91.1**	0.3
2-6	29.10.2015	30.9	10.1	305	-0.1	-1	7.8	**-12.24**	0.07	**-91.0**	0.4
2-6	29.10.2015	33.3	9.4	308	0.0	0	7.8	**-12.22**	0.09	**-91.1**	0.1
2-6	29.10.2015	35.8	8.9	311	-0.1	-1	7.8	**-12.22**	0.06	**-90.6**	0.3
2-6	29.10.2015	41.2	7.5	321	-0.2	-1	7.9	**-12.04**	0.04	**-89.7**	0.1
2-6	29.10.2015	51.5	7.1	325	-0.2	-1	7.8	**-12.06**	0.06	**-89.7**	0.2
2-6	29.10.2015	92.9	6.5	330	-0.2	-1	7.7	**-12.08**	0.08	**-89.7**	0.3
2-5	29.10.2015	0.0						**-12.17**	0.07	**-90.6**	0.2
2-5	29.10.2015	2.3	13.3	286	10.3	99	8.3	**-12.10**	0.10	**-90.5**	0.3
2-5	29.10.2015	10.1	13.2	286	10.1	97	8.3	**-12.15**	0.06	**-90.7**	0.2
2-5	29.10.2015	15.5	13.1	287	9.9	95	8.3	**-12.25**	0.08	**-90.8**	0.2
2-5	29.10.2015	19.4	13.0	288	8.6	82	8.1	**-12.20**	0.10	**-91.1**	0.3
2-5	29.10.2015	20.4	12.6	294	8.4	79	8.0	**-12.25**	0.02	**-91.0**	0.3
2-5	29.10.2015	21.5	12.2	300	8.1	75	7.9	**-12.31**	0.05	**-91.4**	0.1
2-5	29.10.2015	22.8	11.9	298	7.1	66	7.8	**-12.33**	0.06	**-91.6**	0.5
2-5	29.10.2015	24.7	11.1	305	6.3	57	7.7	**-12.32**	0.06	**-91.2**	0.5
2-5	29.10.2015	27.0	10.5	310	6.1	54	7.7	**-12.36**	0.04	**-91.2**	0.3
2-5	29.10.2015	29.0	9.9	314	6.1	54	7.7	**-12.28**	0.09	**-90.9**	0.2
2-5	29.10.2015	30.9	9.3	315	6.6	58	7.7	**-12.21**	0.05	**-90.7**	0.3
2-5	29.10.2015	35.8	8.5	317	7.2	61	7.7	**-12.11**	0.06	**-90.4**	0.5
2-5	29.10.2015	40.8	7.9	320	7.6	65	7.7	**-12.01**	0.04	**-89.8**	0.2
2-5	29.10.2015	51.4	7.2	319	8.9	74	7.8	**-12.16**	0.03	**-89.8**	0.2
2-5	29.10.2015	102.5	6.3	319	10.8	87	7.9	**-12.06**	0.05	**-89.4**	0.4
2-4	29.10.2015	0.0						**-12.19**	0.01	**-90.4**	0.2
2-4	29.10.2015	1.6	13.3	286	10.1	97	8.3	**-12.26**	0.09	**-90.7**	0.4
2-4	29.10.2015	10.6	13.1	286	9.9	94	8.3	**-12.22**	0.09	**-91.0**	0.4
2-4	29.10.2015	18.4	13.0	288	9.5	91	8.2	**-12.25**	0.04	**-90.8**	0.3
2-4	29.10.2015	19.7	12.8	291	9.0	85	8.1	**-12.30**	0.06	**-91.4**	0.3
2-4	29.10.2015	20.7	12.3	294	8.1	75	7.9	**-12.33**	0.05	**-91.4**	0.3
2-4	29.10.2015	21.6	11.9	299	6.9	64	7.9	**-12.25**	0.07	**-91.5**	0.5
2-4	29.10.2015	22.4	10.9	308	6.2	56	7.7	**-12.44**	0.05	**-91.7**	0.1
2-4	29.10.2015	23.4	10.4	312	6.0	54	7.7	**-12.28**	0.10	**-91.2**	0.1
2-4	29.10.2015	24.6	10.1	314	6.0	53	7.7	**-12.36**	0.10	**-90.8**	0.2
2-4	29.10.2015	26.1	9.9	314	6.1	54	7.7	**-12.26**	0.08	**-90.6**	0.3
2-4	29.10.2015	28.4	9.3	318	6.2	54	7.7	**-12.32**	0.03	**-90.5**	0.4
2-4	29.10.2015	30.8	8.9	319	6.4	55	7.7	**-12.29**	0.08	**-90.4**	0.4
2-4	29.10.2015	32.9	8.6	319	6.7	58	7.7	**-12.36**	0.06	**-90.5**	0.2
2-4	29.10.2015	36.2	8.3	319	6.9	59	7.7	**-12.29**	0.10	**-90.7**	0.2
2-4	29.10.2015	41.0	7.6	319	8.2	69	7.8	**-12.14**	0.05	**-90.0**	0.2
2-4	29.10.2015	51.7	7.0	320	9.2	76	7.8	**-12.02**	0.05	**-89.6**	0.2
2-4	29.10.2015	105.0	6.3	317	10.5	86	7.9	**-12.07**	0.04	**-89.7**	0.1
2-3	29.10.2015	0.0						**-12.32**	0.05	**-90.6**	0.5
2-3	29.10.2015	1.5	13.2	286	10.1	97	8.3	**-12.23**	0.03	**-90.7**	0.1

Profile	Sampling date	Depth (m)	T (°C)	K25 (µS/cm)	O_2 (mg/L)	O_2 (% sat.)	pH	**$\delta^{18}O$ VSMOW**	std. dev.	**δD VSMOW**	std. dev.
2-3	29.10.2015	12.4	13.1	287	9.8	93	8.2	**-12.18**	0.06	**-90.8**	0.3
2-3	29.10.2015	16.3	12.8	290	9.4	89	8.1	**-12.23**	0.08	**-91.3**	0.5
2-3	29.10.2015	19.8	12.3	293	8.6	80	8.0	**-12.38**	0.03	**-91.5**	0.3
2-3	29.10.2015	21.1	11.8	298	7.7	71	7.9	**-12.35**	0.05	**-91.6**	0.1
2-3	29.10.2015	22.8	10.5	310	6.6	59	7.8	**-12.36**	0.05	**-91.5**	0.2
2-3	29.10.2015	24.1	10.9	308	6.2	56	7.7	**-12.40**	0.08	**-91.5**	0.2
2-3	29.10.2015	24.8	10.6	310	6.0	54	7.7	**-12.39**	0.08	**-91.2**	0.1
2-3	29.10.2015	25.7	10.1	313	6.0	54	7.7	**-12.30**	0.07	**-90.9**	0.1
2-3	29.10.2015	27.0	9.6	316	6.2	55	7.7	**-12.34**	0.02	**-90.6**	0.2
2-3	29.10.2015	28.8	9.0	318	6.6	57	7.7	**-12.30**	0.09	**-90.7**	0.3
2-3	29.10.2015	31.0	8.5	318	7.0	60	7.7	**-12.19**	0.03	**-90.1**	0.3
2-3	29.10.2015	36.0	7.8	319	7.8	66	7.7	**-12.24**	0.05	**-89.8**	0.4
2-3	29.10.2015	41.0	7.4	320	8.5	71	7.7	**-12.15**	0.05	**-89.6**	0.2
2-3	29.10.2015	51.6	7.0	318	9.4	77	7.8	**-12.14**	0.06	**-89.5**	0.2
2-3	29.10.2015	101.9	6.3	318	10.7	87	7.9	**-12.08**	0.03	**-89.5**	0.4
2-3	29.10.2015	306.1	5.4	335	2.3	18	7.6	**-12.04**	0.07	**-88.7**	0.3
2-2	29.10.2015	0.0						**-12.27**	0.05	**-90.6**	0.4
2-2	29.10.2015	2.4	13.2	286	10.2	97	8.3	**-12.27**	0.09	**-90.6**	0.3
2-2	29.10.2015	10.6	13.2	286	10.2	98	8.3	**-12.25**	0.08	**-91.0**	0.2
2-2	29.10.2015	15.0	13.1	287	10.3	98	8.3	**-12.25**	0.06	**-90.7**	0.3
2-2	29.10.2015	17.2	12.8	289	9.9	94	8.2	**-12.35**	0.06	**-90.6**	0.3
2-2	29.10.2015	19.7	12.2	294	8.0	75	7.9	**-12.52**	0.03	**-92.0**	0.2
2-2	29.10.2015	20.6	11.9	295	7.0	65	7.8	**-12.52**	0.05	**-92.0**	0.1
2-2	29.10.2015	23.0	10.9	307	6.2	56	7.7	**-12.43**	0.05	**-91.1**	0.4
2-2	29.10.2015	25.0	10.4	311	6.1	54	7.7	**-12.44**	0.07	**-90.9**	0.2
2-2	29.10.2015	26.9	9.8	315	6.1	54	7.7	**-12.33**	0.03	**-90.3**	0.3
2-2	29.10.2015	28.6	9.3	317	6.5	56	7.7	**-12.37**	0.07	**-90.1**	0.3
2-2	29.10.2015	30.9	8.8	318	6.8	59	7.7	**-12.31**	0.05	**-90.2**	0.2
2-2	29.10.2015	35.8	8.1	319	7.5	63	7.7	**-12.30**	0.03	**-89.9**	0.5
2-2	29.10.2015	41.0	7.6	320	8.0	67	7.7	**-12.21**	0.07	**-89.8**	0.4
2-2	29.10.2015	51.5	7.1	319	8.8	73	7.8	**-12.21**	0.05	**-89.7**	0.5
2-2	29.10.2015	102.2	6.3	318	10.5	85	7.9	**-12.20**	0.03	**-89.2**	0.5
2-2	29.10.2015	306.3	5.4	335	3.3	26	7.7	**-12.12**	0.08	**-88.8**	0.2
2-1	28.10.2015	0.0						**-12.16**	0.06	**-90.9**	0.3
2-1	28.10.2015	2.3	13.3	286	10.3	99	8.3	**-12.21**	0.03	**-91.0**	0.4
2-1	28.10.2015	10.1	13.2	288	9.9	94	8.2	**-12.22**	0.07	**-90.9**	0.3
2-1	28.10.2015	17.4	13.0	288	9.6	91	8.2	**-12.35**	0.04	**-91.1**	0.3
2-1	28.10.2015	19.3	12.5	293	8.4	79	8.0	**-12.27**	0.06	**-91.1**	0.3
2-1	28.10.2015	21.3	11.5	301	6.4	59	7.8	**-12.33**	0.10	**-91.4**	0.3
2-1	28.10.2015	22.4	11.6	301	7.5	70	7.8	**-12.37**	0.10	**-91.1**	0.3
2-1	28.10.2015	23.3	11.1	307	7.7	70	7.8	**-12.40**	0.07	**-91.3**	0.3
2-1	28.10.2015	24.3	10.0	313	6.4	57	7.7	**-12.28**	0.08	**-90.6**	0.1
2-1	28.10.2015	26.6	9.3	315	6.5	56	7.7	**-12.34**	0.06	**-90.7**	0.3
2-1	28.10.2015	30.5	8.5	319	7.0	60	7.7	**-12.24**	0.08	**-90.2**	0.4
2-1	28.10.2015	32.9	8.1	319	7.3	62	7.7	**-12.17**	0.06	**-90.0**	0.2
2-1	28.10.2015	35.9	7.9	319	7.7	65	7.8	**-12.18**	0.09	**-90.1**	0.4
2-1	28.10.2015	41.1	7.4	320	8.4	70	7.8	**-12.28**	0.07	**-90.0**	0.3
2-1	28.10.2015	51.2	6.9	319	9.4	77	7.8	**-12.21**	0.05	**-90.2**	0.3
2-1	28.10.2015	173.5	5.9	323	9.0	72	7.9	**-12.04**	0.05	**-89.3**	0.3
3-3	26.10.2015	0.0		0				**-12.34**	0.03	**-91.0**	0.3
3-3	26.10.2015	20.6	13.4	285	9.9	95	8.2	**-12.32**	0.04	**-90.6**	0.1
3-3	26.10.2015	25.6	13.2	287	9.5	91	8.1	**-12.32**	0.03	**-90.8**	0.2
3-3	26.10.2015	27.9	12.5	293	7.8	74	7.9	**-12.36**	0.01	**-91.1**	0.2
3-3	26.10.2015	28.9	11.7	302	7.2	67	7.8	**-12.36**	0.01	**-91.1**	0.1
3-3	26.10.2015	30.5	10.1	313	6.7	59	7.7	**-12.36**	0.01	**-91.2**	0.2
3-3	26.10.2015	31.4	9.5	316	6.7	59	7.7	**-12.31**	0.04	**-91.0**	0.2
3-3	26.10.2015	32.8	9.2	317	6.8	59	7.7	**-12.31**	0.02	**-90.7**	0.1
3-3	26.10.2015	35.9	8.4	319	7.3	62	7.7	**-12.29**	0.03	**-90.6**	0.3
3-3	26.10.2015	46.5	7.5	319	8.6	72	7.8	**-12.24**	0.04	**-90.0**	0.2
3-3	26.10.2015	71.4	6.7	320	10.4	85	7.8	**-12.24**	0.02	**-89.9**	0.1
3-2	26.10.2015	0.0						**-12.32**	0.01	**-90.6**	0.1
3-2	26.10.2015	10.8	13.3	285	10.1	97	8.3	**-12.30**	0.02	**-90.7**	0.2

Profile	Sampling date	Depth (m)	T (°C)	K25 (µS/cm)	O_2 (mg/L)	O_2 (% sat.)	pH	**$\delta^{18}O$ VSMOW**	std. dev.	**δD VSMOW**	std. dev.
3-2	26.10.2015	24.4	13.3	287	9.9	95	8.2	**-12.33**	0.03	**-90.8**	0.1
3-2	26.10.2015	26.6	13.2	288	8.7	83	8.0	**-12.36**	0.03	**-90.9**	0.1
3-2	26.10.2015	27.7	12.5	297	7.5	71	7.9	**-12.34**	0.03	**-90.8**	0.1
3-2	26.10.2015	29.2	11.6	304	6.6	61	7.8	**-12.39**	0.03	**-91.0**	0.2
3-2	26.10.2015	30.7	10.1	314	6.1	54	7.7	**-12.40**	0.03	**-91.1**	0.1
3-2	26.10.2015	32.1	9.5	316	6.3	56	7.7	**-12.39**	0.01	**-90.8**	0.1
3-2	26.10.2015	34.0	8.9	319	6.7	58	7.7	**-12.33**	0.02	**-90.4**	0.1
3-2	26.10.2015	36.1	8.5	320	7.3	62	7.7	**-12.29**	0.04	**-90.2**	0.1
3-2	26.10.2015	41.3	7.6	320	8.2	69	7.8	**-12.26**	0.02	**-90.0**	0.1
3-2	26.10.2015	73.6	6.6	319	11.1	91	7.9	**-12.20**	0.02	**-89.6**	0.1
3-1	26.10.2015	0.0						**-12.28**	0.04	**-90.6**	0.1
3-1	26.10.2015	10.0						**-12.33**	0.02	**-90.9**	0.0
3-1	26.10.2015	23.0						**-12.38**	0.01	**-91.0**	0.0
3-1	26.10.2015	25.5						**-12.40**	0.01	**-91.2**	0.1
3-1	26.10.2015	26.5						**-12.41**	0.02	**-91.1**	0.1
3-1	26.10.2015	27.5						**-12.42**	0.01	**-91.0**	0.1
3-1	26.10.2015	30.0						**-12.38**	0.01	**-90.8**	0.1
3-1	26.10.2015	32.0						**-12.28**	0.02	**-90.3**	0.1
3-1	26.10.2015	33.0						**-12.26**	0.04	**-90.0**	0.1
3-1	26.10.2015	35.0						**-12.23**	0.01	**-90.0**	0.1
3-1	26.10.2015	40.0						**-12.25**	0.01	**-90.2**	0.0
3-1	26.10.2015	64.0						**-12.24**	0.02	**-89.7**	0.0
4-3	26.10.2015	0.0						**-12.41**	0.07	**-90.2**	0.5
4-3	26.10.2015	10.7	13.8	282	10.0	97	8.3	**-12.22**	0.02	**-90.0**	0.2
4-3	26.10.2015	20.8	13.7	283	9.7	94	8.2	**-12.19**	0.04	**-90.2**	0.2
4-3	26.10.2015	22.6	13.4	285	8.5	82	8.1	**-12.25**	0.11	**-89.9**	0.2
4-3	26.10.2015	23.7	11.4	302	6.7	61	7.8	**-12.28**	0.09	**-90.4**	0.1
4-3	26.10.2015	24.2	10.7	308	6.1	55	7.8	**-12.31**	0.04	**-90.4**	0.3
4-3	26.10.2015	24.7	10.0	313	6.4	57	7.8	**-12.33**	0.11	**-90.5**	0.3
4-3	26.10.2015	25.3	9.4	317	6.4	56	7.7	**-12.34**	0.08	**-90.4**	0.4
4-3	26.10.2015	26.3	9.0	318	6.5	57	7.7	**-12.31**	0.02	**-89.9**	0.3
4-3	26.10.2015	28.1	8.6	320	6.8	59	7.8	**-12.29**	0.04	**-90.1**	0.2
4-3	26.10.2015	30.9	8.1	321	7.3	62	7.8	**-12.27**	0.10	**-89.9**	0.3
4-3	26.10.2015	41.0	7.8	320	7.9	66	7.8	**-12.36**	0.05	**-90.1**	0.3
4-2	26.10.2015	0.0						**-12.15**	0.03	**-90.4**	0.3
4-2	26.10.2015	10.3	13.8	283	10.1	97	8.3	**-12.04**	0.07	**-90.0**	0.3
4-2	26.10.2015	22.6	13.8	283	9.9	96	8.3	**-12.04**	0.06	**-90.0**	0.4
4-2	26.10.2015	25.2	12.7	293	6.6	62	7.8	**-12.11**	0.08	**-90.0**	0.4
4-2	26.10.2015	26.1	9.9	314	6.3	56	7.7	**-12.14**	0.04	**-90.4**	0.2
4-2	26.10.2015	26.9	9.8	314	6.3	55	7.7	**-12.18**	0.08	**-90.4**	0.5
4-2	26.10.2015	27.9	9.3	317	6.4	56	7.7	**-12.16**	0.09	**-90.1**	0.2
4-2	26.10.2015	28.7	9.1	317	6.5	56	7.7	**-12.13**	0.06	**-90.0**	0.2
4-2	26.10.2015	31.1	8.7	319	6.8	59	7.7	**-12.21**	0.08	**-89.9**	0.3
4-2	26.10.2015	35.9	7.9	320	7.5	63	7.8	**-12.13**	0.06	**-89.9**	0.1
4-2	26.10.2015	63.5	6.9	321	9.0	74	7.8	**-12.09**	0.03	**-89.7**	0.3
4-1	26.10.2015	0.0						**-12.25**	0.02	**-90.3**	0.1
4-1	26.10.2015	10.2	13.8	282	9.8	95	8.3	**-12.21**	0.01	**-90.4**	0.1
4-1	26.10.2015	21.4	13.7	283	9.0	87	8.2	**-12.22**	0.04	**-90.4**	0.1
4-1	26.10.2015	24.6	11.9	299	7.3	67	7.8	**-12.24**	0.03	**-90.6**	0.2
4-1	26.10.2015	25.6	10.6	311	6.4	58	7.8	**-12.29**	0.03	**-90.8**	0.1
4-1	26.10.2015	26.6	9.5	315	6.4	56	7.7	**-12.33**	0.03	**-90.7**	0.2
4-1	26.10.2015	27.7	8.9	317	6.5	56	7.7	**-12.34**	0.02	**-90.6**	0.1
4-1	26.10.2015	28.7	8.8	318	6.5	56	7.7	**-12.33**	0.02	**-90.4**	0.2
4-1	26.10.2015	29.8	8.6	319	6.7	58	7.8	**-12.31**	0.02	**-90.4**	0.1
4-1	26.10.2015	30.8	8.4	319	6.9	59	7.8	**-12.30**	0.03	**-90.2**	0.1
4-1	26.10.2015	32.8	8.1	319	7.4	63	7.8	**-12.28**	0.03	**-90.1**	0.1
4-1	26.10.2015	46.0	7.2	321	8.5	71	7.8	**-12.24**	0.02	**-89.8**	0.1
July 2016											
0	05.07.2016	0.0						**-11.98**	0.02	**-88.5**	0.1
0	05.07.2016	6.4	20.1	292	9.2	102	8.7	**-12.28**	0.05	**-91.0**	0.2
0	05.07.2016	7.5	16.6	293	9.9	102	8.7	**-12.41**	0.05	**-91.6**	0.2
0	05.07.2016	8.2	15.9	319	9.4	96	8.5	**-12.40**	0.01	**-91.3**	0.1

Profile	Sampling date	Depth (m)	T (°C)	K25 (µS/cm)	O_2 (mg/L)	O_2 (% sat.)	pH	**$\delta^{18}O$ VSMOW**	std. dev.	**δD VSMOW**	std. dev.
0	05.07.2016	8.6	16.7	289	9.2	95	8.6	**-12.78**	0.03	**-94.2**	0.0
0	05.07.2016	8.7	15.8	320	9.2	94	8.4	**-12.40**	0.02	**-91.2**	0.2
0	05.07.2016	9.4	16.0	279	9.0	91	8.5	**-12.98**	0.02	**-95.6**	0.2
0	05.07.2016	10.3	14.0	275	8.5	83	8.3	**-12.91**	0.08	**-95.2**	0.4
0	05.07.2016	10.4	14.2	293	9.0	88	8.4	**-12.88**	0.04	**-94.7**	0.0
0	05.07.2016	11.5	12.3	285	8.8	82	8.2	**-12.84**	0.04	**-94.5**	0.1
0	05.07.2016	13.5	11.9	289	8.7	81	8.2	**-12.81**	0.02	**-94.3**	0.1
0	05.07.2016	15.6	11.3	297	8.4	77	8.1	**-12.67**	0.03	**-93.4**	0.0
0	05.07.2016	17.5	10.4	305	8.4	75	8.1	**-12.47**	0.07	**-92.0**	0.1
0	05.07.2016	20.7	9.8	308	8.2	73	8.0	**-12.41**	0.02	**-91.4**	0.1
0	05.07.2016	26.0	8.9	314	8.4	72	8.0	**-12.36**	0.01	**-91.3**	0.1
0	05.07.2016	38.5	7.5	315	8.8	74	8.0	**-12.24**	0.02	**-90.1**	0.1
0	05.07.2016	97.1	7.0	316	9.8	81	8.0	**-12.26**	0.02	**-90.8**	0.3
1-4	05.07.2016	0.0						**-11.93**	0.03	**-88.2**	0.1
1-4	05.07.2016	2.2	20.9	293	9.1	103	8.7	**-11.98**	0.02	**-88.7**	0.3
1-4	05.07.2016	3.8	20.3	286	9.7	108	8.8	**-12.16**	0.03	**-89.9**	0.1
1-4	05.07.2016	5.2	18.7	284	9.5	102	8.7	**-12.56**	0.05	**-92.6**	0.2
1-4	05.07.2016	6.2	16.8	282	9.7	100	8.6	**-12.70**	0.02	**-93.5**	0.2
1-4	05.07.2016	6.9	16.9	280	9.2	95	8.6	**-12.69**	0.02	**-93.5**	0.1
1-4	05.07.2016	8.2	16.2	281	9.4	96	8.6	**-12.69**	0.03	**-93.6**	0.2
1-4	05.07.2016	9.8	15.5	282	8.8	89	8.5	**-12.76**	0.03	**-94.1**	0.2
1-4	05.07.2016	11.4	13.5	285	9.0	86	8.4	**-12.82**	0.03	**-94.5**	0.1
1-4	05.07.2016	13.5	12.9	286	8.9	85	8.3	**-12.80**	0.01	**-94.4**	0.2
1-4	05.07.2016	15.8	12.1	300	9.1	84	8.4	**-12.70**	0.02	**-93.2**	0.1
1-4	05.07.2016	20.3	11.0	307	8.1	74	8.2	**-12.15**	0.06	**-89.5**	0.2
1-4	05.07.2016	25.6	8.7	312	8.3	72	8.0	**-12.31**	0.02	**-91.0**	0.1
1-4	05.07.2016	39.8	7.4	316	8.8	73	8.0	**-12.20**	0.02	**-90.1**	0.1
1-4	05.07.2016	102.3	6.6	319	8.3	68	8.0	**-12.15**	0.03	**-89.8**	0.1
1-4	05.07.2016	205.8	5.7	328	5.6	45	7.9	**-12.00**	0.03	**-88.8**	0.2
1-3	05.07.2016	0.0						**-11.96**	0.01	**-88.5**	0.1
1-3	05.07.2016	3.9	19.0	288	9.5	103	8.8	**-12.34**	0.02	**-91.1**	0.1
1-3	05.07.2016	6.5	17.9	278	9.3	98	8.7	**-12.57**	0.01	**-92.6**	0.0
1-3	05.07.2016	8.6	16.1	287	9.4	96	8.6	**-12.58**	0.02	**-92.9**	0.2
1-3	05.07.2016	10.3	15.1	281	8.8	88	8.5	**-12.77**	0.02	**-94.1**	0.1
1-3	05.07.2016	12.5	13.8	284	8.9	86	8.4	**-12.82**	0.02	**-94.3**	0.1
1-3	05.07.2016	14.4	13.4	285	8.9	85	8.4	**-12.83**	0.01	**-94.1**	0.2
1-3	05.07.2016	16.6	13.1	283	8.5	81	8.3	**-12.74**	0.02	**-94.1**	0.1
1-3	05.07.2016	20.9	11.5	292	8.3	77	8.2	**-12.70**	0.02	**-93.7**	0.1
1-3	05.07.2016	25.5	9.9	309	8.0	71	8.0	**-12.29**	0.04	**-90.8**	0.1
1-3	05.07.2016	41.1	7.3	315	8.7	72	8.0	**-12.19**	0.03	**-90.0**	0.1
1-3	05.07.2016	194.3	5.7	328	5.7	45	7.9	**-12.05**	0.05	**-88.9**	0.3
1-2	05.07.2016	0.0						**-11.93**	0.02	**-88.2**	0.3
1-2	05.07.2016	2.4	21.2	292	8.9	101	8.7	**-12.04**	0.02	**-88.9**	0.1
1-2	05.07.2016	6.2	19.3	288	9.4	103	8.8	**-12.32**	0.01	**-90.7**	0.2
1-2	05.07.2016	7.2	18.2	284	9.2	98	8.7	**-12.52**	0.02	**-92.2**	0.1
1-2	05.07.2016	7.4	18.9	284	9.2	100	8.7	**-12.53**	0.02	**-92.2**	0.2
1-2	05.07.2016	9.4	17.3	282	9.7	101	8.7	**-12.64**	0.01	**-92.6**	0.0
1-2	05.07.2016	10.6	16.9	278	9.1	94	8.6	**-12.82**	0.03	**-94.0**	0.0
1-2	05.07.2016	12.1	15.3	275	9.1	91	8.5	**-12.91**	0.02	**-94.5**	0.1
1-2	05.07.2016	12.8	14.0	283	9.0	87	8.4	**-12.82**	0.02	**-94.1**	0.1
1-2	05.07.2016	14.7	13.1	285	8.4	80	8.3	**-12.75**	0.03	**-93.6**	0.1
1-2	05.07.2016	16.2	11.4	293	8.4	77	8.2	**-12.70**	0.02	**-93.2**	0.2
1-2	05.07.2016	20.9	8.9	312	8.2	71	8.0	**-12.31**	0.02	**-90.4**	0.1
1-2	05.07.2016	25.6	8.3	313	8.4	71	8.0	**-12.30**	0.01	**-90.4**	0.1
1-2	05.07.2016	41.4	7.5	314	8.7	73	8.0	**-12.27**	0.01	**-90.2**	0.2
1-2	05.07.2016	194.1	5.7	327	5.6	45	7.9	**-12.09**	0.02	**-88.7**	0.3
1-1	05.07.2016	0.0						**-11.96**	0.01	**-88.3**	0.1
1-1	05.07.2016	3.3	21.6	292	8.9	101	8.7	**-12.02**	0.02	**-88.7**	0.1
1-1	05.07.2016	5.5	20.7	290	9.1	102	8.7	**-12.13**	0.02	**-89.8**	0.1
1-1	05.07.2016	7.4	20.3	283	8.5	95	8.7	**-12.32**	0.06	**-90.8**	0.5
1-1	05.07.2016	7.6	20.0	289	8.7	96	8.7	**-12.16**	0.06	**-89.9**	0.4
1-1	05.07.2016	8.3	19.7	286	8.6	94	8.7	**-12.59**	0.03	**-92.5**	0.1

Profile	Sampling date	Depth (m)	T (°C)	K25 (µS/cm)	O_2 (mg/L)	O_2 (% sat.)	pH	**$\delta^{18}O$ VSMOW**	std. dev.	**δD VSMOW**	std. dev.
1-1	05.07.2016	9.4	16.8	283	8.9	92	8.6	**-12.62**	0.01	**-93.1**	0.2
1-1	05.07.2016	10.5	13.0	287	8.5	81	8.3	**-12.71**	0.04	**-93.6**	0.1
1-1	05.07.2016	12.4	11.8	294	8.7	80	8.2	**-12.61**	0.10	**-93.1**	0.6
1-1	05.07.2016	14.5	11.3	306	8.4	77	8.2	**-12.45**	0.01	**-91.9**	0.2
1-1	05.07.2016	16.5	10.7	313	8.2	74	8.1	**-12.27**	0.03	**-90.3**	0.1
1-1	05.07.2016	20.7	9.7	314	8.0	71	8.0	**-12.17**	0.08	**-90.0**	0.5
1-1	05.07.2016	25.8	9.1	313	7.9	68	8.0	**-12.21**	0.08	**-90.1**	0.4
1-1	05.07.2016	40.9	7.5	313	8.7	73	8.0	**-12.15**	0.10	**-90.1**	0.8
1-1	05.07.2016	183.7	5.7	328	5.7	45	7.9	**-12.12**	0.03	**-89.1**	0.1
2-6	06.07.2016	0.0						**-11.98**	0.03	**-88.2**	0.2
2-6	06.07.2016	3.3	20.9	293	9.4	105	8.8	**-12.01**	0.03	**-88.8**	0.1
2-6	06.07.2016	5.7	20.1	297	10.2	113	8.8	**-12.08**	0.03	**-88.9**	0.1
2-6	06.07.2016	6.6	18.3	289	11.0	117	8.9	**-12.33**	0.01	**-90.8**	0.3
2-6	06.07.2016	8.1	17.4	286	10.8	113	8.8	**-12.50**	0.02	**-92.1**	0.0
2-6	06.07.2016	8.7	16.8	290	10.9	113	8.8	**-12.47**	0.02	**-91.8**	0.2
2-6	06.07.2016	10.6	15.9	292	10.4	105	8.8	**-12.53**	0.01	**-92.5**	0.2
2-6	06.07.2016	12.4	15.1	291	9.8	98	8.7	**-12.57**	0.00	**-92.7**	0.0
2-6	06.07.2016	14.5	14.1	291	9.3	91	8.6	**-12.66**	0.03	**-93.3**	0.0
2-6	06.07.2016	18.4	10.7	304	8.2	74	8.1	**-12.60**	0.01	**-92.7**	0.1
2-6	06.07.2016	20.9	9.6	310	8.0	70	8.0	**-12.42**	0.01	**-91.4**	0.1
2-6	06.07.2016	24.5	8.7	316	7.9	68	7.9	**-12.26**	0.01	**-90.5**	0.1
2-6	06.07.2016	41.3	7.4	316	8.5	71	8.0	**-12.19**	0.02	**-90.0**	0.2
2-6	06.07.2016	87.0	6.8	317	9.1	75	8.0	**-12.18**	0.02	**-89.9**	0.1
2-5	06.07.2016	0.0						**-12.01**	0.03	**-88.7**	0.1
2-5	06.07.2016	3.1	20.9	293	9.2	104	8.7	**-12.02**	0.05	**-89.0**	0.1
2-5	06.07.2016	5.2	20.8	292	9.7	109	8.8	**-12.31**	0.02	**-90.6**	0.1
2-5	06.07.2016	7.2	17.3	293	11.1	116	8.8	**-12.39**	0.01	**-91.0**	0.2
2-5	06.07.2016	8.1	16.2	295	10.9	112	8.8	**-12.39**	0.03	**-91.2**	0.1
2-5	06.07.2016	8.3	16.8	292	11.0	113	8.8	**-12.39**	0.02	**-91.2**	0.1
2-5	06.07.2016	9.4	16.2	292	10.6	108	8.8	**-12.44**	0.02	**-91.7**	0.1
2-5	06.07.2016	10.3	15.1	293	9.9	99	8.7	**-12.53**	0.02	**-92.4**	0.1
2-5	06.07.2016	12.2	14.3	293	9.9	97	8.7	**-12.56**	0.02	**-92.6**	0.1
2-5	06.07.2016	14.4	13.6	292	9.3	90	8.5	**-12.65**	0.01	**-93.2**	0.1
2-5	06.07.2016	16.4	12.7	295	8.9	84	8.4	**-12.73**	0.03	**-93.7**	0.2
2-5	06.07.2016	18.3	12.2	295	8.7	81	8.2	**-12.74**	0.04	**-93.8**	0.1
2-5	06.07.2016	20.6	11.8	295	8.6	79	8.2	**-12.74**	0.00	**-93.6**	0.1
2-5	06.07.2016	25.8	8.9	316	7.9	68	7.9	**-12.25**	0.01	**-90.2**	0.1
2-5	06.07.2016	40.8	7.3	315	8.6	72	8.0	**-12.24**	0.02	**-90.0**	0.1
2-5	06.07.2016	204.4	5.8	325	6.3	51	7.9	**-12.11**	0.02	**-89.4**	0.0
2-4	06.07.2016	0.0						**-12.11**	0.02	**-88.8**	0.1
2-4	06.07.2016	2.4	21.0	295	9.0	102	8.7	**-12.05**	0.02	**-88.9**	0.1
2-4	06.07.2016	4.4	20.8	297	9.4	105	8.8	**-12.15**	0.02	**-89.2**	0.1
2-4	06.07.2016	5.4	20.4	290	9.9	110	8.8	**-12.18**	0.03	**-89.6**	0.2
2-4	06.07.2016	6.6	19.0	290	10.8	117	8.8	**-12.27**	0.06	**-90.5**	0.4
2-4	06.07.2016	6.8	18.6	288	10.8	116	8.8	**-12.35**	0.02	**-90.6**	0.1
2-4	06.07.2016	7.6	18.2	289	10.9	116	8.8	**-12.30**	0.05	**-90.6**	0.2
2-4	06.07.2016	8.9	16.5	293	11.3	116	8.8	**-12.34**	0.03	**-90.8**	0.2
2-4	06.07.2016	9.9	15.8	294	11.0	111	8.8	**-12.35**	0.02	**-91.0**	0.1
2-4	06.07.2016	11.3	14.2	299	10.7	104	8.8	**-12.46**	0.01	**-91.5**	0.0
2-4	06.07.2016	13.3	13.1	302	11.0	104	8.8	**-12.47**	0.01	**-91.6**	0.2
2-4	06.07.2016	15.8	12.1	296	8.6	81	8.3	**-12.46**	0.02	**-92.0**	0.1
2-4	06.07.2016	20.9	10.9	304	8.2	74	8.1	**-12.64**	0.01	**-92.6**	0.2
2-4	06.07.2016	25.6	9.2	315	7.8	68	8.0	**-12.16**	0.01	**-90.0**	0.1
2-4	06.07.2016	204.1	5.7	326	5.8	47	7.9	**-12.08**	0.02	**-89.0**	0.1
2-3	04.07.2016	0.0						**-11.90**	0.04	**-87.9**	0.2
2-3	04.07.2016	3.1	21.5	296	8.9	102	8.7	**-11.92**	0.01	**-88.1**	0.2
2-3	04.07.2016	5.3	21.1	296	9.4	106	8.7	**-11.93**	0.02	**-88.1**	0.2
2-3	04.07.2016	6.8	20.3	296	10.1	112	8.8	**-11.99**	0.03	**-88.6**	0.2
2-3	04.07.2016	7.4	19.8	293	10.2	112	8.8	**-12.01**	0.02	**-88.7**	0.1
2-3	04.07.2016	8.5	18.8	292	10.2	110	8.8	**-12.30**	0.03	**-90.6**	0.3
2-3	04.07.2016	10.5	15.6	289	9.7	98	8.8	**-12.45**	0.05	**-91.7**	0.2
2-3	04.07.2016	12.5	13.3	294	8.9	86	8.5	**-12.59**	0.02	**-92.5**	0.1

Profile	Sampling date	Depth (m)	T (°C)	K25 (µS/cm)	O_2 (mg/L)	O_2 (% sat.)	pH	**$\delta^{18}O$ VSMOW**	std. dev.	**δD VSMOW**	std. dev.
2-3	04.07.2016	14.7	12.1	298	8.8	82	8.4	**-12.68**	0.01	**-93.0**	0.1
2-3	04.07.2016	16.9	11.6	300	8.4	77	8.2	**-12.62**	0.01	**-92.8**	0.2
2-3	04.07.2016	20.7	9.7	309	8.0	70	8.0	**-12.50**	0.02	**-92.1**	0.3
2-3	04.07.2016	25.8	8.8	313	8.0	69	7.9	**-12.28**	0.06	**-90.3**	0.3
2-3	04.07.2016	40.9	7.2	315	8.9	74	8.0	**-12.23**	0.03	**-90.0**	0.2
2-3	04.07.2016	102.1	6.7	317	8.9	73	8.0	**-12.18**	0.05	**-89.7**	0.1
2-3	04.07.2016	306.2	5.5	334	3.0	24	7.7	**-12.06**	0.03	**-88.9**	0.1
2-2	04.07.2016	0.0						**-11.90**	0.01	**-88.0**	0.1
2-2	04.07.2016	3.2	21.3	296	8.8	100	8.7	**-11.94**	0.02	**-88.0**	0.1
2-2	04.07.2016	5.3	20.3	295	9.8	109	8.7	**-12.00**	0.03	**-88.4**	0.1
2-2	04.07.2016	6.4	17.8	296	11.3	119	8.8	**-12.07**	0.04	**-89.1**	0.1
2-2	04.07.2016	7.4	17.2	297	11.0	115	8.8	**-12.05**	0.02	**-89.0**	0.1
2-2	04.07.2016	8.4	16.6	297	10.6	109	8.8	**-12.29**	0.05	**-90.7**	0.1
2-2	04.07.2016	10.5	14.7	297	9.9	98	8.8	**-12.44**	0.03	**-91.7**	0.1
2-2	04.07.2016	12.4	14.1	287	8.6	84	8.6	**-12.49**	0.03	**-92.3**	0.2
2-2	04.07.2016	14.6	11.7	295	8.6	80	8.3	**-12.71**	0.02	**-93.5**	0.0
2-2	04.07.2016	16.7	11.5	298	8.3	76	8.2	**-12.48**	0.03	**-91.8**	0.2
2-2	04.07.2016	20.8	9.4	313	7.5	66	8.0	**-12.31**	0.02	**-90.9**	0.2
2-2	04.07.2016	26.2	8.3	317	7.7	66	8.0	**-12.19**	0.02	**-90.1**	0.1
2-2	04.07.2016	41.3	7.3	315	8.4	70	8.0	**-12.17**	0.04	**-90.0**	0.1
2-2	04.07.2016	102.2	6.5	318	8.1	66	8.0	**-12.15**	0.01	**-89.8**	0.2
2-2	04.07.2016	204.3	5.7	326	6.1	49	7.9	**-12.06**	0.03	**-88.9**	0.1
2-1	04.07.2016	0.0						**-11.88**	0.03	**-87.8**	0.1
2-1	04.07.2016	3.0	21.2	294	8.3	94	8.7	**-11.92**	0.01	**-88.2**	0.2
2-1	04.07.2016	5.2	20.9	294	8.8	99	8.7	**-11.93**	0.01	**-88.3**	0.2
2-1	04.07.2016	6.4	16.1	291	8.8	90	8.8	**-12.43**	0.03	**-91.5**	0.1
2-1	04.07.2016	7.7	15.5	291	8.9	90	8.8	**-12.53**	0.05	**-92.4**	0.2
2-1	04.07.2016	9.0	14.7	298	8.9	87	8.8	**-12.37**	0.03	**-91.5**	0.2
2-1	04.07.2016	11.3	13.4	304	8.9	85	8.8	**-12.22**	0.03	**-90.3**	0.1
2-1	04.07.2016	13.5	12.8	303	8.4	79	8.8	**-12.33**	0.02	**-91.2**	0.1
2-1	04.07.2016	15.6	11.2	306	7.1	65	8.3	**-12.41**	0.03	**-91.6**	0.2
2-1	04.07.2016	25.5	8.6	314	6.2	53	8.0	**-12.20**	0.01	**-90.0**	0.1
2-1	04.07.2016	41.3	7.4	315	6.7	56	8.0	**-12.19**	0.03	**-90.0**	0.3
2-1	04.07.2016	92.3	6.6	318	6.6	54	8.0	**-12.12**	0.00	**-89.8**	0.1
2-1	04.07.2016	183.5	5.8	324	4.5	36	7.9	**-12.04**	0.01	**-89.0**	0.3
3-3	08.07.2016	0.0						**-11.92**	0.04	**-87.9**	0.2
3-3	08.07.2016	3.0	22.4	296	8.6	100	8.7	**-11.91**	0.02	**-87.9**	0.2
3-3	08.07.2016	5.3	22.0	296	8.9	102	8.7	**-11.92**	0.03	**-87.7**	0.2
3-3	08.07.2016	7.4	21.3	295	10.2	115	8.8	**-11.98**	0.03	**-88.1**	0.2
3-3	08.07.2016	8.3	20.8	295	9.7	109	8.8	**-12.00**	0.01	**-88.4**	0.1
3-3	08.07.2016	8.9	18.9	295	11.8	127	8.8	**-12.01**	0.07	**-88.7**	0.2
3-3	08.07.2016	9.6	17.3	296	11.8	123	8.8	**-12.09**	0.03	**-89.0**	0.1
3-3	08.07.2016	11.2	16.3	298	11.3	116	8.8	**-12.07**	0.06	**-88.9**	0.1
3-3	08.07.2016	12.3	15.5	301	11.3	113	8.8	**-12.09**	0.05	**-89.1**	0.3
3-3	08.07.2016	13.6	14.1	298	10.6	103	8.7	**-12.40**	0.02	**-91.5**	0.2
3-3	08.07.2016	16.1	13.0	303	10.2	98	8.7	**-12.47**	0.06	**-91.6**	0.0
3-3	08.07.2016	21.1	11.5	311	8.6	79	8.2	**-12.30**	0.07	**-90.4**	0.2
3-3	08.07.2016	24.0	10.4	311	8.0	71	8.0	**-12.39**	0.05	**-91.1**	0.1
3-3	08.07.2016	30.7	8.8	317	7.6	66	7.9	**-12.16**	0.03	**-89.7**	0.0
3-3	08.07.2016	41.1	7.6	317	7.8	66	7.9	**-12.09**	0.04	**-89.5**	0.2
3-3	08.07.2016	73.6	6.9	316	8.6	71	8.0	**-12.21**	0.02	**-89.9**	0.1
3-2	08.07.2016	0.0						**-11.84**	0.04	**-87.4**	0.3
3-2	08.07.2016	3.3	22.1	295	8.7	101	8.7	**-11.86**	0.05	**-87.7**	0.0
3-2	08.07.2016	7.4	21.3	294	9.7	110	8.8	**-11.89**	0.04	**-88.0**	0.3
3-2	08.07.2016	8.3	20.5	292	10.6	118	8.8	**-11.94**	0.04	**-88.2**	0.2
3-2	08.07.2016	9.3	19.1	292	11.2	122	8.8	**-12.08**	0.03	**-88.9**	0.3
3-2	08.07.2016	10.3	18.1	291	11.6	123	8.8	**-12.09**	0.02	**-89.2**	0.1
3-2	08.07.2016	11.1	16.5	296	11.6	119	8.8	**-12.02**	0.04	**-88.6**	0.2
3-2	08.07.2016	12.7	14.8	301	10.7	106	8.8	**-12.21**	0.01	**-89.8**	0.2
3-2	08.07.2016	14.5	13.6	304	10.0	97	8.7	**-12.21**	0.02	**-90.0**	0.1
3-2	08.07.2016	17.3	12.1	310	9.2	86	8.5	**-12.20**	0.01	**-89.9**	0.1
3-2	08.07.2016	20.4	11.0	309	8.4	76	8.1	**-12.27**	0.01	**-90.5**	0.1

Profile	Sampling date	Depth (m)	T (°C)	K25 (µS/cm)	O_2 (mg/L)	O_2 (% sat.)	pH	**$\delta^{18}O$ VSMOW**	std. dev.	**δD VSMOW**	std. dev.
3-2	08.07.2016	25.6	10.0	314	7.9	70	8.0	**-12.21**	0.01	**-90.0**	0.1
3-2	08.07.2016	30.9	9.0	316	7.7	67	7.9	**-12.18**	0.01	**-89.7**	0.2
3-2	08.07.2016	41.0	7.4	316	8.1	68	7.9	**-12.21**	0.02	**-89.8**	0.1
3-2	08.07.2016	76.6	6.8	314	8.8	72	8.0	**-12.19**	0.02	**-89.8**	0.1
3-1	08.07.2016	0.0						**-11.92**	0.04	**-87.8**	0.2
3-1	08.07.2016	3.1	22.0	296	8.7	100	8.7	**-11.96**	0.01	**-88.2**	0.1
3-1	08.07.2016	6.4	21.5	295	9.0	102	8.8	**-12.01**	0.03	**-88.5**	0.2
3-1	08.07.2016	7.3	20.2	294	10.6	117	8.8	**-12.05**	0.02	**-88.9**	0.1
3-1	08.07.2016	8.2	18.2	298	11.2	119	8.8	**-12.17**	0.03	**-89.4**	0.0
3-1	08.07.2016	9.3	16.5	297	11.3	116	8.8	**-12.10**	0.05	**-89.0**	0.1
3-1	08.07.2016	10.6	15.3	301	11.3	113	8.8	**-12.16**	0.01	**-89.3**	0.0
3-1	08.07.2016	12.4	14.3	302	10.5	103	8.8	**-12.27**	0.04	**-90.3**	0.3
3-1	08.07.2016	14.5	13.0	307	10.1	96	8.6	**-12.22**	0.03	**-89.8**	0.3
3-1	08.07.2016	17.5	12.3	307	9.5	89	8.5	**-12.29**	0.02	**-90.4**	0.2
3-1	08.07.2016	20.7	11.7	304	8.4	78	8.2	**-12.51**	0.01	**-92.0**	0.0
3-1	08.07.2016	22.8	10.5	312	8.0	72	8.0	**-12.38**	0.06	**-90.8**	0.2
3-1	08.07.2016	25.8	9.8	315	7.7	68	8.0	**-12.20**	0.02	**-89.8**	0.2
3-1	08.07.2016	30.9	9.0	317	7.7	66	7.9	**-12.17**	0.03	**-89.5**	0.2
3-1	08.07.2016	40.9	7.4	316	8.3	69	8.0	**-12.21**	0.01	**-89.9**	0.2
3-1	08.07.2016	66.5	6.7	318	8.2	67	7.9	**-12.19**	0.02	**-89.8**	0.1
4-3	08.07.2016	0.0						**-11.86**	0.04	**-87.5**	0.0
4-3	08.07.2016	3.1	21.7	294	9.1	104	8.7	**-11.90**	0.02	**-87.4**	0.2
4-3	08.07.2016	6.7	21.0	293	10.0	112	8.8	**-11.93**	0.03	**-87.8**	0.2
4-3	08.07.2016	7.7	18.9	297	11.3	122	8.8	**-12.05**	0.02	**-88.7**	0.1
4-3	08.07.2016	8.4	16.9	297	11.1	115	8.8	**-12.15**	0.03	**-88.9**	0.1
4-3	08.07.2016	8.6	18.0	296	11.5	122	8.8	**-12.06**	0.01	**-88.5**	0.1
4-3	08.07.2016	8.6	17.8	294	11.3	119	8.8	**-12.11**	0.02	**-88.7**	0.1
4-3	08.07.2016	9.7	16.5	297	11.1	114	8.8	**-12.12**	0.01	**-89.1**	0.1
4-3	08.07.2016	11.6	15.2	304	10.8	108	8.8	**-12.15**	0.04	**-89.1**	0.1
4-3	08.07.2016	13.4	14.5	304	10.3	102	8.8	**-12.15**	0.01	**-89.3**	0.2
4-3	08.07.2016	14.6	13.7	308	9.4	91	8.5	**-12.16**	0.01	**-89.2**	0.3
4-3	08.07.2016	18.5	12.5	311	8.8	83	8.3	**-12.18**	0.03	**-89.4**	0.2
4-3	08.07.2016	20.8	11.7	313	8.5	79	8.2	**-12.17**	0.01	**-89.4**	0.2
4-3	08.07.2016	23.1	11.0	313	7.9	72	8.1	**-12.18**	0.02	**-89.5**	0.3
4-3	08.07.2016	26.2	9.6	315	7.7	68	7.9	**-12.23**	0.02	**-89.9**	0.0
4-3	08.07.2016	31.4	8.1	315	7.7	65	7.9	**-12.18**	0.04	**-89.8**	0.1
4-3	08.07.2016	46.1	7.1	318	8.0	67	7.9	**-12.21**	0.02	**-89.8**	0.1
4-2	08.07.2016	0.0						**-11.78**	0.07	**-87.7**	0.3
4-2	08.07.2016	3.2	21.8	295	9.3	107	8.7	**-11.88**	0.05	**-87.8**	0.2
4-2	08.07.2016	5.4	21.0	295	9.7	109	8.8	**-11.75**	0.05	**-87.9**	0.2
4-2	08.07.2016	6.5	20.6	295	10.0	112	8.8	**-11.87**	0.07	**-88.1**	0.2
4-2	08.07.2016	7.5	20.3	294	10.6	118	8.8	**-11.92**	0.09	**-88.1**	0.2
4-2	08.07.2016	8.5	19.4	295	11.2	123	8.8	**-11.93**	0.06	**-88.1**	0.4
4-2	08.07.2016	9.5	18.8	296	11.2	120	8.8	**-11.90**	0.04	**-88.6**	0.2
4-2	08.07.2016	9.5	18.0	297	11.5	122	8.8	**-11.93**	0.09	**-88.6**	0.2
4-2	08.07.2016	10.5	17.6	298	11.1	117	8.8	**-11.97**	0.09	**-88.4**	0.3
4-2	08.07.2016	11.5	16.5	300	11.2	115	8.8	**-11.92**	0.06	**-88.5**	0.1
4-2	08.07.2016	12.5	15.7	303	10.5	106	8.8	**-12.05**	0.03	**-89.0**	0.2
4-2	08.07.2016	13.6	14.6	307	10.3	101	8.7	**-11.97**	0.03	**-88.8**	0.4
4-2	08.07.2016	15.7	13.3	308	9.8	94	8.6	**-12.06**	0.06	**-88.9**	0.3
4-2	08.07.2016	17.7	12.7	310	9.3	88	8.5	**-12.08**	0.08	**-89.0**	0.4
4-2	08.07.2016	21.2	11.3	313	8.3	76	8.1	**-12.10**	0.07	**-88.8**	0.3
4-2	08.07.2016	25.8	10.4	315	8.0	72	8.0	**-12.06**	0.03	**-89.0**	0.2
4-2	08.07.2016	31.6	9.3	316	7.9	69	8.0	**-12.09**	0.07	**-88.9**	0.2
4-2	08.07.2016	68.5	6.9	319	7.8	64	7.9	**-12.08**	0.05	**-89.0**	0.3
4-1	08.07.2016	0.0						**-11.91**	0.09	**-88.0**	0.2
4-1	08.07.2016	5.3	21.0	296	9.9	111	8.8	**-11.90**	0.06	**-88.2**	0.4
4-1	08.07.2016	10.5	19.9	295	10.7	118	8.8	**-11.97**	0.08	**-88.6**	0.2
4-1	08.07.2016	12.2	18.4	292	10.6	113	8.8	**-12.06**	0.08	**-89.0**	0.3
4-1	08.07.2016	13.4	15.3	303	11.0	110	8.8	**-12.04**	0.07	**-89.1**	0.3
4-1	08.07.2016	14.5	14.9	305	10.2	101	8.8	**-12.12**	0.06	**-89.3**	0.2
4-1	08.07.2016	16.5	14.1	307	9.5	93	8.6	**-12.07**	0.05	**-89.2**	0.2

4-1	08.07.2016	18.6	12.8	309	9.0	85	8.4	**-12.13**	0.02	**-89.5**	0.3
4-1	08.07.2016	20.6	11.9	311	8.3	77	8.2	**-12.12**	0.07	**-89.8**	0.2
4-1	08.07.2016	25.8	9.9	314	7.7	68	8.0	**-12.17**	0.09	**-89.6**	0.3
4-1	08.07.2016	30.8	8.7	317	7.4	64	7.9	**-12.12**	0.08	**-89.8**	0.3
4-1	08.07.2016	50.4	7.4	318	7.6	63	7.9	**-12.15**	0.07	**-90.0**	0.2

Appendix II

(Chapter II)

Appendix II-1: Positions according to the Swiss coordinate system (CH1903/LV03) and sampling dates of the profiles.

Profile	0	1	2	3	4
X (m)	554725	552000	534700	515000	506100
Y (m)	139048	140000	144950	140000	128040
August 2015	-	27th 12 am	28th 10 am	25th 11 am	25th 3 pm
October 2015	-	28th 12 am	29th 11 am	26th 12 am	26th 3 pm
December 2015	16th 11 am	16th 3 pm	17th 11 am	15th 3 pm	-
July 2016	5th 10 am	5th 12 am	4th 5 pm	8th 3 pm	8th 11 am
February 2017	22nd 10 am	23rd 11 am	-	-	-
May 2017	2nd 10 am 4th 5 pm	3rd 10 am 5th 10 am	2nd 3 pm	2nd 11 am	-

Appendix II-2: Sampling locations in the Haut-Lac of the May 2017 campaign (in yellow = Transect 1, in green = Transect 2, in blue = Transect 3). Locations T1-4 and T3-2 correspond to Profile 1 and T2-3 to Profile 0.

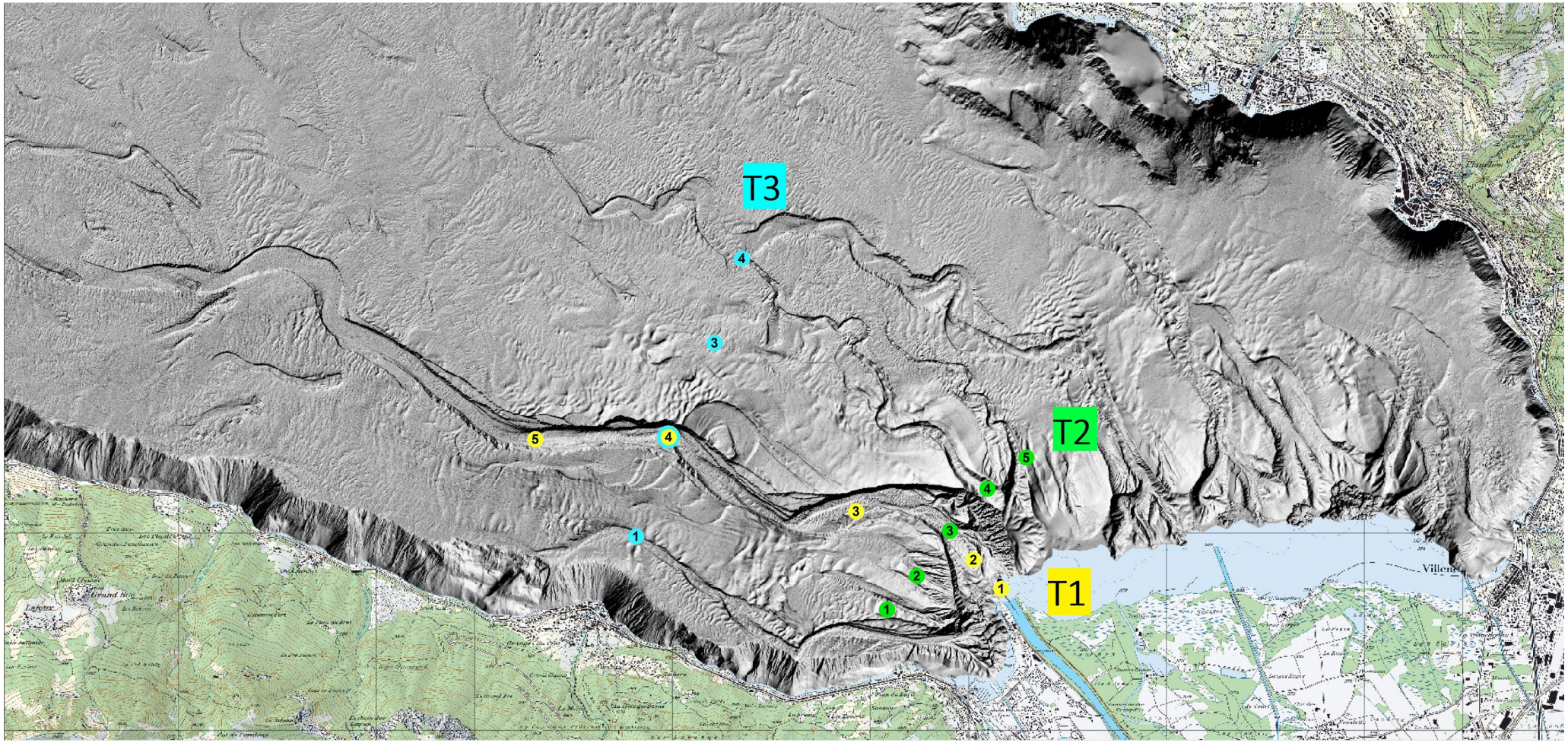

Appendix II-3: CTD profiles of temperature (red), turbidity (brown), conductivity (green) and dissolved oxygen (light blue) with the oxygen isotope composition of water (dark blue) obtained during the campaigns of May 2017.

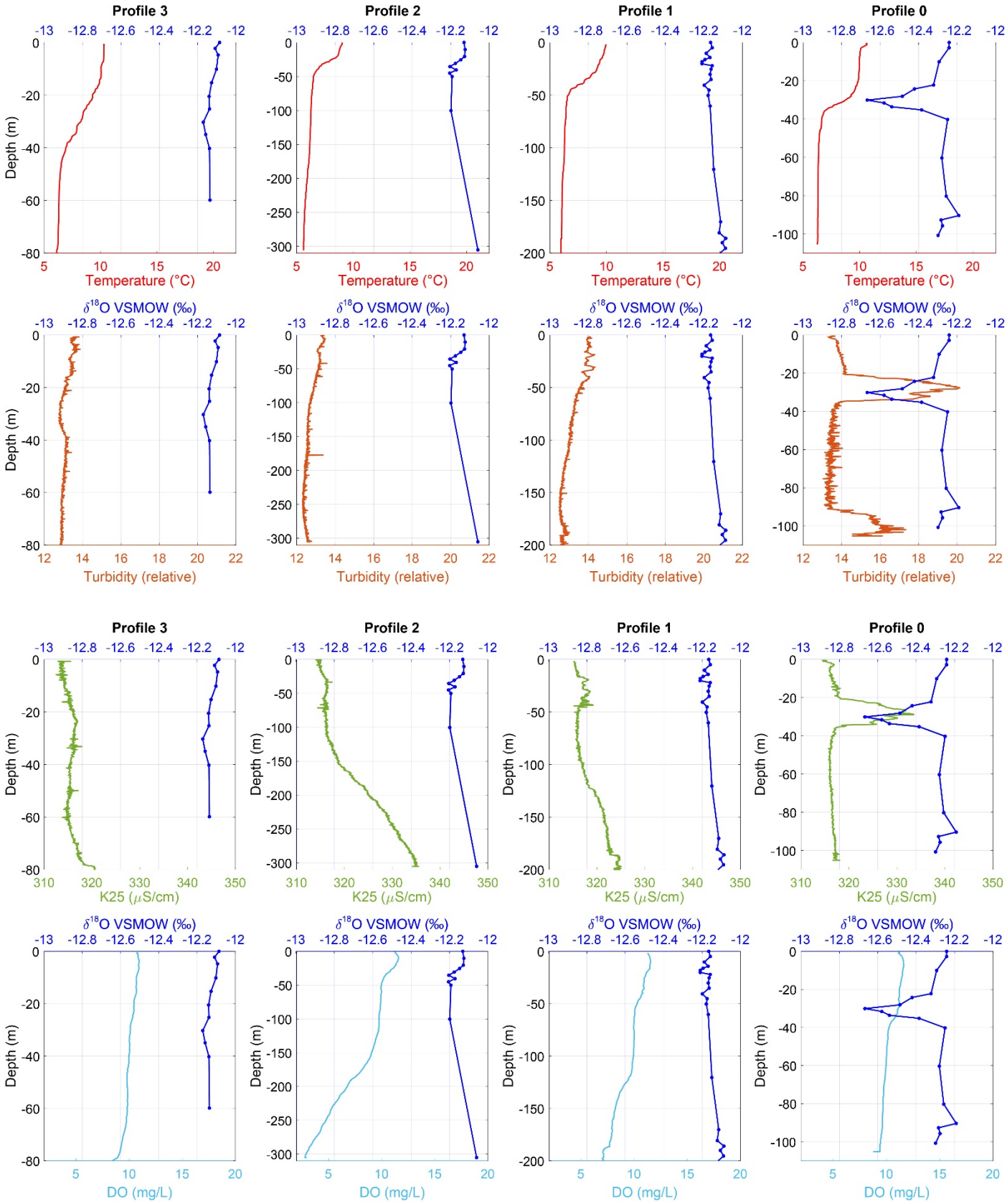

Appendix II-4: CTD profiles of Transect 1 of temperature (red), turbidity (brown), conductivity (green) and dissolved oxygen (light blue) with the oxygen isotope composition of water (dark blue) obtained during the campaigns of May 2017.

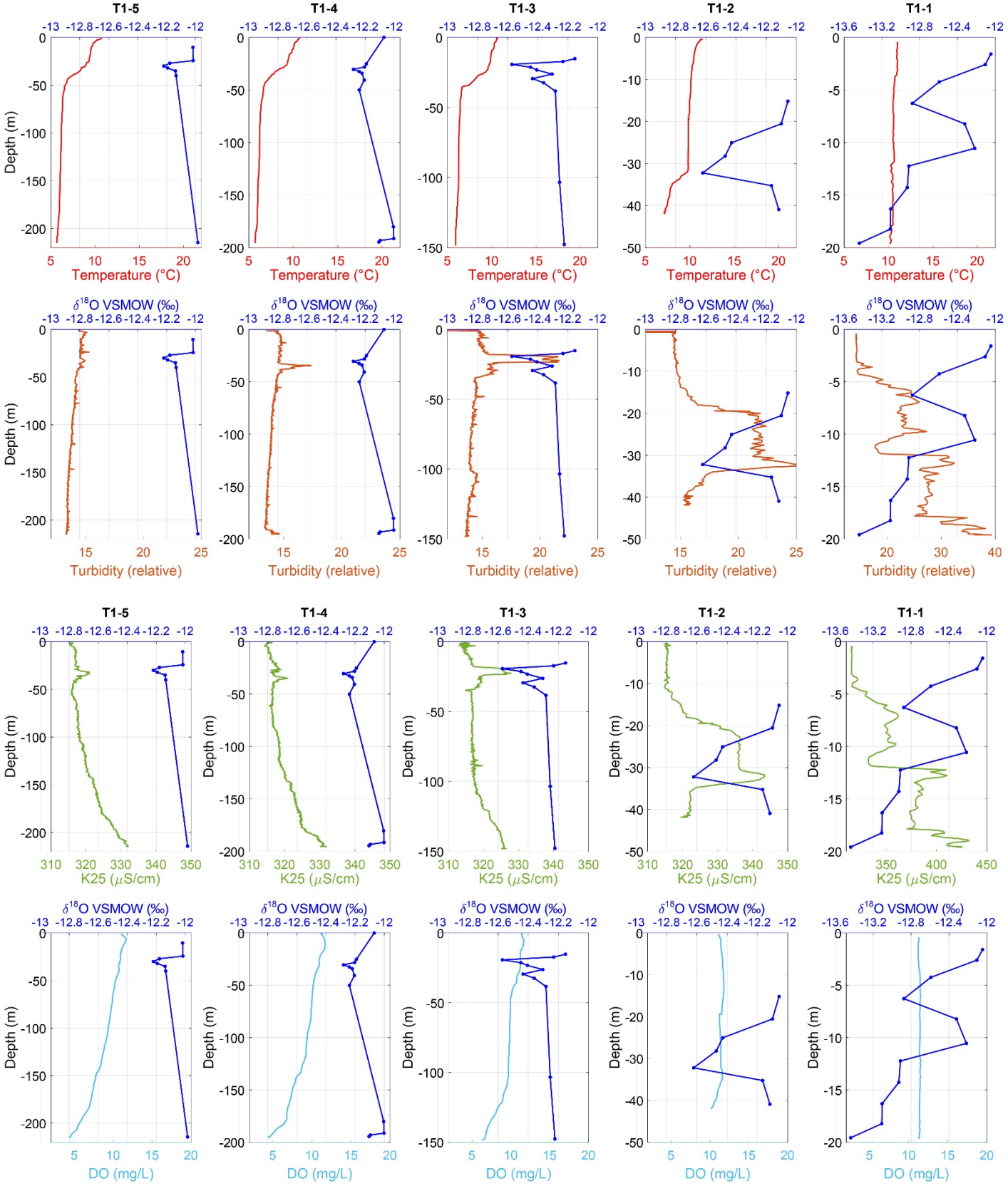

Appendix II-5: CTD profiles of Transect 2 of temperature (red), turbidity (brown), conductivity (green) and dissolved oxygen (light blue) with the oxygen isotope composition of water (dark blue) obtained during the campaigns of May 2017.

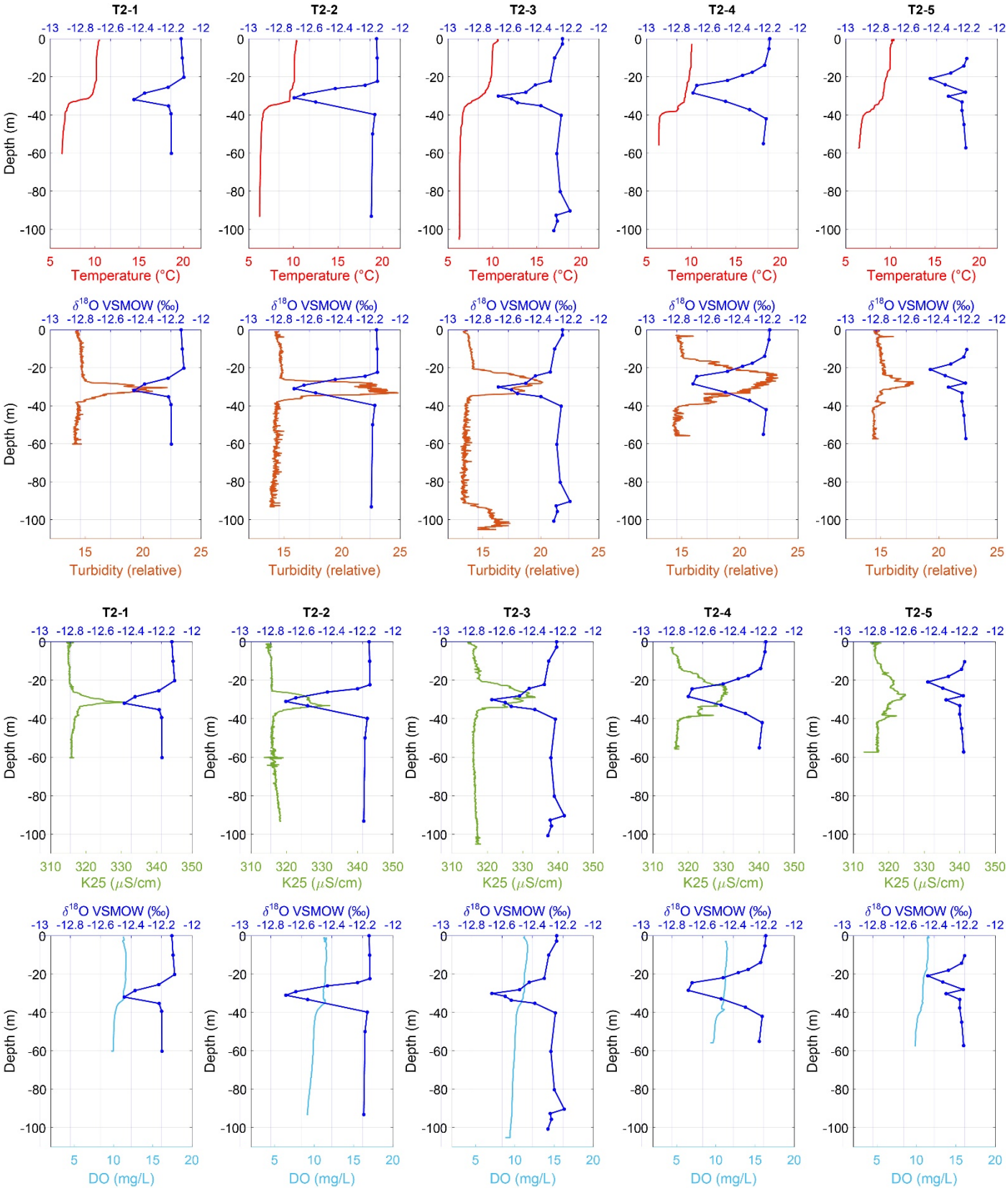

Appendix II-6: CTD profiles of Transect 3 of temperature (red), turbidity (brown), conductivity (green) and dissolved oxygen (light blue) with the oxygen isotope composition of water (dark blue) obtained during the campaigns of May 2017.

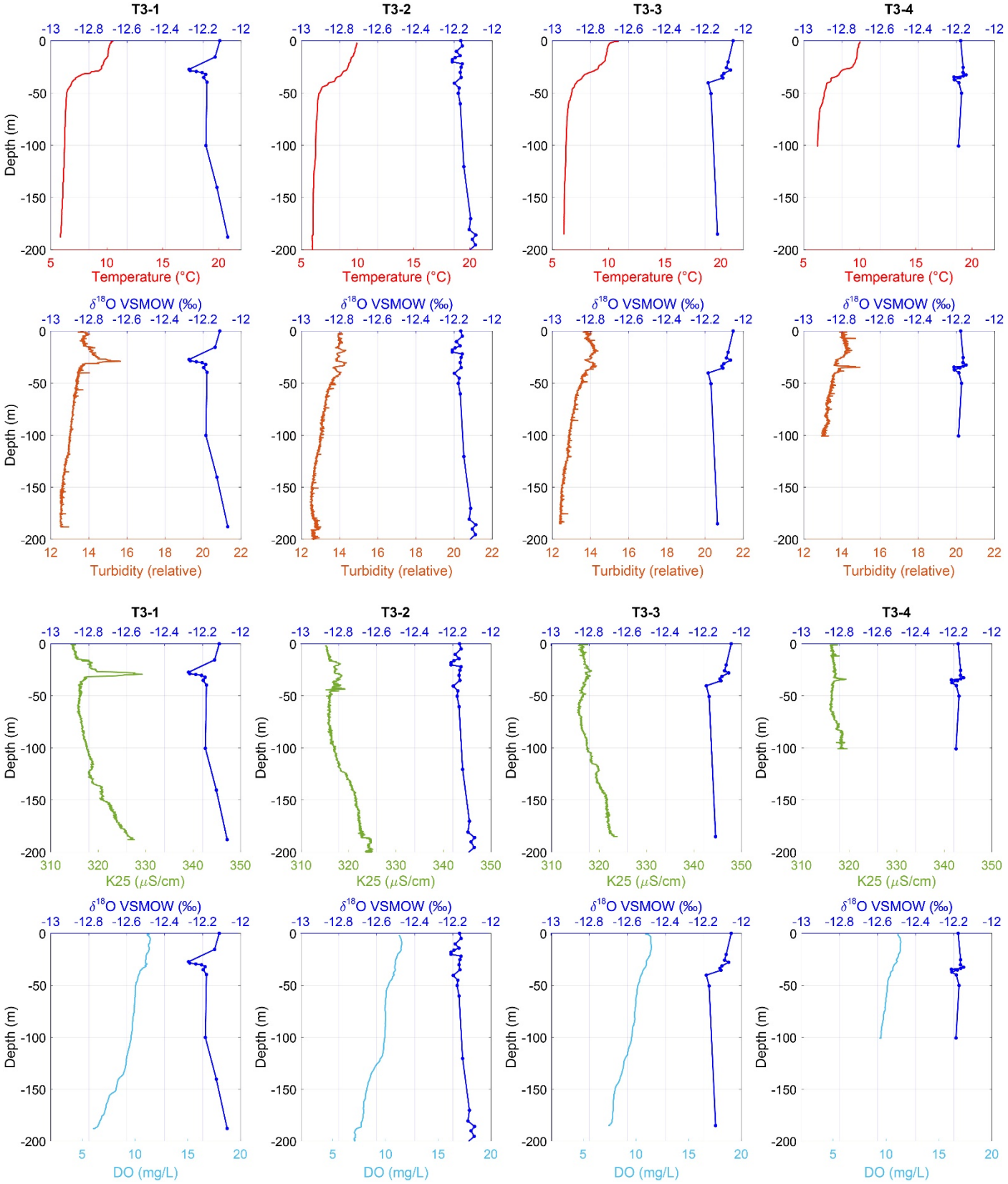

Appendix II-7: Rhône River data (discharge, temperature and turbidity from OFEV/NADUF) and the isotope composition of its water (from our measurements) at the hydrological station of Porte du Scex located 5 km upstream Lake Geneva during the campaigns of February and May 2017.

Sampling time	Discharge (m^3/s)	T (°C)	Turb. (NTU)	**$\delta^{18}O$ VSMOW**	std. dev.	**δD VSMOW**	std. dev.
February 2017							
20.02.2017 09:00	60.8	4.7	15.0	**-14.51**	0.02	**-106.2**	0.1
21.02.2017 05:00	77.3	5.3	16.0	**-14.43**	0.03	**-104.6**	0.0
21.02.2017 08:00	75.7	5.3	15.8	**-14.59**	0.02	**-105.6**	0.2
21.02.2017 11:00	81.8	5.7	16.3	**-14.40**	0.01	**-104.7**	0.2
21.02.2017 14:00	72.1	6.0	28.8	**-14.42**	0.04	**-104.8**	0.1
22.02.2017 02:00	70.1	6.1	15.0	**-14.17**	0.02	**-103.2**	0.1
22.02.2017 04:00	71.4	6.0	15.6	**-14.06**	0.05	**-102.4**	0.2
22.02.2017 06:00	71.9	5.6	16.0	**-14.27**	0.05	**-103.6**	0.6
22.02.2017 08:00	71.3	5.6	14.1	**-14.18**	0.03	**-105.0**	0.1
22.02.2017 10:00	72.7	6.1	17.6	**-14.18**	0.06	**-104.6**	0.1
22.02.2017 12:00	71.1	6.7	30.8	**-14.14**	0.07	**-104.5**	0.2
22.02.2017 14:00	67.4	7.1	36.3	**-14.20**	0.02	**-104.6**	0.1
22.02.2017 16:00	68.8	7.2	32.6	**-14.24**	0.04	**-104.6**	0.2
22.02.2017 18:00	63.3	7.0	29.8	**-14.15**	0.02	**-105.2**	0.2
22.02.2017 20:00	63.4	6.7	22.6	**-14.27**	0.03	**-104.8**	0.2
22.02.2017 22:00	73.7	6.4	17.5	**-14.28**	0.06	**-106.3**	0.2
23.02.2017 00:00	77.5	6.2	16.0	**-14.21**	0.09	**-106.2**	0.5
23.02.2017 02:00	72.8	6.3	13.6	**-14.34**	0.02	**-103.1**	0.2
23.02.2017 04:00	85.4	6.1	17.8	**-14.36**	0.03	**-103.4**	0.0
23.02.2017 06:00	77.0	5.8	17.1	**-14.42**	0.02	**-103.9**	0.1
23.02.2017 08:00	70.4	6.0	16.0	**-14.46**	0.03	**-104.4**	0.1
23.02.2017 10:00	75.5	6.3	17.5	**-14.46**	0.01	**-104.0**	0.0
23.02.2017 12:00	81.7	6.9	20.3	**-14.40**	0.01	**-103.8**	0.1
23.02.2017 14:00	74.1	7.1	25.3	**-14.38**	0.03	**-103.4**	0.2
May 2017							
01.05.2017 19:00	85.5	8.7		**-14.11**	0.01	**-103.8**	0.1
01.05.2017 20:00	83.6	8.5		**-14.13**	0.03	**-103.6**	0.2
01.05.2017 22:00	81.9	8.2		**-14.19**	0.01	**-104.0**	0.1
02.05.2017 00:00	83.2	8.2	25.0	**-14.17**	0.01	**-103.7**	0.1
02.05.2017 02:00	83.7	8.1	24.0	**-14.17**	0.00	**-103.7**	0.1
02.05.2017 04:00	92.7	7.9	28.6	**-14.19**	0.01	**-104.1**	0.0
02.05.2017 06:00	83.8	7.7	30.7	**-14.29**	0.01	**-104.7**	0.2
02.05.2017 08:00	88.6	7.5	29.9	**-14.23**	0.01	**-104.6**	0.3
02.05.2017 10:00	102.1	7.6	34.6	**-14.24**	0.02	**-104.6**	0.0
02.05.2017 12:00	147.1	7.7	55.3	**-14.29**	0.02	**-105.0**	0.1
02.05.2017 14:00	118.0	7.3	88.6	**-14.30**	0.02	**-104.6**	0.1
03.05.2017 19:00	88.6	7.9	30.0	**-14.34**	0.01	**-104.9**	0.2
03.05.2017 20:00	89.3	7.7	30.8	**-14.16**	0.02	**-103.9**	0.0
03.05.2017 22:00	125.9	7.9	37.0	**-14.03**	0.02	**-102.9**	0.3
04.05.2017 00:00	128.5	8.2	39.8	**-14.11**	0.04	**-103.7**	0.1

04.05.2017 02:00	114.1	8.6	37.3	**-14.25**	0.01	**-105.3**	0.1
04.05.2017 04:00	94.0	8.5	30.5	**-14.14**	0.04	**-104.4**	0.3
04.05.2017 06:00	81.6	8.4	30.9	**-14.30**	0.03	**-105.3**	0.1
04.05.2017 08:00	81.7	8.3	37.9	**-14.02**	0.02	**-103.3**	0.2
04.05.2017 10:00	95.2	8.4	52.7	**-14.10**	0.00	**-103.7**	0.1
04.05.2017 12:00	100.1	8.4	51.0	**-14.28**	0.02	**-105.2**	0.0
04.05.2017 14:00	95.4	8.4	43.2	**-14.18**	0.02	**-105.1**	0.2
04.05.2017 16:00	92.1	8.3	42.0	**-14.29**	0.04	**-105.4**	0.1
04.05.2017 18:00	93.6	8.3	36.2	**-14.25**	0.00	**-105.4**	0.1
04.05.2017 20:00	86.1	8.3	32.8	**-14.20**	0.02	**-104.5**	0.3
04.05.2017 22:00	93.4	8.3	31.5	**-14.03**	0.02	**-103.0**	0.2
05.05.2017 00:00	101.6	8.2	36.2	**-13.91**	0.02	**-102.4**	0.1
05.05.2017 02:00	87.1	8.2	33.3	**-14.02**	0.03	**-103.0**	0.1
05.05.2017 04:00	78.9	8.4	31.1	**-14.00**	0.00	**-102.9**	0.2
05.05.2017 06:00	74.9	8.2	26.7	**-14.05**	0.04	**-103.5**	0.1
05.05.2017 14:00	80.9	10.5	25.6	**-14.02**	0.04	**-103.2**	0.1
05.05.2017 16:00	79.1	10.5	25.8	**-13.97**	0.01	**-103.0**	0.1

Appendix II-8: CTD data (depth, temperature, conductivity, oxygen concentration, oxygen saturation and pH) and stable isotope composition of the lake water samples for the sampling campaigns of December 2015, February 2017 and May 2017.

Profile	Sampling time	Depth (m)	T (°C)	K25 (µS/cm)	O_2 (mg/L)	O_2 (% sat.)	pH	**$\delta^{18}O$ VSMOW**	std. dev.	**δD VSMOW**	std. dev.
December 2015											
3	15.12.2015	0.0						**-12.23**	0.01	**-90.4**	0.1
3	15.12.2015	20.8	9.6	297	10.2	90	8.1	**-12.23**	0.01	**-90.4**	0.1
3	15.12.2015	30.8	9.6	298	10.0	88	8.1	**-12.22**	0.03	**-90.4**	0.1
3	15.12.2015	40.9	9.0	38	8.4	73	7.9	**-12.20**	0.03	**-90.1**	0.1
3	15.12.2015	46.0	8.6	313	8.3	71	7.8	**-12.19**	0.04	**-89.9**	0.2
3	15.12.2015	51.3	7.8	315	8.2	69	7.8	**-12.15**	0.03	**-89.7**	0.2
3	15.12.2015	56.4	7.3	316	8.4	70	7.8	**-12.15**	0.04	**-89.6**	0.1
3	15.12.2015	61.3	6.9	318	8.7	71	7.8	**-12.14**	0.02	**-89.5**	0.3
3	15.12.2015	66.0	6.7	318	8.8	72	7.8	**-12.13**	0.03	**-89.4**	0.2
3	15.12.2015	71.7	6.5	320	9.0	73	7.9	**-12.14**	0.02	**-89.4**	0.1
3	15.12.2015	74.8	6.4	319	9.2	75	7.9	**-12.13**	0.02	**-89.4**	0.1
3	15.12.2015	78.7	6.4	318	9.5	77	7.9	**-12.14**	0.04	**-89.5**	0.4
2	17.12.2015	0.0	9.4	322	9.6		7.7	**-12.28**	0.01	**-90.5**	0.1
2	17.12.2015	150.0	6.1	347	8.4		7.5	**-12.13**	0.01	**-89.2**	0.2
2	17.12.2015	200.0	5.9	35	8.0		7.8	**-12.08**	0.02	**-88.8**	0.1
2	17.12.2015	250.0	5.7	352	6.4		7.4	**-12.05**	0.03	**-88.8**	0.1
2	17.12.2015	280.0	5.7	356	5.6		7.6	**-12.05**	0.01	**-88.6**	0.1
2	17.12.2015	290.0	5.7	356	5.4		7.4	**-12.05**	0.03	**-88.6**	0.3
2	17.12.2015	300.0	5.7	358	4.7		7.4	**-12.09**	0.01	**-89.0**	0.1
2	17.12.2015	308.0	5.6	359	3.4		7.2	**-12.09**	0.02	**-89.3**	0.4
1	16.12.2015	0.0	9.6	246			7.8	**-12.26**	0.02	**-90.5**	0.2
1	16.12.2015	160.0	6.4	243			7.8	**-12.08**	0.04	**-89.2**	0.1
1	16.12.2015	180.0	6.5	266			7.6	**-12.06**	0.01	**-88.9**	0.1
1	16.12.2015	200.0	6.8	254			7.8	**-12.05**	0.02	**-88.8**	0.1
0	16.12.2015	0.0	9.5	248			7.8	**-12.32**	0.03	**-90.8**	0.1
0	16.12.2015	25.0	9.5	322	7.6		7.7	**-12.30**	0.02	**-90.8**	0.1
0	16.12.2015	50.0	8.1	336	6.5		7.6	**-12.35**	0.01	**-91.1**	0.1
0	16.12.2015	60.0	7.5	342	6.8		7.6	**-12.20**	0.03	**-89.8**	0.2
0	16.12.2015	70.0	7.0	344	7.0		7.7	**-12.08**	0.14	**-89.1**	0.9
0	16.12.2015	80.0	7.0	344	6.8		7.6	**-12.15**	0.03	**-89.4**	0.1
0	16.12.2015	85.0	7.0	344	7.0		7.6	**-12.16**	0.02	**-89.5**	0.2
0	16.12.2015	90.0	7.0	344	7.2		7.7	**-12.13**	0.03	**-89.4**	0.1
0	16.12.2015	95.0	7.1	342	6.9		7.8	**-12.14**	0.02	**-89.5**	0.1
0	16.12.2015	100.0	7.4	343	6.9		7.7	**-12.13**	0.02	**-89.5**	0.2
0	16.12.2015	105.0	7.2	343	7.2		7.9	**-12.14**	0.04	**-89.4**	0.2
February 2017											
1	23.02.2017 12:00	25.9	6.3	314	8.4	68	8.2	**-12.21**	0.02	**-88.6**	0.0
1	23.02.2017 12:00	76.8	6.2	317	8.4	68	8.2	**-12.33**	0.06	**-89.3**	0.1
1	23.02.2017 12:00	93.9	6.2	318	8.4	68	8.1	**-12.35**	0.04	**-89.6**	0.1
1	23.02.2017 12:00	105.1	6.2	32	8.4	68	8.2	**-12.33**	0.02	**-89.6**	0.1
1	23.02.2017 12:00	114.2	6.2	33	8.5	69	8.2	**-12.44**	0.08	**-89.9**	0.3

Profile	Sampling time	Depth (m)	T (°C)	K25 (µS/cm)	O_2 (mg/L)	O_2 (% sat.)	pH	**$\delta^{18}O$ VSMOW**	std. dev.	**δD VSMOW**	std. dev.
1	23.02.2017 12:00	117.2	6.2	321	8.4	68	8.2	**-12.40**	0.03	**-89.7**	0.2
1	23.02.2017 12:00	122.5	6.2	322	7.9	64	8.1	**-12.41**	0.00	**-89.8**	0.1
1	23.02.2017 12:00	126.3	6.2	33	7.6	61	8.1	**-12.30**	0.03	**-89.4**	0.3
1	23.02.2017 12:00	129.6	6.1	318	7.6	62	8.1	**-12.18**	0.04	**-88.4**	0.3
1	23.02.2017 12:00	137.8	6.1	320	7.3	59	8.1	**-12.20**	0.04	**-88.6**	0.3
1	23.02.2017 12:00	145.2	6.1	322	7.7	62	8.1	**-12.25**	0.03	**-89.1**	0.2
1	23.02.2017 12:00	150.4	6.1	324	7.9	64	8.1	**-12.37**	0.03	**-89.6**	0.2
1	23.02.2017 12:00	155.5	6.1	323	7.8	63	8.1	**-12.34**	0.01	**-89.3**	0.2
1	23.02.2017 12:00	158.3	6.1	322	7.5	61	8.1	**-12.30**	0.02	**-89.0**	0.2
1	23.02.2017 12:00	173.5	6.0	323	6.2	50	8.0	**-12.16**	0.05	**-88.2**	0.1
1	23.02.2017 12:00	183.8	5.9	325	5.9	48	8.0	**-12.18**	0.02	**-88.5**	0.1
1	23.02.2017 12:00	198.1	5.9	326	5.5	44	8.0	**-12.21**	0.02	**-88.4**	0.1
1	23.02.2017 12:00	191.8	5.9	324	5.8	47	8.0	**-12.19**	0.01	**-88.2**	0.4
1	23.02.2017 12:00	195.8	5.9	326	5.7	46	8.0	**-12.17**	0.05	**-88.4**	0.3
1	23.02.2017 12:00	200.4	5.9	327	5.6	45	8.0	**-12.16**	0.02	**-88.7**	0.4
0	22.02.2017 10:00	82.0	6.3	322	8.6	70	8.2	**-12.34**	0.03	**-89.2**	0.1
0	22.02.2017 10:00	91.5	6.3	327	8.7	71	8.2	**-12.42**	0.02	**-89.6**	0.1
0	22.02.2017 10:00	103.2	6.3	336	9.0	73	8.2	**-12.59**	0.02	**-90.6**	0.1
0	22.02.2017 10:00	102.3	6.3	336	8.9	73	8.2	**-12.60**	0.05	**-90.8**	0.1
0	22.02.2017 10:00	96.9	6.3	332	8.9	72	8.2	**-12.48**	0.03	**-90.0**	0.1
0	22.02.2017 10:00	106.0	6.2	336	9.0	73	8.2	**-12.63**	0.04	**-91.0**	0.0
0	22.02.2017 10:00	105.1	6.3	338	9.0	73	8.2	**-12.55**	0.01	**-90.8**	0.1
0	22.02.2017 10:00	104.2	6.3	336	9.0	73	8.2	**-12.60**	0.02	**-90.9**	0.1
0	22.02.2017 10:00	107.1	6.3	338	9.0	73	8.2	**-12.61**	0.02	**-91.0**	0.0
0	22.02.2017 10:00	108.1	6.3	338	9.0	73	8.2	**-12.61**	0.04	**-91.0**	0.1
0	22.02.2017 10:00	109.3	6.2	341	8.8	71	8.2	**-12.71**	0.04	**-91.8**	0.1
May 2017											
3	02.05.2017	0.0						**-12.09**	0.03	**-89.3**	0.2
3	02.05.2017	2.3	10.3	314	11.0	98	8.6	**-12.11**	0.05	**-89.7**	0.1
3	02.05.2017	4.8	10.2	314	10.9	97	8.6	**-12.09**	0.03	**-89.2**	0.1
3	02.05.2017	10.2	10.1	315	10.8	96	8.5	**-12.10**	0.01	**-89.7**	0.2
3	02.05.2017	15.3	10.0	315	10.9	97	8.5	**-12.13**	0.02	**-89.6**	0.1
3	02.05.2017	20.5	9.3	316	10.3	90	8.4	**-12.14**	0.02	**-89.6**	0.1
3	02.05.2017	25.2	8.8	316	10.0	86	8.3	**-12.14**	0.02	**-89.6**	0.1
3	02.05.2017	30.3	8.1	316	9.8	83	8.2	**-12.17**	0.01	**-89.7**	0.2
3	02.05.2017	35.0	7.7	315	9.7	82	8.2	**-12.16**	0.01	**-89.8**	0.2
3	02.05.2017	40.2	6.9	318	9.7	80	8.1	**-12.14**	0.02	**-89.9**	0.1
3	02.05.2017	59.9	6.3	312	9.6	78	8.1	**-12.14**	0.03	**-89.8**	0.1
2	02.05.2017	0.0						**-12.13**	0.01	**-89.6**	0.1
2	02.05.2017	10.4	8.7	315	10.8	93	8.4	**-12.13**	0.03	**-89.8**	0.0
2	02.05.2017	20.6	8.3	315	10.1	86	8.2	**-12.13**	0.02	**-89.8**	0.2
2	02.05.2017	25.5	7.7	316	10.0	84	8.2	**-12.15**	0.03	**-89.8**	0.1
2	02.05.2017	30.7	7.2	316	9.8	82	8.1	**-12.18**	0.01	**-90.1**	0.0
2	02.05.2017	35.4	7.0	316	10.0	83	8.1	**-12.20**	0.03	**-90.1**	0.2
2	02.05.2017	40.5	6.8	315	9.7	80	8.1	**-12.17**	0.02	**-90.1**	0.2

Profile	Sampling time	Depth (m)	T (°C)	K25 (µS/cm)	O_2 (mg/L)	O_2 (% sat.)	pH	**$\delta^{18}O$ VSMOW**	std. dev.	**δD VSMOW**	std. dev.
2	02.05.2017	45.1	6.6	316	9.7	79	8.1	**-12.21**	0.00	**-90.2**	0.1
2	02.05.2017	50.1	6.5	315	9.8	80	8.1	**-12.19**	0.03	**-90.0**	0.3
2	02.05.2017	100.3	6.3	317	9.6	78	8.1	**-12.20**	0.01	**-90.2**	0.1
2	02.05.2017	305.2	5.6	335	2.8	22	7.8	**-12.06**	0.04	**-89.2**	0.1
1	03.05.2017	0.0						**-12.17**	0.02	**-89.9**	0.2
1	03.05.2017	5.0	9.9	315	11.1	99	8.6	**-12.16**	0.03	**-89.6**	0.2
1	03.05.2017	10.2	9.7	315	11.0	97	8.5	**-12.19**	0.01	**-89.9**	0.0
1	03.05.2017	14.3	9.5	316	10.7	94	8.5	**-12.17**	0.02	**-89.8**	0.1
1	03.05.2017	16.2	9.4	318	10.6	93	8.4	**-12.19**	0.02	**-90.1**	0.2
1	03.05.2017	18.2	9.4	318	10.6	92	8.4	**-12.21**	0.03	**-90.0**	0.2
1	03.05.2017	20.2	9.3	317	10.6	93	8.4	**-12.21**	0.04	**-90.0**	0.1
1	03.05.2017	22.1	9.2	317	10.6	92	8.4	**-12.16**	0.02	**-90.0**	0.1
1	03.05.2017	25.3	9.1	317	10.6	92	8.4	**-12.16**	0.01	**-90.0**	0.1
1	03.05.2017	30.3	8.6	316	10.3	89	8.3	**-12.17**	0.02	**-90.0**	0.0
1	03.05.2017	35.1	8.0	316	10.2	87	8.2	**-12.16**	0.03	**-89.9**	0.1
1	03.05.2017	40.6	7.3	316	10.1	84	8.1	**-12.20**	0.02	**-90.1**	0.1
1	03.05.2017	45.2	6.8	316	9.8	80	8.1	**-12.17**	0.01	**-90.1**	0.1
1	03.05.2017	50.3	6.5	316	9.7	80	8.1	**-12.18**	0.01	**-90.1**	0.1
1	03.05.2017	60.3	6.4	316	9.8	80	8.1	**-12.17**	0.00	**-89.9**	0.1
1	03.05.2017	120.5	6.2	319	8.8	71	8.0	**-12.15**	0.01	**-89.8**	0.2
1	03.05.2017	170.3	6.0	322	7.7	62	8.0	**-12.11**	0.04	**-89.7**	0.1
1	03.05.2017	180.7	6.0	322	7.1	57	7.9	**-12.12**	0.02	**-89.5**	0.2
1	03.05.2017	186.0	6.0	325	6.9	56	7.9	**-12.09**	0.02	**-89.3**	0.1
1	03.05.2017	190.1	6.0	324	6.8	55	7.9	**-12.10**	0.05	**-89.3**	0.0
1	03.05.2017	195.4	6.0	324	6.9	55	7.9	**-12.09**	0.02	**-89.5**	0.3
1	03.05.2017	200.2	6.0	324	7.1	57	7.9	**-12.12**	0.03	**-89.2**	0.1
0	03.05.2017	0.0						**-12.24**	0.02	**-89.4**	0.1
0	03.05.2017	2.8	10.2	314	11.4	101	8.6	**-12.24**	0.01	**-89.5**	0.1
0	03.05.2017	10.1	10.0	316	11.1	99	8.6	**-12.29**	0.02	**-89.8**	0.1
0	03.05.2017	20.1	9.9	318	11.0	97	8.5				
0	03.05.2017	22.2	9.8	320	10.8	95	8.5	**-12.32**	0.02	**-89.9**	0.1
0	03.05.2017	24.3	9.7	325	10.9	97	8.5	**-12.42**	0.02	**-90.6**	0.2
0	03.05.2017	26.0	9.6	326	10.9	96	8.5				
0	03.05.2017	28.1	9.5	329	10.8	95	8.4	**-12.48**	0.01	**-91.2**	0.2
0	03.05.2017	30.1	9.3	330	10.4	91	8.4	**-12.67**	0.03	**-92.4**	0.2
0	03.05.2017	31.6	8.9	334	10.2	88	8.3	**-12.58**	0.01	**-91.9**	0.2
0	03.05.2017	33.6	7.7	324	10.1	85	8.2	**-12.54**	0.01	**-91.3**	0.0
0	03.05.2017	35.2	7.6	325	10.0	84	8.2	**-12.38**	0.02	**-90.4**	0.1
0	03.05.2017	40.2	6.7	316	9.8	80	8.1	**-12.25**	0.02	**-89.5**	0.0
0	03.05.2017	60.3	6.4	316	10.0	81	8.1	**-12.28**	0.02	**-89.7**	0.1
0	03.05.2017	80.3	6.3	317	9.5	77	8.1	**-12.26**	0.01	**-89.1**	0.1
0	03.05.2017	90.4	6.3	317	9.3	76	8.1	**-12.19**	0.03	**-89.1**	0.1
0	03.05.2017	92.7	6.3	317	9.2	75	8.1	**-12.28**	0.02	**-89.6**	0.1
0	03.05.2017	95.7	6.3	317	9.3	75	8.1	**-12.28**	0.02	**-89.7**	0.2
0	03.05.2017	100.8	6.3	317	9.4	76	8.1	**-12.30**	0.02	**-89.5**	0.1

Appendix III

(Chapter III)

Appendix III-1: Depth profiles of the different forms of P (a) and N (b) measured at the LéXPLORE platform during the study period. The profiles in colour correspond to the measurements of the APHYS team (EPFL), the black stars to ours.

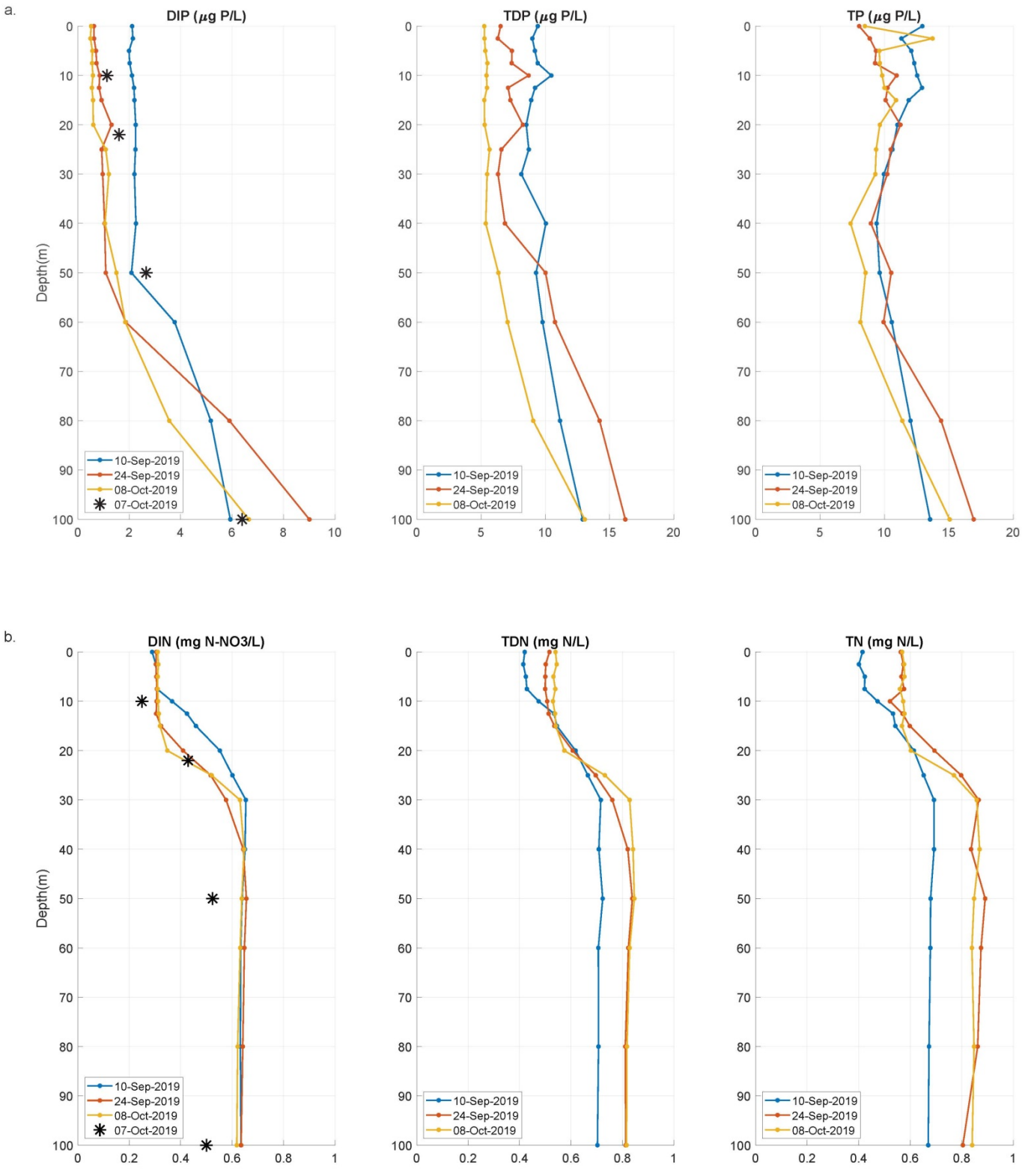

Appendix III-2: Nutrient concentration profiles (orthophosphate, nitrate and silicate) measured at SHL2 (Figure 1) by the CIPEL during the study period. The averaged profiles are shown in dashed line.

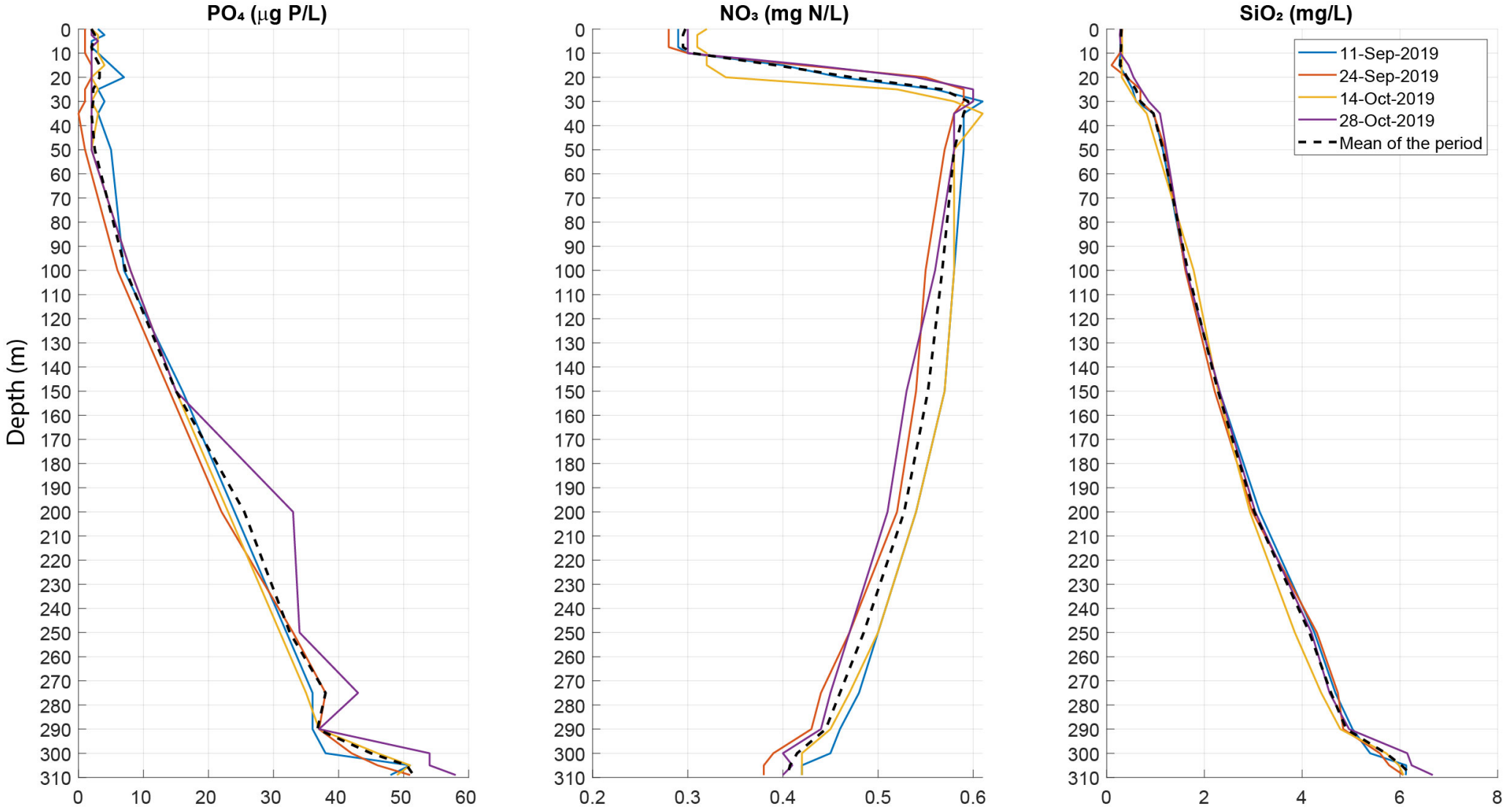

Appendix III-3: Meteolakes screenshots (http://meteolakes.ch).

a. Downwelling event of September 13th.

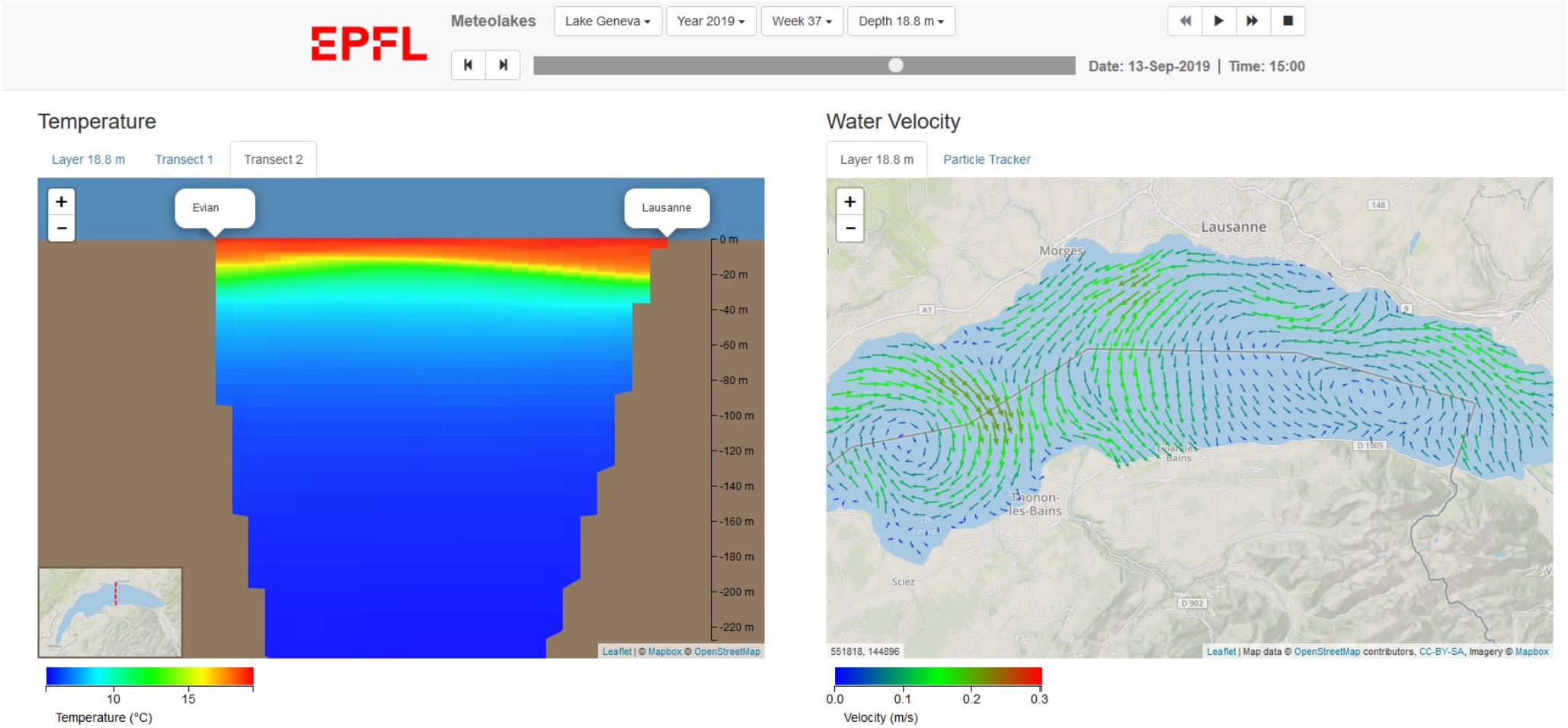

b. Downwelling event of October 24th.

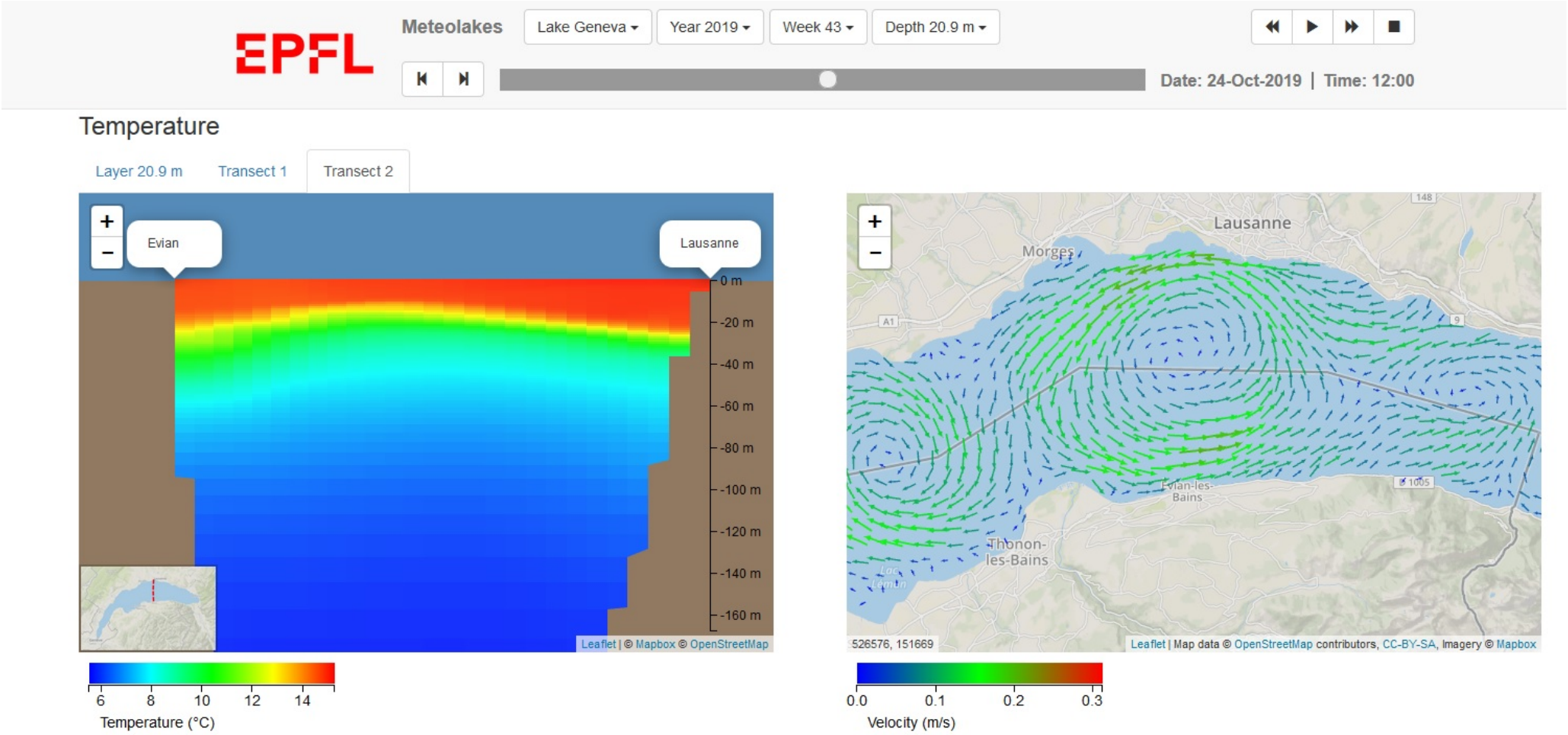

Appendix III-4: Thermocline depth, stable isotope composition of water and related Rhône fractions.

Sample	Sampling time	Sampler	Filtration day	Thermocline depth (m)	$\delta^{18}O$ VSMOW	std dev.	δD VSMOW	std dev.	% *Rhône* ($\delta^{18}O$)	% *Rhône* (δD)
1	13.09.2019 18:00	ISCO	16.09.2019	16.25	**-12.53**	0.03	**-91.9**	0.5	25.4	28.2
2	13.09.2019 21:00	ISCO	-	13.75	**-12.42**	0.04	**-91.0**	0.2	17.7	15.7
3	14.09.2019 00:00	ISCO	-	13.75	**-12.44**	0.04	**-91.1**	0.1	19.0	18.1
4	14.09.2019 03:00	ISCO	-	16.25	**-12.40**	0.03	**-90.9**	0.1	16.8	15.3
5	14.09.2019 06:00	ISCO	-	16.25	**-12.42**	0.03	**-91.0**	0.1	17.7	15.6
6	14.09.2019 09:00	ISCO	-	16.25	**-12.46**	0.04	**-91.1**	0.2	20.7	17.6
7	14.09.2019 12:00	ISCO	-	16.25	**-12.37**	0.04	**-90.8**	0.2	14.3	13.1
8	14.09.2019 15:00	ISCO	-	18.75	**-12.37**	0.04	**-90.9**	0.1	14.4	14.7
9	14.09.2019 18:00	ISCO	-	16.25	**-12.41**	0.04	**-91.0**	0.2	17.0	15.6
10	14.09.2019 21:00	ISCO	-	18.75	**-12.41**	0.01	**-90.9**	0.2	16.9	14.4
11	15.09.2019 00:00	ISCO	-	16.25	**-12.39**	0.03	**-90.8**	0.1	15.6	13.7
12	15.09.2019 03:00	ISCO	-	16.25	**-12.41**	0.02	**-91.0**	0.1	17.5	16.4
13	15.09.2019 06:00	ISCO	-	16.25	**-12.38**	0.04	**-91.0**	0.1	15.0	15.9
14	15.09.2019 09:00	ISCO	-	16.25	**-12.40**	0.03	**-91.0**	0.2	16.5	15.6
15	16.09.2019 20:00	manual	-	13.75	**-12.41**	0.04	**-91.2**	0.1	17.0	18.3
16	16.09.2019 23:00	ISCO	20.09.2019	11.25	**-12.48**	0.03	**-92.5**	0.1	21.6	35.7
17	17.09.2019 02:00	ISCO	no F	13.75	**-12.45**	0.04	**-91.5**	0.3	20.1	22.5
18	17.09.2019 05:00	ISCO	no F	13.75	**-12.45**	0.02	**-91.0**	0.1	19.7	16.8
19	17.09.2019 08:00	ISCO	no F	16.25	**-12.46**	0.01	**-91.0**	0.1	20.6	16.6
20	17.09.2019 11:00	ISCO	no F	13.75	**-12.42**	0.05	**-91.1**	0.2	18.0	17.3
21	17.09.2019 14:00	ISCO	no F	13.75	**-12.49**	0.04	**-91.2**	0.1	22.5	18.2
22	17.09.2019 17:00	ISCO	no F	13.75	**-12.39**	0.03	**-90.8**	0.1	15.8	14.1
23	17.09.2019 20:00	ISCO	no F	11.25	**-12.38**	0.05	**-90.9**	0.2	15.2	15.1
24	17.09.2019 23:00	ISCO	no F	13.75	**-12.41**	0.07	**-91.1**	0.5	17.2	17.6
25	18.09.2019 02:00	ISCO	no F	13.75	**-12.42**	0.04	**-91.1**	0.2	18.0	16.8
26	18.09.2019 05:00	ISCO	no F	13.75	**-12.40**	0.04	**-91.1**	0.4	16.7	17.6
27	18.09.2019 08:00	ISCO	no F	11.25	**-12.39**	0.05	**-90.9**	0.2	15.9	14.7
28	18.09.2019 11:00	ISCO	no F	13.75	**-12.44**	0.06	**-91.1**	0.3	19.2	17.4
29	18.09.2019 14:00	ISCO	no F	13.75	**-12.42**	0.08	**-90.9**	0.4	17.7	15.5
30	20.09.2019 19:00	manual	no F	16.25	**-12.32**	0.02	**-90.5**	0.1	11.1	10.1
31	20.09.2019 22:00	ISCO	no F	16.25	**-12.28**	0.06	**-89.9**	0.2	8.8	1.9
32	21.09.2019 01:00	ISCO	no F	8.75	**-12.43**	0.02	**-90.9**	0.1	18.8	15.0
33	21.09.2019 04:00	ISCO	no F	8.75	**-12.41**	0.07	**-90.8**	0.2	16.9	14.1
34	21.09.2019 07:00	ISCO	no F	8.75	**-12.47**	0.04	**-91.2**	0.1	21.5	19.4
35	21.09.2019 10:00	ISCO	no F	8.75	**-12.50**	0.05	**-91.3**	0.3	23.0	19.9
36	21.09.2019 13:00	ISCO	no F	6.25	**-12.47**	0.04	**-91.3**	0.4	21.2	20.0
37	21.09.2019 16:00	ISCO	no F	11.25	**-12.50**	0.08	**-91.4**	0.4	23.3	21.3
38	21.09.2019 19:00	ISCO	no F	11.25	**-12.52**	0.05	**-91.4**	0.1	24.2	21.2
39	21.09.2019 22:00	ISCO	no F	11.25	**-12.52**	0.01	**-91.5**	0.1	24.7	22.5
40	22.09.2019 01:00	ISCO	no F	13.75	**-12.47**	0.06	**-91.2**	0.2	20.9	18.2
41	22.09.2019 04:00	ISCO	no F	6.25	**-12.41**	0.05	**-91.1**	0.3	17.1	18.0
42	22.09.2019 07:00	ISCO	no F	13.75	**-12.43**	0.05	**-91.4**	0.3	18.7	20.8
43	22.09.2019 10:00	ISCO	no F	8.75	**-12.34**	0.02	**-90.9**	0.1	12.4	14.9
44	22.09.2019 13:00	ISCO	no F	8.75	**-12.45**	0.04	**-91.0**	0.3	19.6	16.4
45	30.09.2019 16:00	manual	no F	16.25	**-12.31**	0.09	**-90.3**	0.5	10.9	7.0
46	01.10.2019 12:00	ISCO	04.10.2019	16.25	**-12.11**	0.04	**-89.3**	0.2	-2.5	-6.2
47	01.10.2019 15:00	ISCO	-	16.25	**-12.32**	0.05	**-90.5**	0.4	11.6	9.4
48	01.10.2019 18:00	ISCO	-	16.25	**-12.42**	0.02	**-90.9**	0.2	17.7	15.0
49	01.10.2019 21:00	ISCO	-	16.25	**-12.39**	0.05	**-90.6**	0.1	15.9	11.5
50	02.10.2019 00:00	ISCO	-	16.25	**-12.36**	0.06	**-90.7**	0.2	13.7	11.8
51	02.10.2019 03:00	ISCO	-	16.25	**-12.42**	0.01	**-91.1**	0.1	17.7	17.1
52	02.10.2019 06:00	ISCO	-	18.75	**-12.24**	0.06	**-89.8**	0.2	5.9	0.6
53	02.10.2019 09:00	ISCO	-	16.25	**-12.28**	0.03	**-90.0**	0.2	8.7	3.2
54	02.10.2019 12:00	ISCO	-	18.75	**-12.31**	0.01	**-90.2**	0.1	10.8	6.3
55	02.10.2019 15:00	ISCO	-	21.25	**-12.24**	0.03	**-89.8**	0.2	5.9	-0.1
56	02.10.2019 18:00	ISCO	-	16.25	**-12.29**	0.04	**-90.2**	0.1	9.6	6.3

57	02.10.2019 21:00	ISCO	-	16.25	**-12.32**	0.05	**-90.1**	0.2	11.2	4.2
58	03.10.2019 00:00	ISCO	-	18.75	**-12.32**	0.01	**-90.3**	0.0	11.1	6.8
59	03.10.2019 03:00	ISCO	-	21.25	**-12.40**	0.02	**-90.7**	0.1	16.7	12.8
60	03.10.2019 14:00	manual	-	26.25	**-12.10**	0.03	**-88.9**	0.2	-3.3	-11.5
61	05.10.2019 12:00	ISCO	08.10.2019	18.75	**-12.05**	0.04	**-88.6**	0.3	-6.7	-14.5
62	05.10.2019 15:00	ISCO	-	23.75	**-12.09**	0.04	**-89.1**	0.5	-4.2	-8.1
63	05.10.2019 18:00	ISCO	-	28.75	**-12.01**	0.06	**-88.4**	0.2	-9.1	-17.1
64	05.10.2019 21:00	ISCO	-	23.75	**-12.01**	0.05	**-88.4**	0.2	-9.2	-18.1
65	06.10.2019 00:00	ISCO	-	21.25	**-11.99**	0.06	**-88.3**	0.3	-10.7	-18.8
66	06.10.2019 03:00	ISCO	-	23.75	**-12.10**	0.01	**-89.0**	0.2	-3.4	-9.8
67	06.10.2019 06:00	ISCO	-	23.75	**-12.00**	0.05	**-88.6**	0.1	-9.9	-15.7
68	06.10.2019 09:00	ISCO	-	18.75	**-12.20**	0.06	**-89.8**	0.2	3.1	0.9
69	06.10.2019 12:00	ISCO	-	18.75	**-12.16**	0.03	**-89.3**	0.4	0.8	-6.3
70	06.10.2019 15:00	ISCO	-	23.75	**-12.20**	0.02	**-89.5**	0.1	3.2	-3.6
71	06.10.2019 18:00	ISCO	-	16.25	**-12.21**	0.06	**-89.6**	0.3	4.1	-1.8
72	06.10.2019 21:00	ISCO	-	11.25	**-12.28**	0.03	**-90.3**	0.2	8.3	6.8
73	07.10.2019 00:00	ISCO	-	13.75	**-12.26**	0.06	**-90.1**	0.3	7.5	4.5
74	07.10.2019 03:00	ISCO	-	11.25	**-12.32**	0.04	**-90.6**	0.1	11.3	10.8
75	**07.10.2019 17:00**	**manual**	**-**	**21.25**	**-12.36**	0.04	**-91.0**	0.1	14.0	15.6
76	07.10.2019 20:00	ISCO	-	28.75	**-12.31**	0.04	**-90.3**	0.3	10.7	7.3
77	07.10.2019 23:00	ISCO	-	23.75	**-12.17**	0.03	**-89.4**	0.2	1.6	-4.4
78	11.10.2019 13:00	manual	16.10.2019		**-12.25**	0.02	**-89.8**	0.1	6.4	0.5
79	09.10.2019 18:15	ISCO	-		**-12.32**	0.03	**-90.0**	0.1	11.1	3.7
80	09.10.2019 21:15	ISCO	-		**-12.30**	0.02	**-90.1**	0.0	9.8	4.0
81	16.10.2019 13:30	manual	-		**-12.13**	0.02	**-89.2**	0.0	-1.6	-7.9
82	16.10.2019 18:00	ISCO	18.10.2019		**-12.20**	0.02	**-89.3**	0.0	3.5	-6.3
83	16.10.2019 21:00	ISCO	-		**-12.18**	0.02	**-89.1**	0.1	2.0	-9.0
84	17.10.2019 00:00	ISCO	-		**-12.13**	0.02	**-89.1**	0.1	-1.5	-9.0
85	17.10.2019 03:00	ISCO	-		**-12.12**	0.03	**-89.0**	0.1	-1.9	-9.4
86	17.10.2019 06:00	ISCO	-		**-12.08**	0.02	**-88.7**	0.1	-4.8	-14.4
87	17.10.2019 09:00	ISCO	-		**-12.11**	0.03	**-89.1**	0.1	-2.7	-8.1
88	17.10.2019 12:00	ISCO	-		**-12.42**	0.02	**-91.1**	0.1	17.9	17.4
89	18.10.2019 16:30	manual	-		**-12.25**	0.02	**-90.2**	0.1	7.0	5.7
90	19.10.2019 18:00	ISCO	22.10.2019		**-12.27**	0.04	**-90.4**	0.5	8.0	8.2
91	19.10.2019 21:00	ISCO	-		**-12.17**	0.02	**-89.5**	0.1	1.5	-3.6
92	20.10.2019 00:00	ISCO	-		**-12.27**	0.04	**-90.0**	0.2	8.0	3.7
93	20.10.2019 03:00	ISCO	-		**-12.25**	0.03	**-90.1**	0.2	6.9	4.1
94	20.10.2019 06:00	ISCO	-		**-12.26**	0.03	**-90.1**	0.2	7.2	3.8
95	20.10.2019 09:00	ISCO	-		**-12.26**	0.02	**-90.0**	0.1	7.0	3.3
96	20.10.2019 12:00	ISCO	-		**-12.25**	0.02	**-90.0**	0.1	6.7	2.6
97	20.10.2019 15:00	ISCO	-		**-12.28**	0.05	**-90.2**	0.2	8.5	6.1
98	20.10.2019 18:00	ISCO	-		**-12.29**	0.03	**-90.2**	0.2	9.4	6.1
99	20.10.2019 21:00	ISCO	-		**-12.22**	0.03	**-90.0**	0.1	4.7	3.0
100	21.10.2019 00:00	ISCO	-		**-12.22**	0.04	**-89.8**	0.2	4.9	-0.1
101	21.10.2019 03:00	ISCO	-		**-12.35**	0.06	**-90.5**	0.3	13.4	10.1
102	21.10.2019 06:00	ISCO	-		**-12.36**	0.04	**-90.6**	0.3	14.1	11.6
103	21.10.2019 09:00	ISCO	-		**-12.35**	0.06	**-90.6**	0.4	13.2	10.5
104	22/10/2019 14:30	manual	-		**-12.36**	0.03	**-90.4**	0.2	14.0	8.6
105	23.10.2019 18:00	ISCO	25.10.2019	18.75	**-12.36**	0.03	**-90.5**	0.2	13.7	9.2
106	23.10.2019 21:00	ISCO	-	16.25	**-12.32**	0.04	**-90.3**	0.3	11.3	7.4
107	24.10.2019 00:00	ISCO	-	16.25	**-12.32**	0.04	**-90.3**	0.1	11.4	7.2
108	24.10.2019 03:00	ISCO	-	16.25	**-12.37**	0.04	**-90.5**	0.1	14.7	9.6
109	24.10.2019 06:00	ISCO	-	18.75	**-12.34**	0.04	**-90.3**	0.2	12.9	6.6
110	24.10.2019 09:00	ISCO	-	16.25	**-12.39**	0.01	**-90.5**	0.1	15.7	10.1
111	24.10.2019 12:00	ISCO	-	11.25	**-12.36**	0.02	**-90.5**	0.1	14.0	9.6
112	24.10.2019 15:00	ISCO	-	13.75	**-12.32**	0.03	**-90.0**	0.3	11.4	3.4
113	24.10.2019 18:00	ISCO	-	23.75	**-12.32**	0.02	**-90.0**	0.2	11.5	2.8
114	24.10.2019 21:00	ISCO	-	26.25	**-12.31**	0.05	**-90.0**	0.2	10.6	2.6
115	25/10/2019 00:00	ISCO	-	23.75	**-12.30**	0.04	**-89.9**	0.3	10.0	1.4
116	25/10/2019 03:00	ISCO	-	23.75	**-12.31**	0.03	**-89.8**	0.1	10.7	0.8
117	25/10/2019 06:00	ISCO	-	23.75	**-12.26**	0.01	**-89.6**	0.1	7.0	-2.5

118	25/10/2019 09:00	ISCO	-	18.75	**-12.22**	0.01	**-89.5**	0.2	4.9	-3.8
119	25/10/2019 10:00	manual	-	21.25	**-12.23**	0.06	**-89.5**	0.2	5.4	-3.6

Appendix III-5: Isotope composition and concentration of DIC and nutrient concentrations. Samples 17 to 45 were not filtrated in time so were not analysed.

Sample	Sampling time	Sampler	Filtration day	**$\delta^{13}C$ VPDB**	DIC (mg/L)	**PO_4^{3-} (mg/L)**	std dev.	**SiO_2 (mg/L)**	std dev.	**NO_3^- (mg N/L)**	std dev.
1	13/09/2019 18:00	ISCO	16/09/2019	**-5.74**	80	10.2	1.20	0.37	0.00	0.333	0.005
2	13/09/2019 21:00	ISCO	-	**-3.83**	83	15.7	1.20	0.47	0.01	0.398	0.003
3	14/09/2019 00:00	ISCO	-	**-4.47**	75	21.0	1.79	0.48	0.01	0.399	0.003
4	14/09/2019 03:00	ISCO	-	**-6.72**	79	33.7	1.79	0.49	0.01	0.429	0.000
5	14/09/2019 06:00	ISCO	-	**-4.22**	73	6.6	0.84	0.40	0.00	0.383	0.002
6	14/09/2019 09:00	ISCO	-	**-4.74**	74	8.6	0.84	0.42	0.00	0.373	0.003
7	14/09/2019 12:00	ISCO	-	**-5.15**	70	12.4	0.21	0.51	0.01	0.395	0.000
8	14/09/2019 15:00	ISCO	-	**-4.56**	80	9.0	0.40	0.47	0.00	0.370	0.000
9	14/09/2019 18:00	ISCO	-	**-6.36**	74	7.8	0.40	0.50	0.01	0.395	0.000
10	14/09/2019 21:00	ISCO	-	**-4.37**	76	7.3	0.40	0.52	0.00	0.398	0.000
11	15/09/2019 00:00	ISCO	-	**-3.51**	75	3.9	0.11	0.50	0.00	0.308	0.001
12	15/09/2019 03:00	ISCO	-	**-4.63**	79	5.5	0.40	0.52	0.00	0.396	0.002
13	15/09/2019 06:00	ISCO	-	**-5.55**	77	6.9	0.40	0.48	0.00	0.365	0.001
14	15/09/2019 09:00	ISCO	-	**-6.20**	75	3.2	0.11	0.44	0.01	0.359	0.001
15	16/09/2019 20:00	manual	-	**-4.76**	82	0.7	0.13	0.43	0.00	0.362	0.001
16	16/09/2019 23:00	ISCO	20/09/2019	**-4.33**	80	3.5	0.11	0.53	0.00	0.424	0.001
17			no F								
17→45			no F								
45			no F								
46	01/10/2019 12:00	ISCO	04/10/2019	**-4.79**	79	0.7	0.13	0.31	0.00	0.198	0.000
47	01/10/2019 15:00	ISCO	-	**-5.85**	79	1.1	0.13	0.47	0.01	0.300	0.002
48	01/10/2019 18:00	ISCO	-	**-5.53**	78	5.7	0.40	0.49	0.00	0.317	0.001
49	01/10/2019 21:00	ISCO	-	**-4.69**	74	1.2	0.13	0.43	0.00	0.320	0.004
50	02/10/2019 00:00	ISCO	-	**-5.90**	82	1.7	0.13	0.42	0.01	0.246	0.002
51	02/10/2019 03:00	ISCO	-	**-6.18**	83	1.0	0.13	0.42	0.01	0.373	0.001
52	02/10/2019 06:00	ISCO	-	**-4.80**	77	0.6	0.13	0.36	0.00	0.269	0.000
53	02/10/2019 09:00	ISCO	-	**-5.36**	79	2.4	0.11	0.41	0.00	0.278	0.001
54	02/10/2019 12:00	ISCO	-	**-5.78**	85	1.6	0.13	0.43	0.00	0.240	0.001
55	02/10/2019 15:00	ISCO	-	**-5.21**	78	2.4	0.11	0.38	0.01	0.278	0.001
56	02/10/2019 18:00	ISCO	-	**-5.51**	86	2.4	0.11	0.40	0.00	0.113	0.000
57	02/10/2019 21:00	ISCO	-	**-7.17**	87	1.3	0.13	0.47	0.01	0.425	0.004
58	03/10/2019 00:00	ISCO	-	**-7.10**	94	2.0	0.11	0.46	0.02	0.445	0.000
59	03/10/2019 03:00	ISCO	-	**-6.12**	76	2.6	0.11	0.46	0.03	0.352	0.001
60	03/10/2019 14:00	manual	-	**-4.50**	78	0.4	0.13	0.31	0.00	0.249	0.001
61	05/10/2019 12:00	ISCO	08/10/2019	**-4.82**	81	0.9	0.13	0.35	0.00	0.270	0.001
62	05/10/2019 15:00	ISCO	-	**-5.78**	84	0.7	0.13	0.39	0.00	0.248	0.000
63	05/10/2019 18:00	ISCO	-	**-4.74**	79	2.4	0.11	0.31	0.00	0.252	0.000
64	05/10/2019 21:00	ISCO	-	**-4.84**	66	1.5	0.13	0.31	0.01	0.237	0.002
65	06/10/2019 00:00	ISCO	-	**-5.17**	79	1.4	0.13	0.34	0.00	0.132	0.000
66	06/10/2019 03:00	ISCO	-	**-5.06**	66	3.4	0.06	0.23	0.00	0.247	0.001
67	06/10/2019 06:00	ISCO	-	**-5.44**	82	3.4	0.06	0.26	0.00	0.265	0.002
68	06/10/2019 09:00	ISCO	-	**-6.26**	74	3.0	0.06	0.40	0.02	0.243	0.002
69	06/10/2019 12:00	ISCO	-	**-5.55**	82	2.2	0.06	0.39	0.03	0.293	0.005
70	06/10/2019 15:00	ISCO	-	**-5.85**	70	2.8	0.06	0.29	0.02	0.300	0.004
71	06/10/2019 18:00	ISCO	-	**-5.92**	74	3.3	0.06	0.38	0.00	0.311	0.002
72	06/10/2019 21:00	ISCO	-	**-6.98**	81	2.7	0.06	0.44	0.00	0.242	0.000
73	07/10/2019 00:00	ISCO	-	**-7.51**	94	4.2	0.06	0.50	0.00	0.352	0.000
74	07/10/2019 03:00	ISCO	-	**-7.29**	87	2.3	0.06	0.53	0.02	0.420	0.002
75	**07/10/2019 17:00**	**manual**	**-**	**-6.78**	83	1.6	0.10	0.47	0.00	0.429	0.002
76	07/10/2019 20:00	ISCO	-	**-6.70**	79	1.2	0.13	0.46	0.00	0.375	0.000
77	07/10/2019 23:00	ISCO	-	**-5.55**	85	1.6	0.13	0.37	0.01	0.307	0.000
78	11/10/2019 13:00	manual	16/10/2019	**-6.04**	82	1.1	0.13	0.50	0.00	0.321	0.000
79	09/10/2019 18:15	ISCO	-	**-7.14**	89	0.8	0.13	0.45	0.01	0.456	0.001
80	09/10/2019 21:15	ISCO	-	**-7.08**	89	1.1	0.13	0.49	0.00	0.451	0.001
81	16/10/2019 13:30	manual	-	**-5.52**	78	1.1	0.13	0.52	0.01	0.298	0.000

82	16/10/2019 18:00	ISCO	18/10/2019	**-6.26**	73	1.7	0.13	0.58	0.05	0.275	0.001
83	16/10/2019 21:00	ISCO	-	**-5.51**	72	1.4	0.13	0.58	0.08	0.305	0.001
84	17/10/2019 00:00	ISCO	-	**-5.83**	80	2.6	0.11	0.54	0.00	0.313	0.000
85	17/10/2019 03:00	ISCO	-	**-5.70**	85	3.2	0.11	0.60	0.05	0.308	0.001
86	17/10/2019 06:00	ISCO	-	**-5.48**	86	2.9	0.04	0.48	0.00	0.308	0.001
87	17/10/2019 09:00	ISCO	-	**-5.86**	85	2.9	0.04	0.48	0.00	0.311	0.000
88	17/10/2019 12:00	ISCO	-	**-6.86**	86	2.3	0.04	0.60	0.00	0.403	0.000
89	18/10/2019 16:30	manual	-	**-7.11**	91	2.3	0.04	0.52	0.01	0.404	0.000
90	19/10/2019 18:00	ISCO	22/10/2019	**-5.89**	86	1.1	0.01	0.48	0.00	0.298	0.001
91	19/10/2019 21:00	ISCO	22/10/2019	**-6.79**	88	1.0	0.01	0.48	0.00	0.384	0.005
92	20/10/2019 00:00	ISCO	22/10/2019	**-7.45**	92	3.4	0.04	0.54	0.01	0.462	0.000
93	20/10/2019 03:00	ISCO	22/10/2019	**-7.40**	83	1.7	0.01	0.55	0.01	0.474	0.001
94	20/10/2019 06:00	ISCO	22/10/2019	**-7.48**	94	2.8	0.04	0.52	0.00	0.500	0.001
95	20/10/2019 09:00	ISCO	22/10/2019	**-7.34**	91	2.4	0.04	0.52	0.02	0.488	0.000
96	20/10/2019 12:00	ISCO	22/10/2019	**-6.93**	90	1.8	0.01	0.48	0.00	0.438	0.004
97	20/10/2019 15:00	ISCO	22/10/2019	**-7.19**	86	0.9	0.08	0.54	0.02	0.463	0.001
98	20/10/2019 18:00	ISCO	22/10/2019	**-7.27**	80	1.7	0.01	0.52	0.00	0.472	0.002
99	20/10/2019 21:00	ISCO	22/10/2019	**-7.32**	89	3.9	0.04	0.50	0.01	0.476	0.003
100	21/10/2019 00:00	ISCO	22/10/2019	**-6.60**	74	3.0	0.04	0.43	0.00	0.436	0.003
101	21/10/2019 03:00	ISCO	22/10/2019	**-6.07**	75	2.2	0.04	0.52	0.01	0.433	0.000
102	21/10/2019 06:00	ISCO	22/10/2019	**-6.32**	68	3.6	0.04	0.51	0.00	0.448	0.002
103	21/10/2019 09:00	ISCO	22/10/2019	**-6.46**	72	1.4	0.01	0.52	0.00	0.443	0.001
104	22/10/2019 14:30	manual	22/10/2019	**-6.15**	70	1.8	0.01	0.63	0.01	0.417	0.001
105	23/10/2019 18:00	ISCO	25/10/2019	**-6.69**	74	2.2	0.04	0.63	0.02	0.422	0.002
106	23/10/2019 21:00	ISCO	25/10/2019	**-6.46**	71	3.4	0.04	0.63	0.02	0.417	0.000
107	24/10/2019 00:00	ISCO	25/10/2019	**-6.58**	77	3.6	0.04	0.62	0.00	0.434	0.001
108	24/10/2019 03:00	ISCO	25/10/2019	**-6.61**	81	2.2	0.04	0.70	0.07	0.454	0.002
109	24/10/2019 06:00	ISCO	25/10/2019	**-6.62**	74	2.7	0.04	0.64	0.01	0.463	0.000
110	24/10/2019 09:00	ISCO	25/10/2019	**-6.53**	72	2.6	0.04	0.69	0.20	0.426	0.003
111	24/10/2019 12:00	ISCO	25/10/2019	**-5.93**	72	2.0	0.04	0.71	0.04	0.187	0.001
112	24/10/2019 15:00	ISCO	25/10/2019	**-5.69**	74	1.7	0.01	0.83	0.01	0.349	0.001
113	24/10/2019 18:00	ISCO	25/10/2019	**-5.40**	75	1.7	0.01	0.87	0.00	0.137	0.000
114	24/10/2019 21:00	ISCO	25/10/2019	**-5.50**	77	2.4	0.04	0.88	0.01	0.369	0.001
115	25/10/2019 00:00	ISCO	25/10/2019	**-5.65**	72	2.1	0.04	0.92	0.01	0.361	0.003
116	25/10/2019 03:00	ISCO	25/10/2019	**-5.96**	69	2.0	0.04	0.78	0.01	0.375	0.002
117	25/10/2019 06:00	ISCO	25/10/2019	**-5.70**	72	2.3	0.04	0.73	0.01	0.089	0.000
118	25/10/2019 09:00	ISCO	25/10/2019	**-5.61**	73	1.7	0.01	0.70	0.02	0.340	0.001
119	25/10/2019 10:00	manual	25/10/2019	**-5.74**	73	1.3	0.01	0.74	0.01	0.355	0.000

Appendix III-6: Time series of Rhône fractions, nutrients and DIC concentration with its isotopic composition (left axis). The dissolved oxygen is in black full line (right axis).

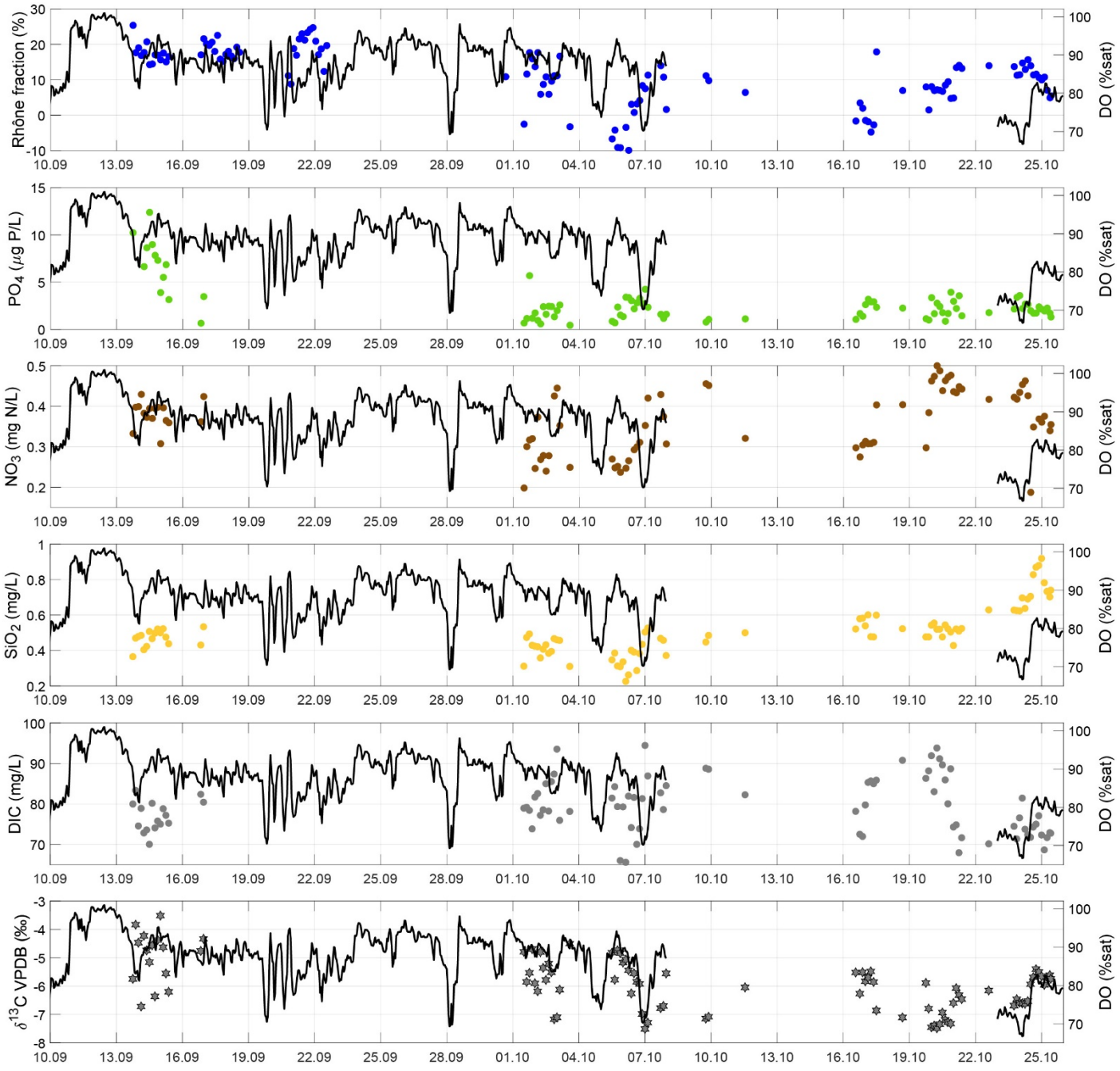

Appendix III-7: Period 1 (Summer Period). Time series of Rhône fractions, nutrients and DIC concentration with its isotopic composition (left axis). The dissolved oxygen is in dashed line (first right axis) while the thermocline depth is in full line (second right axis).

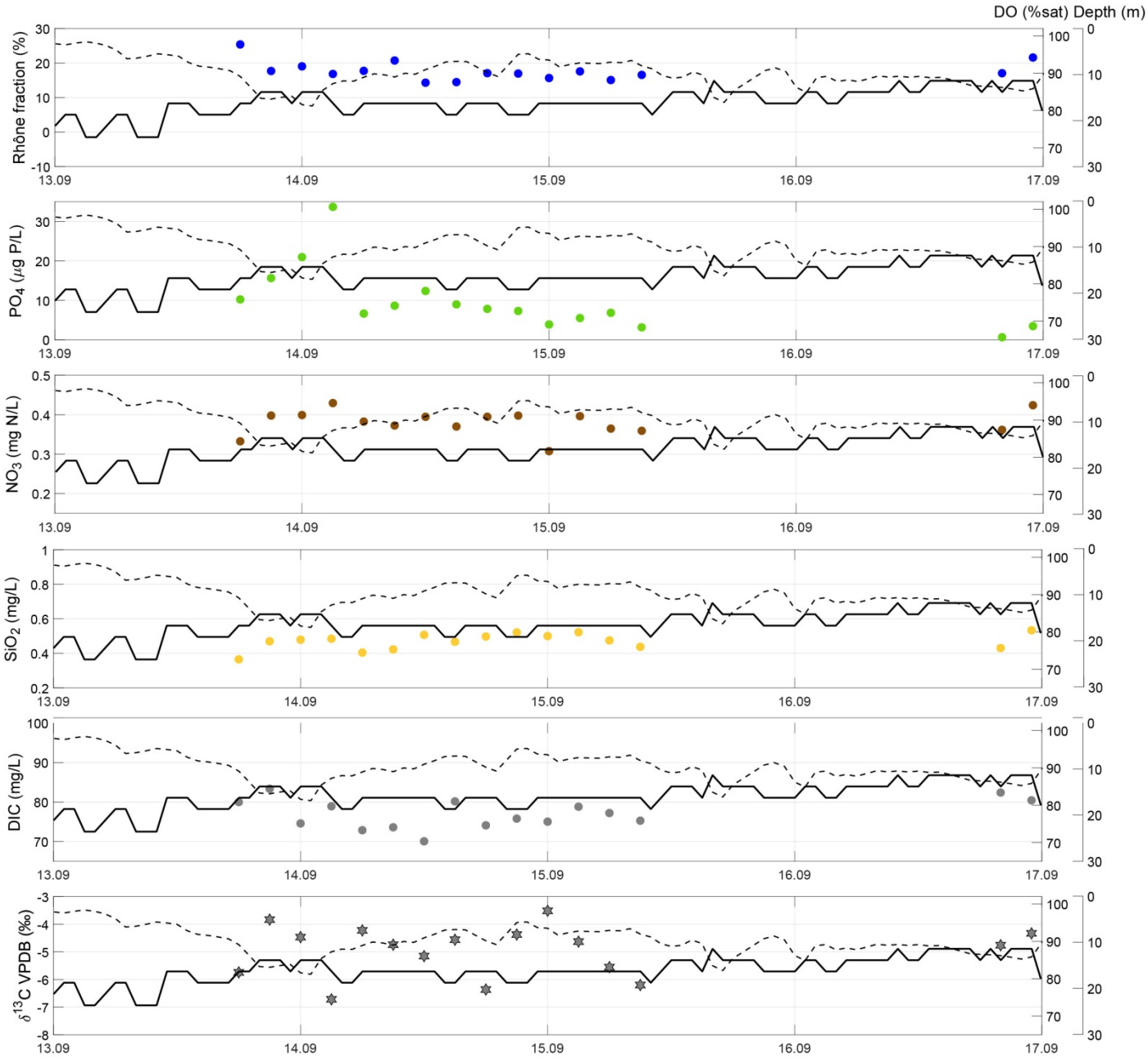

Appendix III-8: Period 2 (Windy Period). Time series of Rhône fractions, nutrients and DIC concentration with its isotopic composition (left axis). The dissolved oxygen is in dashed line (first right axis) while the thermocline depth is in full line (second right axis).

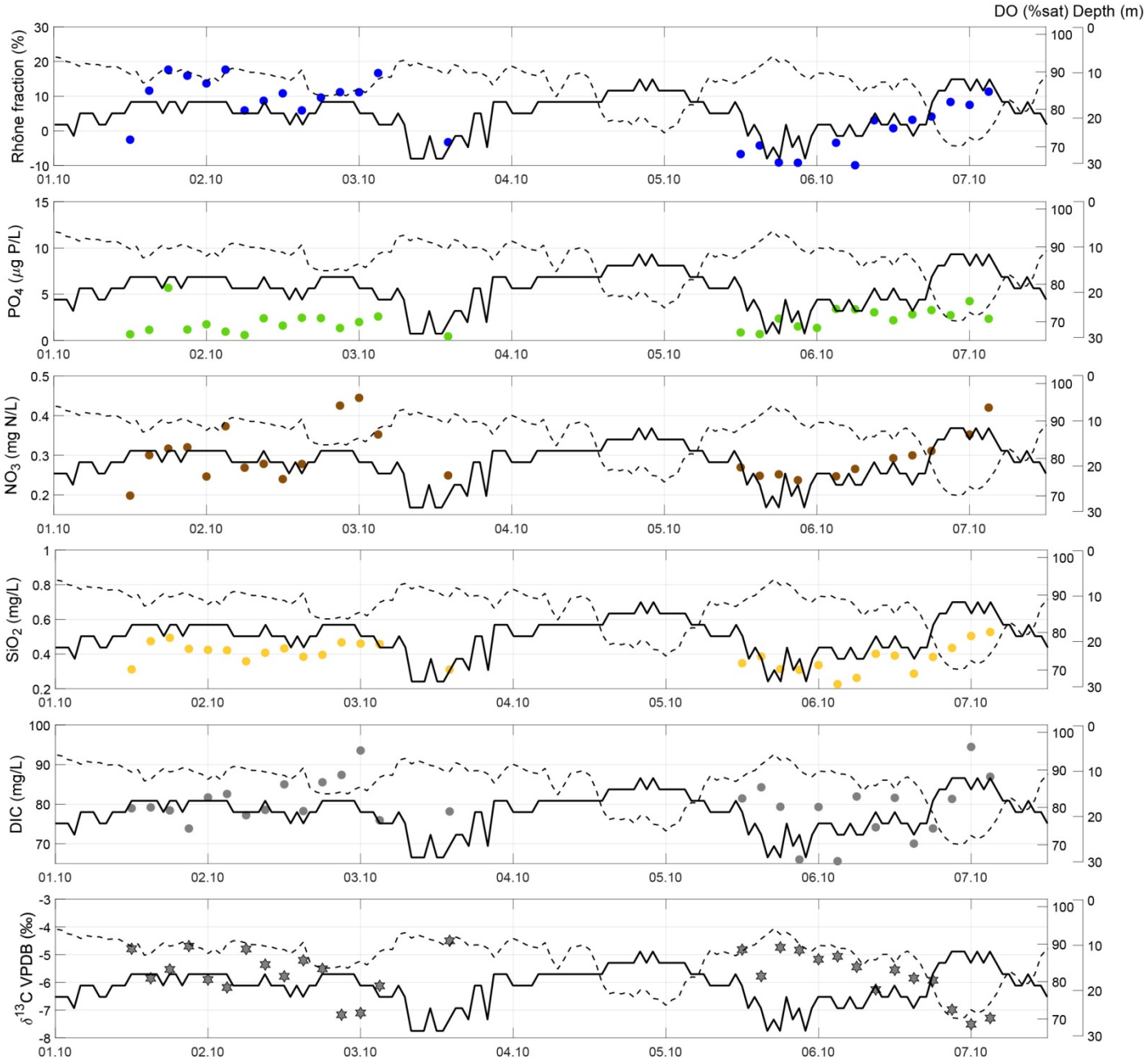

Appendix III-9: Period 3 (Autumn Period). Time series of Rhône fractions, nutrients and DIC concentration with its isotopic composition (left axis). The dissolved oxygen is in dashed line (first right axis) while the thermocline depth is in full line (second right axis).

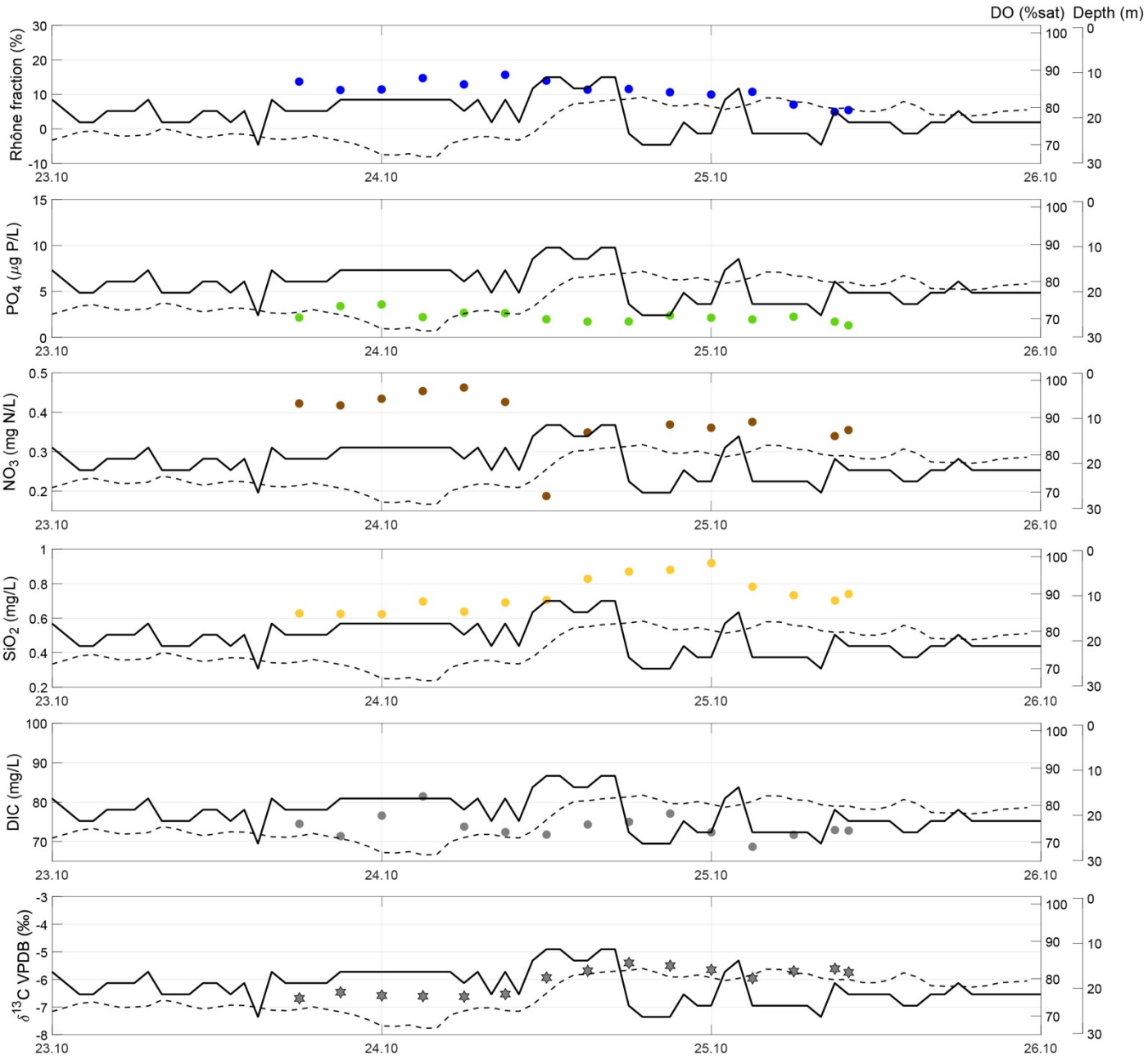

Appendix IV

(Chapter IV)

Appendix IV-1: Location according to the Swiss Coordinate System (CH1903/LV03) and sampling date of the different sampling stations (first: April campaign, second: September campaign).

Station	Depth (m)	Distance from river mouth (m)	X (m)	Y (m)	Date of sampling (2019)
A	109	1000	554725	139048	2nd of April 17:30
B	175	5110	554966	143380	2nd of April 16:00
C	230	14000	545027	147694	2nd of April 14:00
D	309	21700	534700	144950	2nd of April 10:00
Ibis	219	5100	550589	139956	4th of April 11:20
I	109	1000	554725	139048	4th of April 12:20
II	50	550	555059	138720	4th of April 13:10
III	20	420	555517	138710	4th of April 15:00
IV	35	280	555147	138374	4th of April 16:10
V	20	180	555322	138470	4th of April 17:15

Station	Depth (m)	Distance from river mouth (m)	X (m)	Y (m)	Date of sampling
1	50	400	555210	138680	24th of September 12:00
2	40	-	554860	138480	24th of September 13:00
3	45	-	555040	138580	24th of September 14:00
4	35	-	555380	138780	24th of September 15:30
5	30	-	555560	138880	24th of September 16:30
A	50	400	555210	138680	26th of September 09:45
B	105	800	554850	138925	26th of September 11:00
C	120	1200	554500	139150	26th of September 12:30
C1	133	1600	554100	139250	26th of September 14:10
D	160	2000	553650	139300	26th of September 17:30
E	200	4000	552000	140000	26th of September 16:10

Appendix IV-2: Meteolake simulation showing a cyclonic gyre in the main basin deflecting the water towards the northern shore on the 2nd of April 2019 at 3 pm (http://meteolakes.ch).

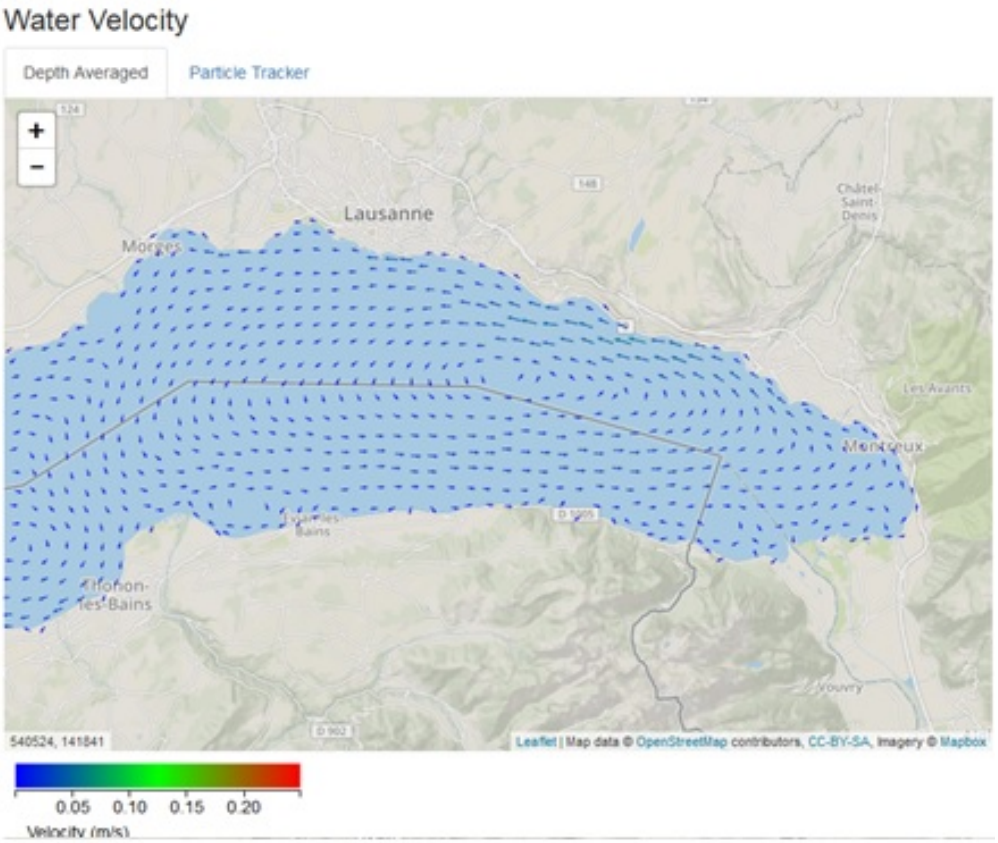

Appendix IV-3: CTD profiles at station Ibis, located 5 km in front of the Rhône River mouth on the 4th of April 2019.

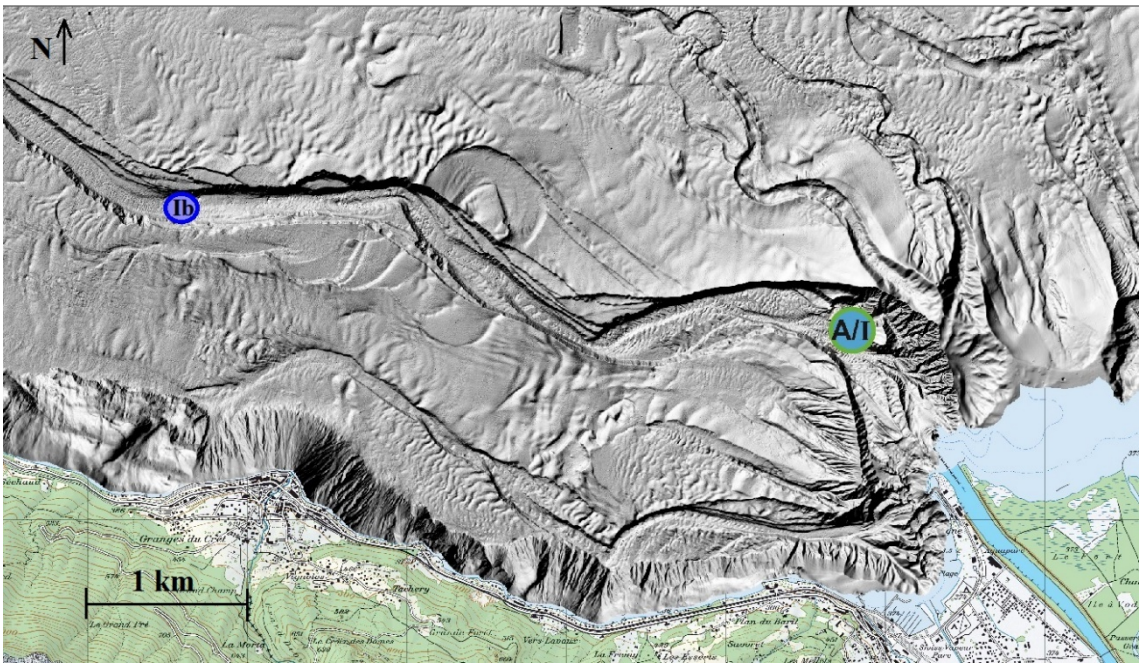

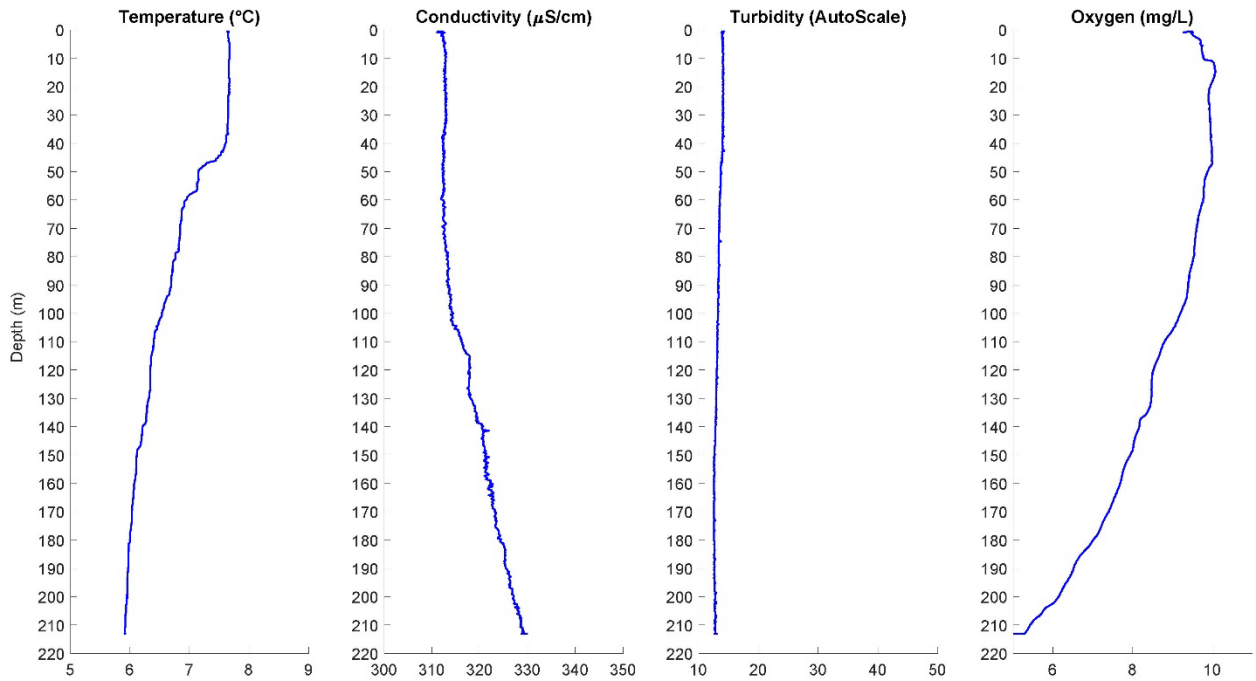

Appendix IV-4: Isotopic and chemical analyses results (first: April campaign, second: September campaign). "R" corresponds to the Rhône River samples during the sampling campaigns.

April 2019

Sample	Depth (m)	**$\delta^{18}O$ VSMOW**	std. dev.	**δD VSMOW**	std. dev.	**% Rhône ($\delta^{18}O$)**	**$\delta^{13}C$ VPDB**	DIC (mg/L)	**PO_4^{3-} (µgP/L)**	std dev.	**SiO_2 (mg/L)**	std dev.	**NO_3^- (mgN/L)**	std dev.
R'1	-	**-13.44**	0.02	**-99.2**	0.21	-	**-6.41**	117.4	8.4	0.5	3.65	0.06	-	-
R'2	-	**-14.00**	0.02	**-102.1**	0.07	-	**-7.29**	93.8	4.2	0.0	3.42	0.01	0.427	0.000
R'3	-	**-14.11**	0.07	**-102.7**	0.42	-	**-6.92**	72.0	10.1	0.9	2.32	0.00	0.301	0.000
A10	1.5	**-12.34**	0.03	**-88.0**	0.10	0	**-6.46**	98.4	0.3	0.2	1.50	0.02	0.435	0.000
A9	2.5	**-12.30**	0.04	**-88.2**	0.06	0	**-6.18**	105.6	1.0	0.2	0.91	0.01	0.423	0.000
A8	5.0	**-12.31**	0.04	**-88.1**	0.27	0	**-6.46**	94.8	2.3	0.2	1.16	0.00	-	-
A7	7.5	**-12.33**	0.06	**-87.8**	0.32	0	**-6.37**	99.7	0.2	0.2	2.00	0.02	-	-
A6	10.1	**-12.33**	0.04	**-87.6**	0.17	0	**-6.87**	88.9	0.7	0.2	0.99	0.01	0.456	0.000
A5	15.0	**-12.37**	0.03	**-87.9**	0.08	0	**-6.68**	103.5	1.1	0.2	2.29	0.03	0.468	0.000
A4	20.1	**-12.34**	0.05	**-88.1**	0.09	0	**-6.88**	93.2	1.2	0.2	1.73	0.04	0.473	0.000
A3	30.1	**-12.32**	0.03	**-87.9**	0.02	0	**-7.28**	82.2	1.4	0.2	2.03	0.16	0.480	0.000
A2	100.9	**-12.40**	0.03	**-88.2**	0.09	0	**-7.29**	106.2	5.0	0.2	2.03	0.08	0.512	0.000
A1	305.0	**-12.36**	0.01	**-88.7**	0.60	0	**-9.17**	120.7	29.0	0.5	11.75	0.01	0.412	0.000
B10	1.0	**-12.22**	0.04	**-88.6**	0.24	0	**-6.36**	98.5	0.7	0.2	0.77	0.02	0.458	0.000
B9	2.5	**-12.33**	0.03	**-88.7**	0.20	0	**-6.39**	99.6	0.7	0.2	0.83	0.01	0.453	0.000
B8	5.1	**-12.28**	0.02	**-88.5**	0.10	0	**-6.29**	116.2	0.7	0.2	0.76	0.01	0.452	0.000
B7	7.6	**-12.28**	0.01	**-88.5**	0.10	0	**-6.40**	114.4	0.6	0.2	0.82	0.01	0.358	0.000
B6	9.6	**-12.34**	0.03	**-88.4**	0.08	0	**-6.50**	105.2	2.3	0.2	1.21	0.00	0.467	0.000
B5	14.9	**-12.25**	0.03	**-88.6**	0.20	0	**-6.62**	100.0	0.5	0.2	0.90	0.01	0.810	0.000
B4	20.1	**-12.19**	0.05	**-88.7**	0.06	0	**-6.61**	111.0	5.5	0.2	1.68	0.00	0.475	0.000
B3	29.9	**-12.28**	0.03	**-88.5**	0.18	0	**-6.67**	108.6	1.9	0.2	1.08	0.00	0.474	0.000
B2	100.4	**-12.29**	0.04	**-88.6**	0.14	0	**-7.28**	114.1	6.3	0.2	3.38	0.07	0.516	0.000
B1	210.4	**-12.31**	0.06	**-88.3**	0.17	0	**-8.05**	120.2	18.5	0.5	3.05	0.02	0.487	0.000
C10	1.2	**-12.23**	0.05	**-89.2**	0.17	0	**-6.37**	93.0	0.6	0.2	0.79	0.00	0.428	0.000
C9	2.0	**-12.21**	0.05	**-89.3**	0.13	0	**-6.67**	70.8	0.2	0.2	0.71	0.01	0.422	0.000
C8	5.1	**-12.24**	0.01	**-88.8**	0.07	0	**-6.37**	105.8	0.2	0.2	0.68	0.02	0.455	0.000
C7	7.6	**-12.28**	0.03	**-88.6**	0.04	0	**-6.30**	107.2	0.4	0.2	0.79	0.04	0.457	0.000
C6	10.3	**-12.34**	0.01	**-88.5**	0.07	0	**-6.33**	113.9	0.5	0.2	0.76	0.02	0.405	0.000
C5	14.9	**-12.31**	0.06	**-88.5**	0.10	0	**-6.78**	105.9	1.2	0.2	1.04	0.00	0.477	0.000
C4	20.3	**-12.36**	0.05	**-88.4**	0.12	0	**-6.84**	107.9	1.1	0.2	0.91	0.00	0.470	0.000
C3	30.0	**-12.30**	0.03	**-88.6**	0.08	0	**-6.73**	117.7	1.5	0.2	0.83	0.01	0.479	0.000
C2	47.5	**-12.29**	0.04	**-88.7**	0.13	0	-	-	3.2	0.2	1.57	0.04	0.503	0.000
C1	175.3	**-12.23**	0.01	**-88.3**	0.10	0	**-8.37**	112.4	18.5	0.5	3.60	0.01	0.772	0.000
D10	1.0	**-12.01**	0.11	**-90.3**	0.25	0	**-6.51**	109.2	0.3	0.2	0.89	0.01	0.258	0.000
D9	2.3	**-12.22**	0.05	**-91.3**	0.28	6	**-5.85**	107.4	0.4	0.2	1.46	0.02	0.473	0.000
D8	5.1	**-12.48**	0.02	**-92.8**	0.13	20	**-6.35**	111.4	0.7	0.2	1.76	0.01	0.173	0.000
D7	7.5	**-12.50**	0.02	**-93.0**	0.09	21	**-6.69**	109.9	1.1	0.2	2.00	0.06	0.394	0.000
D6	10.6	**-12.69**	0.12	**-92.4**	0.29	31	**-5.70**	110.4	6.2	0.2	1.84	0.01	0.505	0.000
D5	15.1	**-12.60**	0.11	**-92.7**	0.26	26	**-5.98**	114.8	1.5	0.2	1.77	0.01	0.411	0.000
D4	20.0	**-12.76**	0.04	**-91.7**	0.20	35	**-6.77**	107.3	1.1	0.2	2.11	0.01	0.503	0.000
D3	29.9	**-12.28**	0.05	**-89.7**	0.10	9	**-6.79**	101.8	0.8	0.2	1.09	0.03	0.474	0.000
D40	40.4	**-12.11**	0.14	**-89.4**	0.29	1	**-7.09**	114.8	0.9	0.2	1.05	0.02	0.479	0.000
D2	65.4	**-12.20**	0.01	**-89.3**	0.16	5	**-6.80**	101.9	2.0	0.2	1.25	0.10	0.494	0.000
D1	100.5	**-12.31**	0.06	**-89.0**	0.10	11	**-6.85**	120.4	3.8	0.2	1.86	0.01	0.373	0.000
I10	1.3	**-12.13**	0.02	**-89.3**	0.09	2	**-6.57**	111.4	0.3	0.3	0.91	0.02	0.446	0.000
I9	2.6	**-12.08**	0.07	**-89.2**	0.46	0	**-6.55**	110.6	0.1	0.3	0.76	0.02	0.444	0.000
I8	5.2	**-12.11**	0.07	**-89.3**	0.43	0	**-7.15**	109.8	0.4	0.3	0.75	0.02	0.450	0.000
I7	7.5	**-12.07**	0.05	**-89.2**	0.21	0	**-6.46**	112.2	0.0	0.3	0.85	0.02	0.450	0.000

I6	10.2	**-12.08**	0.03	**-89.3**	0.17	0	**-6.56**	101.7	0.0	0.3	0.85	0.01	0.450	0.000
I5	15.4	**-12.10**	0.04	**-89.1**	0.24	0	**-6.41**	113.6	0.0	0.3	0.79	0.02	0.453	0.000
I4	20.3	**-12.13**	0.05	**-89.7**	0.14	2	**-6.56**	110.3	0.1	0.3	0.74	0.01	0.448	0.000
I3	29.2	**-12.08**	0.02	**-89.3**	0.27	0	**-6.75**	104.5	0.3	0.3	0.82	0.00	0.453	0.000
I2	65.3	**-12.41**	0.03	**-91.3**	0.17	20	**-6.72**	112.8	1.6	0.0	1.32	0.00	0.467	0.000
I1	101.4	**-12.24**	0.05	**-90.8**	0.68	9	**-7.43**	133.5	7.9	0.5	1.58	0.00	0.504	0.000
I75	76.2	**-12.30**	0.06	**-90.7**	0.32	13	**-6.69**	112.3	-	-	-	-	-	-
II10	1.2	**-12.16**	0.06	**-89.7**	0.39	4	**-6.48**	114.2	-	-	0.90	0.02	0.442	0.000
II9	2.5	**-12.12**	0.01	**-89.4**	0.17	1	**-6.62**	105.8	0.0	0.3	0.81	0.05	0.444	0.000
II8	5.5	**-12.10**	0.04	**-89.5**	0.04	0	**-6.49**	113.2	0.0	0.3	0.73	0.00	0.443	0.000
II6	7.5	**-12.12**	0.01	**-89.6**	0.02	1	**-6.53**	109.3	0.1	0.3	0.84	0.01	0.451	0.000
II7	10.2	**-12.12**	0.02	**-89.4**	0.06	1	**-6.63**	106.8	0.1	0.3	0.73	0.00	0.448	0.000
II5	15.2	**-12.03**	0.03	**-89.0**	0.06	0	**-6.66**	99.7	0.1	0.3	0.80	0.00	0.449	0.000
II4	20.7	**-12.08**	0.03	**-89.0**	0.21	0	**-6.84**	112.7	0.2	0.3	0.85	0.02	0.454	0.000
II3	30.5	**-12.09**	0.02	**-89.4**	0.27	0	**-6.72**	111.4	0.3	0.3	1.19	0.01	0.457	0.000
II2	45.5	**-12.16**	0.03	**-89.7**	0.19	4	**-6.65**	116.5	0.1	0.3	0.88	0.01	0.457	0.000
II1	50.2	**-12.16**	0.04	**-89.7**	0.35	4	**-6.59**	114.4	0.2	0.3	0.88	0.01	0.460	0.000
II40	40.5	**-12.17**	0.09	**-89.7**	0.23	5	**-6.51**	104.4	0.1	0.3	-	-	-	-
III8	1.4	**-12.14**	0.04	**-89.8**	0.26	2	**-6.51**	110.1	0.2	0.3	0.83	0.01	0.440	0.000
III7	2.5	**-12.10**	0.07	**-89.4**	0.34	0	**-6.55**	101.2	0.3	0.3	0.87	0.00	0.449	0.000
III6	5.0	**-12.16**	0.05	**-89.7**	0.22	3	**-6.47**	109.7	0.0	0.3	0.80	0.00	0.399	0.000
III5	7.3	**-12.12**	0.06	**-89.6**	0.13	1	**-6.60**	107.2	0.1	0.3	0.90	0.00	0.440	0.000
III4	9.5	**-12.21**	0.05	**-90.2**	0.21	5	**-6.65**	108.5	0.6	0.3	1.03	0.02	0.445	0.000
III3	15.4	**-12.51**	0.08	**-91.9**	0.24	20	**-6.68**	104.8	5.7	0.5	1.31	0.00	-	-
III2	20.2	**-12.59**	0.05	**-92.7**	0.29	24	**-6.66**	112.0	4.6	0.0	1.44	0.00	0.449	0.000
III1	21.5	**-12.60**	0.05	**-92.5**	0.15	25	**-6.56**	114.8	3.4	0.0	1.36	0.01	0.448	0.000
IV9	0.9	**-12.22**	0.01	**-90.0**	0.05	6	**-6.53**	107.8	0.0	0.3	0.81	0.00	-	-
IV8	2.5	**-12.18**	0.01	**-89.9**	0.20	4	**-6.52**	108.7	0.0	0.3	0.81	0.00	0.366	0.000
IV7	5.2	**-12.12**	0.07	**-89.5**	0.31	1	**-6.38**	111.7	0.0	0.3	0.77	0.01	0.443	0.000
IV6	7.5	**-12.16**	0.02	**-89.8**	0.11	3	**-6.45**	106.0	0.0	0.3	0.80	0.03	0.450	0.000
IV5	10.6	**-12.13**	0.06	**-89.7**	0.26	2	**-6.52**	105.1	0.0	0.3	0.84	0.03	-	-
IV4	15.1	**-12.12**	0.06	**-89.5**	0.19	1	**-6.50**	102.3	0.0	0.3	0.77	0.00	0.454	0.000
IV3	20.2	**-12.17**	0.03	**-89.8**	0.10	4	**-6.48**	108.3	0.0	0.3	0.65	0.00	0.434	0.000
IV2	30.2	**-12.15**	0.09	**-89.8**	0.13	3	**-6.52**	110.9	0.0	0.3	0.89	0.01	0.445	0.000
IV1	33.8	**-12.14**	0.01	**-89.6**	0.14	2	**-6.59**	105.6	0.2	0.3	0.90	0.00	0.448	0.000
V9	1.0	**-13.15**	0.06	**-96.3**	0.15	52	**-7.00**	90.3	5.9	0.5	1.55	0.02	0.383	0.000
V8	2.6	**-12.89**	0.05	**-94.8**	0.22	39	**-6.45**	124.5	3.2	0.0	1.47	0.00	0.398	0.000
V7	5.2	**-13.16**	0.00	**-96.5**	0.09	53	**-6.85**	88.8	4.8	0.0	1.61	0.03	0.343	0.000
V6	7.5	**-13.12**	0.02	**-96.2**	0.11	51	**-6.86**	90.6	4.3	0.0	1.85	0.00	0.384	0.000
V5	10.3	**-13.04**	0.02	**-95.5**	0.18	47	**-6.61**	97.5	4.8	0.0	1.80	0.02	0.413	0.000
V4	15.3	**-13.30**	0.00	**-97.2**	0.06	60	**-6.92**	90.3	6.5	0.5	1.78	0.01	0.383	0.000
V3	20.2	**-12.08**	0.03	**-92.2**	0.15	0	**-6.73**	100.7	3.6	0.0	1.19	0.00	0.212	0.000
V2	25.6	**-12.50**	0.20	**-92.6**	0.72	20	**-6.63**	99.0	3.0	0.0	0.91	0.01	0.377	0.000
V1	30.1	**-12.64**	0.05	**-92.9**	0.20	27	**-6.96**	93.2	2.7	0.0	1.32	0.01	0.413	0.000

September 2019

Sample	Depth (m)	**$\delta^{18}O$ VSMOW**	std. dev.	**δD VSMOW**	std. dev.	**% Rhône ($\delta^{18}O$)**	**$\delta^{13}C$ VPDB**	DIC (mg/L)	**PO_4^{3-} (µgP/L)**	std dev.	**SiO_2 (mg/L)**	std dev.	**NO_3^- (mgN/L)**	std dev.
R'1	-	**-14.17**	0.05	**-103.0**	0.35	-	**-6.62**	51.0	2.0	0.4	2.29	0.00	0.345	0.001
R'2	-	**-14.11**	0.04	**-102.4**	0.20	-	**-6.90**	46.4	2.9	0.4	1.97	0.03	0.265	0.002
R'3	-	**-13.96**	0.02	**-102.4**	0.10	-	**-5.25**	42.9	6.0	0.1	2.13	0.12	0.344	0.003
R'4	-	**-13.97**	0.05	**-101.4**	0.17	-	**-6.33**	56.9	2.4	0.4	2.40	0.16	0.375	0.000
R'5	-	**-14.04**	0.02	**-101.7**	0.14	-	**-6.53**	55.1	4.7	0.4	1.89	0.03	0.273	0.000
1-1	1.4	**-12.03**	0.04	**-89.4**	0.16	0.00	**-3.84**	73.2	0.5	0.4	0.26	0.00	0.218	0.001
1-2	2.5	**-12.01**	0.02	**-88.6**	0.05	0.00	**-4.34**	56.2	0.6	0.4	0.25	0.01	0.215	0.001
1-3	5.3	**-12.01**	0.02	**-88.3**	0.39	0.00	**-3.79**	73.0	0.6	0.4	0.28	0.01	0.225	0.001
1-4	7.6	**-11.83**	0.03	**-87.7**	0.15	0.00	**-4.23**	55.7	0.5	0.4	0.29	0.00	0.223	0.001
1-5	10.0	**-11.89**	0.02	**-87.7**	0.33	0.00	**-3.86**	77.3	0.9	0.4	0.17	0.00	0.224	0.000
1-6	15.6	**-12.02**	0.05	**-88.8**	0.30	0.00	**-4.55**	76.3	0.7	0.4	0.37	0.03	0.242	0.000
1-7	20.8	**-12.70**	0.02	**-93.1**	0.18	29.89	**-5.57**	62.4	2.8	0.4	1.17	0.00	0.315	0.002
1-8	25.6	**-12.73**	0.03	**-93.1**	0.22	31.18	**-6.31**	65.7	1.4	0.4	1.11	0.00	0.309	0.001
1-9	30.7	**-12.32**	0.02	**-91.1**	0.20	10.93	**-6.87**	84.6	1.3	0.4	1.08	0.02	0.450	0.008
1-10	45.7	**-12.12**	0.04	**-89.8**	0.07	0.81	**-7.26**	88.7	1.6	0.4	0.98	0.01	0.485	0.001
2-1	1.4	**-12.01**	0.05	**-88.4**	0.13	0.00	**-3.88**	80.7	0.5	0.4	0.27	0.01	0.217	0.002
2-2	2.5	**-12.02**	0.03	**-88.6**	0.13	0.00	**-4.23**	61.1	0.6	0.4	0.24	0.01	0.222	0.000
2-3	5.2	**-12.02**	0.03	**-88.4**	0.20	0.00	**-4.05**	63.1	0.5	0.4	0.27	0.01	0.218	0.000
2-4	7.5	**-12.01**	0.02	**-88.4**	0.34	0.00	**-3.92**	75.0	0.4	0.4	0.26	0.01	0.220	0.002
2-6	14.9	**-12.02**	0.04	**-88.8**	0.09	0.00	**-4.26**	62.0	0.3	0.4	0.40	0.00	0.231	0.000
2-7	20.1	**-12.52**	0.04	**-91.7**	0.15	21.06	**-5.69**	66.5	1.0	0.4	0.77	0.00	0.329	0.000
2-8	25.4	**-12.33**	0.01	**-90.6**	0.20	11.60	**-6.80**	91.6	1.0	0.4	0.67	0.01	0.445	0.001
2-9	30.2	**-12.26**	0.03	**-90.3**	0.13	7.87	**-7.34**	78.6	0.7	0.4	0.75	0.01	0.340	0.003
2-10	40.3	**-12.23**	0.05	**-89.8**	0.19	6.52	**-7.10**	105.7	1.4	0.4	1.00	0.00	0.474	0.000
3-1	1.5	**-11.99**	0.04	**-88.5**	0.17	0.00	**-4.00**	72.2	0.5	0.4	0.33	0.03	0.217	0.004
3-2	2.6	**-11.97**	0.05	**-88.3**	0.14	0.00	**-3.99**	69.9	0.9	0.4	0.31	0.01	0.217	0.004
3-3	5.5	**-11.98**	0.05	**-88.2**	0.12	0.00	**-3.77**	82.0	0.7	0.4	0.28	0.01	0.221	0.000
3-4	7.3	**-11.98**	0.05	**-88.4**	0.13	0.00	**-4.15**	68.9	0.6	0.4	0.33	0.01	0.218	0.003
3-5	9.7	**-12.01**	0.01	**-88.4**	0.06	0.00	**-3.72**	-	0.6	0.4	0.28	0.00	-	-
3-6	15.4	**-12.01**	0.03	**-88.5**	0.09	0.00	**-3.91**	72.0	0.9	0.4	0.26	0.10	0.225	0.000
3-7	19.9	**-12.60**	0.01	**-92.3**	0.24	24.81	**-5.63**	65.9	1.1	0.4	0.93	0.10	0.324	0.004
3-8	25.3	**-12.30**	0.06	**-90.6**	0.13	9.96	**-7.05**	76.0	1.2	0.4	0.69	0.01	0.466	0.003
3-9	30.2	**-12.23**	0.05	**-90.2**	0.19	6.25	**-7.17**	82.9	1.3	0.4	0.84	0.00	0.498	0.006
3-10	40.3	**-12.18**	0.06	**-90.2**	0.26	4.20	**-7.48**	85.1	1.5	0.4	1.06	0.05	0.504	0.004
4-1	1.5	**-11.97**	0.06	**-88.5**	0.26	0.00	**-4.26**	66.5	1.2	0.4	0.27	0.00	0.223	0.003
4-2	2.5	**-11.98**	0.04	**-88.4**	0.19	0.00	**-3.94**	67.5	1.1	0.4	0.29	0.00	0.223	0.005
4-3	5.1	**-11.98**	0.05	**-88.4**	0.35	0.00	**-4.14**	82.2	1.2	0.4	0.27	0.00	0.233	0.000
4-4	7.3	**-11.99**	0.06	**-88.4**	0.14	0.00	**-3.95**	73.4	0.9	0.4	0.30	0.01	0.216	0.002
4-5	9.9	**-12.04**	0.03	**-88.8**	0.17	0.00	**-4.03**	70.4	1.2	0.4	0.35	0.00	0.222	0.002
4-6	14.9	**-12.29**	0.02	**-90.3**	0.03	9.42	**-4.28**	67.5	1.0	0.4	0.52	0.00	0.204	0.001
4-7	19.9	**-12.78**	0.03	**-93.5**	0.09	33.80	**-6.03**	-	1.6	0.4	0.94	0.00	-	-
4-8	25.2	**-12.29**	0.03	**-90.8**	0.28	9.33	**-7.25**	84.8	1.1	0.4	0.82	0.03	0.513	0.010
4-9	30.5	**-12.02**	0.03	**-88.4**	0.15	0.00	**-4.40**	69.8	1.8	0.1	0.27	0.00	0.230	0.001
4-10	40.8	**-12.18**	0.04	**-89.9**	0.25	4.12	**-7.20**	83.7	1.3	0.4	0.93	0.03	0.515	0.001
5-1	1.5	**-11.98**	0.04	**-88.6**	0.11	0.00	**-4.35**	59.7	1.1	0.4	0.34	0.00	0.219	0.002
5-2	2.6	**-12.00**	0.05	**-88.6**	0.15	0.00	**-3.90**	67.3	1.8	0.1	0.28	0.01	0.221	0.003
5-3	5.1	**-12.05**	0.05	**-88.8**	0.09	0.00	**-4.46**	-	0.7	0.2	0.18	0.04	-	-
5-4	7.5	**-12.03**	0.05	**-88.6**	0.17	0.00	**-4.34**	62.3	0.6	0.2	0.29	0.00	0.225	0.004
5-5	10.2	**-12.02**	0.04	**-88.8**	0.14	0.00	**-4.31**	-	0.4	0.2	0.30	0.02	-	-
5-6	15.0	**-12.45**	0.01	**-91.6**	0.02	17.39	**-6.16**	58.0	0.9	0.2	0.74	0.01	0.320	0.002
5-7	17.4	**-12.50**	0.02	**-91.9**	0.11	19.98	**-6.21**	67.8	1.1	0.1	0.74	0.01	0.335	0.007

5-8	19.9	**-12.54**	0.03	**-92.4**	0.27	21.98	**-6.32**	66.1	1.0	0.1	0.82	0.01	0.333	0.002
5-9	23.0	**-12.59**	0.03	**-92.5**	0.02	24.28	**-6.83**	55.9	1.7	0.1	0.88	0.00	0.354	0.002
5-10	26.0	**-12.56**	0.06	**-92.4**	0.20	22.75	**-6.99**	66.8	1.6	0.1	0.77	0.01	0.364	0.000
A-1	1.4	**-12.10**	0.02	**-90.6**	1.10	0.08	**-4.33**	69.9	0.4	0.2	0.31	0.00	0.226	0.005
A-2	2.3	**-12.07**	0.03	**-88.7**	0.04	0.00	**-4.49**	62.9	1.3	0.2	0.32	0.00	0.236	0.003
A-3	5.1	**-12.03**	0.01	**-88.4**	0.07	0.00	**-4.60**	66.1	1.2	0.2	0.32	0.00	0.233	0.002
A-4	7.6	**-12.01**	0.03	**-88.2**	0.05	0.00	**-4.51**	67.0	0.2	0.2	0.32	0.01	0.232	0.001
A-5	10.2	**-12.03**	0.04	**-88.2**	0.16	0.00	**-4.63**	62.4	2.9	0.2	0.35	0.00	0.207	0.001
A-6	15.6	**-12.19**	0.02	**-89.4**	0.01	4.89	**-4.44**	71.6	5.2	0.1	0.50	0.01	0.223	0.001
A-7	20.7	**-12.49**	0.04	**-91.3**	0.10	20.46	**-4.69**	-	1.7	0.2	0.83	0.00	-	-
A-8	24.9	**-12.63**	0.03	**-92.0**	0.12	27.68	**-6.57**	77.6	0.7	0.2	1.13	0.02	0.416	0.003
A-9	30.3	**-12.25**	0.03	**-90.1**	0.15	7.90	**-7.18**	83.0	1.1	0.2	0.87	0.00	0.515	0.004
A-10	40.4	**-12.19**	0.04	**-89.9**	0.16	4.64	**-7.16**	94.0	3.9	0.2	1.29	0.01	0.508	0.008
B-1	1.6	**-12.05**	0.04	**-88.6**	0.10	0.00	**-4.35**	72.1	0.9	0.2	0.27	0.01	0.226	0.000
B-2	2.4	**-12.01**	0.05	**-88.3**	0.13	0.00	**-4.44**	-	0.9	0.2	0.27	0.00	-	-
B-3	5.0	**-12.05**	0.02	**-88.5**	0.15	0.00	**-4.11**	-	0.3	0.2	0.25	0.00	-	-
B-4	7.6	**-12.05**	0.02	**-88.4**	0.25	0.00	**-4.07**	63.8	2.0	0.2	0.28	0.01	0.170	0.001
B-5	10.1	**-12.04**	0.04	**-88.5**	0.22	0.00	**-4.28**	63.4	0.1	0.2	0.31	0.00	0.228	0.001
B-6	14.9	**-12.05**	0.01	**-88.7**	0.24	0.00	**-4.34**	-	1.4	0.2	0.32	0.00	-	-
B-7	20.5	**-12.52**	0.02	**-91.4**	0.01	21.83	**-5.55**	69.6	1.2	0.2	0.69	0.02	0.296	0.002
B-8	25.7	**-12.63**	0.03	**-92.2**	0.03	27.87	**-6.27**	73.8	2.1	0.2	1.05	0.02	0.386	0.000
B-9	30.1	**-12.23**	0.04	**-90.2**	0.32	6.78	**-7.25**	96.9	1.0	0.2	0.81	0.00	0.513	0.008
B-10	95.3	**-12.21**	0.02	**-90.0**	0.07	5.64	**-7.53**	81.2	6.3	0.1	1.53	0.03	0.504	0.006
C-1	1.5	**-12.05**	0.04	**-88.6**	0.08	0.00	**-3.96**	-	0.4	0.2	0.25	0.01	-	-
C-2	2.3	**-12.03**	0.02	**-88.3**	0.07	0.00	**-4.30**	68.2	0.2	0.2	0.25	0.00	0.224	0.000
C-3	5.0	**-12.05**	0.01	**-88.4**	0.20	0.00	**-5.01**	75.6	1.2	0.2	0.28	0.00	0.225	0.003
C-4	7.6	**-12.04**	0.03	**-88.5**	0.18	0.00	**-4.33**	74.1	1.5	0.2	0.27	0.00	0.225	0.004
C-5	10.2	**-12.06**	0.06	**-88.5**	0.17	0.00	**-4.17**	80.6	0.8	0.2	0.28	0.00	0.227	0.002
C-6	15.2	**-12.13**	0.01	**-88.9**	0.14	1.74	**-4.34**	81.4	2.1	0.2	0.35	0.00	0.250	0.004
C-7	20.1	**-12.45**	0.03	**-91.1**	0.22	18.14	**-5.46**	69.1	0.6	0.2	0.67	0.00	0.301	0.001
C-8	25.3	**-12.73**	0.03	**-92.9**	0.22	32.96	**-6.05**	66.1	0.9	0.2	1.35	0.01	0.270	0.001
C-9	30.2	**-12.27**	0.03	**-90.3**	0.12	9.13	**-7.33**	82.7	0.4	0.2	0.70	0.00	0.518	0.009
C-10	110.3	**-12.17**	0.03	**-89.6**	0.28	3.62	**-7.63**	80.2	6.3	0.1	1.69	0.03	0.504	0.011
D-1	1.7	**-12.03**	0.02	**-88.2**	0.06	0.00	**-4.21**	67.2	0.0	0.2	0.26	0.01	0.228	0.002
D-2	2.6	**-12.04**	0.02	**-88.5**	0.11	0.00	**-4.22**	-	-0.1	0.2	0.27	0.00	-	-
D-3	5.0	**-12.02**	0.05	**-88.5**	0.17	0.00	**-4.02**	79.0	0.5	0.2	0.28	0.00	0.228	0.004
D-4	7.2	**-12.05**	0.06	**-88.6**	0.15	0.00	**-4.30**	-	0.3	0.2	0.28	0.00	-	-
D-5	10.2	**-12.09**	0.04	**-88.8**	0.05	0.00	**-4.16**	73.6	-0.4	0.2	0.27	0.00	0.231	0.003
D-6	15.4	**-12.13**	0.04	**-89.1**	0.13	1.71	**-4.33**	73.5	0.0	0.2	0.33	0.01	0.241	0.003
D-7	20.3	**-12.44**	0.05	**-91.0**	0.25	17.81	**-5.11**	75.9	0.3	0.2	0.69	0.04	0.298	0.001
D-8	24.9	**-12.52**	0.03	**-91.7**	0.19	22.24	**-6.43**	88.2	0.6	0.2	0.69	0.00	0.390	0.003
D-9	29.6	**-12.26**	0.05	**-90.0**	0.07	8.52	**-7.18**	95.0	0.2	0.2	0.76	0.00	0.507	0.002
D-10	155.6	**-12.21**	0.06	**-89.8**	0.10	6.02	**-7.56**	97.1	10.7	0.3	2.02	0.00	0.481	0.006
E-1	1.6	**-12.03**	0.05	**-88.6**	0.10	0.00	**-3.91**	-	1.2	0.2	0.28	0.00	-	-
E-2	2.7	**-12.03**	0.04	**-88.5**	0.21	0.00	**-3.89**	-	0.5	0.2	0.29	0.00	-	-
E-3	5.1	**-12.05**	0.04	**-88.6**	0.09	0.00	**-4.11**	73.1	0.4	0.2	0.27	0.01	0.227	0.001
E-4	7.6	**-12.07**	0.05	**-88.6**	0.25	0.00	**-4.07**	75.5	-0.3	0.2	0.28	0.00	0.225	0.002
E-5	10.0	**-12.06**	0.06	**-88.7**	0.14	0.00	**-4.14**	76.1	0.0	0.2	0.29	0.00	0.232	0.004
E-6	15.2	**-12.11**	0.04	**-89.0**	0.23	0.34	**-4.32**	-	0.6	0.2	0.30	0.00	-	-
E-7	20.3	**-12.48**	0.06	**-91.3**	0.29	19.69	**-5.28**	78.6	0.9	0.2	0.60	0.00	0.302	0.004
E-8	25.3	**-12.51**	0.06	**-91.5**	0.27	21.39	**-5.88**	85.0	0.3	0.2	0.43	0.01	0.340	0.003
E-9	30.2	**-12.36**	0.02	**-90.6**	0.23	13.69	**-7.20**	96.0	0.1	0.2	0.84	0.00	0.487	0.001
E-10	198.5	**-12.21**	0.01	**-89.7**	0.10	5.89	**-7.95**	105.4	22.6	0.3	2.77	0.02	0.458	0.001

Appendix IV-5: Monthly (main box) and daily (small boxes) fluctuations of oxygen isotope composition of the Rhône River water.

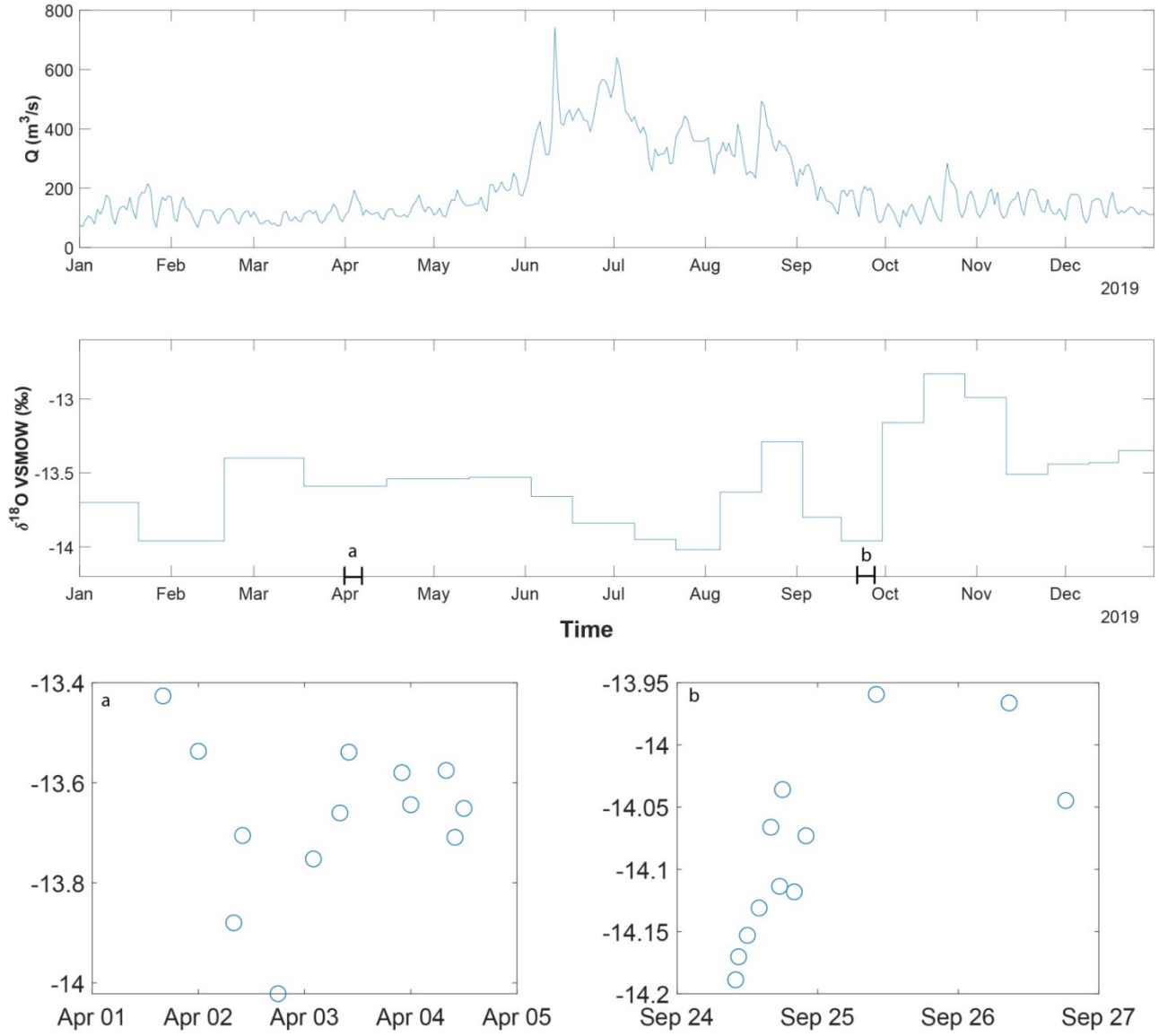

Appendix IV-6: Time series of meteorological parameters during the April 2019 sampling week (Le Bouveret – MeteoSwiss).

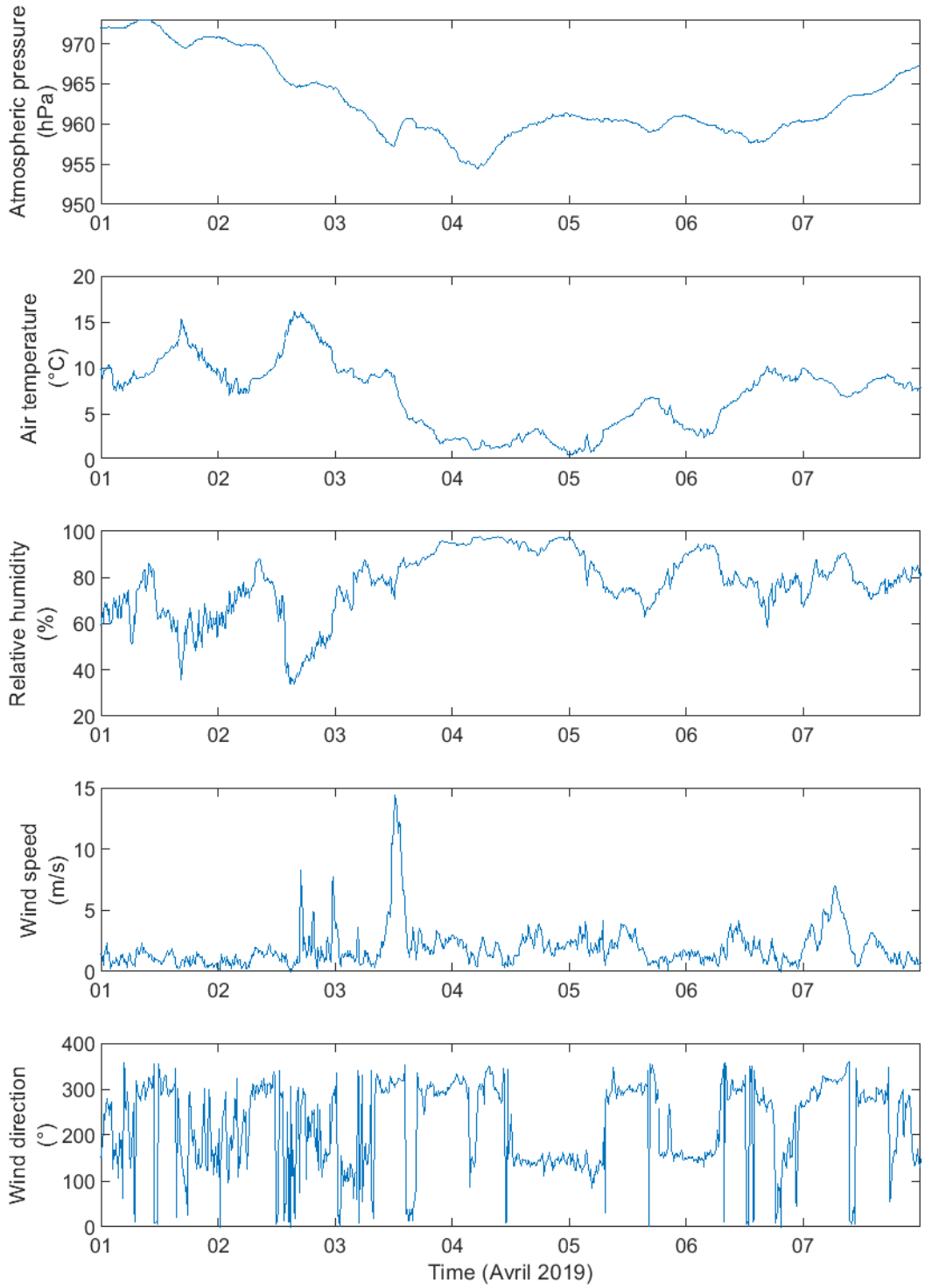

Appendix IV-7: Boxplot of meteorological parameters during the April 2019 sampling campaign (Le Bouveret – MeteoSwiss).

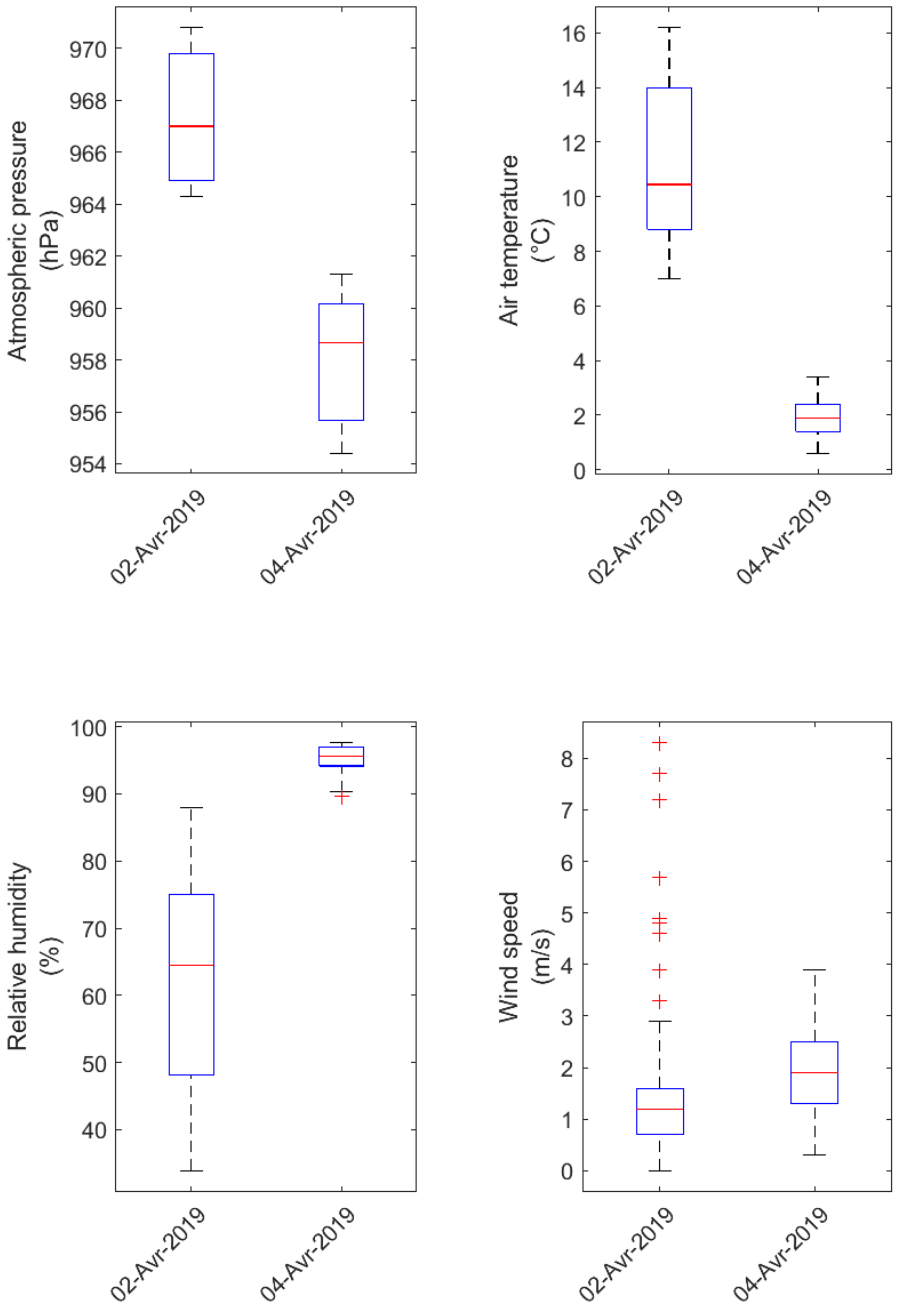

Appendix IV-8: Meteolake simulation showing strong eastward currents in the Haut-Lac on the 3rd of April 2019 at 3 pm (http://meteolakes.ch).

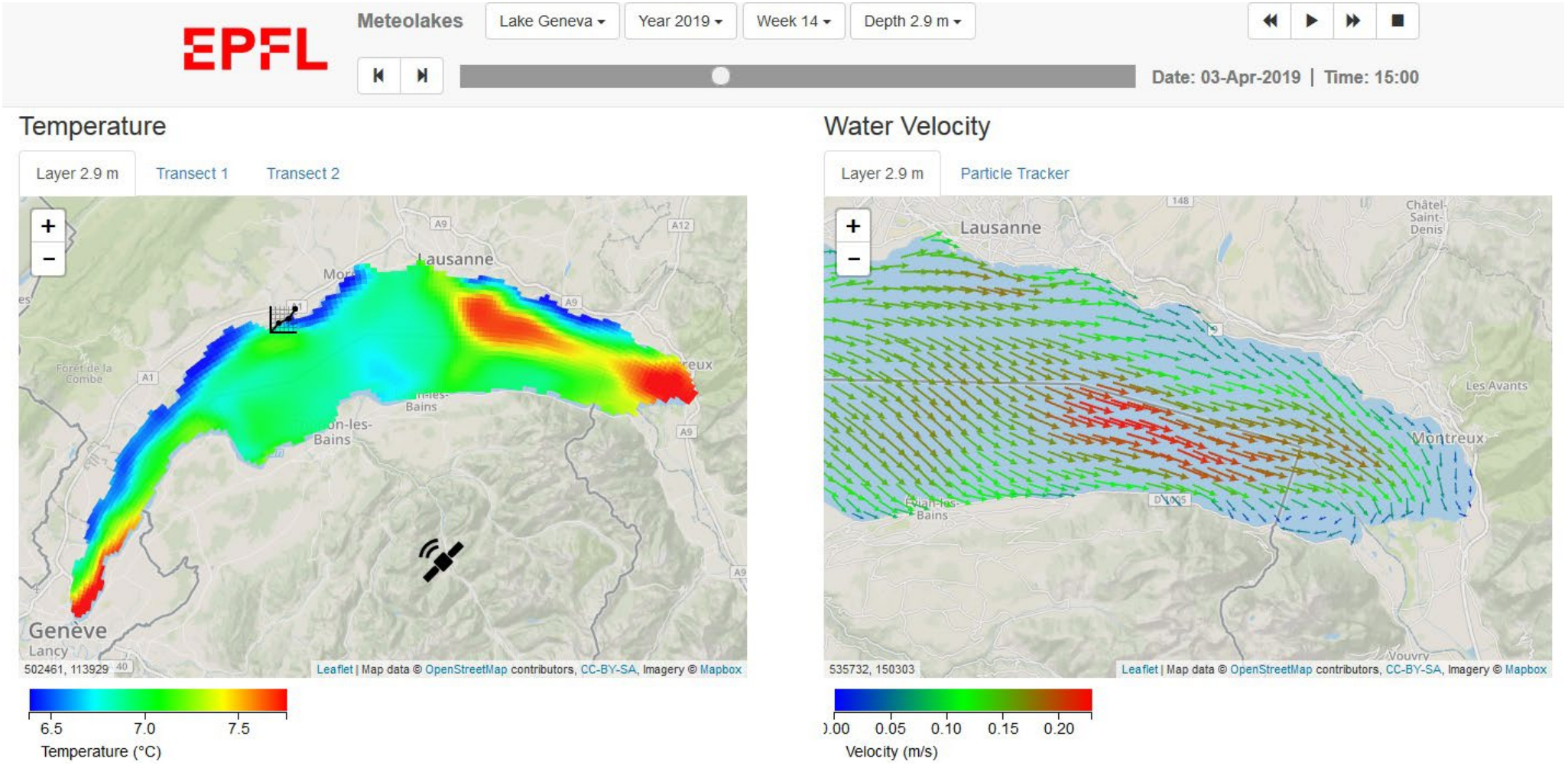

Appendix IV-9: Time series of river parameters during the April 2019 sampling week (Porte du Scex – OFEV).

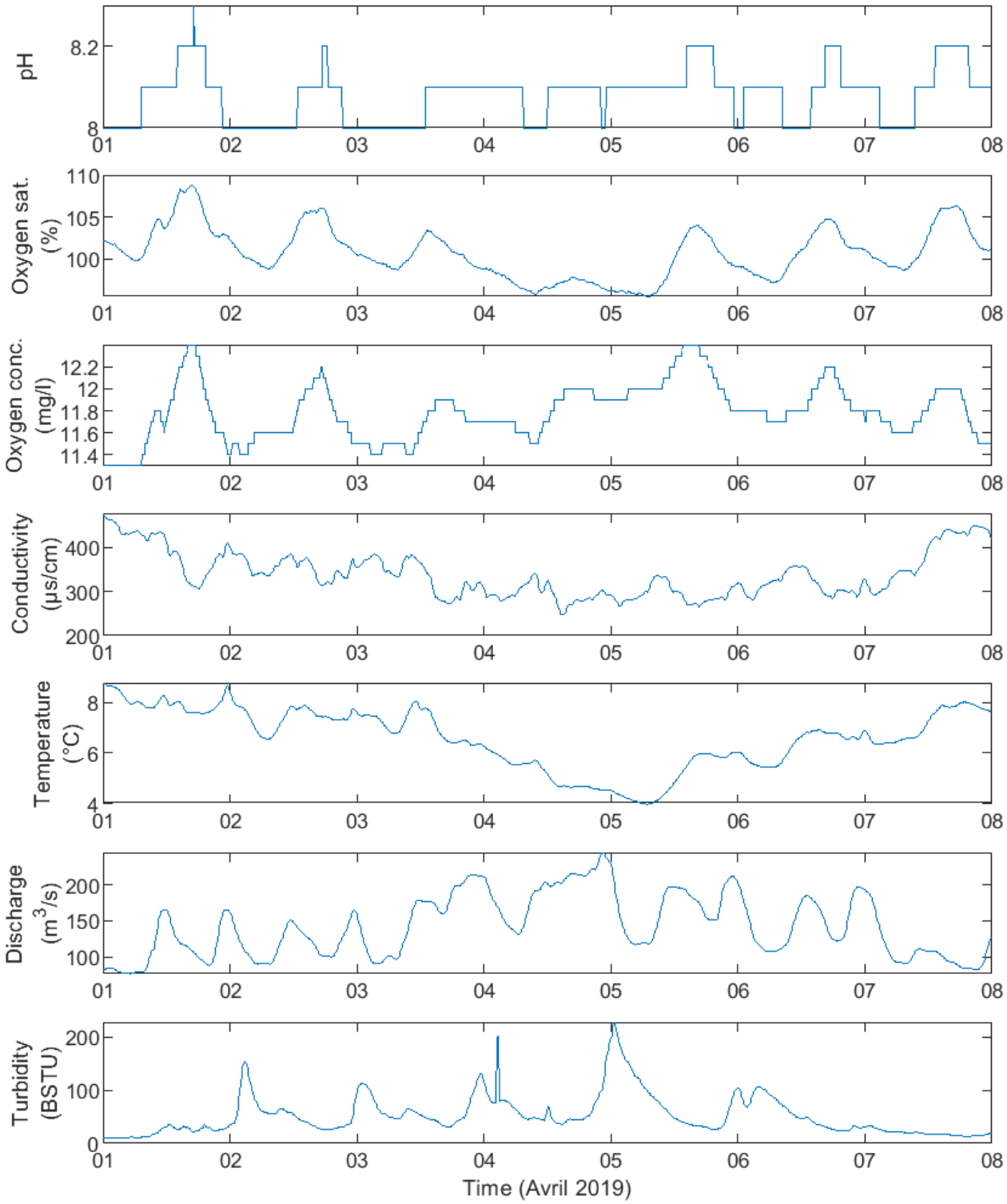

Appendix IV-10: Vertical profiles of lake parameters for the April 1st 2019 (SHL2 station – CIPEL).

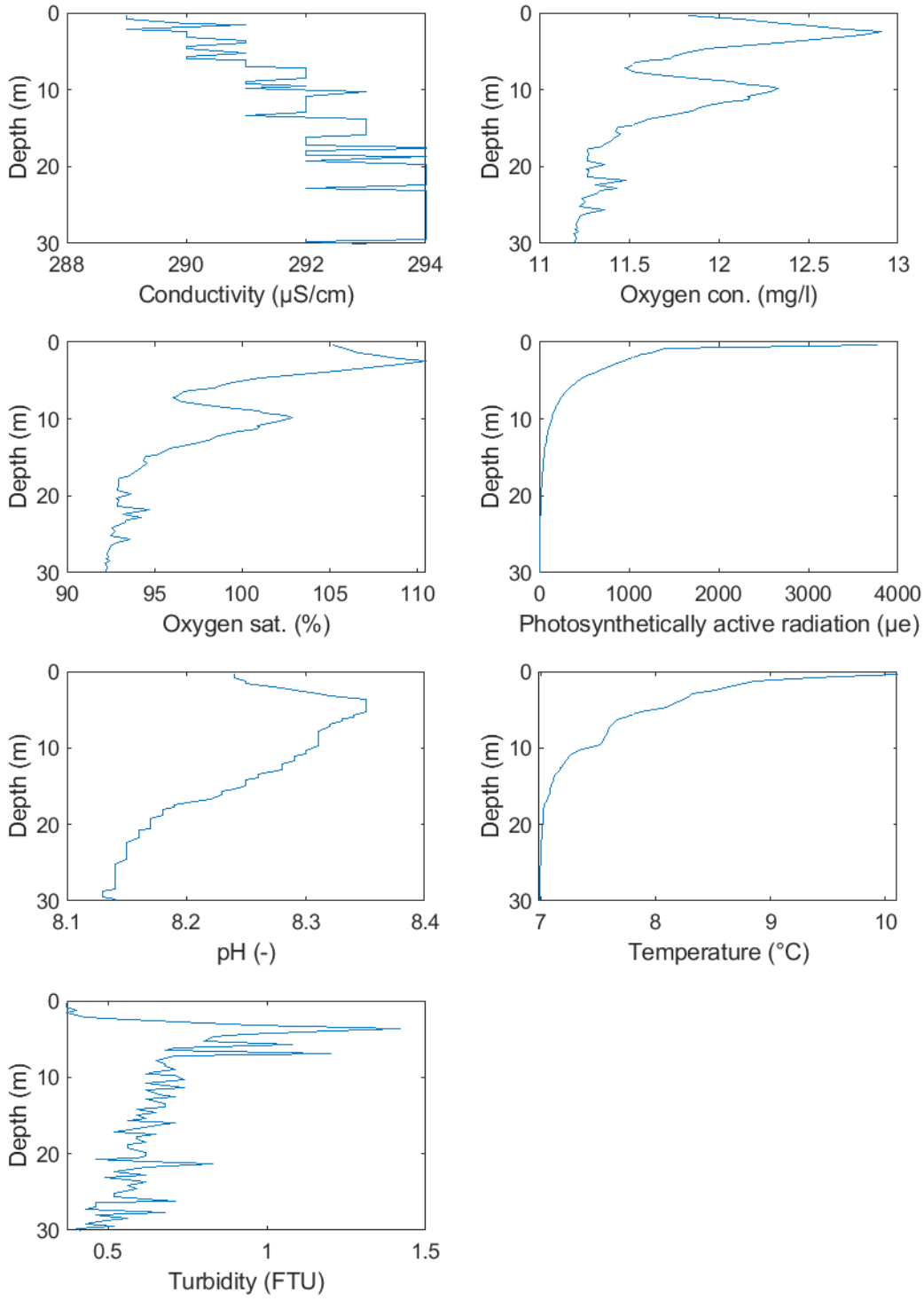

Appendix IV-11: Vertical profiles of lake physico-chemical parameters for the April 1st 2019 (SHL2 station – CIPEL).

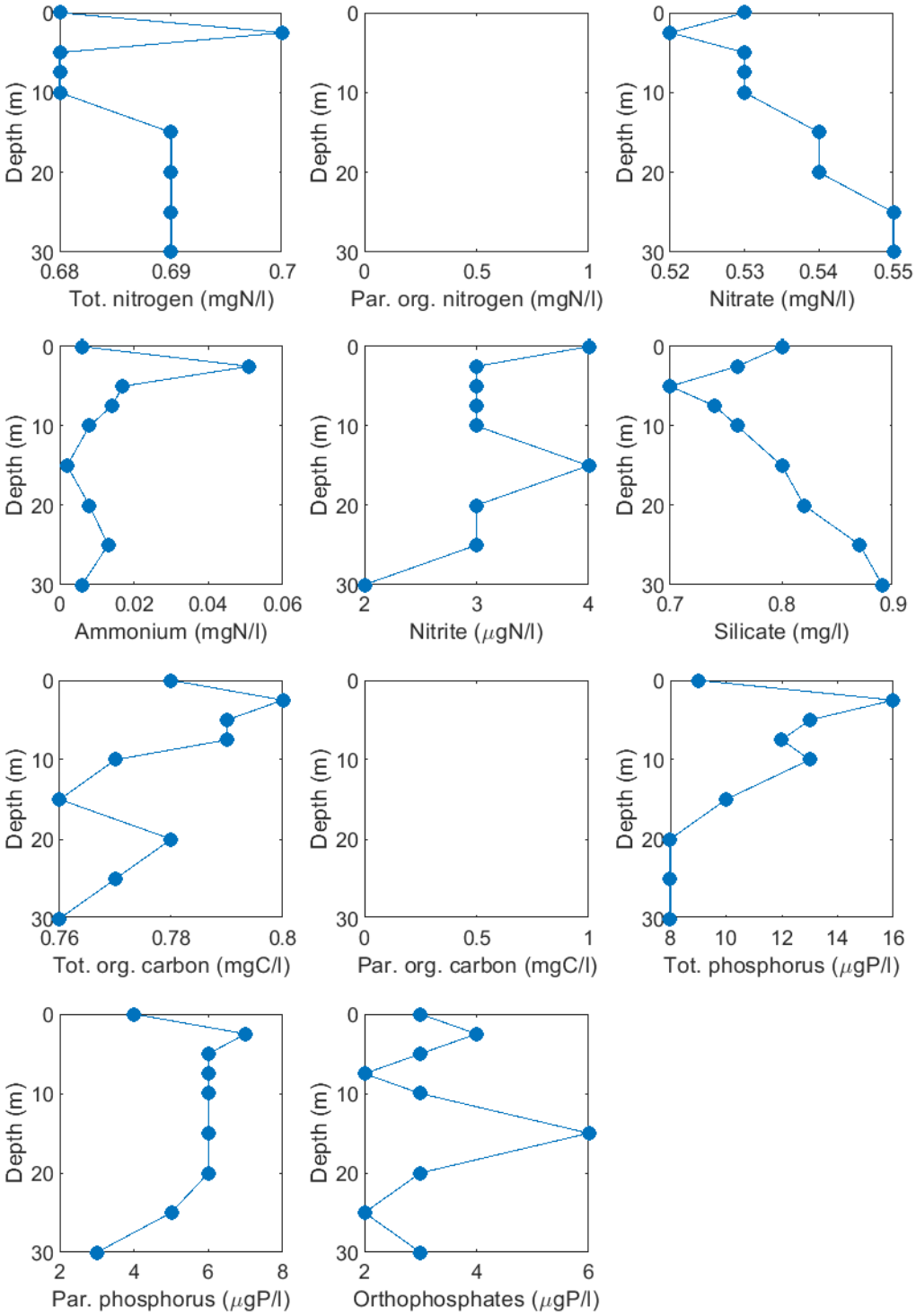

Appendix IV-12: Monitoring profiles of nutrient concentration during winter 2019 (CIPEL).

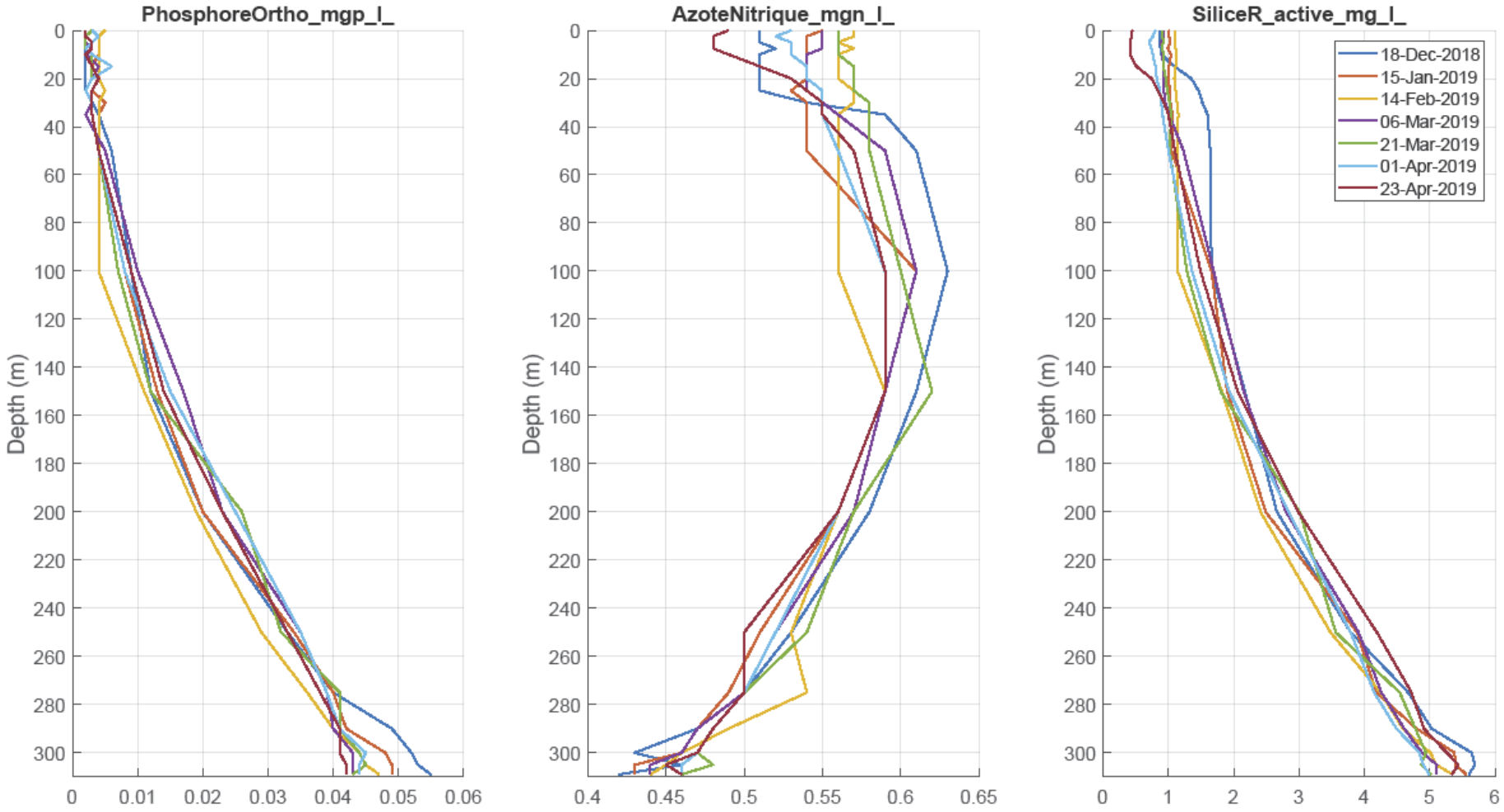

Appendix IV-13: Time series of meteorological parameters during the September 2019 sampling week (Le Bouveret – MeteoSwiss).

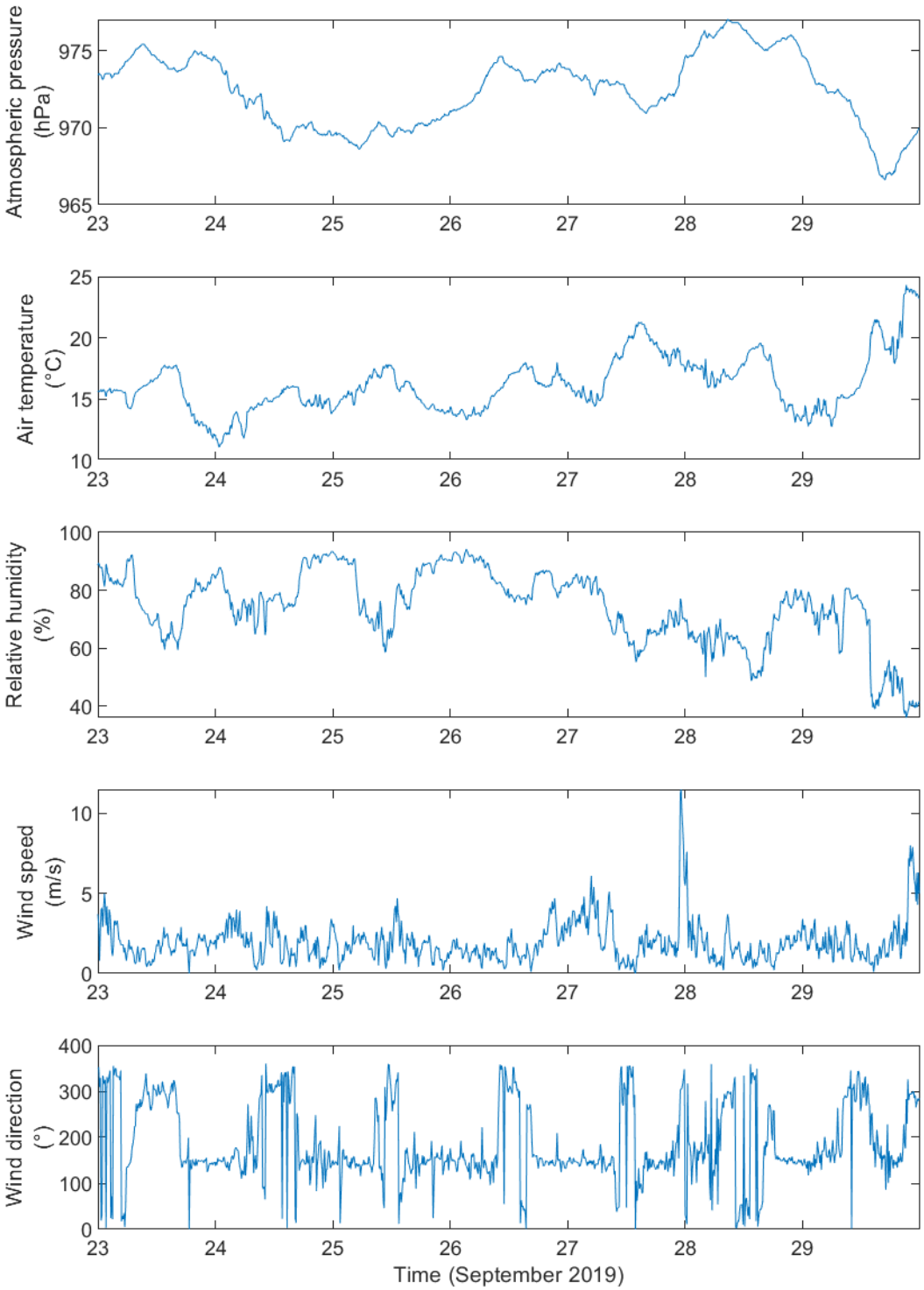

Appendix IV-14: Boxplot of meteorological parameters during the September 2019 sampling campaign (Le Bouveret – MeteoSwiss).

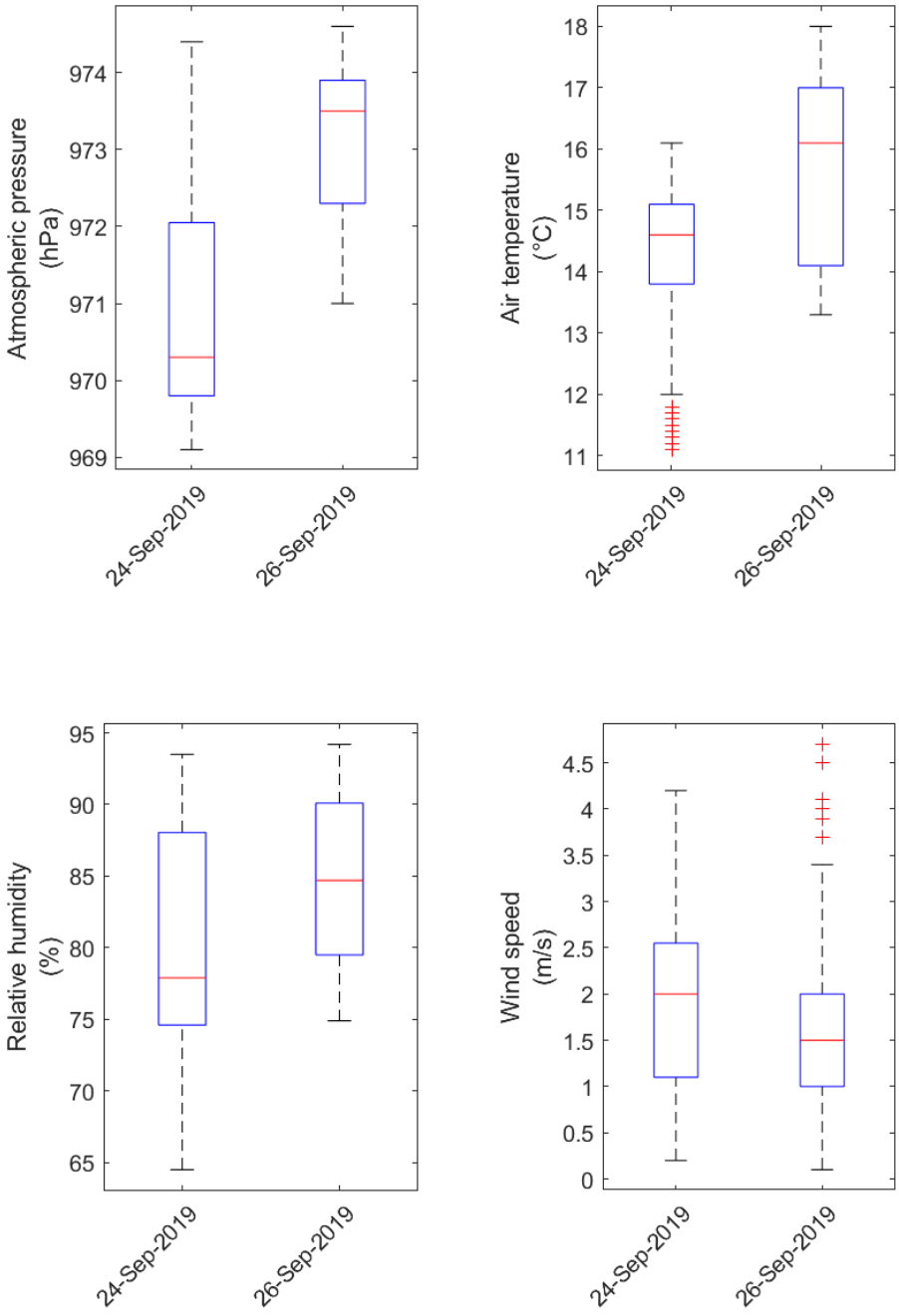

Appendix IV-15: Time series of river parameters during the September 2019 sampling week (Porte du Scex – OFEV).

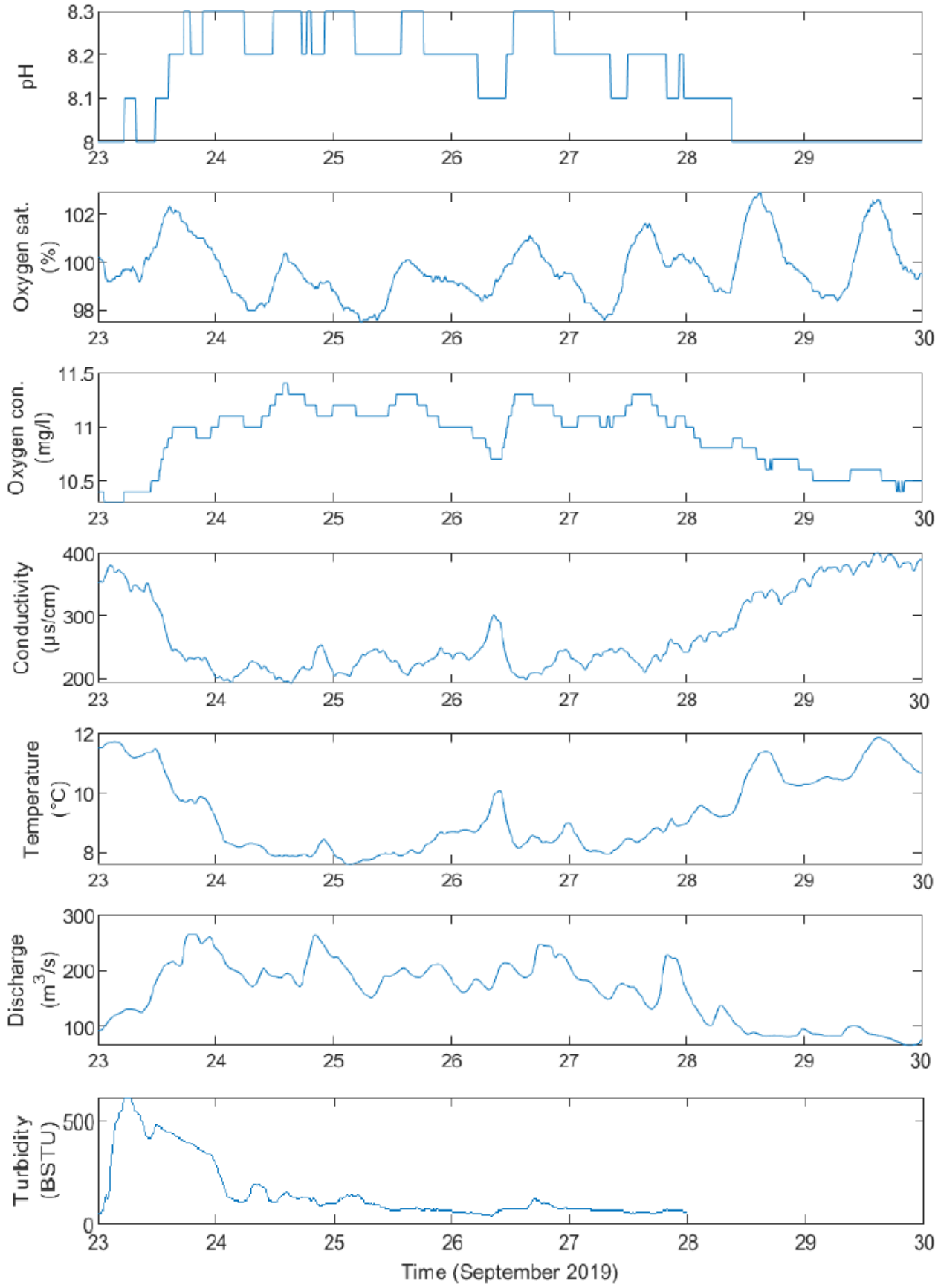

Appendix IV-16: Vertical profiles of lake parameters for the September 24th 2019 (SHL2 station – CIPEL).

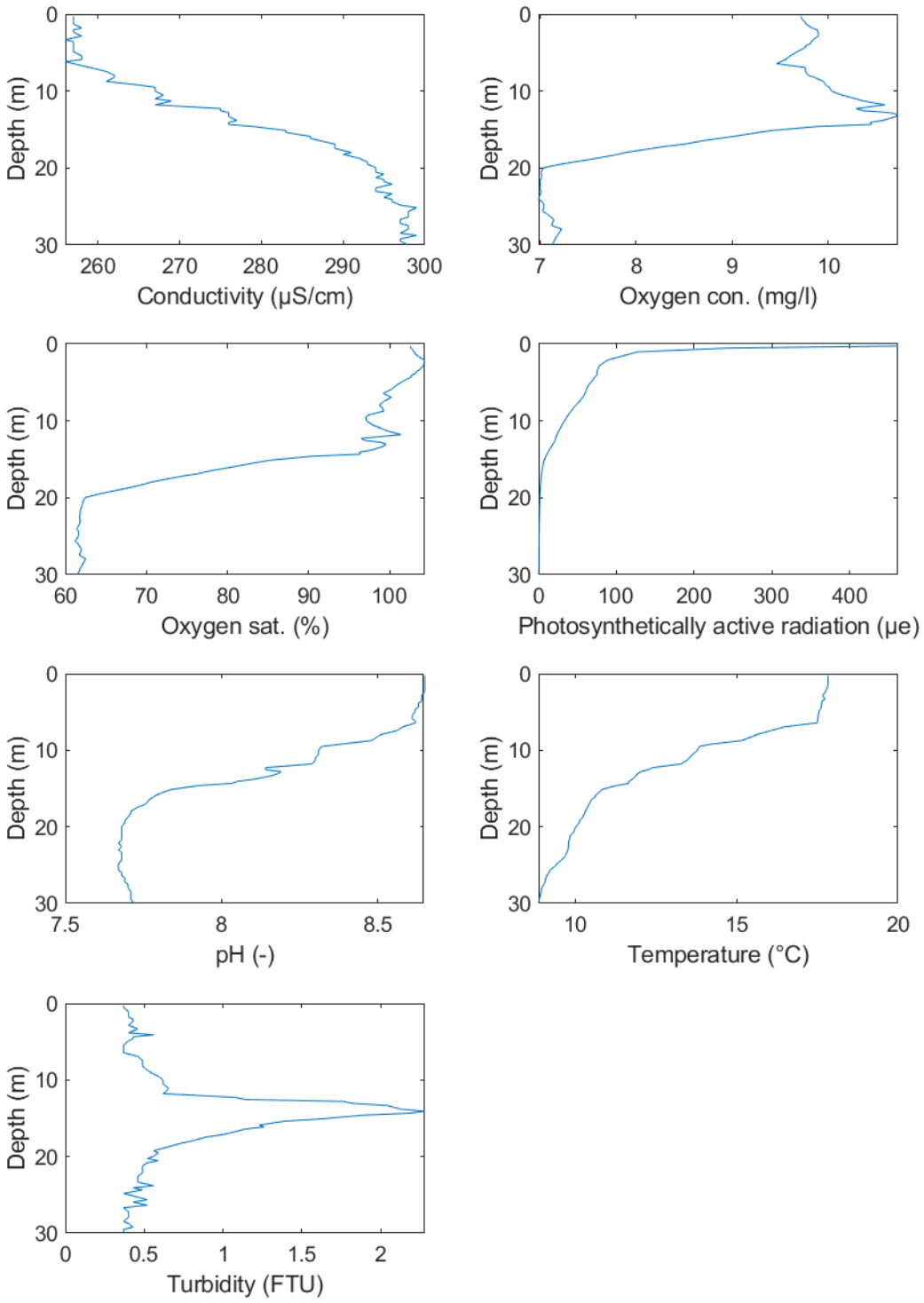

Appendix IV-17: Vertical profiles of lake physico-chemical parameters for the September 24th 2019 (SHL2 station – CIPEL).

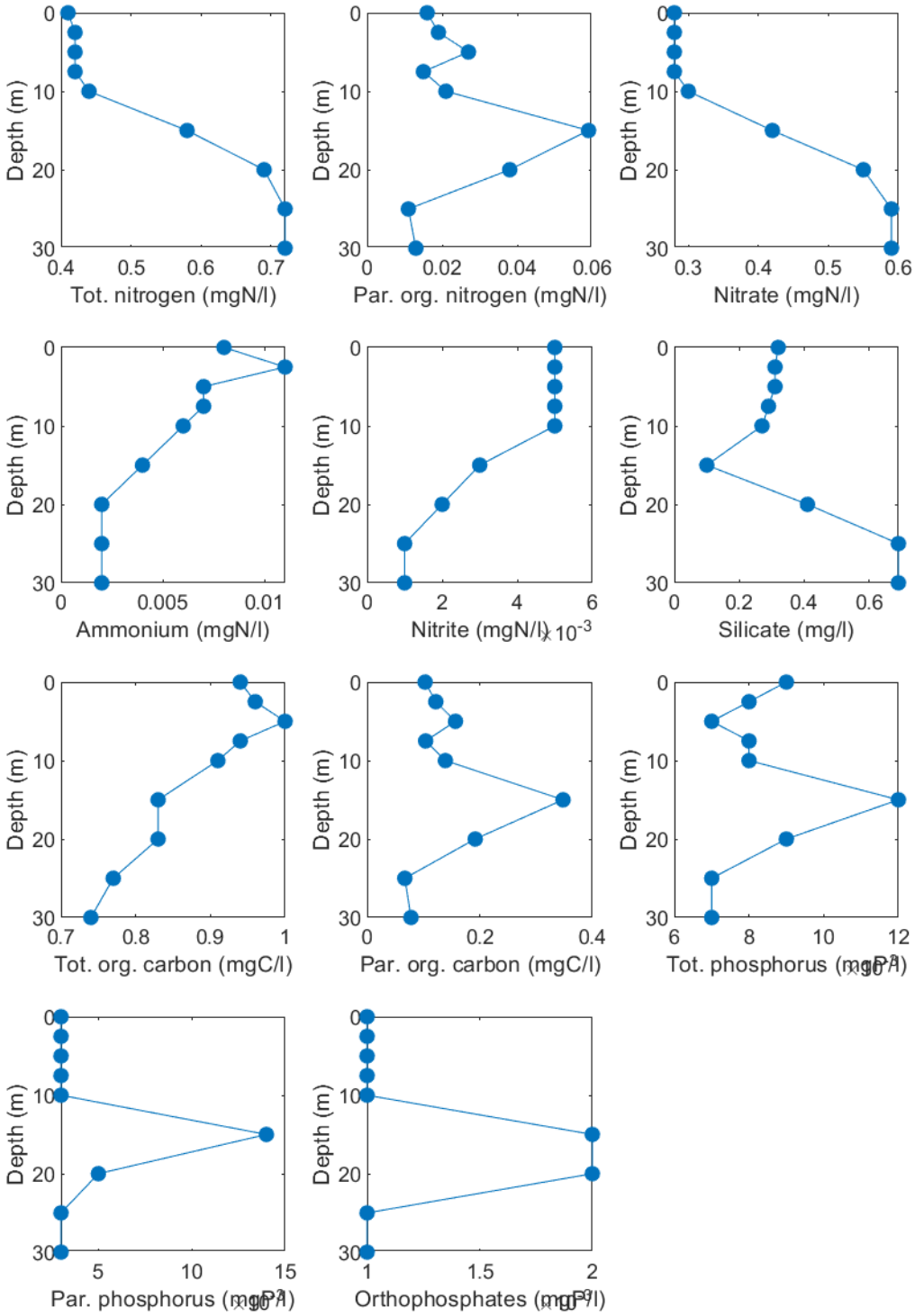

Appendix IV-18: CTD profiles of transects T1-A and T2-A.

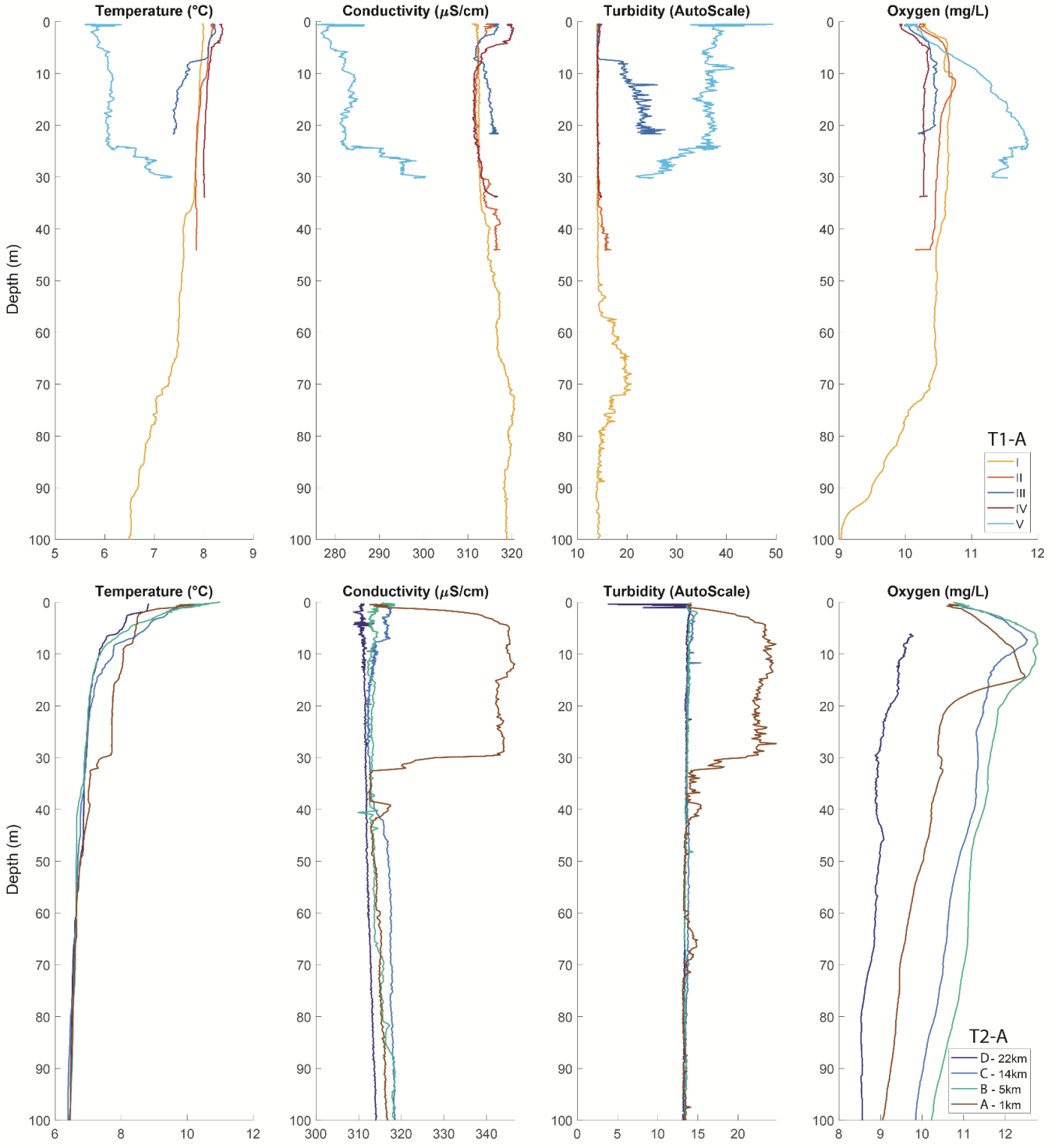

Appendix IV-19: CTD profiles of transects T1-S and T2-S.

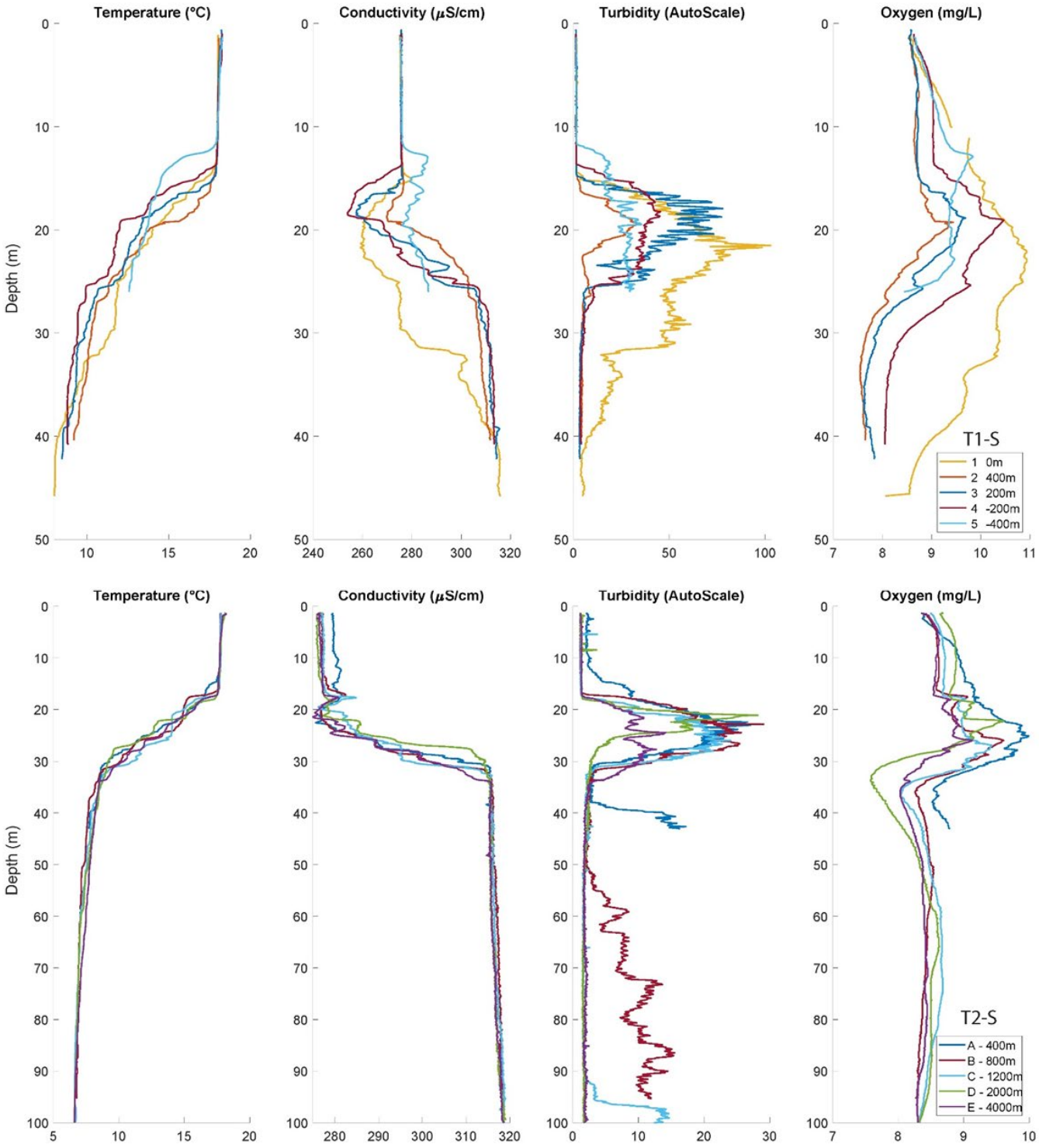

Appendix IV-20: Lake Analyser calculations. The Brunt-Väisälä buoyancy frequency (N^2) is expressed in s^{-2} while the top and lower limits of the metalimnion (metaT and metaB), the thickness of the metalimnion (h(meta)) and the thermocline depth (thermD) are expressed in meters.

Profile	N^2	metaT	thermD	metaB	h(meta)
1	1.4E-03	12.4	14.8	25.5	13.0
2	2.4E-03	12.7	18.7	27.2	14.4
3	2.8E-03	13.5	16.4	26.3	12.7
4	2.1E-03	12.6	15.3	20.4	7.8
5	3.2E-03	10.6	12.6	18.7	8.2
A	1.4E-03	16.6	22.5	30.9	14.3
B	2.6E-03	14.9	16.7	19.4	4.5
C	2.9E-03	15.6	17.6	21.2	5.6
D	2.9E-03	16.3	21.5	23.4	7.1
E	1.9E-03	15.6	17.5	32.5	16.9

Appendix IV-21: Results of ANOVA tests (MATLAB) with groups corresponding to the clusters (first: April campaign, second: September campaign).

	Source	SS	df	MS	F	p-value
PO_4^{3-}	Groups	229.574	3	76.5246	43.4	**7.10E-16**
	Error	121.655	69	1.7631		
	Total	351.229	72			
NO_3^-	Groups	0.03686	3	0.01229	2.32	**0.0837**
	Error	0.33901	64	0.0053		
	Total	0.37587	67			
SiO_2	Groups	17.3437	3	5.78125	46.85	**1.01E-16**
	Error	8.6387	70	0.12341		
	Total	25.9824	73			
Phytoplankton	Groups	2.05E+07	2	1.02E+07	8.57	**0.0005**
	Error	7.16E+07	60	1.19E+06		
	Total	9.21E+07	62			

	Source	SS	df	MS	F	p-value
PO_4^{3-}	Groups	38.9617	3	12.9872	19.6	**8.55E-10**
	Error	57.6574	87	0.6627		
	Total	96.6192	90			
NO_3^-	Groups	0.42341	3	0.14114	39.44	**2.91E-15**
	Error	0.26123	73	0.00358		
	Total	0.68464	76			
SiO_2	Groups	19.0111	3	6.33705	517.81	**2.41E-55**
	Error	1.0647	87	0.01224		
	Total	20.0759	90			
Phytoplankton	Groups	412648.3	2	206324.2	5.02	**0.0088**
	Error	3287468.6	80	41093.4		
	Total	3700116.9	82			

Appendix IV-22: Pictures of a part of the team (top: 4th of April, bottom: 26th of September 2019).

Appendix V

(Upper Rhône River)

Appendix V-1: Stable isotope composition ($\delta^{18}O$ values presented in ‰) of the Rhône water (in bold) and some of its tributaries (boxed text) in December 2015.

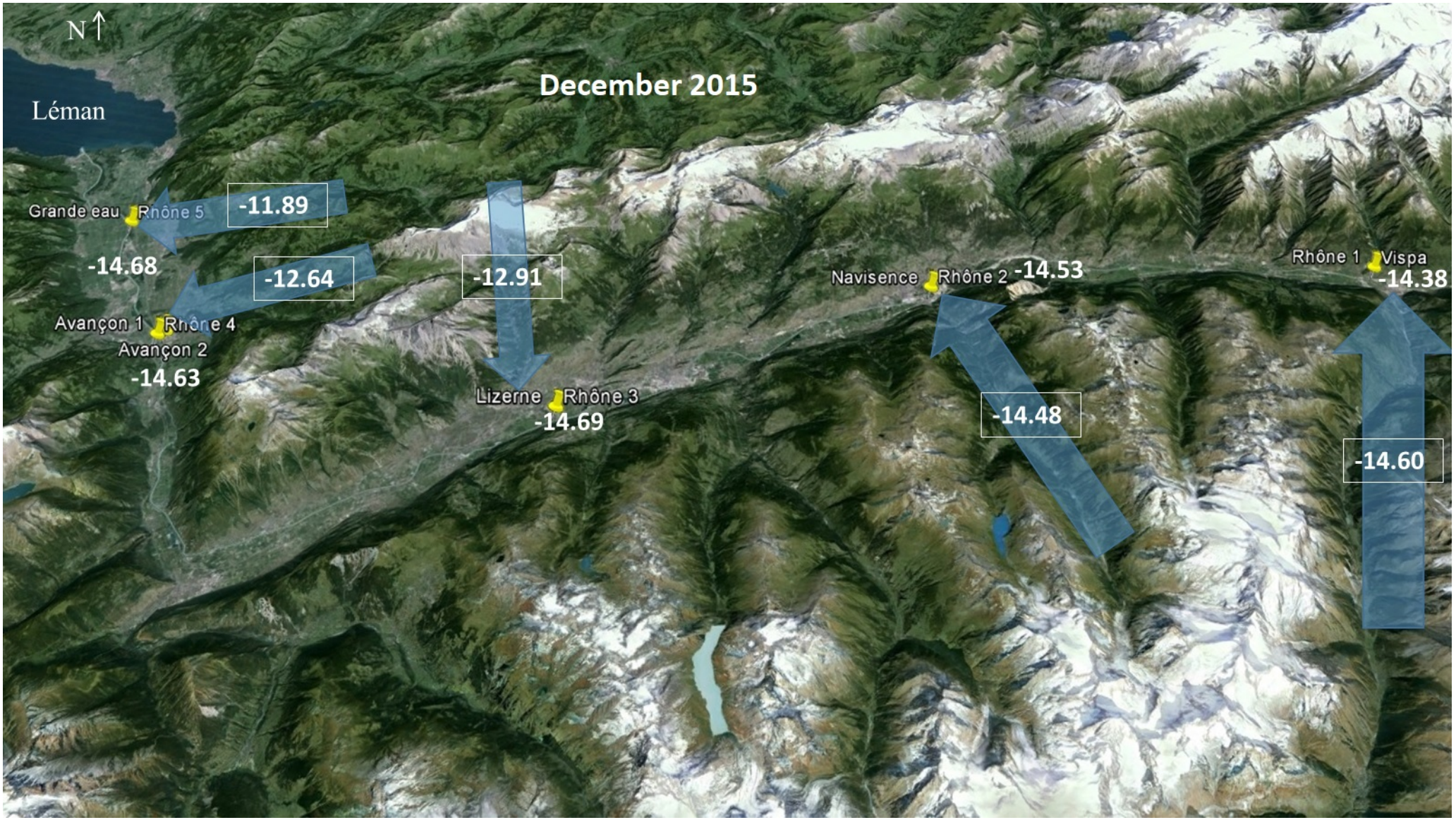

Appendix V-2: Stable isotope composition ($\delta^{18}O$ values presented in ‰) of the Rhône water (in bold), some of its tributaries (in blue) and dam outputs (normal font) in March 2017.

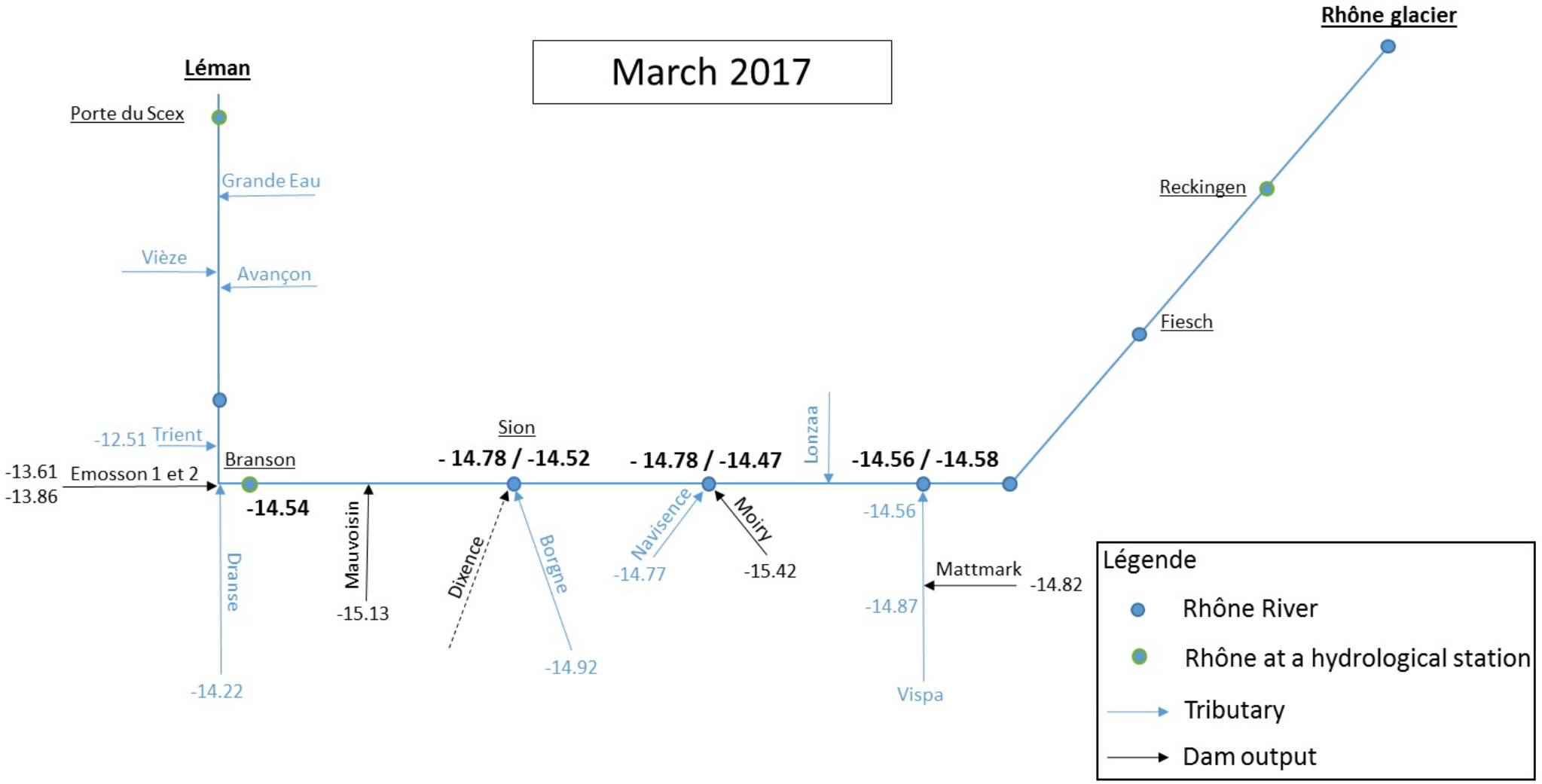

Appendix V-3: Stable isotope composition ($\delta^{18}O$ values presented in ‰) of the Rhône water (in bold), some of its tributaries (in blue) and dam outputs (normal font) in September 2017.

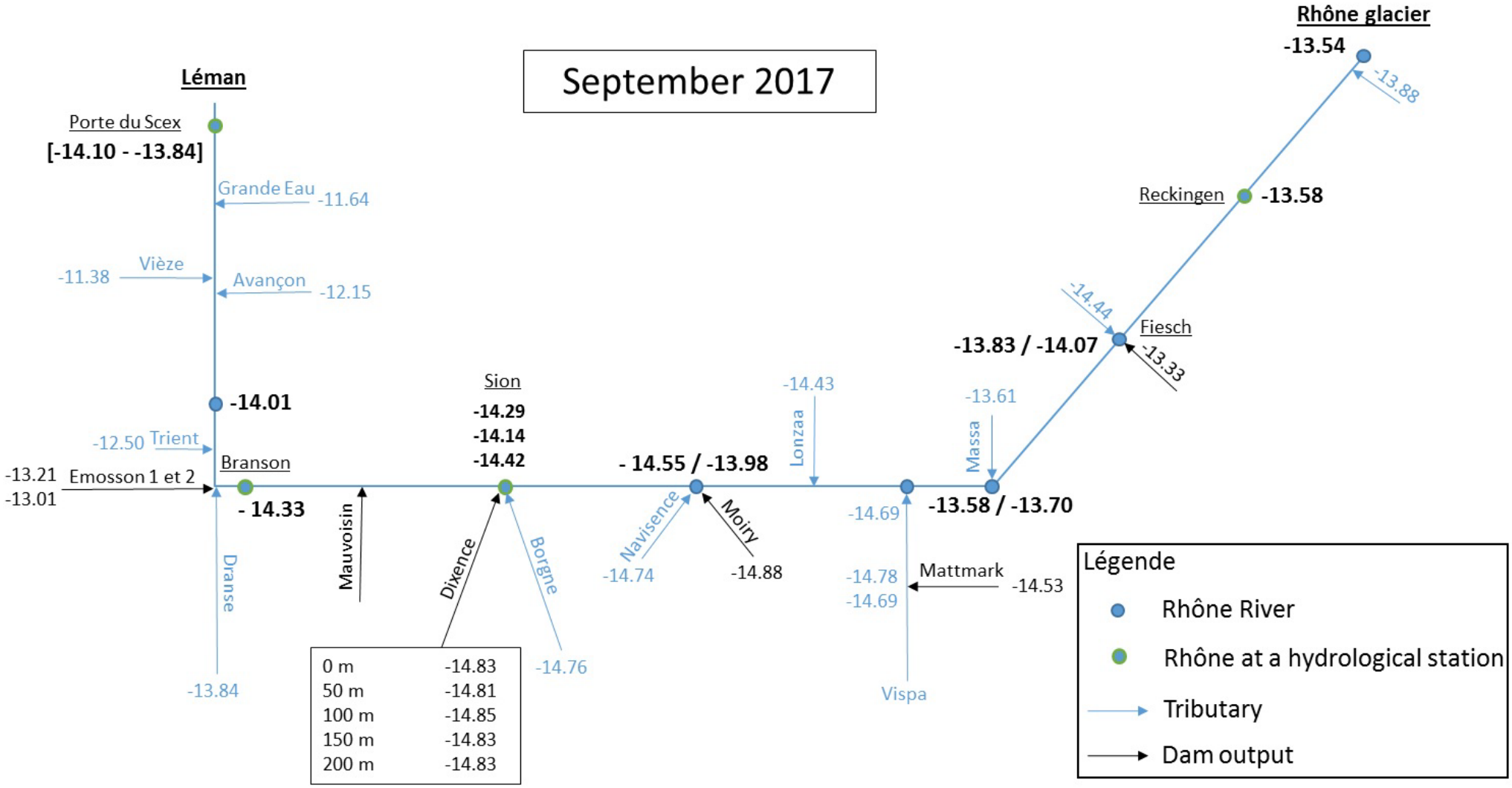

Appendix V-4: Stable isotope composition of the water (March 2017). Rhône water samples are indicated by a "R" (with "am" for upstream and "av" for downstream), the tributaries samples by a "T" and the dam outputs samples by "CF".

Sample	Location	Time	**$\delta^{18}O$ VSMOW**	std. dev.	**δD VSMOW**	std. dev.
6-CF	Moiry	16.03.2017	**-15.42**	0.03	**-114.2**	0.08
6-Ram	Navisence	-	**-14.47**	0.03	**-106.5**	0.11
6-Rav	Navisence	-	**-14.78**	0.04	**-109.2**	0.17
6-T	Navisence	-	**-14.77**	0.01	**-110.0**	0.04
7-CF	Mattmark	-	**-14.82**	0.03	**-109.1**	0.15
7-Vam	Vispa	-	**-14.87**	0.01	**-110.5**	0.18
8-Ram	Vispa	-	**-14.58**	0.03	**-107.0**	0.15
8-Rav	Vispa	-	**-14.56**	0.03	**-106.6**	0.16
8-TV	Vispa	-	**-14.56**	0.01	**-106.5**	0.05
10-CF	Chandolin	-	**-13.38**	0.03	**-99.9**	0.34
11-Ram	Borgne	-	**-14.52**	0.03	**-107.1**	0.17
11-T	Borgne	-	**-14.92**	0.01	**-110.6**	0.14
11-Rav	Borgne	-	**-14.78**	0.03	**-109.5**	0.18
13-CF	Mauvoisin	-	**-15.13**	0.03	**-110.8**	0.06
13-Rav	Mauvoisin	-	**-14.70**	0.02	**-108.1**	0.07
14-CF	Emosson	-	**-13.86**	0.03	**-99.9**	0.22
14-Ram	Dranse	-	**-14.54**	0.02	**-106.9**	0.13
14-Rav	Dranse	-	**-14.34**	0.02	**-105.0**	0.18
14-T	Dranse	-	**-14.22**	0.02	**-103.8**	0.16
15-CF	Emosson	-	**-13.61**	0.02	**-98.0**	0.05
15-T	Trient	-	**-12.51**	0.02	**-91.8**	0.06

Appendix V-5: Stable isotope composition of the water and the DIC (September 2017). Rhône water samples are indicated by a "R" (with "am" for upstream and "av" for downstream), the tributaries samples by a "T" and the dam outputs samples by "CF".

Sample	Location	Time	$\delta^{13}C$ VPDB	std. dev.	DIC (mg/L)	$\delta^{18}O$ VSMOW	std. dev.	δD VSMOW	std. dev.
1-R	glacier du Rhône	20.09.2017 11:00	**-11.31**	0.08	**4.6**	**-13.54**	0.05	**-95.8**	0.18
1-T	Muttbach	20.09.2017 11:30	**-6.10**	0.06	**60.3**	**-13.88**	0.02	**-99.6**	0.36
2-R	Reckingen	20.09.2017 13:40	**-5.81**	0.07	**33.4**	**-13.58**	0.03	**-97.7**	0.11
3-CF	Fiesch	20.09.2017 16:30	**-2.84**	0.04	**75.0**	**-13.33**	0.05	**-94.5**	0.15
3-Ram	Fiesch	20.09.2017 17:00	**-4.92**	0.07	**50.5**	**-14.07**	0.05	**-101.9**	0.18
3-Rav	Fiesch	20.09.2017 17:00	**-4.40**	0.06	**50.9**	**-13.83**	0.05	**-99.7**	0.18
3-T	Fiesch	20.09.2017 17:00	**-7.95**	0.05	**36.6**	**-14.44**	0.03	**-105.3**	0.14
4-Ram	Massa	20.09.2017 18:00	**-4.29**	0.07	**46.0**	**-13.70**	0.06	**-98.5**	0.21
4-Rav	Massa	20.09.2017 18:00	**-4.35**	0.05	**49.9**	**-13.58**	0.05	**-97.5**	0.30
4-T	Massa	20.09.2017 18:00	**-4.34**	0.08	**45.6**	**-13.61**	0.05	**-97.7**	0.19
5.1-R	Sion	20.09.2017 20:00	**-6.04**	0.03	**49.1**	**-14.29**	0.05	**-103.6**	0.23
5.2-R	Sion					**-14.14**	0.02	**-102.6**	0.07
5.3-R	Sion	21.09.2017 09:30	**-6.19**	0.03	**76.5**	**-14.42**	0.03	**-104.9**	0.11
6-CF	Moiry	21.09.2017 10:30	**-4.54**	0.04	**42.9**	**-14.88**	0.03	**-108.7**	0.25
6-Ram	Navisence	21.09.2017 11:00	**-6.04**	0.03	**66.8**	**-13.98**	0.03	**-101.0**	0.19
6-Rav	Navisence	21.09.2017 11:30	**-5.46**	0.04	**57.2**	**-14.55**	0.02	**-106.3**	0.14
6-T	Navisence	21.09.2017 10:00	**-3.78**	0.04	**81.7**	**-14.74**	0.04	**-108.7**	0.11
7-CF	Mattmark	21.09.2017 13:00	**-3.19**	0.06	**38.3**	**-14.53**	0.02	**-106.3**	0.19
7-Vam	Vispa	21.09.2017 13:00	**-5.08**	0.05	**56.6**	**-14.69**	0.01	**-108.4**	0.16
7-Vav	Vispa	21.09.2017 13:00	**-3.93**	0.04	**59.4**	**-14.78**	0.03	**-108.8**	0.09
8-Ram	Vispa	21.09.2017 15:00	**-5.00**	0.08	**52.3**	**-13.70**	0.04	**-98.3**	0.24
8-Rav	Vispa	21.09.2017 15:00	**-4.72**	0.04	**46.0**	**-13.71**	0.04	**-98.6**	0.30
8-TRD	Vispa	21.09.2017 15:00	**-3.33**	0.05	**37.5**	**-14.01**	0.05	**-102.3**	0.21
8-TV	Vispa	21.09.2017 15:00	**-4.39**	0.05	**52.7**	**-14.69**	0.04	**-108.0**	0.29
9-T	Lonza	21.09.2017 15:30	**-3.90**	0.04	**59.0**	**-14.43**	0.02	**-105.6**	0.17
10-CF	Chandolin	21.09.2017 16:30	**-9.32**	0.02	**139.4**	**-14.36**	0.03	**-105.8**	0.12
11-T	Borgne	21.09.2017 17:00	**-3.82**	0.03	**91.2**	**-14.76**	0.01	**-109.1**	0.07
12-0	Grande Dixence	21.09.2017 19:00	**-4.71**	0.11	**25.4**	**-14.83**	0.04	**-107.5**	0.19
12-50	Grande Dixence	21.09.2017 19:00	**-5.07**	0.12	**22.8**	**-14.81**	0.02	**-107.3**	0.37
12-100	Grande Dixence	21.09.2017 19:00	**-5.16**	0.11	**22.8**	**-14.85**	0.03	**-107.6**	0.10
12-150	Grande Dixence	21.09.2017 19:00	**-5.53**	0.09	**25.3**	**-14.83**	0.03	**-107.4**	0.19
12-200	Grande Dixence	21.09.2017 19:00	**-5.06**	0.11	**25.3**	**-14.83**	0.02	**-107.5**	0.19
13-CF	Mauvoisin	22.09.2017 14:00	**-5.42**	0.05	**41.4**	**-14.70**	0.04	**-106.7**	0.09
14-CF	Emosson	25.09.2017 16:00	**-7.40**	0.08	**31.6**	**-13.01**	0.06	**-93.0**	0.37
14-Ram	Dranse	25.09.2017 15:30	**-5.79**	0.05	**59.8**	**-14.33**	0.03	**-104.2**	0.11
14-Rav	Dranse	25.09.2017 16:00	**-5.72**	0.05	**71.7**	**-14.20**	0.03	**-103.2**	0.11
14-T	Dranse	25.09.2017 16:30	**-4.81**	0.04	**73.0**	**-13.84**	0.07	**-100.6**	0.20
15-CF	Emosson	25.09.2017 17:00	**-6.30**	0.07	**25.3**	**-13.21**	0.02	**-94.1**	0.27
15-Rav	Trient	25.09.2017 17:30	**-5.68**	0.06	**57.8**	**-14.01**	0.04	**-102.0**	0.17
15-T	Trient	25.09.2017 17:00	**-4.38**	0.05	**59.5**	**-12.50**	0.02	**-90.7**	0.09
16-T	Avançon	25.09.2017 18:30	**-5.38**	0.02	**122.3**	**-12.15**	0.02	**-85.6**	0.08
17-T	Vièze	25.09.2017 19:00	**-5.90**	0.03	**146.4**	**-11.38**	0.01	**-80.6**	0.18
18-T	Grande Eau	25.09.2017 19:10	**-6.55**	0.02	**147.0**	**-11.64**	0.31	**-83.1**	1.45

R1 PdS	Porte du Scex	19.09.2017 16:00	**-6.33**	0.18	**78.7**	**-13.93**	0.03	**-100.4**	0.29
R1	Porte du Scex	20.09.2017 14:00	**-6.76**	0.08	**74.4**	**-13.95**	0.03	**-100.6**	0.05
R2	Porte du Scex	20.09.2017 15:00	**-6.66**	0.06	**70.7**	**-13.91**	0.01	**-100.4**	0.15
R3	Porte du Scex	20.09.2017 16:00	**-6.35**	0.11		**-13.88**	0.02	**-100.0**	0.04
R4	Porte du Scex	20.09.2017 17:00	**-6.11**	0.10	**57.3**	**-13.84**	0.02	**-99.8**	0.10
R5	Porte du Scex	20.09.2017 18:00	**-6.11**	0.07	**86.4**	**-13.88**	0.02	**-100.1**	0.29
R6	Porte du Scex	20.09.2017 19:00	**-6.29**	0.03	**68.8**	**-13.89**	0.04	**-100.2**	0.15
R7	Porte du Scex	20.09.2017 20:00	**-6.33**	0.04	**65.6**	**-13.89**	0.02	**-99.9**	0.09
R8	Porte du Scex	20.09.2017 21:00	**-5.99**	0.03	**81.4**	**-13.85**	0.03	**-99.8**	0.12
R9	Porte du Scex	20.09.2017 22:00	**-5.82**	0.05	**85.8**	**-13.85**	0.03	**-99.8**	0.06
R10	Porte du Scex	20.09.2017 23:00	**-5.78**	0.03	**83.1**	**-13.85**	0.02	**-100.0**	0.15
R11	Porte du Scex	21.09.2017 00:00	**-5.84**	0.04	**82.8**	**-13.91**	0.04	**-100.4**	0.09
R12	Porte du Scex	21.09.2017 01:00	**-6.14**	0.05	**66.1**	**-14.00**	0.03	**-101.2**	0.17
R13	Porte du Scex	21.09.2017 02:00	**-5.96**	0.04	**82.0**	**-13.97**	0.03	**-101.0**	0.11
R14	Porte du Scex	21.09.2017 03:00	**-5.80**	0.03	**79.1**	**-13.92**	0.03	**-100.7**	0.16
R15	Porte du Scex	21.09.2017 04:00	**-6.07**	0.06	**63.7**	**-13.90**	0.05	**-100.5**	0.12
R2 PdS	Porte du Scex	22.09.2017 16:25	**-6.55**	0.15	**98.1**	**-13.87**	0.03	**-100.4**	0.19
R3 PdS	Porte du Scex	25.09.2017 19:25	**-6.01**	0.10	**65.2**	**-14.10**	0.03	**-102.2**	0.20

Appendix VI

(SPIKE II project)

Appendix VI-1: Description of the research project.

SPIKE II – Following a rainfall injection through the entire hydrologic cycle (including vegetation)

Research groups involved:

- EPFL ENAC ECHO: Andrea Rinaldo and Paolo Benettin
- EPFL ENAC CEL: Michaël Bensimon
- University of Saskatchewan, Saskatoon (CA): Jeff McDonnell, Magali Furlan Nehemy, Dyan Pratt, Cody Millar, Kim Janzen
- UNIL: Torsten Vennemann and Gabriel Cotte

Project description:

An unresolved problem in catchment hydrology pertains the fate of precipitation after it lands on a soil surface. After infiltration takes place, it is still very debated how long water takes before reaching a river network and how much of that water will actually not reach any river network because it will be uptaken by vegetation. The research objective of this experiment is to shed light on where rainfall goes after it infiltrates into the soil, with particular focus on when and where it becomes the source water for vegetation. To achieve this goal, we will use a unique facility at the ECHO laboratory: a large (2.5 x 1 meters) weighed lysimeter, filled with soil and with 2 small willow trees planted since 2015. After a first warm-up period, where the system will be let to evolve under natural climate conditions, we will manually inject a 20-mm precipitation with a labeled isotopic composition. This special injection will be tracked in time for at least 40 days, by frequently taking samples of: soil, plant tissues, soil water, bottom leakage water, atmospheric vapor. At the end of the experiment, both the soil and the trees will be destructively sampled to allow a full recovery of the labeled injection.

Specific Objectives:

The main goals of the experiment can be summarized as follows:

1) Obtain a high-quality tracer breakthrough curve in the trees' water uptake and transpiration fluxes
2) Quantitatively evaluate the effect of tree transpiration on water vapor sampled at the canopy level
3) Reconstruct the infiltration profile of the labeled injection in the soil column
4) Close the tracer mass balance: where is the injected precipitation mass 40 days after injection?
5) Investigate whether the isotopic composition of the more mobile water is significantly different from that of the water that is tightly bound to the soil particles.

Highlights:

An innovative aspect of this experiment is that it will blend different techniques to monitor the evolution of the system, allowing a new and complete view on the infiltration-uptake processes. The bulk soil and vegetation samples will be analyzed using the Koeniger cryogenic extraction method at the University of Saskatchewan (CA). The isotopic analyses of liquid water samples will be carried out at EPFL by Michaël Bensimon. The vapor analyses will be done in collaboration with the group of Torsten Vennemann (University of Lausanne).

Appendix VI-2: Calendar of the experiment and positions of the Picarro sampling tube.

07.05.2018 10:52	1st position, fixed to a branch of teh tree
11.05.2018 16:30	in the middle of the leaves fixed with scotch
14:05:2018 20:00	free air (at 2 m from the tree)
16.05.2018 16:26	leaves (fixed with a rope)
16.05.2018 23:59	Spike water injection (leaves)
29.06.2018 11:12	free air (at 2 m from the tree)
03.07.2018 11:30	Picarro switched off

Appendix VI-3: Stable isotope composition of the vapour water and the CO_2 sampled in the vacuum bottles.

			H_2O		CO_2
Sample	Location	Date & Time	**$\delta^{18}O$ VSMOW**	**δD VSMOW**	**$\delta^{13}C$ VPDB**
B1	free air	18.05.2018 14:35	-19.88	-129.4	**-10.16**
B2	leaves	18.05.2018 14:45	-18.63	-125.6	**-11.09**
B3	leaves	30.05.2018 10:15	-18.64	-124.4	**-10.00**
B4	leaves	30.05.2018 18:30	-17.69	-117.1	**-9.44**
B5	leaves	20.05.2018 15:57	-	-	**-10.40**
B6	free air	29.06.2018 08:22	-19.72	-144.0	**-9.30**
B7	leaves	29.06.2018 08:20	-	-	**-8.93**
B8	free air	28.06.2018 23:40	-21.66	-148.2	**-**
B9	free air	27.06.2018 12:45	-18.71	-128.9	**-9.37**
B10	leaves	22.06.2018 19:25	-10.79	-120.5	
B11	leaves	27.06.2018 12:45	-	-	**-9.36**

Appendix VI-4: Local Meteoric Water Line and stable isotope composition of the vapour water extracted from the bottles (left), calibration curve for the correction of the Picarro data via the extracted data (right).

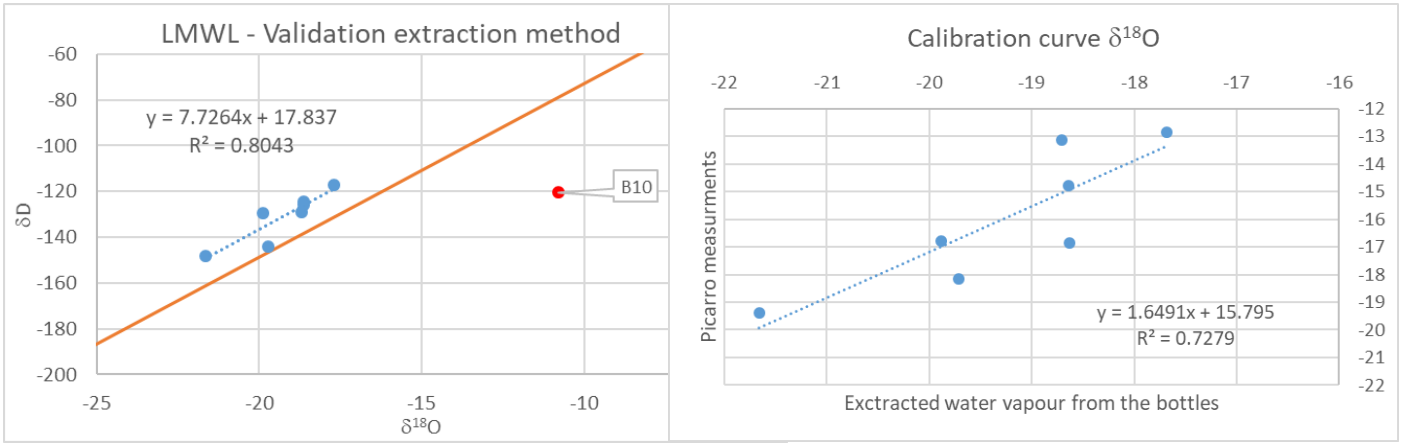

Appendix VI-5: Corrected vapour water data. The spike water was injected the 17th of May at 00:00.

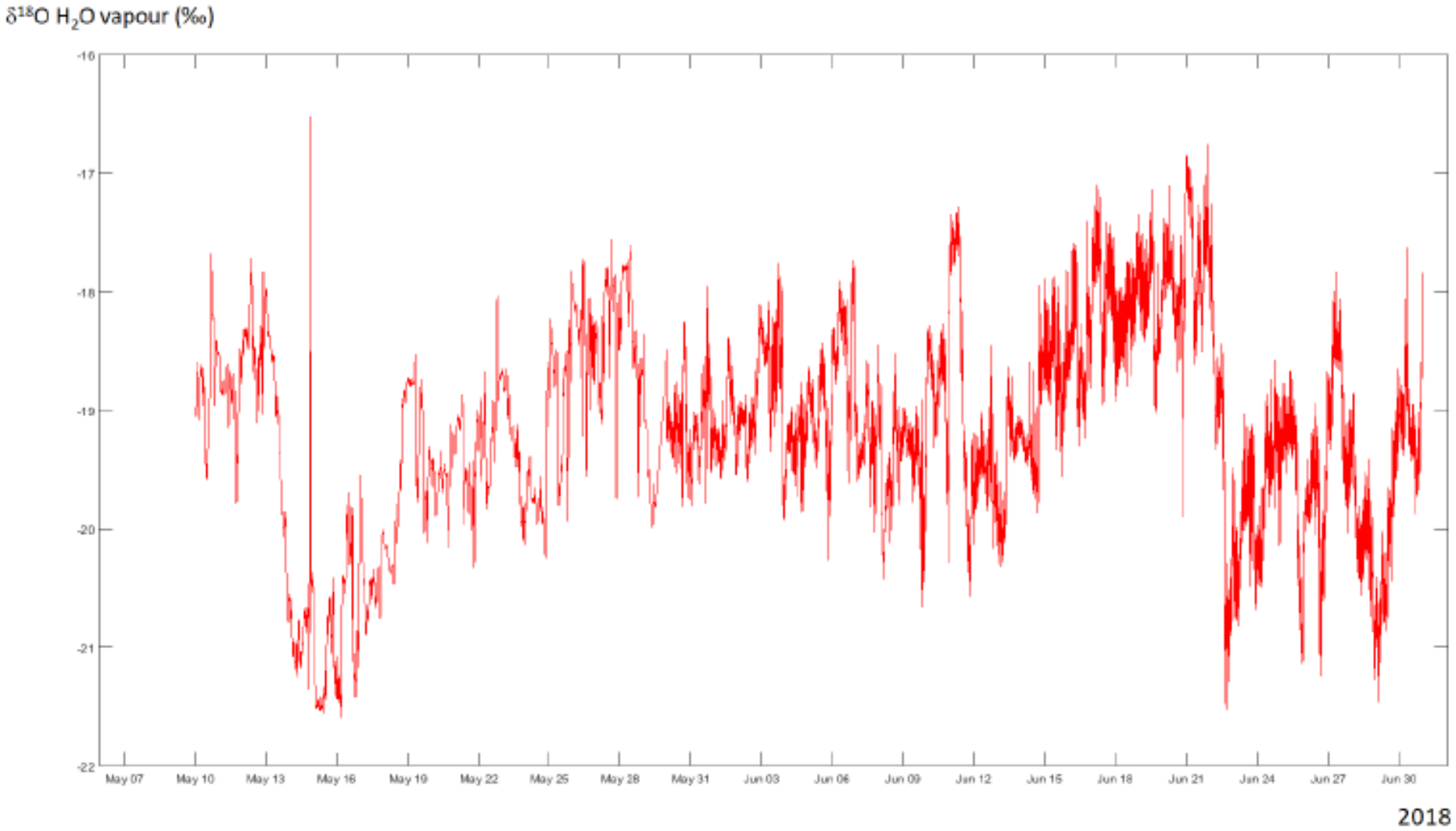

Appendix VI-6: Picture of a part of the team and of the tree during its cutting (29th of June 2018).